# Visible Light Photocatalysis: Mechanisms and Reaction Development




Mihai Viorel Popescu

University of Oxford

A thesis submitted for the degree of
Doctor of Philosophy

2021

# Declaration

This dissertation describes work carried out in the Chemistry Research Laboratory at the University of Oxford between October 2018 and August 2021 under the supervision of Prof. Martin D. Smith. Computational work was undertaken at Colorado State University between June and July 2019 in collaboration with Prof. Robert S. Paton. The dissertation is the product of my own work and includes no results obtained through collaboration, except where specifically indicated in the text.

Mihai Viorel Popescu

# Acknowledgments

First and foremost, I would like to thank Prof. Martin D. Smith for all his support and guidance throughout my Ph.D. I am very grateful for the opportunity to work in his group and his advice has enabled me to grow as a scientist and as a person.

I would like to thank Prof. Robert S. Paton for providing me the opportunity to visit his group in Colorado. It was a very enjoyable experience, during which I've learned a lot about computational chemistry from his group. In particular, I would like to thank Dr. Juan Alegre-Requena for his mentorship and patience throughout our numerous collaborations, for which I am very grateful.

My stay in the Smith group has also been very enjoyable. I owe special thanks to Dr. Aroonroj "Yao" Makareeya and Zachariah Lockhart for their contributions to the projects that form the basis of this thesis. I am also grateful for all the other collaborators: Benjamin "Badger" Jones, Pearse Solon, Dr. Nicolas Parker, Dr. Jia Zhuqing and Owen Smith. Thanks to the remaining members of the Smith groups (past and present): Alison, Minh, Arseni, Kat, Ricky, Benjamin Danet, Elliot (member of the quarantine squad), Maddie, Morgan, Xiangqian, Jiyuan and all the part 2 and SBM rotation students. Special mention goes to the other members of the "Power Hour" gang: Zachariah Lockhart, Owen Smith and Benjamin Jones. Also, thank you Pearse for making sure the lab kept running!

# Abstract

This thesis describes the development and mechanistic investigations into novel photochemical transformations mediated by visible light.

Chapter one introduces key concepts pertaining to excited state chemistry, mainly the interaction between matter and light, fundamental photophysical events, and the subsequent changes in physical and chemical properties that ensue upon excitation.

Chapter two provides an overview of recent developments into visible light mediated [2+2] photocyclizations, with the emphasis being placed on photocyclizations of indoles. Although the synthesis of cyclobutanes *via* photochemical [2+2] processes is highly facile, deviations from standard behaviour do occasionally occur, leading to the formation of novel chemical scaffolds. Here we describe the development of an interrupted [2+2]-photochemical process that leads to the formation of highly functionalized heterocycles with the aid of visible-light mediated energy transfer catalysis.

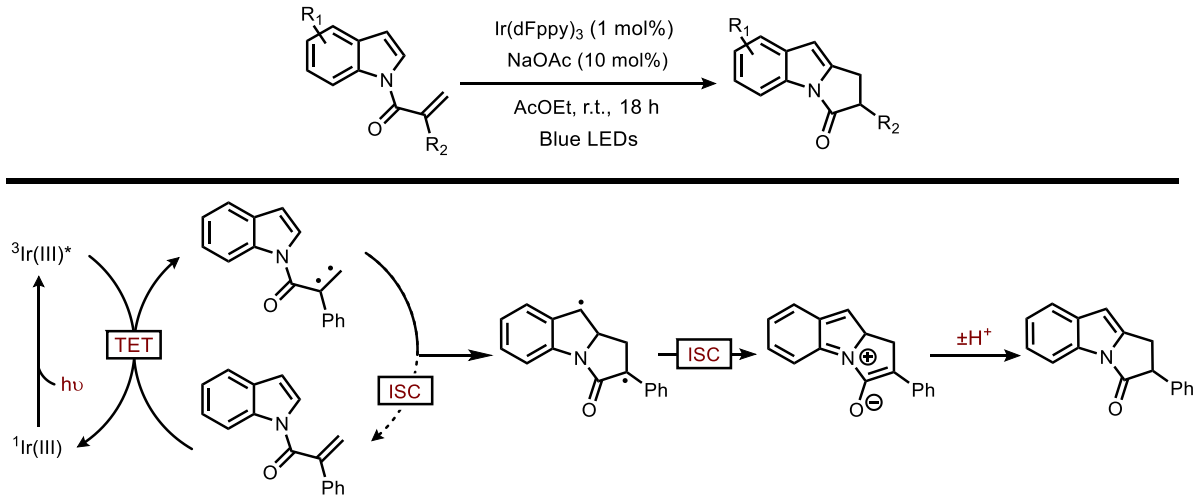



***Figure I**: Visible-light-mediated heterocycle functionalization via geometrically interrupted [2+2] cycloaddition*

Chapter 3 describes mechanistic investigations into the regioselectivity of the visible light mediated photocyclization of 2-*N*-arylamino-cyclohexenones bearing an *ortho*-iodo substituent. These substrates undergo cyclization exclusively on the carbon bearing the iodine

substituent, which upon loss of the iodine atom, leads to the formation of iminium ions capable of trapping numerous nucleophiles. The reactivity displayed by these substrates is completely orthogonal to that of their 2-aryloxy analogues, which lead to the cyclization at the *ipso*-H position. Here we investigate the mechanism of this transformation with the aid of quantum chemical calculations.

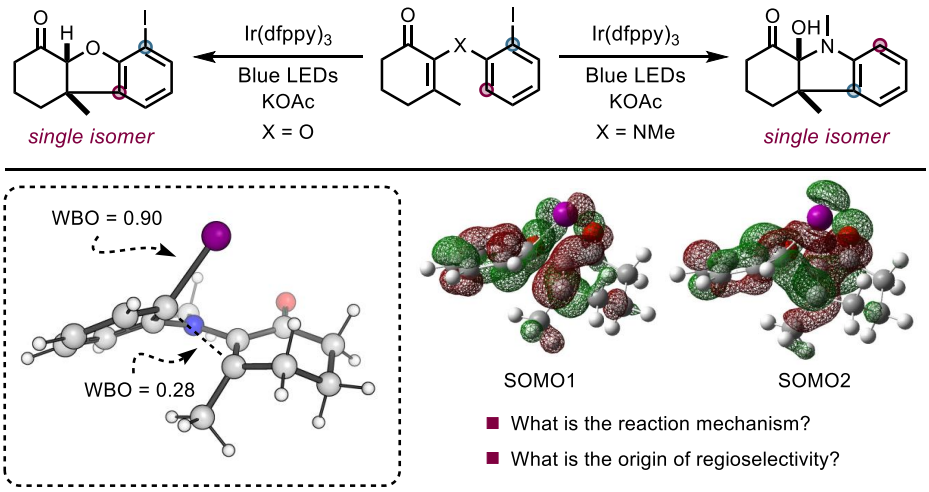



***Figure II**: Mechanistic investigations into visible-light-mediated photoeliminative cyclizations of O-iodo N-2-iodoaryl enaminones*

# List of Abbreviations

| | |
|---|---|
| [O] | oxidant |
| [Q] | concentration of quencher |
| A | ampere |
| μA | micro ampere |
| a.u. | atomic units |
| Ac | acetyl |
| aq. | aqueous |
| Å | Armstrong |
| ATR | attenuated total reflectance |
| Bn | benzyl |
| Boc | *tert*-butyloxycarbonyl |
| cat. | catalytic |
| CASSCF | complete active space self-consistent field |
| CCSD(T) | coupled-cluster with single and double (triple) |
| CI | chemical ionization |
| cm | centimetre |
| COSY | correlation spectroscopy |
| CPCM | conductor-like polarizable continuum model |
| d | doublet |
| DCC | *N*,*N*-dicyclohexylcarbodiimide |
| DCE | 1,2-dichloroethane |
| d.r. | diastereoisomeric ratio |
| DFT | density functional theory |
| DLPNO | domain-based local pair natural orbital |
| DMF | dimethyl formamide |
| DMAP | 4-dimethylaminopyridine |
| DMSO | dimethyl sulfoxide |
| E | energy |
| $E^+$ | electrophile |
| EI | electron ionization |
| equiv. | equivalents |

| | |
|---|---|
| ESI | electron spray ionization |
| $E_{SPC}$ | energy with single point corrections |
| $E_T$ | triplet energy |
| Et | ethyl |
| ET | electron transfer |
| et al. | and others |
| Fc | ferrocene |
| $Fc^+$ | ferrocenium ion |
| FT-IR | Fourier-transformed infrared spectroscopy |
| g | gram |
| G | free energy |
| $G_{SPC}$ | free energy with single point correction |
| H | enthalpy |
| HAT | hydrogen atom transfer |
| HMBC | heteronuclear multiple bond correlation |
| HOMO | highest occupied molecular orbital |
| HPCL | high performance liquid chromatography |
| HRMS | high resolution mass spectrometry |
| $H_{SO}$ | spin-orbit coupling |
| $\widehat{H_{SO}}$ | spin-orbit coupling operator |
| HSQC | heteronuclear single quantum correlation |
| Hz | hertz |
| hν | photon |
| I | light intensity |
| $I_0$ | initial light intensity |
| IC | internal conversion |
| *imag.υ* | imaginary frequency |
| *i*Pr | *iso*-propyl |
| IRC | intrinsic reaction coordinate |
| IUPAC | International Union of Pure and Applied Chemistry |
| ISC | intersystem crossing |
| *J* | coupling constant |
| kcal | kilocalorie |

| | |
|---|---|
| KHMDS | potassium bis(trimethylsilyl)amide |
| $k_{SV}$ | Ster-Volmer quenching constant |
| KIE | kinetic isotope effect |
| L | litre |
| LED(s) | light emitting diode(s) |
| LUMO | lowest unoccupied molecular orbital |
| m | multiplet |
| *m* | meta |
| M | molar |
| Me | methyl |
| MECP | minimum energy crossing point |
| mg | milligram |
| mL | millilitre |
| mM | millimolar |
| mmol | millimole |
| MO | molecular orbital |
| mol | mole |
| MOM | methoxymethyl ether |
| Ms | methane sulfonyl |
| mV | millivolt |
| NBO | natural bonding orbitals |
| MHz | megahertz |
| nm | nanometre |
| nM | nanomolar |
| NMR | nuclear magnetic resonance |
| NOESY | nuclear Overhauser effect spectroscopy |
| ns | nanosecond |
| $Nu^-$ | nucleophile |
| *o* | ortho |
| *p* | para |
| $p_i$ | probability |
| ppm | parts per million |
| Ph | phenyl |
| PMP | *para*-methoxy phenyl |

| | |
|---|---|
| R | universal gas constant |
| qh. | quasiharmonic |
| r.r. | regioisomeric ratio |
| S | entropy / singlet |
| $S_{conf}$ | configurational entropy |
| SCE | saturated calomel electrode |
| SEM | trimethylsilylethoxymethyl |
| sens. | sensitizer |
| SMD | solvation model based on density |
| $S_0$ | singlet ground state |
| $S_1$ | 1$^{st}$ singlet excited state |
| $S_2$ | 2$^{nd}$ singlet excited state |
| $S_n$ | n$^{th}$ singlet excited state |
| SOMO | singly occupied molecular orbital |
| T | temperature |
| t | triplet |
| TBAB | tetrabutyl ammonium bromide |
| TBS | *tert*-butyldimethylsilyl |
| *t*Bu | *tert*-butyl |
| TD-DFT | time dependent density functional theory |
| TET | triplet energy transfer |
| Tf | trifluoromethanesulfonate |
| TFE | 2,2,2-trifluoroethanol |
| THF | tetrahydrofuran |
| TLC | thin layer chromatography |
| TS | transition state |
| $T_1$ | 1$^{st}$ triplet excited state |
| $\tilde{T}_1$ | perturbed 1$^{st}$ triplet state |
| $T_2$ | 2$^{nd}$ triplet excited state |
| $T_3$ | 3$^{rd}$ triplet excited state |
| UV | ultraviolet |
| UV-Vis | ultraviolet and visible |
| U(eq) | third of the trace of the orthogonalized $U^{ij}$ tensor |
| V | volt |

| | |
|---|---|
| w/o | without |
| WBO | Wiberg bond order |
| ZPE | zero-point energy |
| $\Delta$ | difference or high temperature |
| $\delta$ | chemical shift |
| $\varepsilon$ | extinction coefficient |
| $\lambda$ | wavelength |
| $\lambda_{Longest}$ | highest wavelength cut-off |
| $\lambda_{max}$ | wavelength maximum |
| $\mu s$ | microsecond |
| $\tau$ | lifetime |
| $\tau^{o}$ | initial lifetime |
| $\Phi$ | quantum yield |
| $\Phi_{ISC}$ | quantum yield of intersystem crossing |
| ‡ | transition state |
| $^{o}$ | degrees |
| $^{o}C$ | degrees Celsius |
| (±) | racemic mixture |

# Table of Contents

**Chapter 1: Introduction to excited state chemistry ..... 1**

1.1 Elements of photochemistry ..... 1

1.2 Excited state properties ..... 4

1.3 Excited state lifetime ..... 6

1.4 Energy transfer catalysis ..... 8

1.5 Stern-Volmer quenching ..... 12

1.6 Baldwin's rules ..... 13

1.7 Computational methods and triplet state chemistry ..... 14

1.8 Aims of this work ..... 18

**Chapter 2: Visible-light-mediated heterocycle functionalization *via* geometrically interrupted [2+2] cycloaddition ..... 19**

2.1 Introduction ..... 19

2.1.1 Visible light mediated [2+2] cycloadditions ..... 19

2.1.2 Interrupted [2+2] cycloadditions ..... 28

2.1.3 Project Aim ..... 33

2.2 Results and Discussions ..... 35

2.2.1 Substrate Synthesis ..... 35

2.2.2 Reaction Optimization ..... 38

2.2.3. Substrate Scope ..... 39

2.2.4. Mechanistic Investigations ..... 44

2.3 Mechanistic summary and conclusions ..... 55

**Chapter 3: Mechanistic investigations into visible-light-mediated photoeliminative cyclizations of *O*-iodo *N*-2-iodoaryl enaminones ..... 58**

3.1 Introduction ..... 58

3.1.1 Photoeliminative cyclizations ..... 58

3.1.3 Project Aim ..... 68

3.2 Results and Discussions ..... 70

*3.2.1 Geometry Benchmarking* ..... 70

*3.2.2 Mechanistic investigation* ..... 72

*3.2.3 Origin of regioselectivity* ..... 80

*3.2.4 Comparison to 2-(2-iodophenoxy)-cyclohexenones reactivity* ..... 87

*3.2.5 Influence of ortho-substituents* ..... 90

3.3 Mechanistic summary and conclusions ..... 98

**Supplementary Information ..... 102**

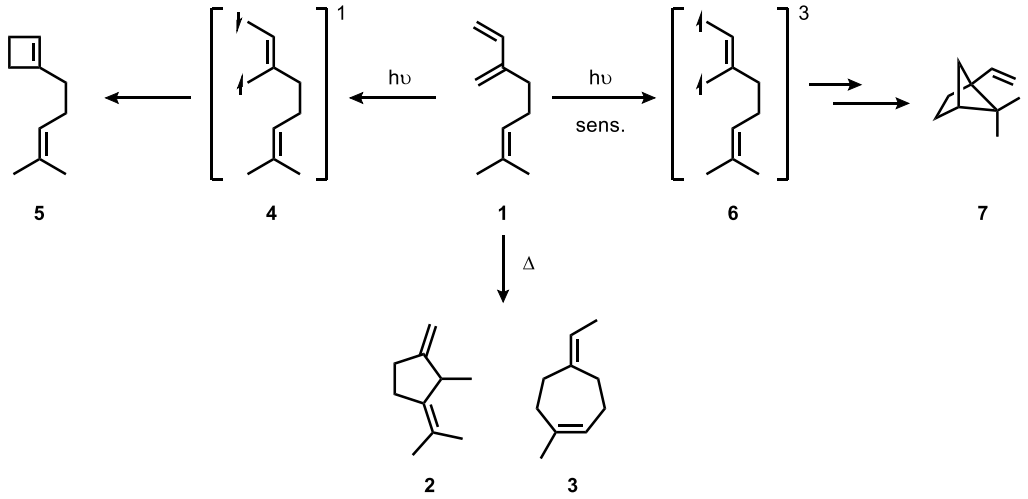
1. Instrumentation, methods and materials ..... 102

2. General synthetic procedures..... 104
3. Characterization of compounds..... 105
4. Large Scale Synthesis of compound 179..... 132
5. Stern-Volmer Quenching..... 132
6. Square wave voltammetry..... 133
7. General Computational Methods..... 133
9. Thermochemical Data..... 138
10. TD-DFT results..... 145
11. X-Ray Crystallography..... 156
**References..... 158**

# Chapter 1: Introduction to excited state chemistry

## 1.1 Elements of photochemistry

Photochemistry and photophysical processes are fundamental physical phenomena that form the basis of life on Earth. Light from the Sun provides the energy source required to sustain life *via* complex chemical processes referred collectively as photosynthesis, but also numerous other metabolic and sensory processes such as vision and hormone synthesis. The study of interactions between matter and electromagnetic radiation and the resulting changes that ensue fall within the field of study of photochemistry.[1]




***Scheme 1****: Chemical behaviour of b-myrcene on the S0, S1 and T1 potential energy surface*

Although the absorption of light by matter can be viewed as an alternative source of energy, in reality, it is much more than that, as the excitation of molecules fundamentally alters their electronic nature.[2] This results in being able to access new chemical pathways *via* different potential energy surfaces and is best illustrated by the chemical behaviour of β-myrcene **1** (***Scheme 1)***, which is a room temperature stable natural product. Upon providing energy from three different sources, thermally and photochemically (by direct irradiation or sensitization), different distributions of products can be observed. Flash vacuum pyrolysis of **1** leads to a mixture of products **2** and **3** *via* the $S_0$ potential energy surface. On the other hand, direct

irradiation with UV-light leads to the population of the $S_1$ state **4**, which in turn facilitates the selective formation of cyclobutene derivate **5**. Alternatively, population of the $T_1$ state **6** *via* sensitization, leads to the isolation of polycyclic derivative **7** as the sole reaction product.[3]

Although molecules can interact with electromagnetic radiation spanning a wide range of wavelengths, absorption of high energy visible and ultraviolet light are associated chemical with changes.[1-2] As most organic molecules possess singlet multiplicity in the ground state, absorption of a high energy photon leads to the population of an excited singlet state $S_n$ of a particular vibrational state.

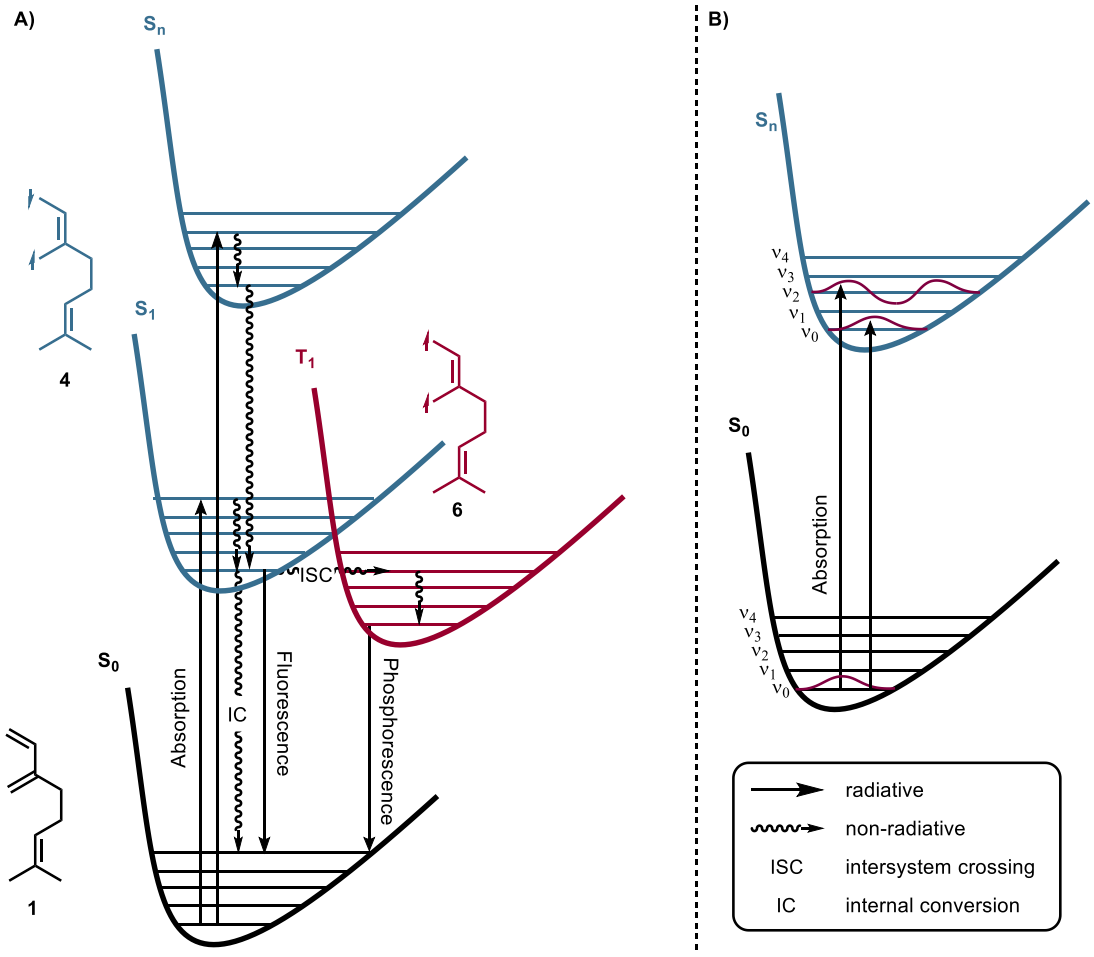



***Figure 1**: A) Jablonski diagram illustrating general photochemical processes; B) Jablonski diagram showcasing wavefunction overlap between ground state vibrational level and different excited state vibrational levels*

The efficiency of the absorption process is proportional to the overlap between the wavefunction of the initial and final vibrational states. Due to the large mass difference

between electrons and nuclei, electronic and nuclear motion happen on different timescales, with electrons moving much faster than the nuclei. As such electronic transitions take place faster than nuclear rearrangement, process that can be visualised as a "vertical"-transition on a potential energy diagram (**Figure 1**, **B**). Under this vertical transition requirement, a change in electronic transitions may also happen concurrently with a change in vibrational level. As such, the *Frank-Condon principle* states that the intensity of this resulting vibronic transition will be proportional to the square of the overlap integral of two vibrational wavefunction of the two states at the same nuclear coordinates.[1-2, 4]

Once in the excited sate, molecules undergo rapid relaxation to lower energy states. This can be achieved non-radiatively by vibrational relaxation through energy exchange with the surrounding environment. An additional non-radiatively relaxation mechanism internal conversion (IC) to a lower electronic state with the same spin multiplicity. These processes are generally exceedingly fast, with rates generally higher than $10^{-12}\ s^{-1}$, and forms the basis of *Kasha's rule*, which stipulates that higher-level $S_n$ (n>1) excited states undergo preferential relaxation to the lowest vibrational level of the $S_1$ state. [1-2, 5-6] Once in the $S_1$ state, molecules can than proceed to react or relax back to the ground state either by internal conversion or by the emission of a photon, in a process known as fluorescence.

An alternative relaxation pathway is intersystem crossing (ISC) into lower energy triplet states such as $T_1$.[5-6] Generally, triplet states are lower in energy than their corresponding singlet states due to additional stabilisation arising from electron exchange correlation energies (*Hund's rules*).[2] However, crossing of states from a singlet to a triplet is a forbidden process as it violates conservation of spin selection rules, or more specifically, conservation of angular momentum. Therefore, processes that involve a change of spin are slow. However, the magnetic moment of an electrons spin can couple with the orbital angular momentum. As such, the change in electron angular momentum associated with the spin state can be relieved

by a change in orbital angular momentum such that the total angular momentum of the system is conserved.[2, 7] Under the effect of spin-orbit coupling, intersystem crossing is allowed through the mixing of the singlet and triplet wavefunctions. Using 1st order perturbation theory, the perturbed $\widetilde{T_1}$ state can be described according to equation [**EQ1**]:

$$\widetilde{T_1} = T_1 + \sum_n \delta_n S_n \qquad [\boldsymbol{EQ1}]$$

where $T_1$ is the unperturbed triplet wavefunction, $S_n$ is the n[th] singlet wavefunction and $\delta_n$ is the admixture coefficient.[7] The admixture coefficient term can be further expanded according to equation [**EQ2**]:

$$\delta_n = \frac{\langle T_1 | \widehat{H_{SO}} | S_n \rangle}{E(T_1) - E(S_n)} \qquad [\mathbf{EQ2}]$$

where $\widehat{H_{SO}}$ is the spin orbit operator, and $E(T_1)$ and $E(S_n)$ are the energies or the $T_1$ and $S_n$ states, respectively.[7] According to [**EQ2**], the degree of mixing between the two states and consequently the rate of intersystem crossing, will increase with an increase of the $\langle T_1 | \widehat{H_{SO}} | S_n \rangle$ integral or by a decrease in the energy gap between the two states.[7]

Upon intersystem crossing, molecules in the triplet state are also capable of undergoing chemical transformation, or relaxation back to the ground state. Like the $S_1$ state, $T_1$ relaxation can happen radiationlessly *via* intersystem crossing or *via* a slow photon emission known as phosphorescence. In both cases, the processes are formally spin forbidden therefore slow.

## 1.2 Excited state properties

As excitation of molecules fundamentally alters the electronic makeup of the system, it leads to the generation of new species with unique chemical properties. Taking ethene (**8**) as an example (***Figure 2***), excitation to the first triplet state $T_1$ (**9**) involves moving an electron from a bonding π orbital to a non-bonding π* orbital (i.e. a ππ* state). This has the overall effect of

breaking the alkene π bond, thus leading to the lengthening of the central C–C bond. To further minimise internal electronic repulsions, the resulting two radicals occupying p-orbitals twist 90º across the central C–C axis, leading to an overall drastic departure from ground state geometry.[8] This change in electronic structure also leads to overall changes in chemical properties such as chemical reactivity, dipole moments, reduction, and oxidation potentials.[2]

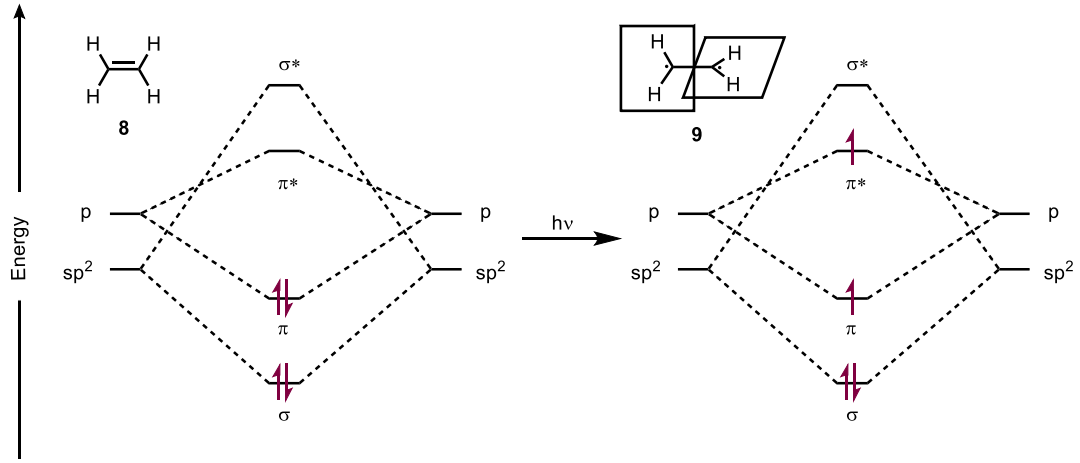



***Figure 2****: MO diagram of the central C=C bond of ethene*

This orthogonal geometry of excited state alkenes provides the basis of excited state alkene isomerization. Like ethene, the excitation of *trans-β*-methylstyrene **10** to either its $T_1$ or $S_1$ state leads to the 90º dihedral structure **11**. Vertical relation back to the ground state (Frank-Condon principle)[9-11], leads to the transition state structure **11** that connects the *trans* isomer **10** to the *cis* isomer **12**. This 90º intermediate has an effectively equal probability of relaxing to either of the two isomers. As such, by selectively exciting one of the two isomers (either by direct irradiation or sensitization), enrichment of the opposite diastereoisomer occurs over time (***Figure 3***).[12-13] This process has thus been exploited as a synthetic tool, but also as a signalling mechanism in molecular switches.[14]

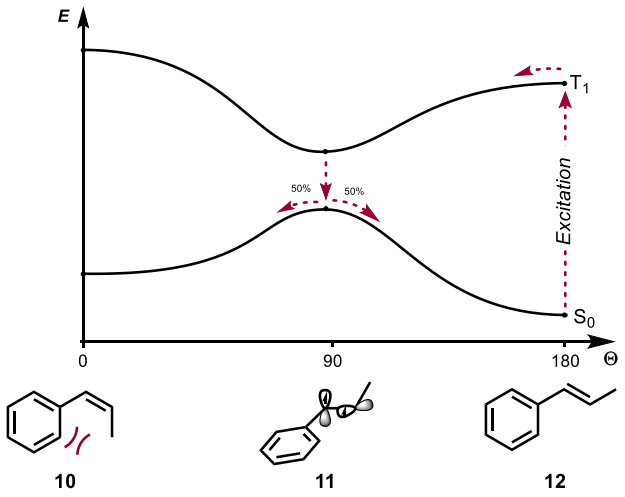



***Figure 3**: Excited and ground state potential energy surfaces of stilbene*

## 1.3 Excited state lifetime

Contrary to most ground state molecules, excited state species only exist for relatively short periods of time. As excited state molecules rapidly decay to the ground state *via* unimolecular radiative and non-radiative processes, the lifetime of the system ($\tau$) is inversely proportional to the 1$^{st}$ order rate constant of de-excitation.[2] Depending on the nature of the system, the excited state lifetime can vary from picosecond up to tens of second. The value of the lifetime can play a significant role in determining reaction outcome, especially for bimolecular processes.

Excited states that possess different multiplicity than their corresponding grounds state are usually long lived, as the relaxation mechanism *via* emission of a photon is spin forbidden. Such examples include most $T_1$ excited state organic molecules which normally possess singlet grounds state multiplicity. However, even in the case of spin-forbidden transitions, substantial variation in lifetimes exist (***Figure 4***). For example, 4-methoxy-styrene **13** displays a triplet lifetime of 22±1 ns. By increasing the degree of substitution, a substantial increase in triplet lifetime can be observed, as exemplified by tetrasubstituted derivative **17**, which possesses a triplet lifetime of 91±1 ns. A possible explanation for this phenomenon has been associated with the degree of torsional excursion between the orthogonal orientation of the

triplet minimum and planar geometry of the ground state. A drastic increase in lifetime is observed when the alkene is bound to a ring system, with 1-(4-methoxyphenyl)cyclopentene **18** displaying over 1000-fold increase in lifetime compared to that of the parent molecule **13**. However, further increase in ring size does not display such drastic effects, with the 7-membered ring analogue **20** displaying similar lifetimes to that of the acyclic-1,2-disubstituted analogue **15**.[15]

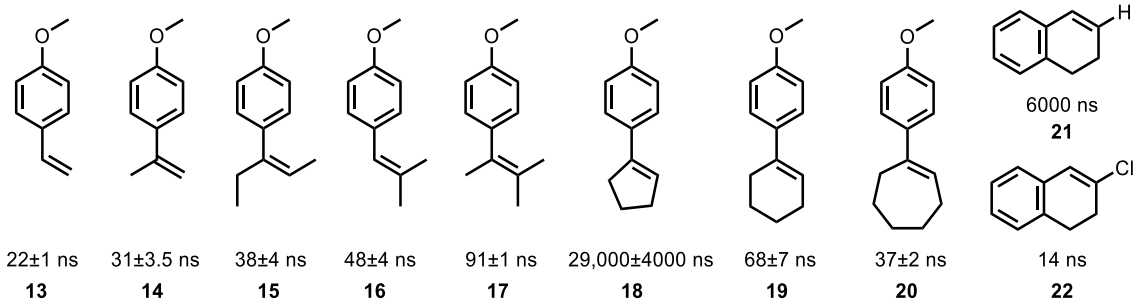



***Figure 4**: $T_1$ state lifetimes of styrenes[15-16]*

As previously mentioned thermal deactivation *via* intersystem crossing is highly dependent on spin-orbit coupling constants.[17] Studies from Rowland and Salem have shown that 1,2-birradiaclas, spin-orbit coupling interactions are maximised when the $p_z$ atomic orbitals of the vicinal radicals are non-parallel.[18] By incorporating the alkene in a ring system, strain prevents perpendicularity in the $T_1$ state. This leads to partial overlap between the p-orbitals of the triplet biradical, which is expected to minimise spin-orbit coupling interactions and consequently increase the triplet lifetime of cyclic alkenes. In the case of cyclopentene derivative **18**, strain induced by the ring system leads to an almost planar geometry in the triplet state.[15] An increase in carbocyclic rings size enable greater degrees of twisting along the 1,2-birradiaclas C-C axis, alleviating some of the overlap between the $p_z$ orbitals and consequently decreasing their excited state lifetimes.[15] As such, large ring systems such as cycloheptane derivate **20** possesses a similar triplet lifetime to its acyclic alkene analogue **15**. This strategy of binding alkenes and imines in small ring systems has been exploited as a means of improving the efficiency of bimolecular photochemical transformations.[17, 19]

Other structural influences include degrees of delocalization and presence of polar substituents and the degree of ionic character of the corresponding singlet wavefunction.[15, 17, 20] An important structural feature worth noting that can substantially affect lifetime, is the presence of heavy atoms. For a hydrogen-like atom, it is known that spin-orbit coupling is directly proportional to the fourth power of the nuclear atomic number ($H_{SO} \sim Z^4$). Due to this strong dependence of spin-orbit coupling on atomic number, incorporation of large atoms can be detrimental to the excited state lifetime. Therefore, groups such as Cl, Br and I are capable of substantially increasing the spin-orbit coupling between the triplet and singlet states. For example, 1,2-dihydronaphthalene **21** possesses a relatively large lifetime of 6000 ns in the triplet state. Upon addition of a chlorine atom at the 3-position (**22**) a drastic lowering of triplet lifetime to 14 ns occurs (***Figure 4***). It is important to note that the heavy atom effect is conformationally dependent and highly regiospecific, with the greatest effects being noticeable when the heavy atom is placed at positions where the excited state radicals have the highest probability densities.[16]

## 1.4 Energy transfer catalysis

As previously mentioned, relaxation of excited triplet state molecules back to the ground $S_0$ state by emission of a photon is a slow process, as it is spin forbidden. Conversely, direct excitation of singlet ground state molecules to excited triplet states is also not allowed. As such, access to the triplet state relies heavily on intersystem crossing events. For systems that do not possess high spin orbit coupling constant between the $S_1$ and $T_1$ states, the efficiency of intersystem crossing can small when compared to spin allowed processes such as internal conversion, intersystem crossing, and chemical transformations on the $S_1$ surface.

An alternative approach to accessing the triplet state of molecules is through a process known as triplet energy transfer.[21] By exciting a sensitiser molecule with high absorption coefficients and high quantum yields for intersystem crossing into the triplet state, transfer of spin state

can occur indirectly to an acceptor molecule. This process can happen *via* two mechanisms: coulombic-interaction or electron exchange.[22-23] The latter, also known as *Dexter energy transfer*, is the most common sensitization process in energy transfer catalysis. Fundamentally, Dexter energy transfer can be viewed as a concurrent donation of an electron from the SOMO2 orbital of the excited state donor, to the LUMO of the ground state acceptor and donation of an electron from the HOMO of the acceptor to the SOMO1 orbital of the donor (***Figure 5***). As such, the overall spin of the system is conserved. In general, for an efficient energy transfer process, the triplet energy of the sensitizer must be higher than that of the acceptor (exergonic energy transfer) (***Figure 6***).[23]

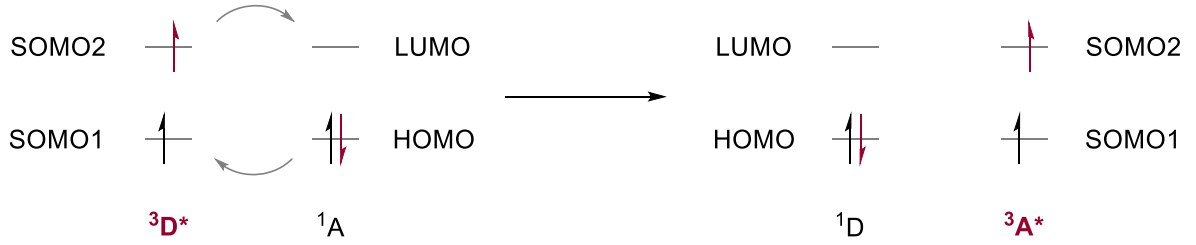



***Figure 5****: Graphical representation of Dexter energy transfer mechanism*

Direct irradiation of organic molecules that are not heavily conjugated may also require photons of very high energy. These conditions can be very harsh and potentially hazardous to operate. Furthermore, they may also lead to the degradation of either the starting materials or products, thus lowering reaction yields. The addition of sensitizers molecule to the chemical reaction that possesses an absorbing state (e.g. **S1**) lower than that of the acceptor molecule can enable access of the triplet state of the desired substrate, while also necessitating photons of lower energies that those required to directly excite the substrate (***Figure 6***).[21] As such, over the same photochemical outcome is achieved, while using photons of lower energy, making the process more efficient.

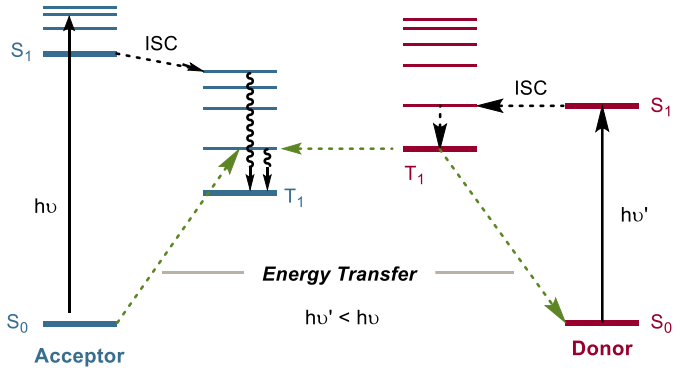



***Figure 6**: Jablonski diagram showcasing the mechanism of accessing the triplet sate of a molecule via direct irradiation and via sensitization. Due to the lower energy S1 state of the Donor, sensitization requires a photon of lower energy then the alternative mechanism of excitation by direct absorption of the Acceptor molecule*

Besides improved rates of triplet state population for substrates that do not possess efficient mechanisms of intersystem crossing, energy transfer does offer other advantages. For example, if alternative excited state reactivity from the $S_1$ state is competitive, mixtures containing undesired reaction by-products can be obtained, leading to lower yields and isolation issues (***Figure 7***). Irradiation of azo-compound **23** leads to a mixture of three hydrocarbons, bicyclo[2.2.2]octa-2,5-diene **24**, semibullvalene **25**, and cyclooctatetraene **26**, in a 24:73:3 ratio. Conversely, the addition of a sensitizer leads to the formation of semibullvalene **25** as the sole reaction product.[24]

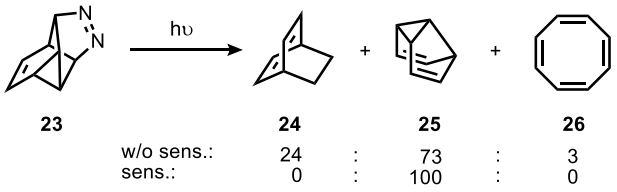



***Figure 7**: Product distribution upon irradiation of **23** in the absence and presence of a sensitizer*

Ketones are common photosensitizers employed for energy transfer, either as solvent (e.g. acetone) or catalysts (e.g. benzophenone **27**), in conjunction with UV-irradiation. Recent developments in organic light-emitting diodes have led to discoveries of novel organometallic complexes with adequate photophysical properties for visible-light photocatalysis. One of the most popular class of organometallic complexes employed in photocatalysis are based around cyclometalated iridium(III) complex such as **28**. Although these complexes have been extensively employed in photo-redox catalysis,[25] they have also found recent applications in

energy transfer catalysis.[21] Their high excitation coefficient in the visible range, high triplet energy, efficiency of intersystem crossing to the triplet state due to the heavy atom effect exhibited by iridium, as well as high chemical stability, make them ideal catalysts for visible light energy transfer.[26-27] Due to the diffuse nature and of the 5d orbitals on iridium and strong octahedral field exhibited by the phenyl-pyridine ligands, octahedral iridium(III) complexes exhibit large crystal field splitting.[28] Coupled with the strong π-accepting capabilities of phenyl-pyridine and bipyridine ligands, the lowest energy excited state can be described as a transition from the highest occupied molecular orbitals that possess metal character, to the lowest energy unoccupied orbitals that possess ligand character (*i.e.* a metal to ligand charge transfer state) (***Figure 8B***). Due to this high ligand character of the excited sate, the emission properties of these complexes are highly tuneable. As such, by functionalizing the ligands in order to increase their π-accepting capabilities (*e.g.* by adding electron withdrawing group such as fluorine and trifluoromethyl), complexes of higher triplet energies can be synthesised.[28] However, changes in ligand architecture can have unforeseen changes in their σ and π-donor capabilities of the ligand. As such, quantitative predictions of excited state energies are difficult, and constructions of models that are capable of accurately predicting excited state properties of iridium complex is an ongoing field of research of high interest.[29]

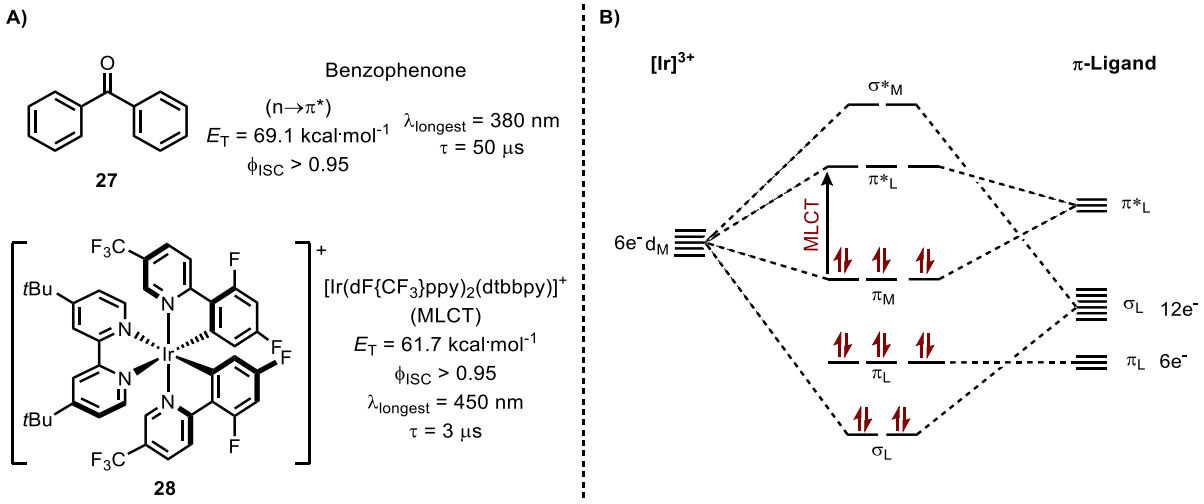



***Figure 8****: A) structures and properties of two commonly employed sensitizers[26]; B) simplified MO-diagram of an octahedral iridium complex; correlations with empty s and p orbitals on iridium are omitted for clarity*

Besides improvements in energy efficiency and increased user safety, the use of visible light instead of harsh UV-light can lead to improved chemical transformations. For example, as most organic functional groups display absorption in the UV, non-participating functional groups in the desired transformation can absorb UV-irradiation instead, leading to undesired side-reactivity and thus subsequent decomposition of both starting materials and products.[21] As such, the use of visible light energy transfer catalysis as an alternative synthetic methodology to direct UV-light irradiation may lead to improved reaction yields and increased functional group tolerance. Overall, these novel complexes have led to a renaissance in energy transfer catalysis, entailing the reinvestigation of older UV-mediated processes, as well as the discovery of novel transformations, with the aid of visible light.

## 1.5 Stern-Volmer quenching

An important experiment used in mechanistic studies of catalysed photochemical processes involves measurement of change in fluorescence/phosphorescence intensity of the photocatalyst in presence of various quencher molecules. This experiment in referred to as Stern-Volmer quenching, and the relationship between the emission intensity and quencher concentration is described by the Stern-Volmer equation:

$$\frac{I^0}{I} = 1 + \tau^0 k_q [Q] \qquad [\boldsymbol{EQ3}]$$

$$\frac{d\left(\frac{I^0}{I}\right)}{d[Q]} = \tau^0 k_q = k_{SV} \qquad [\boldsymbol{EQ4}]$$

where $I^0$ is the emission intensity in the absence of a quencher, $I$ is the emission intensity in the presence of a quencher of set concentration, $\tau^0$ is the lifetime of the photocatalyst in the absence of the quencher, $k_q$ is the quenching rate constant and $[Q]$ represent the quencher concentration.[1] By plotting the emission intensity ratio ($I^0/I$) as a function of quencher

concentration $[Q]$, a linear plot with the slope equal to $\tau^0 k_q$, product also known as the Stern-Volmer constant $k_{SV}$. As such, by measuring the Stern-Volmer quenching constant $k_{SV}$ for each component present a photochemical reaction mixture, we can estimate which chemical species will most likely interact with the catalyst. However, although this experiment does provide kinetic information regarding quenching, no information can be extract with regards to the nature of the quenching process.

## 1.6 Baldwin's rules

Due to short lifetimes associated with excited state transformations, quite often photochemical reactions undergo intramolecularly, leading to the formation of complex polycyclic systems. When studying cyclization reactions, one cannot avoid mentioning Baldwin's rules.[30] In his seminal paper in 1976, Baldwin disclosed a set of empirically derived rules that summarise the relative rates of different types of cyclization, as well as the terminology required to discuss cyclization reactions. The classification of cyclizations is based upon three parameters: a) the size of the resulting ring system; b) position of the bond cleaved during cyclization, with external bonds being labelled as "*exo*" and internal bonds as "*endo*"; and c) the hybridization of the atom attacked, which are labelled as "tet", "trig" and "dig" for $sp^3$, $sp^2$ and sp hybridizations, respective (***Figure 9***). Based on proposed stereochemical requirements of transition states for various class of ring-closures, as well as strong empirical evidence, Baldwin disclosed a set of guidelines for the prediction of favoured and disfavoured cyclization processes, which have been summarised in ***Table 1***.[30] With subsequent developments and reinvestigations, exceptions and revisions to Baldwin's original rules have been identified.[31] However, for the purpose of this Thesis, of importance is the nomenclature developed by Baldwin, as it enables up to clearly summarise what happens during the course of a set transformation, while also providing us a point of comparison between different cyclizations.

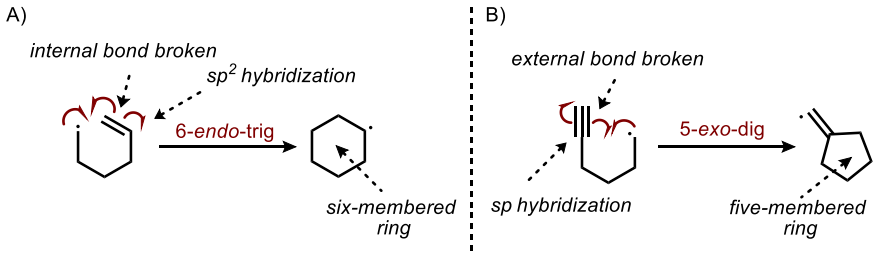



***Figure 9**: Diagram showcasing Baldwin's classification for: A) a 6-endo-trig radical cyclization; B) a 5-exo-trig radical cyclization*

| Ring Size | | 3 | 4 | 5 | 6 | 7 |
|---|---|---|---|---|---|---|
| ***endo*** | **tet** | N/A | N/A | | | |
| | **trig** | | | | | |
| | **dig** | | | | | |
| ***exo*** | **tet** | | | | | |
| | **trig** | | | | | |
| | **dig** | | | | | |

***Table 1**: Summary of Baldwin's rules as proposed in 1976; green boxes denote favoured cyclizations, while red boxes denote disfavoured cyclizations.[30]*

## 1.7 Computational methods and triplet state chemistry

One of the most popular method used for the computational investigation of chemical reactions is density functional theory (DFT). DFT is based on the Hohenberg-Kohn theorem, which states the properties of a system are contained within its ground state electron density and can be expressed by a unique functional of the electron density.[32] Although the theorem proves the existence of such a functional, no additional information can be derived regarding the nature of this functional. Later on, Kohn and Sham introduced the idea that the electron density of a system can be instead expressed by an equivalent fictitious system constructed non-interaction electrons with the same density.[33] As such, under the Kohn-Sham formalism, the ground state energy $E[\rho(r)]$ can be expressed as follows:

$$E[\rho(r)] = T_{ni}[\rho(r)] + V_{ne}[\rho(r)] + V_{ee}[\rho(r)] + V_{xc}[\rho(r)] \qquad [\boldsymbol{EQ5}]$$

where $T_{ni}[\rho(r)]$ is the kinetic energy of non-interacting electrons, $V_{ne}[\rho(r)]$ is the electron-nuclear Coulomb interactions, $V_{ee}[\rho(r)]$ is the electron-electron Coulomb repulsion, and $V_{xc}[\rho(r)]$ is the exchange correlation potential, which also encapsulates corrections associated

with the difference between the kinetic energy of the non-interacting electrons and that of the real system. Under this form, exact solutions are available for all terms expect the exchange correlation potential, $V_{xc}[\rho(r)]$. As the exact nature of the $V_{xc}[\rho(r)]$ remains unknown, numerous density functional approximations (DFAs) have been developed in order to account for exchange correlation interactions. Such approximations include the local density approximation (LDA), which treats the electron-electron interactions based exclusively on the electron density at a particular point in space, the generalized gradient approximation (GGA), which includes dependencies on the gradient of the electron density and the meta-generalized gradient approximation (meta-GGA) which also includes the 2$^{nd}$ derivative of the electron density. Additional improvements have been obtained through the development of hybrid functionals with the inclusion of a proportion exact Hartree-Fock exchange in the estimation of exchange correlations, as well as hybrid range-separated functionals, which treat the percentage of exact Hartree-Fock exchange as a function of distance.[34]

Throughout this work, the M06-2X hybrid-meta-GGA functional has been used in DFT calculations.[35] The Minnesota family of functions, of which M06-2X belongs to, were derived by empirical parameterization against large datasets, while also being constrained to the uniform-electron-gas limit and the absence of absence of self-correlation energy. The M06-2X functional possesses 32 paraments fitted to 314 experimental data points and twice the amount of HF exchange (54%) than the parent functional M06. Out the 06' generation of Minnesota functionals, M06-2X displays the best performance when predicting main group thermochemistry, reaction kinetics and non-covalent interactions.[35] Further benchmarking studies have shown that it compares favourably against other hybrid functionals being one of the best performers,[36] while also performing well in the description of radicals,[37-38] thus making it a good candidate to describe triplet state reactivity.

As most DFT functionals fail to reproduce the $1/R^6$ distance dependence of long-range London dispersion, which can cause inaccuracies in thermochemical calculations, corrections factors have been developed. One such correction factor that has been employed in this work, is Grimme's D3 dispersion.[39] The atom pair dispersion energy correction can be expressed according to equation [**EQ6**]:

$$E_{disp} = \sum_{A \neq B} \sum_{n=6,8} s_n \frac{C_n^{AB}}{R_{AB}^n} f_{damp,n}(R_{AB}) \qquad [\boldsymbol{EQ6}]$$

where $C_n^{AB}$ is the averaged n$^{th}$ dispersion term, $R_{AB}$ is the internuclear distance, $s_n$ is the n$^{th}$ order scaling factor, and $f_{damp,n}$ is the Head-Gordon damping function.[39] Benchmarking studies have shown that including of long-range dispersion correction factors can improve accuracy of thermochemical calculations, reaction kinetics and description of non-covalent interactions at minimal additional computational cost.[36, 40]

In recent years, DFT has also seen increased use in the study of triplet state photochemical transformations, especially in the determination of excited state triplet energy.[21] Experimentally, the determination of triplet energy can be achieved spectroscopically from the highest energy band of the phosphorescence spectrum. In practice obtaining a good phosphoresce spectrum can be difficult due to low emission intensities associated with thermal deactivation of the triplet state, as well as poor special resolution of the phosphorescence bands. As such, determination of triplet energy often requires access to specialised equipment capable of recording data at cryogenic conditions. Due to these constraints, DFT has risen as an alternative for the prediction of triplet energies, with hybrid functionals such as B3LYP[41-44] and M06-2X,[35] in conjunction with triple-ζ basis, being able to reliably describe triplet energies for molecules composed of main-group elements.[21] Although, most often DFT has been used as a post rationalization method to provide evidence for or against energy transfer

mechanisms, recent studies how also showcased the power of DFT as a predictive tool in the design of substrates that possess low triplet energies for applications in visible light energy transfer reaction development.[45]

One of the major challenges associated with excited state calculations, which require calculations to be performed under unrestricted formalism, is spin contamination. Spin contamination arises from mixing of wave functions of the desired spin state with the wavefunction of other spin states.[46] In cases where high amounts of spin contamination are present, large errors can be introduced, leading to poor estimations of geometries and reaction energetics. Multireference methods such as CASSCF,[47] CASPT2[48-49] and NEVPT2[50] provide a solution to such spin contamination issues, however at large increase in computational cost.[51]

Additional complexities associated with the study of exited state reactivity, lies with calculation of excited state dynamics, such as internal conversion and intersystem crossing rates. Accurate determination of intersystem crossing rates is still an ongoing challenge,[52] with state-of-the-art methodologies employing non-adiabatic “surface hopping" *ab initio* molecular dynamics calculations (*e.g.,* AIMS-CASSCF,[53] AIMS-DFT[54] and SHARC[55]). However, the computational cost of such methods makes it prohibitive for studies involving large systems. A qualitative alternative commonly employed in the study of transformations involving changes in spin multiplicity, is the identification of minimum energy crossing points (MECP). As the name suggests, an MECP is the lowest energy point between two surfaces of different multiplicities. According to equation [**EQ2**], the probability of intersystem crossing is inversely proportional to the difference in energy between the singlet and triplet state. As such, the relative energy of MECPs provide a good qualitative indicator of the likelihood of intersystem crossing.

## 1.8 Aims of this work

As seen up to now, photochemical excitation of organic molecules leads to altered electronic states with substantially different physical and chemical properties to that of their ground state forms. This opens access to unique modes of reactivity that are often difficult to reproduce using traditional thermal methods.

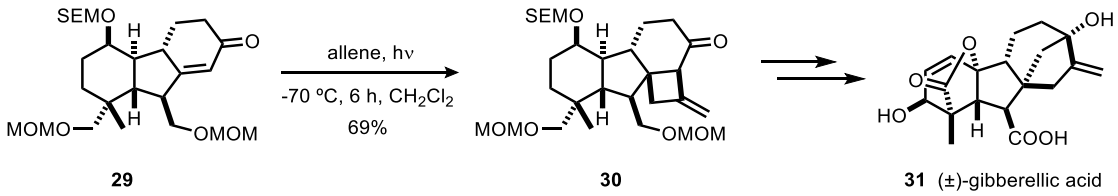
Recent progress in the field of visible light photochemistry has revolutionized the way we approach the development of exited state transformations, facilitating the discovery of energetically more efficient, functional group tolerant, and higher yielding transformations. Improvements in blue LED technology, coupled with the discovery of visible light photocatalysts, have been instrumental to this field by making photochemistry accessible to synthetic organic research groups, without the need of highly specialised UV-reactors.[56] This has substantially bolstered the interest in this field, leading to the discovery of new and exciting chemical transformations.[21, 25] The purpose of this Thesis is to further expand on our understanding of these transformations through the discovery and development of novel modes of chemical reactivity in the excited state. We aim to understand the nature and selectivity of these transformations with the aid of computational and experimental techniques, in hopes of further informing future developments in this field. We have thus identified two novel photochemical transformations, an interrupted [2+2]-cyclization of nitrogen containing heterocycles and a regioselective photoeliminative cyclization. These transformations provide access to pyrrolo[1,2*a*]indoles and tetrasubstituted indolines, two important chemical motifs commonly found in natural products and pharmacologically active compounds.[57-62] The development of these transformations will be discussed in subsequent chapters, in the context of the appropriate literature.

# Chapter 2: Visible-light-mediated heterocycle functionalization *via* geometrically interrupted [2+2] cycloaddition

## 2.1 Introduction

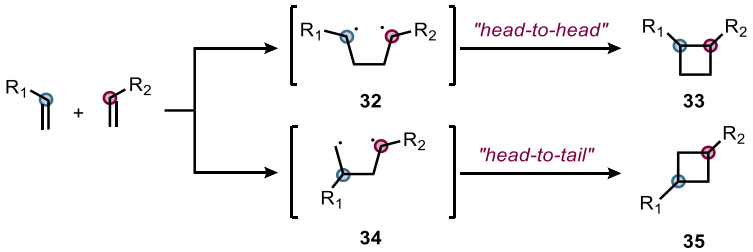
### 2.1.1 Visible light mediated [2+2] cycloadditions

The [2+2] cycloaddition is one of the most studied photochemical processes.[63] The reaction involves taking two π-systems, most commonly alkenes, and generating 4-membered rings in a single step with perfect atom economy. This transformation has been employed in numerous total syntheses, either as a method to construct highly strained molecular systems, or to introduce the 4-membered ring as highly strained reactive intermediates for further functionalization (***Scheme 2***).[64]




***Scheme 2****: Total synthesis of (±)-gibberellic acid*

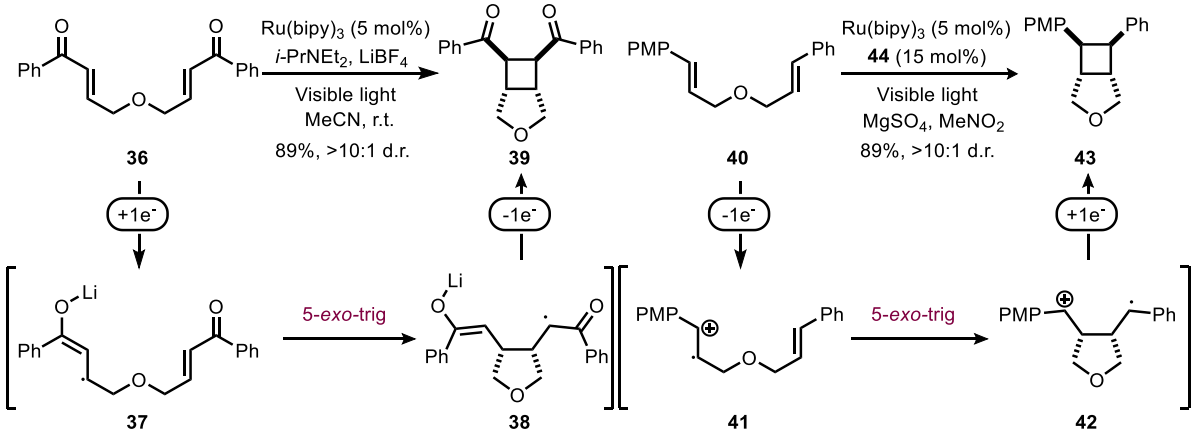
An important aspect of the [2+2] cycloaddition is the regioselectivity of the cyclization when two unsymmetrical alkenes are involved. Two possible products **33** and **35** can be isolated, either from "head-to-head" or "head-to-tail" recombination of diradical intermediates **32** and **34** respectively (***Scheme 3***).[65]




***Scheme 3****: Regioselectivity and nomenclature of [2+2] cycloadditions*

Although this degree of freedom can lead to complex product mixtures, in practice, the regioselectivity of the reaction can be controlled by electronic factors, which lead to the preferential formation of the most stable 1,4-diradical intermediate, and the use of intramolecular tethers.[65]

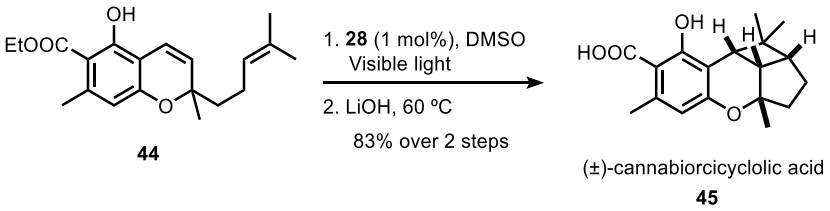
Despite extensive study of the UV-mediated [2+2] cycloaddition, the use of a photocatalyst under visible light under visible light irradiation to complete the same transformation has attracted substantial attention, due to its increased functional group compatibility.[21] The Yoon group employed photoredox catalysis, utilizing a reductive quencher or oxidant (such as tertiary amines or methyl viologen **44**, respectively), to generate oxidised (**41**) or reduced (**37**) alkene species. These undergo 5-*exo*-trig cyclization to their corresponding 1,4-radical-anion (**38**) or 1,4-radical-cation (**42**), which are then then quenched by electron transfer to 1,4-diradicals, followed by recombination to give the desired cyclobutane (***Scheme 4***).[66-67] Although these initially reported cyclizations were solely intramolecular, both intermolecular and asymmetric variants have recently been developed since.[68-69]



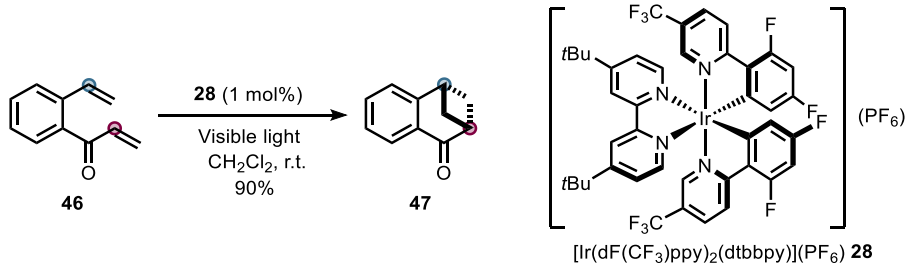

***Scheme 4**: A [2+2] photoredox cycloaddtion via an oxidative or reductive cycle*

As modern dyes can act as both photoredox and energy transfer catalysts, the possibility of visible light energy transfer mediated analogous transformation has also been explored. Pioneering work from the Yoon group has shown that styrenes and dienes possess low energy triplet states that are accessible to iridium-based photosensitizers. Using intramolecular

tethers, a wide range of complex three-dimensional scaffolds were synthesized, including natural products such as (±)-cannabiorcicyclolic acid **45** (***Scheme 5***).[70] Subsequent work by Kwon *et. al.* demonstrated that by controlling the orientation of the carbon tether, head-to-tail type scaffolds such as **47** can also be synthesized in high yield (***Scheme 6***).[71] Notable other developments include visible light catalyzed asymmetric variants, as well as visible light-mediated Paterno-Büchi and aza-Paterno-Büchi transformations, where one of the alkenes is replaced by a carbonyl group or an imine respectively.[19, 72-74]



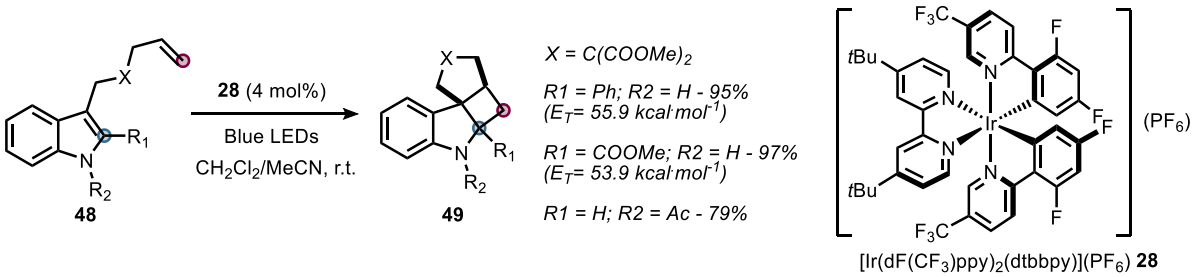

***Scheme 5****: Synthesis of (±)-cannabiorcicyclolic acid using visible light energy transfer catalysis*




***Scheme 6****: Head-to-tail [2+2] photocyclization of styrene **47**.*

In recent years, the [2+2] cycloaddition of heterocycles, in particular indoles, has become a common method for installing structural complexity, with particular interest being drawn towards sensitization of the heterocycle itself, rather than the alkene partner. However, the high triplet energy of the heterocycles and the additional energy required for dearomarization have hindered this area of research. For example, indoles possess a triplet energy of approximately 65 kcal·mol$^{-1}$,[75] which is outside the energy available to iridium based photosensitizers. The You group managed to circumvent this issue by computationally screening indole substitution patterns by lower the triplet energy of the heterocycle. Using DFT at the B3LYP/6-311+G(2d,p)//B3LYP/6-31+G(d,p)[41-44, 76-79] in conjunction with the universal solvation model (SMD)[80-84] for dichloromethane, the authors identified that the

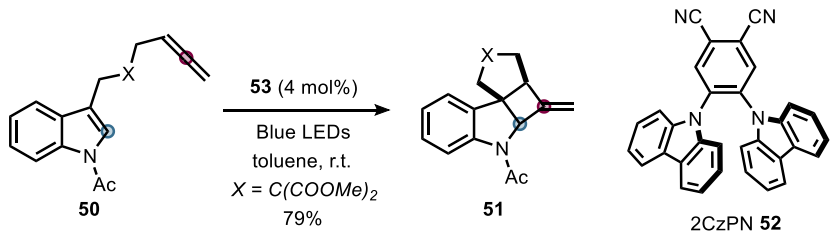
presence of aryl or carbonyl substituent at the C2 position of the indole lowered the triplet energy to 55.9 kcal·mol$^{-1}$ and 53.9 kcal·mol$^{-1}$, respectively. These groups lower the triplet energy of the substrate by stabilising the resulting triplet biradical relative to the ground state energy. In the case of phenyl substituted substrates the radical is stabilised by additional delocalization across the phenyl substituent, while carbonyl groups captodatively stabilise the radical at the C2 position of the indole. These substrates possess triplet energies which are accessible to iridium-based photocatalysts such as **28**, and as such are amenable to sensitization in presence of blue light. By attaching a tether bearing an alkene at the C3 position, the authors were able to synthesize a wide range of complex three-dimensional scaffolds such as **49**. Furthermore, they found that *N*-acylation of the indole also lowered the triplet energy, thus improving the versatility of this transformation (***Scheme 7***).[45] An alternative photoredox mechanistic hypothesis was disproven with the aid of electrochemical measurement, while further evidence towards the proposed energy transfer mechanism was provided by a thorough investigation of the reaction energy profile with the aid of DFT performed at the B3LYP/6-31+G(d,p) level of theory, with the SMD model for dichloromethane .




***Scheme 7**: Visible light [2+2] cycloaddition of C3-tethered indoles*

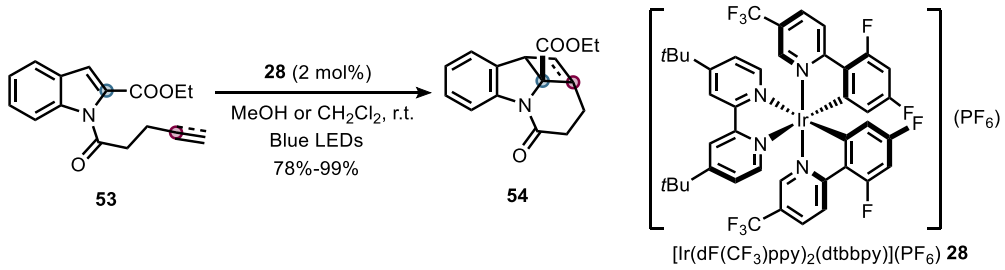
Using a similar scaffold, Rolka and Kening reported the direct [2+2] cycloaddition of indoles with allenes.[85] Although this reaction was previously developed by using UV irradiation,[86] the authors showcased, similar to You *et. al.*,[45] that C2-substituted indoles and *N*-acylated indoles can undergo sensitization using visible light (***Scheme 8***). The organic dye 2CzPN (**52**), was

found to be an effective catalyst, leading to the formation of the exocyclic alkene bearing cyclobutene derivative **51** in 79% yield.

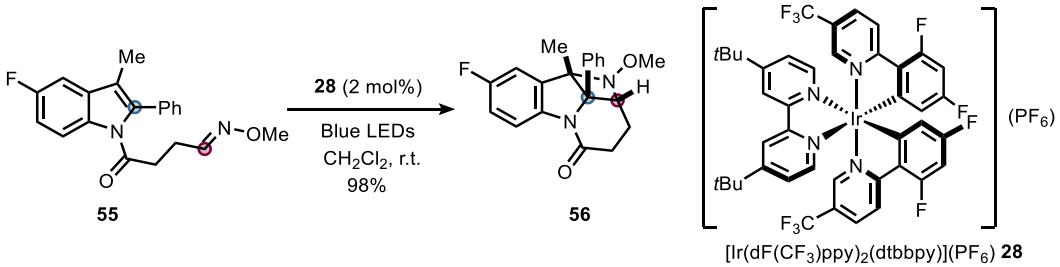



***Scheme 8**: Intramolecular [2+2] cycloaddition of indoles and allenes*

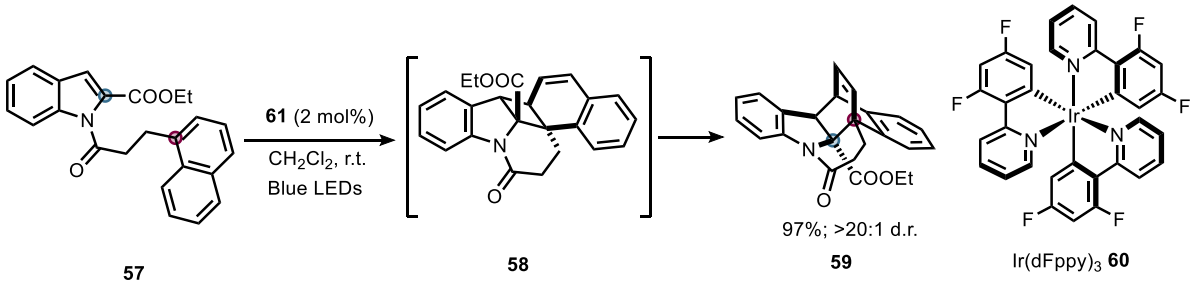
Expanding on their original work, the You group demonstrated that the reactive tether can also be attached to the *N*-acyl substituent, rather than the C3 position for the [2+2] cycloaddition. They found that alkynes are compatible as coupling partners, yielding cyclobutenes (***Scheme 9***),[87] and that oximes (***Scheme 10***)[88] and naphthalenes (***Scheme 11***)[89] are also well tolerated. When using naphthalene tethers, the styrene moiety present in the cyclobutene intermediate **58** is further sensitized, resulting in the isolation of the formal [4+2] cycloaddition adduct **59** in 97% yield. A similar sensitization cascade involving naphthalenes was also reported by Glorius *et. al.*[90]




***Scheme 9**: Intramolecular [2+2] cycloaddition of indoles and alkenes or alkynes via a N-acylated tether*



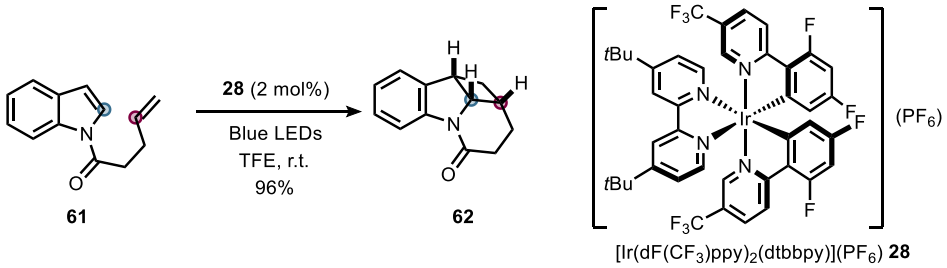

***Scheme 10**: Intramolecular [2+2] cycloaddition of indoles and alkenes or alkynes via a N-acylated tether*




***Scheme 11**: Intramolecular photocycloaddition of indole and naphthalene*

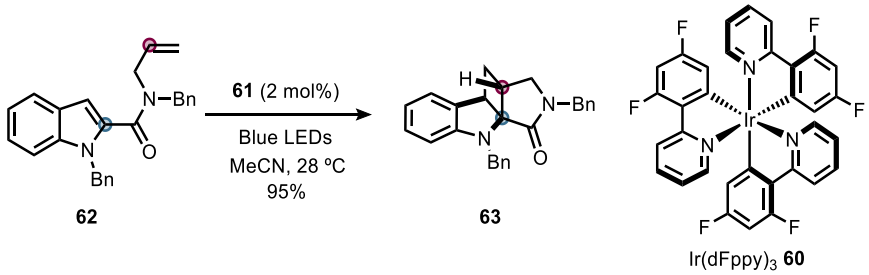
Concurrent with the discoveries from the You group, Fu and co-workers reported that the [2+2]-cycloaddition of indoles *via* an *N*-acylated tether can be performed in the absence of the C2-triplet energy lowering group, through the use of trifluoroethanol (***Scheme 12***). Although the You group demonstrated that *N*-acylated compounds do undergo sensitization in the absence of a C2-triplet lowering substituent, computational work from Fu indicates that the reaction is slightly endothermic when coupled with photocatalyst **28** ($E_T$(**62**) = 62.5 kcal·mol$^{-1}$ vs. $E_T$(**28**) = 60.3 kcal·mol$^{-1}$). It is well established that molecules in the excited possess different physical and chemical properties their corresponding ground states, such as dipole moments. As such, excited state molecules will interact differently with their solvation environment and therefore a change in solvent can influence the energetics of the excited state relative to the corresponding ground state structure.[1] Based on this observation, by using trifluoroethanol as the reaction solvent, the authors suggest that the triplet energy of **61** is lowered within the range of photocatalyst **28**, leading to improved photo-kinetics and overall increased reaction yields.[91] This is substantiated upon with the aid of computational modelling using DFT at the B3LYP/def2-SVP[41-44, 92-93] level of theory, in conjunction with the polarizable continuum model for trifluoroethanol, which shown that the triplet energy of substrate **62** can go down to 58.2 kcal·mol$^{-1}$ when four explicit molecules of trifluoroethanol are involved in hydrogen bonding with the carbonyl group. This interaction is also observed experimentally during $^{13}$C-NMR titration of substrate **61** with trifluoroethanol. The authors also proceed to study the energy profile of the transformation using DFT at the

B3LYP/def2-TZVPP[41-44, 92-93] level of theory in conjunction CPCM solvation model for trifluoroethanol in the absence of explicit solvation molecules, which they use to explain the observed regio- and diastereoselectivity of the [2+2] cycloaddition.

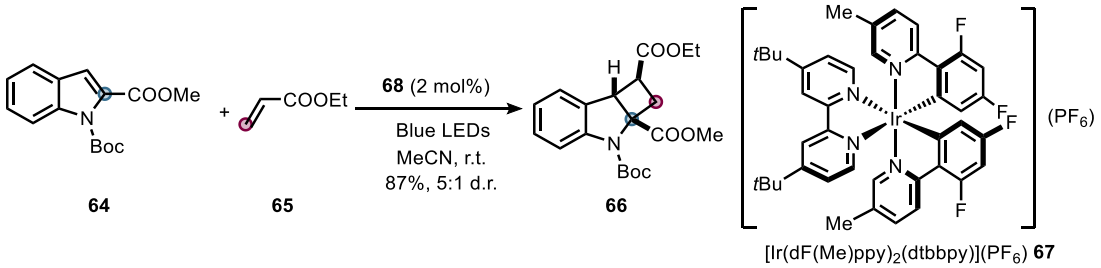



***Scheme 12**: Intramolecular [2+2] cycloaddition via N-acylated tethers in the absence of a C2 substituent*

Following in the footsteps of You *et. al.*, Oderinde and co-workers directly attached the tether onto the triplet energy lowering functional group at the C2 position of the indole. With the aid of DFT calculations performed at the B3LYP/6-311+G(2d,p)//B3LYP/6-31+G(d,p)[41-44, 76-79] with the SMD model for acetonitrile,[80-84] the authors demonstrated that by using the amide as both the tethering and the triplet energy lowering group, exoergic energy transfer can still occur leading to the formation of novel three-dimensional scaffolds such as **63** in excellent yield (***Scheme 13***).[94] Oderinde and co-workers continued their investigation into the [2+2] photocyclization of indoles by developing an intermolecular variant. Using the C2 substituted indole as their starting point, the authors quickly discovered that the presence of an *N*-acyl group such as Boc is essential for a successful transformation. Based on this discovery, the authors continued to investigate the substrate scope and laminations, showcasing that the *N*-Boc indole **64** is compatible with a wide range of alkenes, giving the desired cyclobutanes in good yields with modest diastereoselectivity (***Scheme 14***).[95] Subsequent DFT studies performed at the B3LYP/6-31+G(d,p) level of theory using the SMD continuum model for acetonitrile provide evidence for an energy transfer mechanism, while also corroborating the experimentally observed regio- and diastereoselectivity.

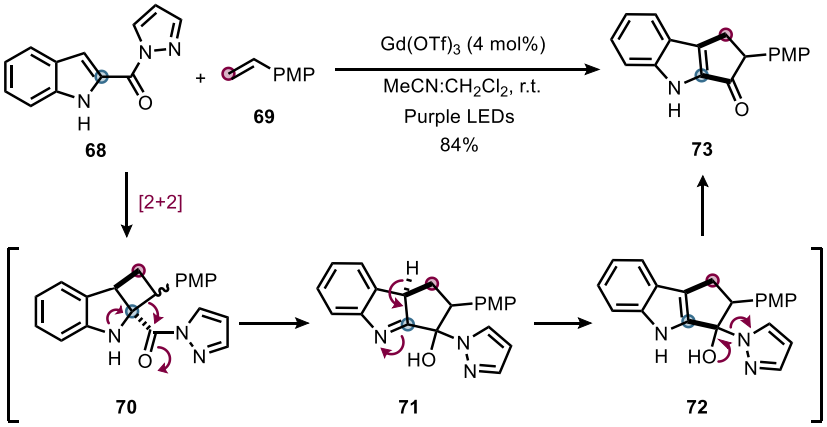



***Scheme 13**: Intramolecular [2+2] cycloaddition of indoles bearing a tether at the C2 position*



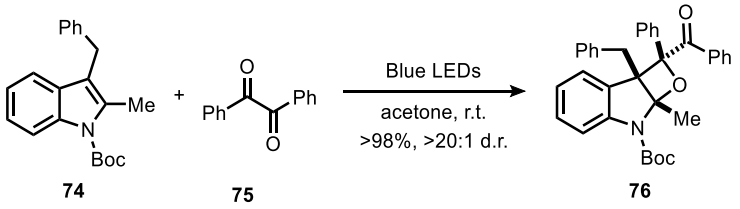

***Scheme 14**: Intermolecular [2+2] cycloaddition of indoles bearing a tether at the C2 position*

Prior to Oderinde's work into intermolecular [2+2] cycloadditions on indoles, Glorius and co-workers disclosed a bimolecular cyclization between C2-substituted indoles bearing an *N*-acyl pyrazole substituent (**68**) and styrenes. Although the reaction resulted in the formation of cyclopenta[*b*]indole derivative **73**, the reaction is hypothesized to proceed *via* the [2+2]-cycloaddition product **70**, which undergoes a semi-pinacol rearrangement to the hemiaminal **72**. Subsequent aromatization and collapse of tetrahedral intermediate **72** gives the cyclopenta[*b*]indole derivative **73** in high yield. Intriguingly, the reaction does not require the presence of a visible light photosensitizer, instead, the addition of $Gd(OTf)_3$ results in a bathochromic shift that facilitates direct absorption in the visible range of the **68**-$Gd(OTf)_3$ Lewis acid complex.[96]




***Scheme 15**: Cascade [2+2] bimolecular cycloaddition between indoles and styrenes, followed by rearrangement*

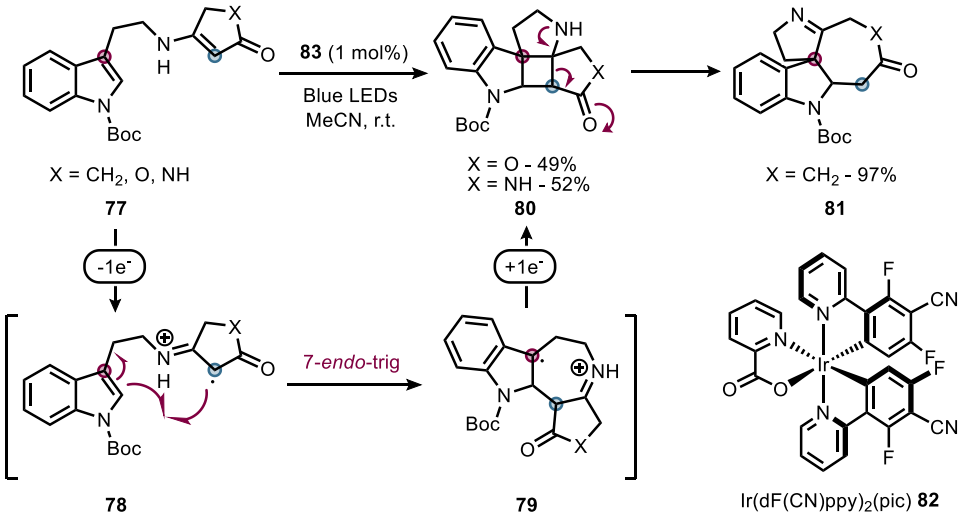
Another photocatalyst-free [2+2]-cycloaddition was reported by Dell'amico *et. al.*, where a Paterno-Büchi photocyclization between indoles and benzophenones occurs in the presence of 405 nm purple LEDs. In this particular transformation, the authors rely on the excitation of benzophenone, which then undergoes the [2+2] cycloaddition in the triplet state. The reaction works well on a wide range of indoles and benzophenones, as well as benzil derivatives (which are capable of absorbing 450 nm photons), leading to the formation of complex oxetanes such as **76** in very high yields in excellent diastereoselectivity (***Scheme 16***).[97]




***Scheme 16**: Cascade [2+2] bimolecular cycloaddition between indoles and styrenes followed by rearrangement*

Taking inspiration from Yoon's seminal work in redox-mediated [2+2]-cycloadditions (***Scheme 4***), Yang and co-workers disclosed an intramolecular cyclization *via* an oxidative catalytic cycle (***Scheme 17***). Using Stern-Volmer quenching studies, the authors show that the photocatalyst **82** is quenched selectively by the enaminone moiety, while electrochemical studies showed that single electron oxidation of the enaminone group is thermochemically viable. Though an energy transfer process can also be hypothesised, studies on model substrates using direct UV-irradiation show no relativity. The authors further study the potential energy surface of the proposed photo-redox pathway using DFT performed at the wB97M-V/def2-QZVP//wB97X-D/def-TZVP[92-93, 98] level of theory, and solvation effects were accounted for at the M05-2X/6-31G(d)[76-79, 99] level of theory using the SMD continuum model for acetonitrile. The authors also estimated the rates of single electron transfer to and from the iridium complex **82** with the aid of Marcus-Hush theory, using computational values obtained at the PBE0/def-TZVP[92-93, 100] level of theory. Similarly, solvation effects were accounted for iridium-complex structures using the M05-2X functional and the def2-TZVP

basis set for the iridium atom and the 6-31G(d) basis set for the remaining atoms in conjunction with the SMD model for acetonitrile. Using this model, the authors obtained an activation energy barrier of 11.9 kcal·mol$^{-1}$, thus providing additional evidence that the photoredox mechanism is also kinetically viable. As such, the authors propose that the oxidation of the enamine **77** to the corresponding radical cation **78** can lead kcal·mol$^{-1}$ *via* a 7-*endo*-trig cyclization to 1,4-radical cation **79**. Subsequent oxidation and radical-radical recombination yields [2+2] cycloaddition product **80**. When the carbonyl substituent is a ketone moiety, a concerted Grob fragmentation occurs, leading to the formation of the natural product like scaffold **81** in an excellent 97% yield.[101]

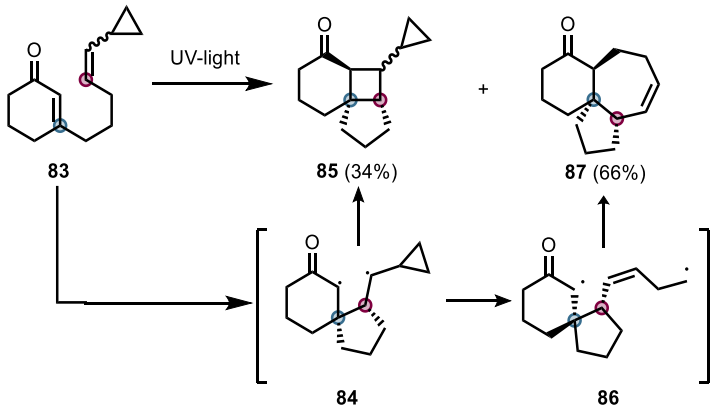



***Scheme 17**: Visible light photoredox mediated [2+2] of indoles and enamines*

### 2.1.2 Interrupted [2+2] cycloadditions

Although the [2+2] cycloaddition is the most ubiquitous processes when thinking about excited state chemistry, occasionally deviations from expected behaviour occur. Even though recombination of 1,4-singlet diradicals is highly facile and results in the formation of exceptionally strained systems, occasionally, alternative competitive pathways become available, leading to unique chemical reactivity. As such, when a resulting 1,4-diradical leads to the formation of other products besides cyclobutane adducts, it could be referred to as an "interrupted"-process.

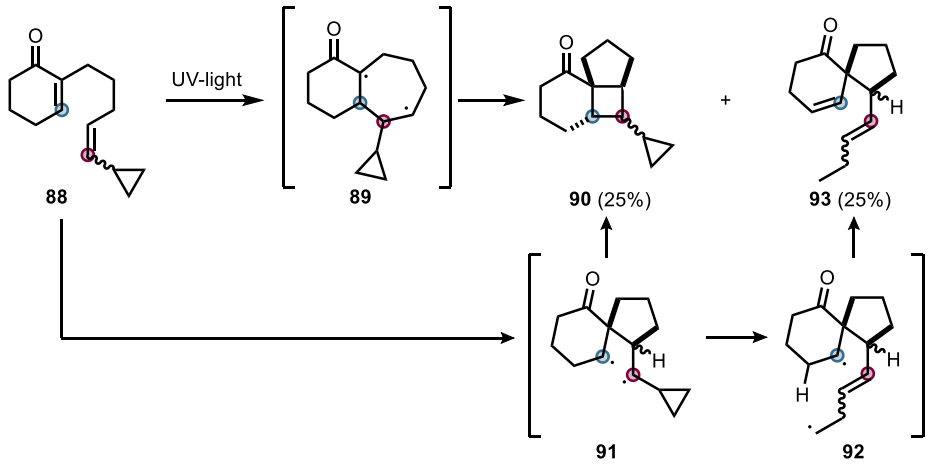
One such example of an interrupted [2+2] process was reported by Becker and co-workers using vinyl cyclopropanes (***Scheme 18***). Initially disclosed in 1989 and further expanded on in 1995, the authors showcased that by tethering a vinyl cyclopropane group to the 3-position of cyclohexanone. Irradiation of **83** leads to a radical addition onto the pendant alkene that can be described as a 5-*exo*-trig cyclization according to Baldwin's classification of ring closures.[30] This process facilitates the formation of 1,4-diradical intermediate **84** which can then undergo a competition between cyclobutene ring closure and cyclopropyl ring opening. Radical recombination leads to the formation of the expected [2+2] product **85** in 34% yield, while cyclopropyl ring opening leads to a hypothetical 1,7-biradical intermediate **86**, which undergoes radical-radical recombination to facilitate the formation of fused tricyclic system **87** as the major product in 66% yield.[102-103]




***Scheme 18:*** *Cycloaddition products of* ***83*** *upon UV-irradiation*

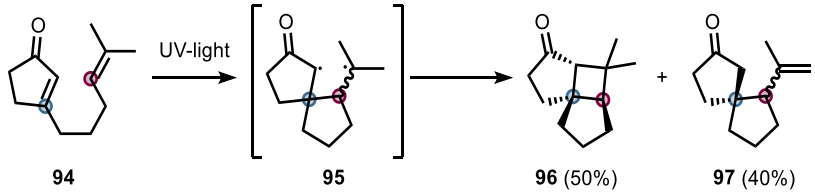
The authors further expanded on this observation in their follow-up paper, by tethering the vinyl cyclopropane to the 2-position of cyclohexanone (***Scheme 19***). In this scenario, upon UV-irradiation of **88**, the resulting diradical can undergo a 7-*endo*-trig cyclization to furnish 1,4-biradical **89**, which can then proceed to generate the [2+2]-cyclization derivative **90** in 25% yield, as a mixture of diastereoisomers. Alternatively, if the initial alkene addition occurs *via* a 5-*exo*-trig pathway to give 1,4-biradical **91**, competition between 1,4-diradical recombination and cyclopropyl ring opening occurs, the latter leading to the generation of

1,7-biradical **92**. Intermediate **92** can then proceed to abstract a hydrogen atom adjacent to the secondary radical in a 1,8-HAT fashion, leading to the formation of spirocyclic diene derivative **93** in a modest 25% yield.[104]




***Scheme 19**: Cycloaddition products of **88** upon UV-irradiation*

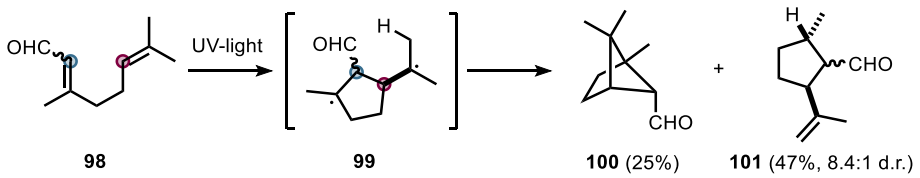
A further example of an interrupted [2+2]-cycloaddition was disclosed by Agosta *et. al.* while studying the [2+2] cycloaddition of 1,6-diene **94** (***Scheme 20***). Upon UV-irradiation, it was found that **94** undergoes a 5-*exo*-trig cyclization that leads to the formation of diradical **95**, which undergoes radical recombination to furnish the head-to-head cyclobutene adduct **96** in 50% yield. Intriguingly, alkene **97** was also isolated in a 40% yield, presumably arising from a 1,5-HAT process.[105]




***Scheme 20**: Cycloaddition products of **94** upon UV-irradiation*

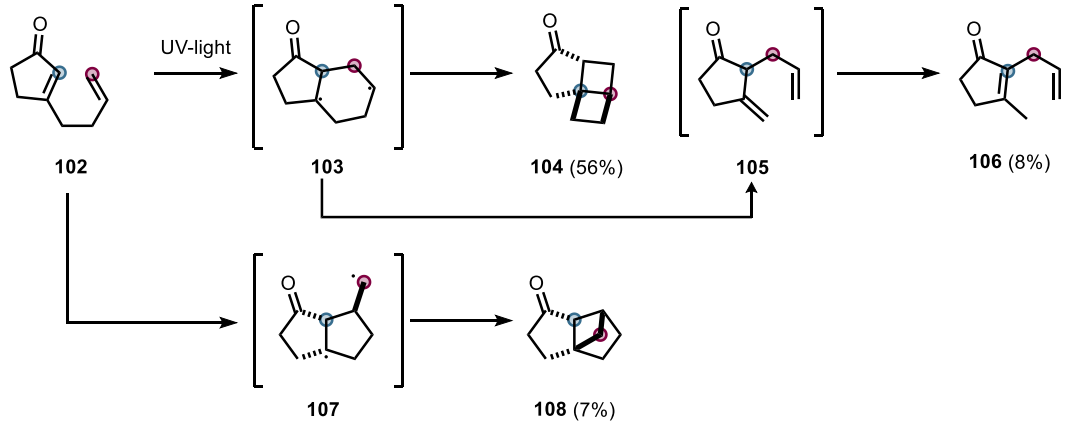
The authors also studied the behaviour of 1,5-dienes (***Scheme 21***). In this seminal work, the authors studied a wide range of substitution patterns and their photochemical behaviour. One interesting example is the cycloaddition of 1,5-diene **98**, where the carbonyl group is not bound in a cyclic system. In this scenario, the reaction proceeds to generate the 1,4-diradical **99** *via* a 5-*exo*-trig pathway, which then furnishes the head-to-tail [2+2] cyclization product

**100**. However, the major product in this reaction is alkene **101** which is generated in 47% yield *via* a 1,5-HAT process.[105]




***Scheme 21**: Cycloaddition products of **98** upon UV-irradiation*

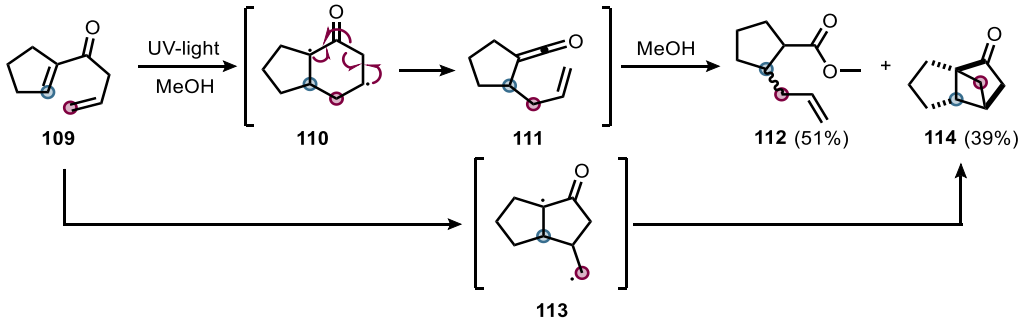
An alternative chemical behaviour was also observed for 1,5-diene **102**, which is very similar to scaffold **94** (***Scheme 22***). UV-irradiation of 1,5-diene **102** leads to the formation of the head-to-head [2+2] cycloaddition product **104** in 56% yield as the major reaction product *via* a 6-*endo*-trig pathway, while the head-to-tail derivative **108,** arising from the 5-*exo*-trig pathway, was only observed in 7% yield. The difference in selectivity can be attributed to the relative stability of the putative 1,4 radicals formed, as 6-*endo*-trig pathway leads to the formation of secondary radical **103**, which is more stable than the primary radical **107** arising from the 5-*exo*-trig pathway. Along with these two products, the 1,4-diene **106** was isolated in a marginal 8% yield. In this case, the formation of the interrupted **106** product was attributed to the fragmentation of 1,4-biradical **103** to yield the 1,5-diene **105**, which tautomerizes to the thermodynamically more stable conjugated enone.[106]




***Scheme 22**: Cycloaddition products of **102** upon UV-irradiation*

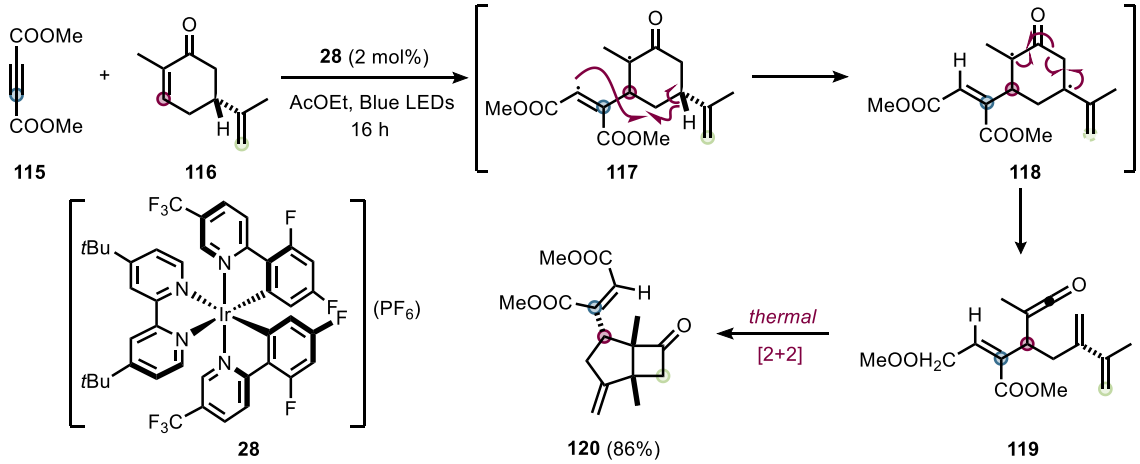
Similar behaviour was observed when the carbonyl group was placed in an endocyclic position as in substrate **109** (***Scheme 23***). Here, the 1,4-biradical **110** arising from the 6-*endo*-trig

cyclization pathway leads to the preferential fragmentation to ketene **111**, which subsequently traps the reaction solvent to form ester **112** as the major reaction product in 51% yield. This was isolated alongside the head-to-tail [2+2] cycloaddition product **114** in a 39% yield.[106]




***Scheme 23**: Cycloaddition products of **109** upon UV-irradiation*

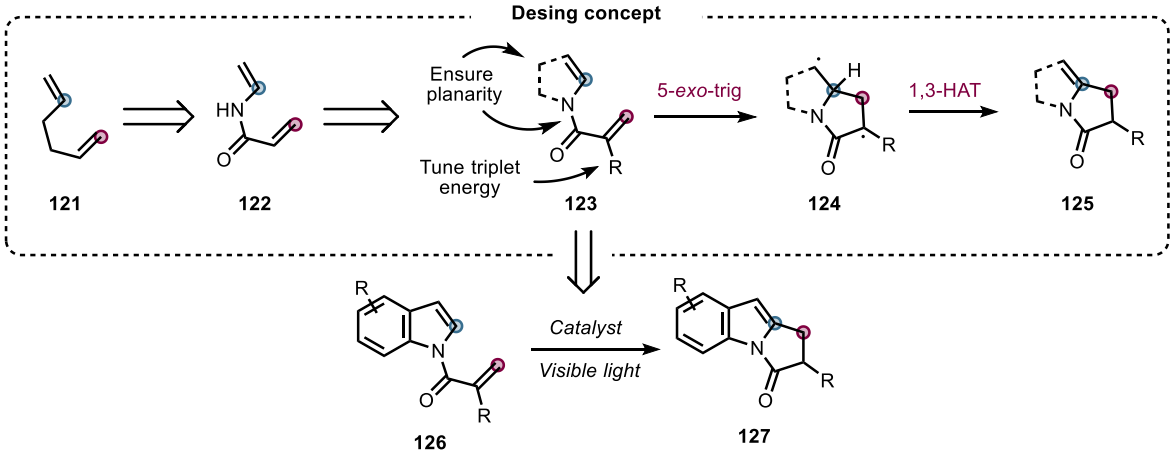
Glorius *et. al.*, reported the serendipitous discovery of an interrupted process during a high throughput screening process involving visible light sensitization of a mixture of carvone (**116**) and electron-deficient alkynes such as **115**, which resulted in the formation of polycyclic derivative **120** as a single diastereoisomer, in a very good 86% yield. The proposed mechanism, supported by DFT computational studies performed at the B3LYP/def2-TZVPP[41-44, 92-93] level of theory, postulates that the reaction proceeds *via* an endergonic energy transfer mechanism that initially generates 1,4-diradical **117**, which undergoes a subsequent 1,5-HAT to give the isomeric diradical **118**. Further fragmentation to ketene **119** and thermal [2+2] cycloaddition yields the observed product **120** (***Scheme 24***).[107]




***Scheme 24**: Cycloaddition product of **115** and **116** via visible light energy transfer*

### 2.1.3 Project Aim

The emergence of heterocycle [2+2] cycloadditions has reinvigorated the interest of organic chemistry community in energy transfer transformations. Although a lot of effort has been place directed towards the development of intermolecular and intramolecular variants, with different tether orientations and coupling partners, no investigations have been conducted towards the development of interrupted alternatives. As seen in **section 2.1.2**, interrupted [2+2] cycloaddition processes where the 1,4-diradical recombination step is avoided, are relatively rare and are usually only minor competitive pathways in [2+2] cycloaddition reactions. However, they do provide access to new and complicated scaffolds, and as such, may be utilized in organic synthesis to quickly install chemical complexity. By combining these two approaches, we aim to develop an interrupted [2+2] cycloaddition on a heterocycle.




***Scheme 25**: Design features behind the proposed transformation*

To ensure its chemical utility and applicability, eliminating the [2+2] pathway is essential. As past literature transformations indicated that 1,5-dienes (such as **121**) appear to lead preferentially to interrupted pathways,[106] it was decided that they represented a good structural starting point. It was envisaged that a planar 1,4-diradical intermediate would maximize and deter recombination. To this extent, *N*-vinyl acrylamides (**122**) are great structural candidates, however, further rotation across the *N*-vinyl group would still be viable and detrimental. The next key structural modification would be the interlocking of the *N*-vinyl group in a ring

system (**123**). The resulting 1,4-diradical intermediate **124** would be completely deterred from recombination due to the spatial orientation of the of the radical centres, thus effectively being "geometrically interrupted". At this point, the only viable alternative that could be envisaged was a 1,3-HAT (or 1,3-H shift) to facilitate the formation of the fused 5,5-heterocycle **125**. The final structural feature that was considered, was the addition of substituents at the 2-position of the acrylamide capable of tuning the triplet energy of the system capable of being sensitized using visible light, without affecting the intrinsic reactivity of C–C bond-forming terminal radical. This was considered a vital requirement of a good transformation, as visible light energy transfer catalysis ensures wide functional group compatibility, as well as increased user safety. Based on all these considerations, we arrived at 2-substituted *N*-acryloyl heterocycles, such as indoles and pyrroles (***Scheme 25***). We decided to focus our attention mainly on indoles, as they are ubiquitous in medicinal chemistry, commercially accessible, as well as chemically stable.[108] Furthermore, the resulting pyrrolo[1,2-*a*]indoles (**127**) represent an important class of molecules commonly found in a wide range of natural products (***Figure 10***).[57-61] Although syntheses of pyrrolo[1,2-*a*]indoles exist, if successful, this transformation would represent the first synthetic strategy using energy transfer catalysis.[109-111]

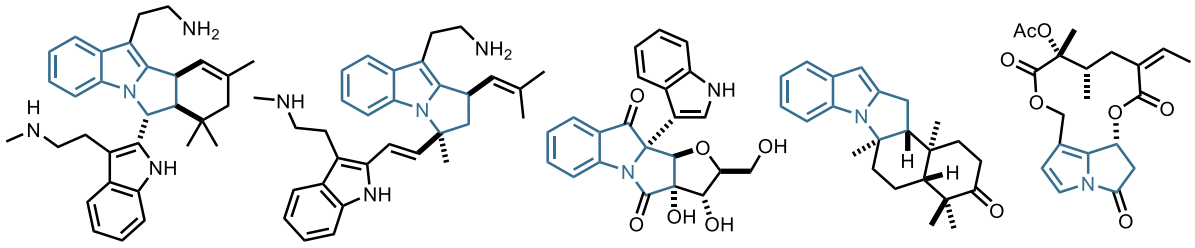
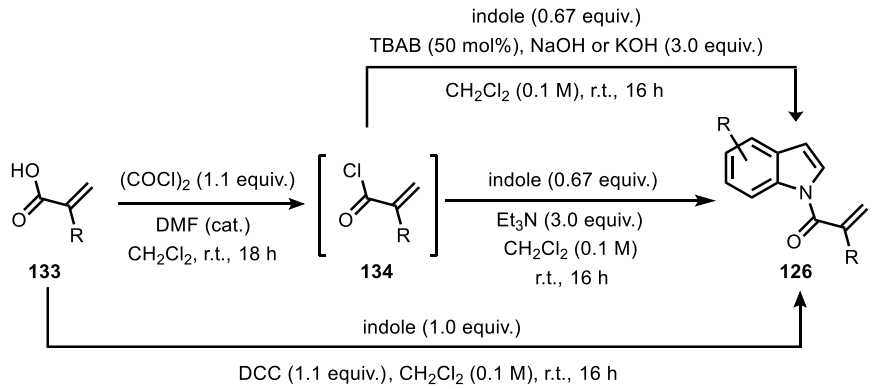



***Figure 10**: Natural products containing pyrrolo[1,2a]indole and pyrrolo[1,2a]pyrrole cores*

## 2.2 Results and Discussions

### 2.2.1 Substrate Synthesis

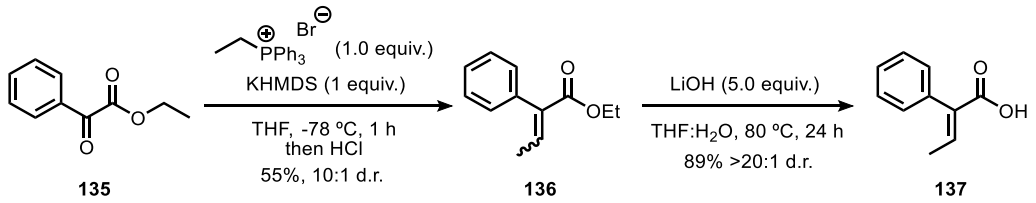
Synthesis of *N*-acryloyl indoles, though retro-synthetically straightforward, proved to be more difficult than initially expected. Conjugate addition indole to the acrylic acid was particularly problematic for acrylates that were substituted at the terminal end. This was further complicated by C3 acylation of indole, competing polymerization of the resulting products, and degradation of the indoles in presence of acids, resulting in complex reaction mixtures that are difficult to purify. A thorough investigation of literature methods resulted in the identification of three general protocols for the synthesis of the desired substrates (***Scheme 26***).[112-113]




***Scheme 26****: Synthetic sequences used in the preparation on N-acryloyl indoles*

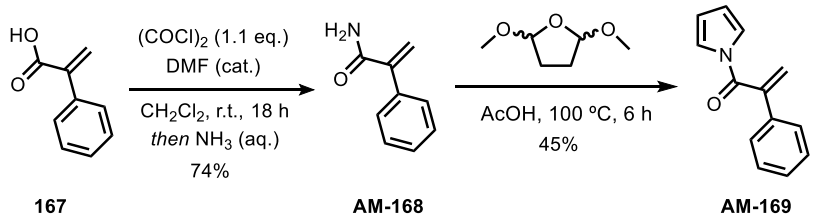
Using these three protocols, a wide range of *N*-acryloyl indole derivatives were synthesized and the results are summarised in ***Figure 11***. Although most of our investigation is focused on indoles, due to their medicinal relevance and commercial availability, other *N*-acryloyl heterocycles were well tolerated, as exemplified by azaindoles **AM-158**, **AM-159** and **AM-160**, imidazole derivative **AM-149** and pyrazole **AM-150**. Due to solubility issues, melatonin-based derivative **165** was synthesized using a modified phase transfer procedure, which involved replacing the solvent with toluene and heating the reaction mixture to 40 $^{o}$C. The (*E*)-2-phenylbut-2-enoic acid **137**, necessary in the synthesis of substrate **163**, was

prepared from α-ketoester **135** *via* Witting olefination, to give the acrylate derivate **136**, followed by hydrolysis (***Scheme 27***).

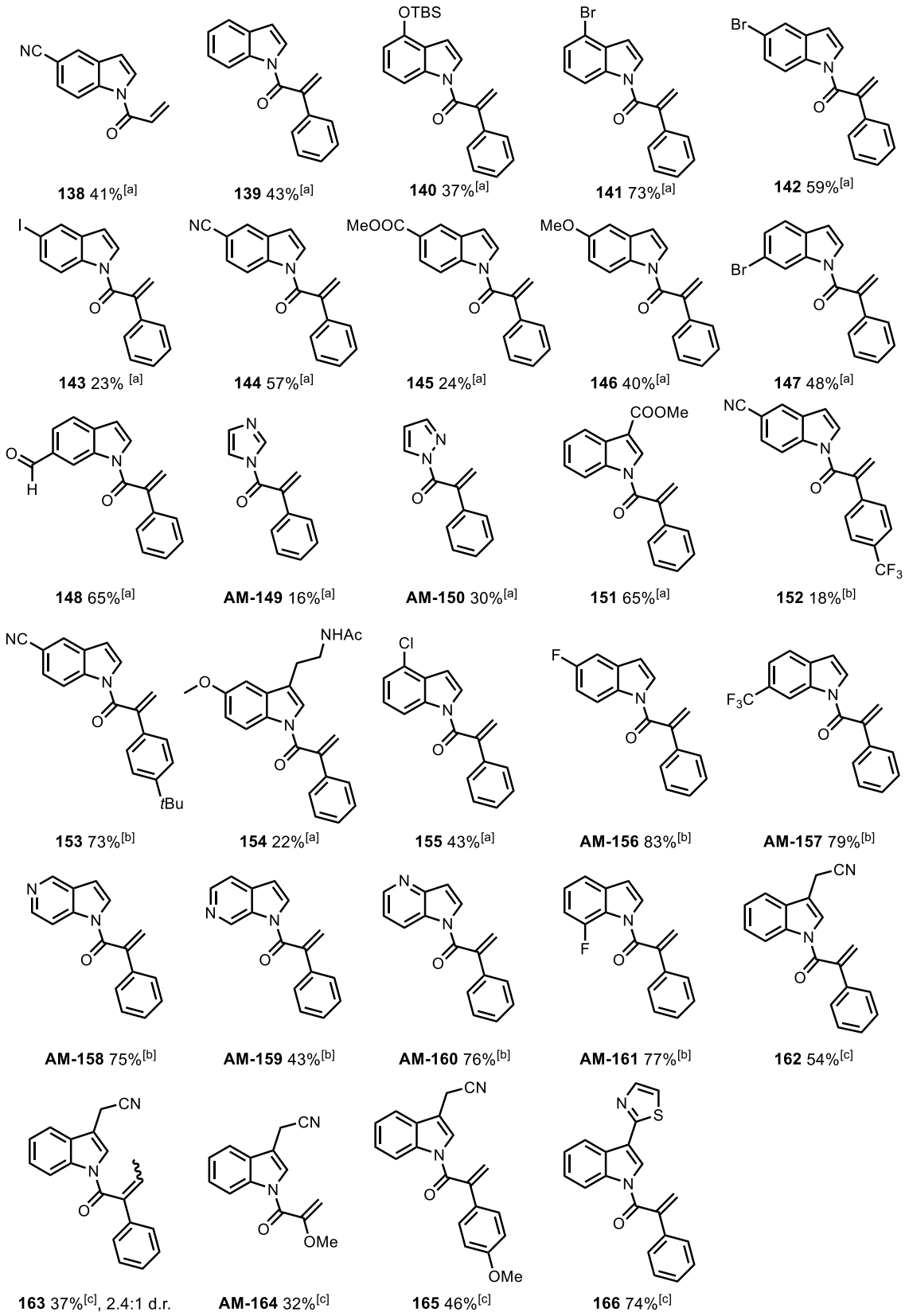



***Scheme 27****: Synthesis of* (E)-2-phenylbut-2-enoic acid

Unfortunately, pyrroles proved incompatible with the three protocols described above. As such, a change in strategy was employed, whereby the heterocycle was synthesized around the acrylamide instead (***Scheme 28***).




***Scheme 28****: Synthesis of N-atropyl pyrrole* ***AM-169****; Synthetic sequence was undertaken by Dr. Aroonroj Mekereeya*




**138** 41%[a] **139** 43%[a] **140** 37%[a] **141** 73%[a] **142** 59%[a]

**143** 23% [a] **144** 57%[a] **145** 24%[a] **146** 40%[a] **147** 48%[a]

**148** 65%[a] **AM-149** 16%[a] **AM-150** 30%[a] **151** 65%[a] **152** 18%[b]

**153** 73%[b] **154** 22%[a] **155** 43%[a] **AM-156** 83%[b] **AM-157** 79%[b]

**AM-158** 75%[b] **AM-159** 43%[b] **AM-160** 76%[b] **AM-161** 77%[b] **162** 54%[c]

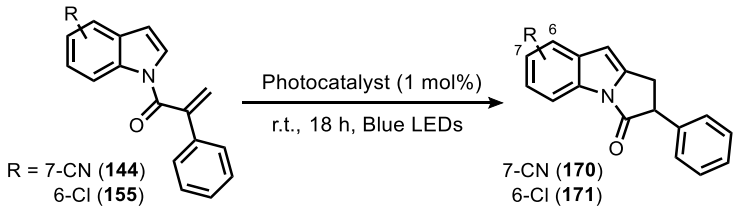
**163** 37%[c], 2.4:1 d.r. **AM-164** 32%[c] **165** 46%[c] **166** 74%[c]

***Figure 11****: Yields of N-acryloyl derivatives synthesized according to the general protocols; [a] Using acid chloride, TBAB and NaOH; [b] Using acid chloride, $Et_3N$; [c] Using carboxylic acid and DCC; [d] using KOH at 40 °C; Compounds labelled with the prefix AM were synthesized by Dr. Aroonroj Mekereeya*

### 2.2.2 Reaction Optimization

We continued our investigation by studying the chemical reactivity of substrate **144** (***Table 1***). Irradiation of **144** in ethyl acetate using blue light led to complete recovery of starting material. The addition of catalytic amounts of $Ru(bipy)_3(PF_6)_2$ (**171**) also gave no conversion to the desired product **170**. Replacement of the ruthenium photocatalyst by $[Ir(ppy)_2(bpy)](PF_6)$ (**173**) led to the first successful hit, where the desired pyrrolo[1,2-*a*]indole derivative **170** was obtained in 6% NMR yield. Encouraged by this result, we proceeded to screen iridium-based photocatalysts with increasing triplet energies. The addition of catalytic amounts of $Ir(ppy)_3$, (**174**), a commonly employed energy transfer catalyst, resulted in a dramatic increase in NMR yield up to 71%; $[Ir(dF(CF_3)ppy)_2(dtbbpy)](PF_6)$ (**28**) lead to the formation of **170** in 81%, while $Ir(dFppy)_3$ (**60**) gave the desired product in 92% NMR yield and 84% isolated yield. Having identified an optimal photocatalyst, we proceeded to screen reaction solvents. Commonly used solvents in photochemistry, such as acetonitrile, toluene and acetone, only resulted in reduced product yields, and as such, no further solvent optimization was conducted. However, during a preliminary substrate scope investigation, *N*-acryloyl derivative **155** bearing a chlorine substituent at the 6-position was found to lead to the formation of polycyclic derivative **171** in 55%. As this result was unsatisfactory, a re-optimization of reaction conditions was conducted on substrate **155**. We continued our investigation by studying the influence of additives. The addition of one equivalent of potassium acetate furnished the desired 6-chloro cyclization product **171** in 74% NMR yield. By switching to sodium acetate, a further increase to 83% NMR yield was observed, while potassium phosphate tribasic resulted in a lower yield of product **171**. Reducing the amount of sodium acetate to 0.1 equivalents and increasing the solvent concentration to 0.1 M had no deleterious effects leading to an isolated yield of 79% of the desired product. Resubjection of the original

optimization substrate to the condition pleasingly led to an increase in the isolated yield of **169** from 85% to 93%.




| Entry | R | Catalyst | Solvent | Base | Yield[a] |
|---|---|---|---|---|---|
| **1** | 7-CN | N/A | AcOEt (0.04 M) | N/A | 0% |
| **2** | 7-CN | $Ru(bipy)_3(PF_6)_2$ | AcOEt (0.04 M) | N/A | 0% |
| **3** | 7-CN | $[Ir(ppy)_2(bpy)](PF_6)$ | AcOEt (0.04 M) | N/A | 6% |
| **4** | 7-CN | $Ir(ppy)_3$ | AcOEt (0.04 M) | N/A | 71% |
| **5** | 7-CN | $[Ir(dF(CF_3)ppy)_2(dtbbpy)](PF_6)$ | AcOEt (0.04 M) | N/A | 81% |
| **6** | 7-CN | $Ir(dFppy)_3$ | AcOEt (0.04 M) | N/A | 92% (85%)[b] |
| **8** | 7-CN | $Ir(dFppy)_3$ | MeCN (0.04 M) | N/A | 74% |
| **9** | 7-CN | $Ir(dFppy)_3$ | PhMe (0.04 M) | N/A | 50% |
| **10** | 7-CN | $Ir(dFppy)_3$ | Acetone (0.04 M) | N/A | 64% |
| **11** | 6-Cl | $Ir(dFppy)_3$ | AcOEt (0.04 M) | N/A | 55% (55%)[b] |
| **12** | 6-Cl | $Ir(dFppy)_3$ | AcOEt (0.04 M) | KOAc (1.0 eq) | 74% |
| **13** | 6-Cl | $Ir(dFppy)_3$ | AcOEt (0.04 M) | NaOAc (1.0 eq) | 83% |
| **14** | 6-Cl | $Ir(dFppy)_3$ | AcOEt (0.04 M) | $K_3PO_4$ (1.0 eq) | 32% |
| **15** | 6-Cl | $Ir(dFppy)_3$ | AcOEt (0.04 M) | NaOAc (0.5 eq) | 82% |
| **16** | 6-Cl | $Ir(dFppy)_3$ | AcOEt (0.04 M) | NaOAc (0.1 eq) | 82% |
| **17** | 6-Cl | $Ir(dFppy)_3$ | AcOEt (0.025 M) | NaOAc (0.1 eq) | 75% |
| **18** | 6-Cl | $Ir(dFppy)_3$ | AcOEt (0.1 M) | NaOAc (0.1 eq) | 81% (79%)[b] |
| **19** | 7-CN | $Ir(dFppy)_3$ | AcOEt (0.1 M) | NaOAc (0.1 eq) | 95% (93%)[b] |

***Table 2**: Reaction conditions: substrate (0.1 mmol), catalyst (1 mol.%), 35 W blue LED (440 nm), r.t., 18 h; [a] $^1$H-NMR yield measured vs. $CH_2Br_2$ as internal standard; [b] yields in parentheses are for isolated material.*

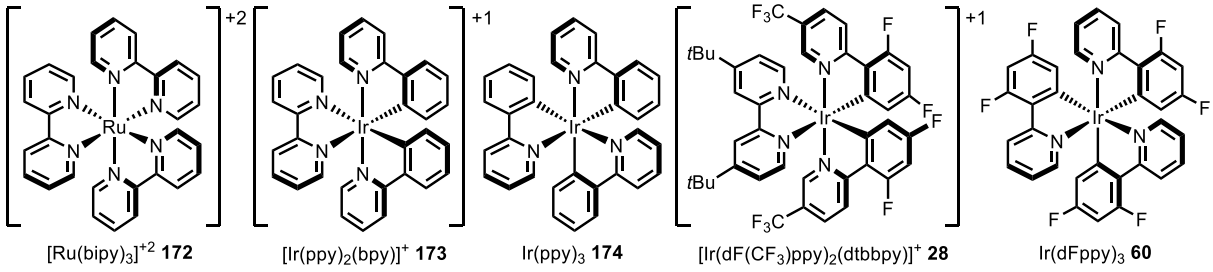



***Figure 12**: Structures of catalysts screened in **Table 2***

## 2.2.3. Substrate Scope

With the optimized reaction conditions in hand, we proceeded to investigate the substrate scope of the chemical transformation (***Figure 13***). The parent molecule bearing no functionality across the heterocycle scaffold, cyclized readily, leading to the isolation of pyrrolo[1,2-*a*]indole **175** in 98% yield. Substituents on the 8-position were well tolerated. The O-*tert*-butyldimethylsilyl derivative **176** was isolated in 85% yield, while halogen bearing

derivatives **171** and **177** were prepared in 79% and 94% yield, respectively. Modifications at the 7-position proved to be compatible, with a wide range of electron-withdrawing and electron-rich substituents being well tolerated. Halogen substituents were well behaved leading to the isolation of the 7-iodo **178**, 7-bromo **179** and 7-fluoro **180** products in 83%, 94% and 95% isolated yields, respectively. We were particularly pleased by the excellent yield of the 7-iodo derivative **178**, as aryl iodides are poorly tolerated under UV-irradiation due to C–I homolysis, thus showcasing the advantage of using visible light. Other electron withdrawing groups such as methyl ester (**181**, 62% yield) and nitrile (**170**, 93% yield) were well behaved, while the electron-rich substrate bearing a methoxy group led to the isolation of product **182** in 70% yield. Substitution at the 6-position was next investigated. Bromine and trifluoromethyl groups readily gave the cyclization products **183** and **184** in very good isolated yields of 94% and 74%, respectively. The addition of an aldehyde was also tolerated, albeit affording compounds **185** in a low yield of 32%. We propose that the majority of the material was consumed in a polymerization reaction, as we observed precipitation of an insoluble white solid from the reaction. An example of 5-position substituted pyrroloindole core was also synthesized, as exemplified by the fluorine bearing derivative **186**, which was isolated in 82% yield. Further investigations into 5-substituted derivatives could not be performed due to difficulties in synthesizing the necessary precursors. The 9-position was also probed, and proved to be well-tolerated, as exemplified by products **187** (92% yield) and **188** (84% yield). Lastly, more complex camalexin and serotonin-derived indoles **189** and **190** were both obtained in 50% yield, respectively.

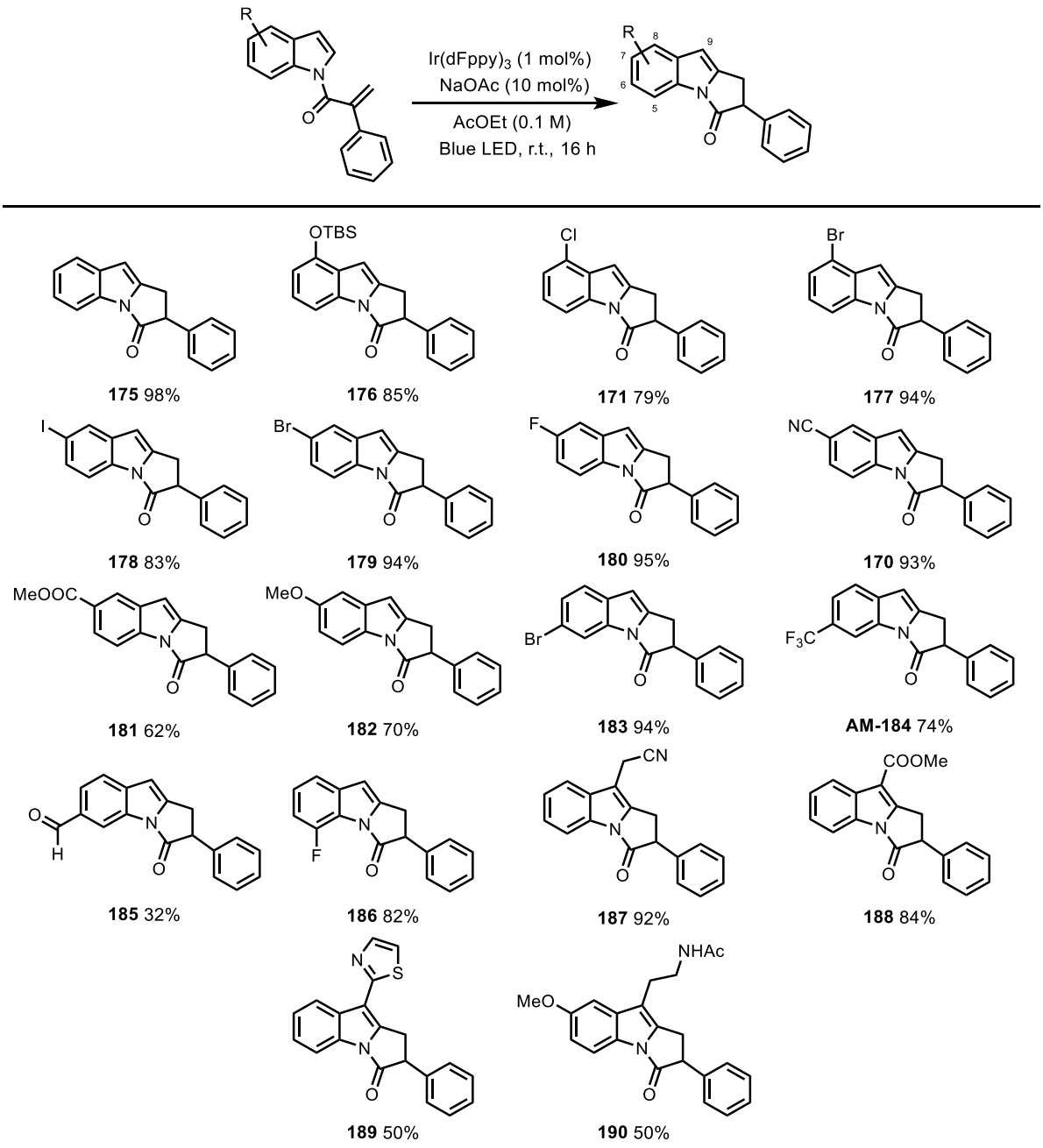



***Figure 13***: *Substrate scope where the indole motif is modified; Compounds labelled AM were synthesized by Dr. Aroonroj Mekereeya*

Having investigated the substitution on the indole motif, we next turned our attention to the chromophore (***Figure 14***). The presence of an additional alkyl substituent at the terminal end of the alkene proved to be compatible with the reaction conditions, leading to the isolation of compound **191** in 88%, albeit with no control over the diastereoselectivity. Modification of the aryl group showcased no deleterious effects. The addition of electron-rich groups such as a *p*-OMe substituent or *p*-*t*Bu led to the isolation of pyrroloindole derivatives **192** and **193** in

92% and 93% yield, respectively. The electron-deficient substituent *p*-$CF_3$ also led to the desired product **194** in 93% isolated yield. Satisfyingly, the aromatic substituent of the *N*-acyl motif can be replaced altogether by a methoxy ether group, leading to the formation of **AM-195** in 74% yield, thus further improving the versatility of this transformation.

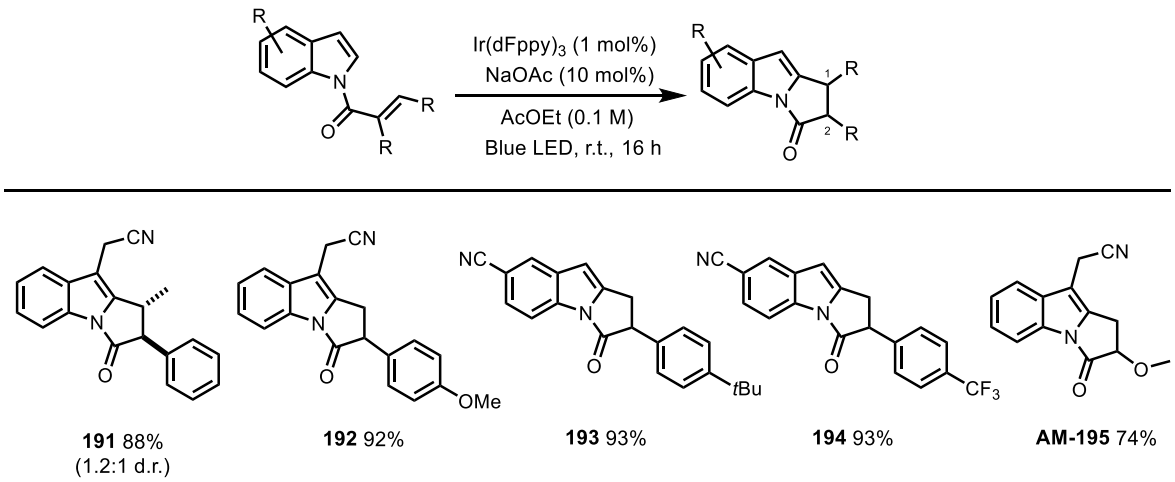



***Figure 14***: *Substrate scope where the chromophore is modified; Compounds labelled AM were synthesized by Dr. Aroonroj Mekereeya*

Finally, we investigated the scope of other 5-membered ring *N*-heterocycles (***Figure 15***). The reaction behaved excellently on a series of azaindoles, leading to the formation of 6-azaindole derivate **196** (77% yield), 7-azaindole **197** (90% yield) and 8-azaindole **198** (88%) in very good yields. Starting from *N*-atropyl pyrrole **AM-169**, irradiation under the normal reaction conditions provided access to the pyrrolo[1,2-*a*]pyrrole scaffold **AM-199** in 85% yield. Lastly, bicyclic derivative **AM-200** was obtained in a poor 21% yield, as a 1.3:1 mixture of regioisomers. The poor yield for this substrate was attributed to the instability of the *N*-acyl imidazole motif, which readily hydrolyses when dissolved.

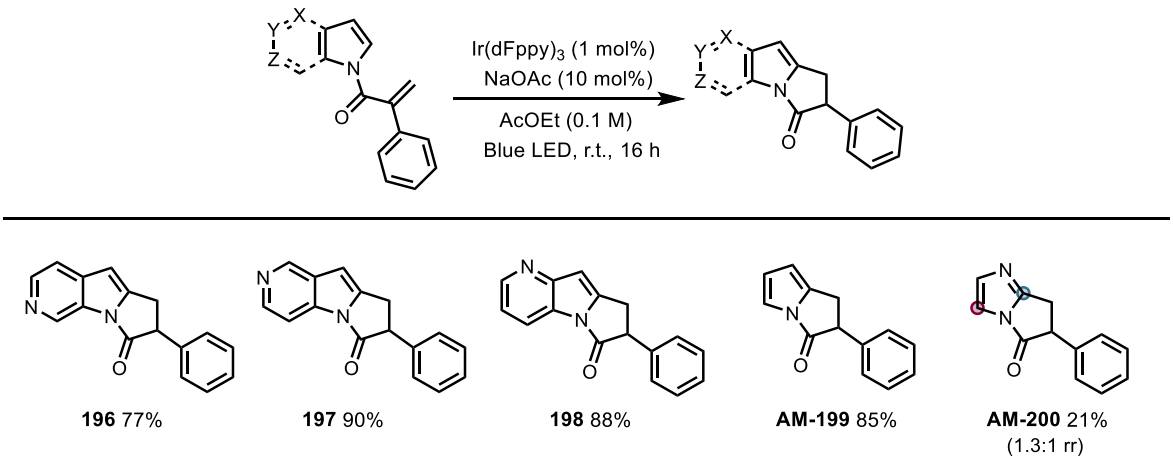
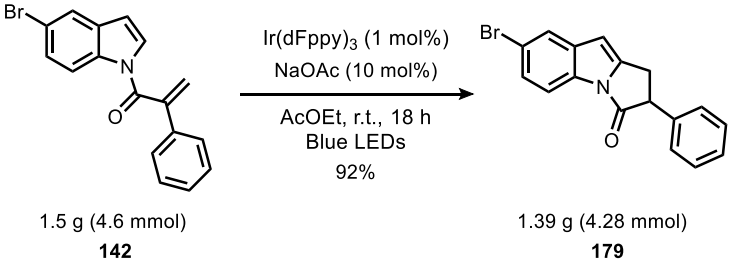



***Figure 15***: *Substrate scope where the indole motif is replaced by other heterocycles; Compounds labelled AM were synthesized by Dr. Aroonroj Mekereeya*

During our investigations, some substrates proved to be incompatible with the reaction conditions. Subjecting *N*-atropyl pyrazole **AM-150** and *N*-acryloyl indole **140** to the reaction conditions resulted in the recovery of the starting materials. The lack of reactivity involving **140** was assigned to an increase in triplet energy. Literature investigations into *N*-acyl pyrazoles revealed that they exist preferentially in the undesired conformer where the proximal carbon atom points towards the carbonyl.[114] This conformational bias arises from the favourable interaction between the lone pair of the aromatic nitrogen and the σ* orbital of the carbonyl C=O bond.

The synthetic utility of this novel protocol was demonstrated in the gram scale synthesis of compound **179**. Irradiation of a reaction mixture containing 1.5 g (4.6 mmol) of **142**, led to the isolation of pyrrolo[1,2-*a*]indole **179** in 92% yield as a white powder. This result is only 1% lower than the isolated yield obtained on a 97.9 mg (0.3 mmol) scale, thus showcasing the robustness of this transformation (***Scheme 29***).




***Scheme 29***: *Gram scale synthesis of substrate **180***

## 2.2.4. Mechanistic Investigations

Having studied this transformation's scope and limitations, we proceeded to investigate the reaction mechanism using a combination of computational and experimental techniques. As modern transition metal-based photosensitizers undergo very efficient electron transfer processes in the excited state, an alternative (or even competitive) photoredox pathway cannot be excluded. To this extent, square wave voltammetry was performed on substrate **144** in acetonitrile using ferrocene as an internal standard (***Figure 16***).

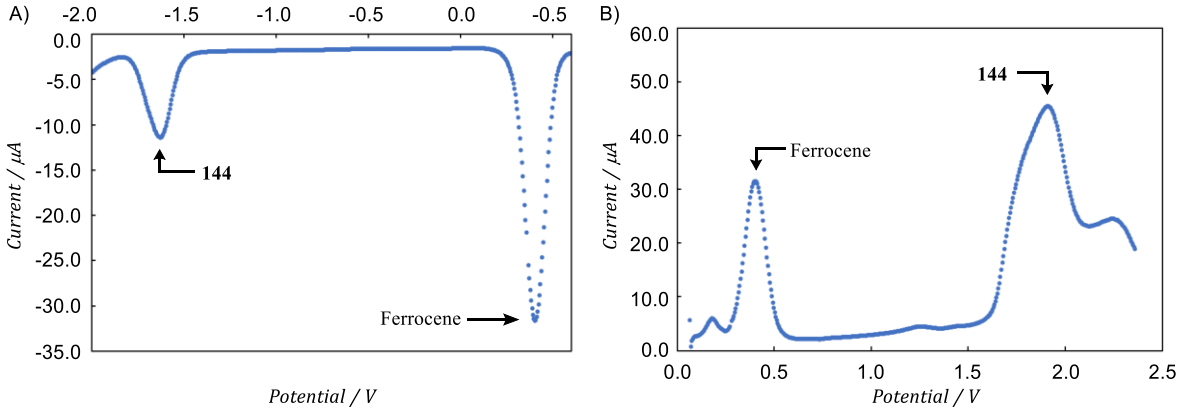



***Figure 16***: Square wave voltammograms of **144** measured in MeCN under: A) negative potential; B) positive potential

A potential scan between 0.6 V and -2.0 V referenced against SCE revealed the presence of a signal at 0.4 V corresponding to ferrocene and an additional signal at -1.62 V, which was assigned to the first electron reduction potential of compound **144**. Similarly, a positive potential voltammogram measured between 0.0 V and 2.5 V revealed the same ferrocene refence signal at 0.4 V vs. SCE as well as an additional signal with a maximum at 1.91 V vs. SCE which was assigned to the first electron oxidation of the measured substrate.

To assess the viability of a photoredox mechanism, the measured reduction and oxidation potentials of substrate **144** were compared against those of the photocatalysts studied during the reaction optimization (**Table 2**). As motioned earlier, iridium photocatalysts are efficient excited state electron donors and acceptor, possessing a wide range of redox potentials. Homoleptic iridium(III) catalysts such as $Ir(ppy)_3$ and $Ir(dFppy)_3$ are generally efficient

excited state reductants due to the increased σ-donor capabilities of phenylpyridine type ligands, compared to that of bipyridine ligands. Conversely, the cationic heterolytic iridium(III) photocatalysts such as $[Ir(ppy)_2(bpy)](PF_6)$ and $[Ir(dF(CF_3)ppy)_2(dtbbpy)](PF_6)$ generally possess good excited state oxidation capabilities due to the decreased electron density at the iridium centre compared to that of the homoleptic analogues. Furthermore, excited state potentials can be tuned by substituting the phenylpyridine and bipyridine ligands. For ease of comparison, the excited state oxidation potential (Ir(IV/III*) vs. SCE) and excited state reduction potentials (Ir(III*/II) vs. SCE) of the photocatalysts studied were compiled in **Table 3**, together with their corresponding triplet energy ($T_E$) and the corresponding NMR yields of the desired cyclization product **170**. As such, it can be observed that the redox potentials of substrate **144** lie outside the redox capabilities of most photocatalysts, with the exception of $Ir(ppy)_3$, which possesses a high excited state reduction potential of -1.91 V vs. SCE.[115] Although a single electron transfer mechanism cannot be excluded when $Ir(ppy)_3$ is used as a catalysts, the two best performing catalysts $Ir(dFppy)_3$ and $[Ir(dF(CF_3)ppy)_2(dtbbpy)](PF_6)$ have redox potentials comfortably outside the redox window of substate **144**, thus providing evidence against a photoredox mechanism for the optimized reaction conditions. Conversely, a correlation can be observed between the triplet energy of the photocatalyst and reaction yield, thus pointing towards an energy transfer mechanism.

| Catalyst | Ir(IV/III*) / V | Ir(III*/II) / V | $E_T$ / kcal·mol$^{-1}$ | Yield |
|---|---|---|---|---|
| $[Ir(ppy)_2(bpy)](PF_6)$ [116] | -1.17 | 1.01 | 48.6 | 6% |
| $Ir(ppy)_3$ [115] | -1.97 | 0.55 | 55.4 | 71% |
| $[Ir(dF(CF_3)ppy)_2(dtbbpy)](PF_6)$ [115] | -1.00 | 1.42 | 60.1 | 81% |
| $Ir(dFppy)_3$ [115] | -1.23 | 0.39 | 60.1 | 92% |

***Table 3**: Compiled literature redox potentials vs. SCE and triplet energies for tested iridium complexes*

Subsequent Stern-Volmer quenching experiments showcased substantial drop of the emission intensity of $Ir(dFppy)_3$ upon addition of increasing concentration of substrate **144** (***Figure 17A***). By plotting the ratio between emission intensities in the absence and presence

of the quencher against the quencher concentration, a linear Stern-Volmer relationship can be observed, indicating a clear interaction between the catalyst and substrate **144** (***Figure 15B***).

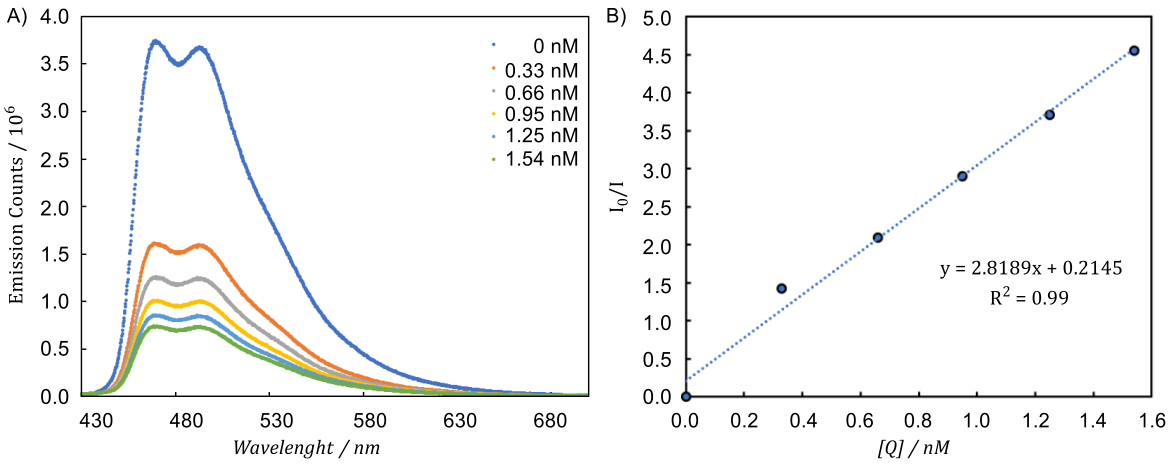



***Figure 17**: A) emission quenching of Ir(dFppy)$_3$ with increasing concentration of **144**; B) Stern-Volmer plot*

To further understand the processes underpinning this transformation, we turned to computational modelling. In recent years DFT has emerged as a compelling alternative for the determination of triplet energy of organic molecules, with hybrid functionals having proven to provide reliable predictions. We thus proceed to investigate the triplet energy of substrate **139** using a range of functionals and basis sets (***Table 4***). The functionals chosen for the triplet energy benchmarking were B3LYP,[41-44] and M06-2X[35] and ωB97xD[98] as they have been used previously for triplet energy determinations.[21, 101, 117-119] Additional D3[39] and D3(BJ)[120] dispersion corrections were included in the calculations involving the M06-2X and B3LYP functionals, respectively, as benchmarking studies have shown to increase computational accuracy at low additional computational cost. All calculations were performed in conjunction with the universal solvation model based on density (SMD)[80-84] for ethyl acetate to describe solvation sphere.

| Optimization | | Single Point Correction | | $T_E$ / $kcal \cdot mol^{-1}$ |
|---|---|---|---|---|
| **Functional** | **Basis Set** | **Functional** | **Basis Set** | |
| B3LYP-D3(BJ) | 6-31++G(d,p) | N/A | N/A | 48.3 |
| ωB97xD | 6-31++G(d,p) | N/A | N/A | 49.4 |
| M06-2X-D3 | 6-31++G(d,p) | N/A | N/A | 51.6 |
| M06-2X-D3 | 6-31++G(d,p) | M06-2X-D3 | 6-311++G(2d,p) | 52.2 |
| M06-2X-D3 | 6-31++G(d,p) | M06-2X-D3 | def2-QZVPP | 52.2 |
| M06-2X-D3 | 6-31++G(d,p) | B3LYP-D3(BJ) | def2-QZVPP | 49.6 |
| M06-2X-D3 | 6-31++G(d,p) | ωB97xD | def2-QZVPP | 49.5 |

***Table 4***: *Adiabatic triplet energy determination for substrate **140**; Triplet energy calculation are based on the lower energy conformer of compound **140***

Comparison of computed adiabatic triplet energies across all levels of theory showed small variation, with predictions ranging from 48.3 kcal·mol$^{-1}$ to 51.6 kcal·mol$^{-1}$ when Pople's double-ζ 6-31++G(d,p)[76-79] basis set is used in the geometry optimization. Single point energy corrections performed at the same optimization geometry, showed similar energy predictions ranging from 49.5 kcal·mol$^{-1}$ for B3LYP-D3(BJ) up to 52.2 kcal·mol$^{-1}$ M06-2X-D3 when computed using Ahlrichs's heavily polarize quadruple-ζ Def2-QZVPP[92-93] basis set. Similarly, the triple-ζ 6.311++G(2d,p) basis set provided similar results to Def2-QZVPP. In all cases, the predicted triplet energies are lower than the three best performing iridium catalysts, $Ir(dFppy)_3$ ($T_E$=60.1 kcal·mol$^{-1}$), $[Ir(dF(CF_3)ppy)_2(dtbbpy)](PF_6)$ ($T_E$=60.1 kcal·mol$^{-1}$) and $Ir(ppy)_3$ ($T_E$=55.4 kcal·mol$^{-1}$) (**Table 3**). Furthermore, the triplet energy of the worst performing catalyst, $[Ir(ppy)_2(bpy)](PF_6)$ ($T_E$=48.6 kcal·mol$^{-1}$), is lower than that of the predicted triplet energies, providing compelling evidence for an efficient exergonic triplet energy transfer mechanism.

We next proceeded to investigate the potential energy surface behind the desired transformation. Although all levels of theory used in the triplet energy determination of substrate **139** provide similar results, we chose the M06-2X-D3/Def2-QZVPP//M06-2X-D3/6-31++G(d,p)[35, 39, 76-79, 92-93, 121] with the SMD solvation model for this investigation. The Minnesota hybrid-meta-GGA functional has been used extensively in the study of triplet state reactivity,[118, 122-126] while also accurately describing radical processes in previous benchmarking studies,[37-38] thus making it a good candidate for this study.

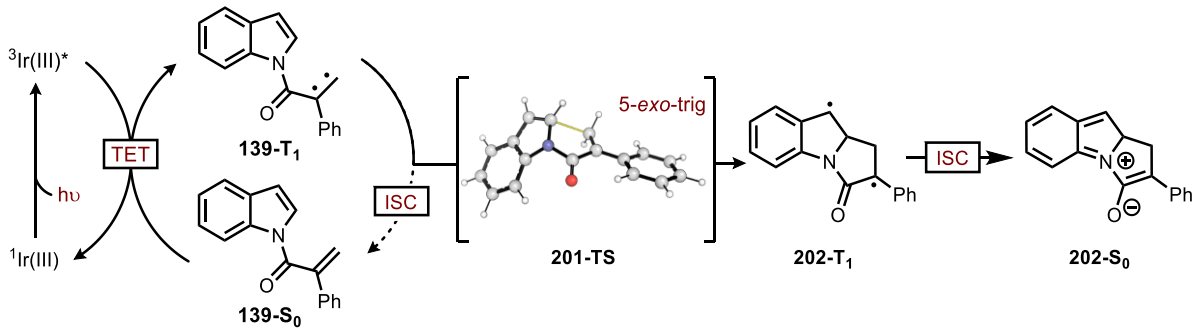



***Figure 18**: Proposed mechanism for excitation and C-C bond formation*

| Entry | $\Delta E$ | $\Delta ZPE$ | $\Delta H$ | $T\Delta S$ | $\Delta G$ |
|---|---|---|---|---|---|
| **139-S$_0$** | -54.2 | 2.5 | -51.7 | -0.5 | -52.2 |
| **139-T$_1$** | 0.0 | 0.0 | 0.0 | 0.0 | 0.0 |
| **201-TS** | 10.1 | -0.1 | 9.4 | -1.2 | 10.6 |
| **202-T$_1$** | -23.1 | 1.8 | -22.0 | -1.3 | -20.7 |
| **202-S$_0$** | -24.9 | 2.9 | -22.7 | -2.2 | -20.6 |

***Table 5**: Boltzmann thermochemical parameters in kcal/mol represented relative to **139-T$_1$**, performed at uM06-2x-D3/Def2-QZVPP(SMD=AcOEt)//uM06-2x-D3/6-31++G(d,p)(SMD=AcOEt) level of theory*

Using this protocol, it was found that upon excitation to the triplet state, the transition state **201-TS** leading the triplet diradical **202-T$_1$** possesses a free energy activation barrier of 10.6 kcal·mol$^{-1}$. The overall change in free energy for this 5-*exo*-trig cyclization process is -20.7 kcal·mol$^{-1}$, making this pathway effectively irreversible. The resulting triplet diradical intermediate **202-T$_1$** can undergo intersystem crossing to the singlet state intermediate **202-S$_0$** *via* minimum energy crossing point **202-MECP** (***Figure 19***).

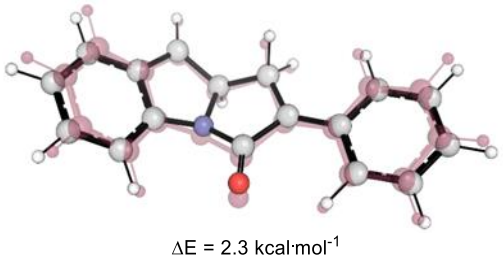
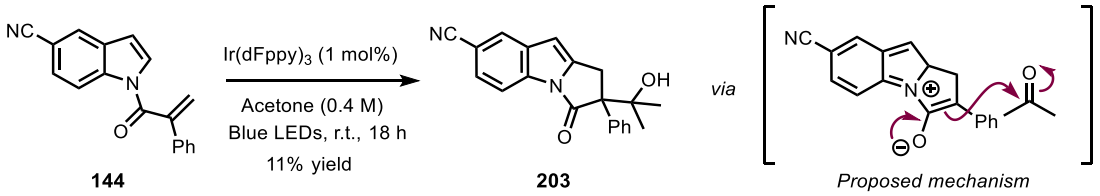



***Figure 19**: Computed structure of **202-MECP** (grey) overlayed with that of intermediate **202-T$_1$**. Little structural rearrangement can be observed between the two structures, thus accounting for the small activation energy required to reach the MECP. MECP was computed by Dr. Juan Alegre-Requena.*

Careful analysis of singlet species **202-S$_0$** suggests that it is best described as a closed shell zwitterion, rather than an open-shell singlet biradical, as indicated by $< \hat{S}^2 > = 0$ in wavefunction stability checks, as well as Mülliken spin densities. This observation was confirmed experimentally by using acetone as a trapping reagent. Under these conditions,

adduct **202** was isolated in 11% yield, alongside the normal cyclization product (***Scheme 30***). Besides providing evidence for zwitterionic intermediates, this experiment reveals a potential decomposition mechanism for the aldehyde bearing pyrrolo[1,2-*a*]indole **185** thus accounting for the modest isolated yield.




***Scheme 30**: Trapping experiment showcasing the presence of a zwitterionic intermediate*

Having experimentally established the presence of zwitterion **203-S$_0$**, we next proceeded to investigate the final mechanistic step. The most straightforward process for regenerating the indole aromaticity is *via* an intramolecular 1,3-H shift (***Figure 20***, ***Table 6***).

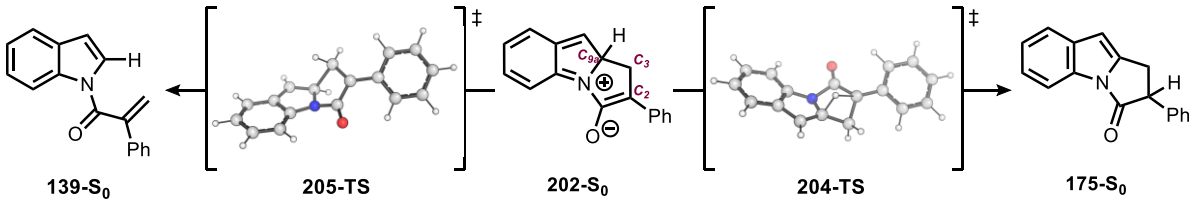



***Figure 20***: Proposed pathways for 1,3-H shift and regeneration of starting materials

| Entry | Δ***E*** | Δ***ZPE*** | Δ***H*** | ***TΔS*** | Δ***G*** |
|---|---|---|---|---|---|
| **139-S$_0$** | -30.9 | -0.4 | -30.9 | 1.7 | -32.5 |
| **204-TS** | 10.6 | -1 | 9.3 | -0.3 | 9.7 |
| **202-S$_0$** | 0 | 0 | 0 | 0 | 0 |
| **205-TS** | 34.9 | -3.3 | 31.3 | -0.3 | 31.7 |
| **175-S$_0$** | -52 | 1.1 | -51 | 0.3 | -51.1 |

***Table 6*: Boltzmann thermochemical parameters in kcal/mol represented relative to *202-S$_0$*, performed at *uM06-2x-D3/Def2-QZVPP(SMD=AcOEt)//uM06-2x-D3/6-31++G(d,p)(SMD=AcOEt) level of theory**

Intriguingly, computational investigation of this process revealed an activation energy barrier of 31.7 kcal·mol$^{-1}$. Careful analysis of the transition state revealed substantial unfavourable structural reorganization *via* pyramidalization of the amide nitrogen, in an effort to deplanarize the polyclinic system, as a mechanism to minimise the distance between positions $C_{9a}$ and $C_2$. The large activation energy required to reach transition state **204-TS** makes this process unfeasible, especially when compared to the activation energy of 9.7 kcal·mol$^{-1}$ (*via* transition state **205-TS**) required for the fragmentation pathway leading back to the starting material

**139-S$_0$**. As the addition of catalytic amounts of base has beneficial effects on this transformation, an intramolecular deprotonation/protonation mechanism was proposed instead (***Figure 21***).

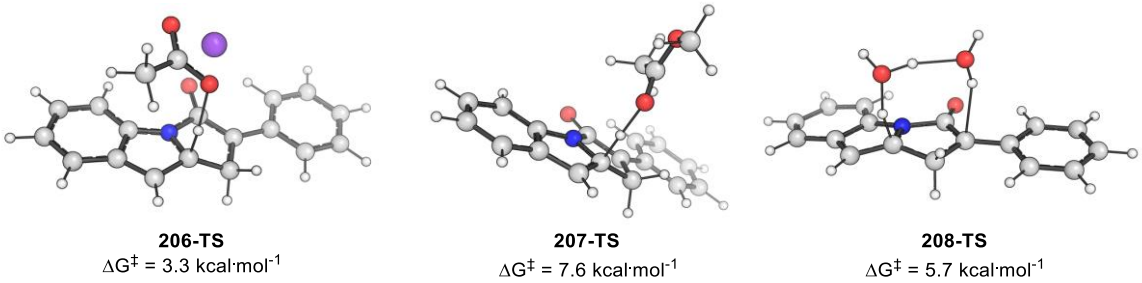



***Figure 21*: *Base mediated (left), solvent mediated (middle) and water mediated (right) proton shuttle transition states; Transition state **208-TS** was computed by Dr. Juan Alegre-Requena***

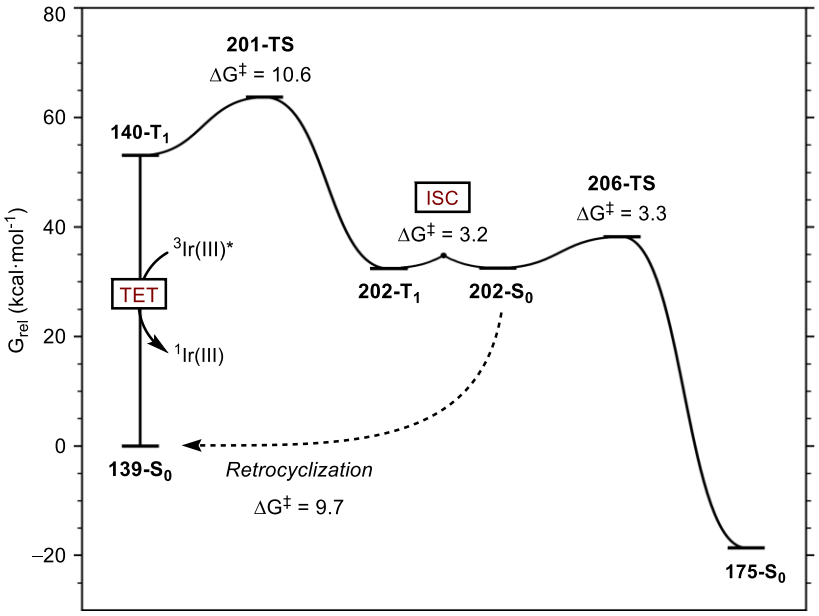



***Figure 22*: *Proposed reaction energy profile based on DFT calculations***

A transition state search revealed a sodium acetate catalyzed pathway, with an activation energy of 3.3 kcal·mol$^{-1}$ (*via* **206-TS**), making this process highly facile. As the reaction works well even in the absence of catalytic amounts of base, it was envisioned that a similar process can be catalyzed by a solvent molecule. Indeed, a transition state (**207-TS**) was found possessing an activation energy of 7.6 kcal·mol$^{-1}$ (for simplicity, methyl acetate was used as a model for the ethyl acetate), which is substantially lower in energy than the competitive retro-cyclization pathway *via* transition state **205-TS**, especially when considering the high effective

concentration of ethyl acetate. Alternatively, as the reaction is not performed under strictly anhydrous conditions, a water-mediated proton shuttle is also possible as exemplified by transition state **207-TS**, which possesses an activation energy of 5.7 kcal·mol$^{-1}$.

Another mechanistic possibility that might explain the formation of the photocyclization product **175-S$_0$** is a stepwise combination of 1,2-H shifts in the triplet state starting from the triplet 1,4-birradical **202-T$_1$** (***Figure 23***). Under this proposal, intermediate **202-T$_1$** can undergo 1,2-H shift to furnish 1,3-dirradical **210-T$_1$** *via* transition state **209-TS**, which in turn can then undergo an additional 1,2-H shift to give the excited triplet state of the experimentally observed product **175**. When investigated computationally, **203-TS** was found to require a 45.7 kcal·mol$^{-1}$, which is not easily accessible at room temperature. Similarly, the subsequent 1,2-H shift required to reach intermediate **175-T1** also possesses a high activation energy barrier of 44.9 kcal·mol$^{-1}$. Although, the barriers required to undertake the two 1,2-H shifts in the triplet state are high, it has been shown that quantum mechanical tunnelling can play an important role in hydrogen-shift processes.[127]

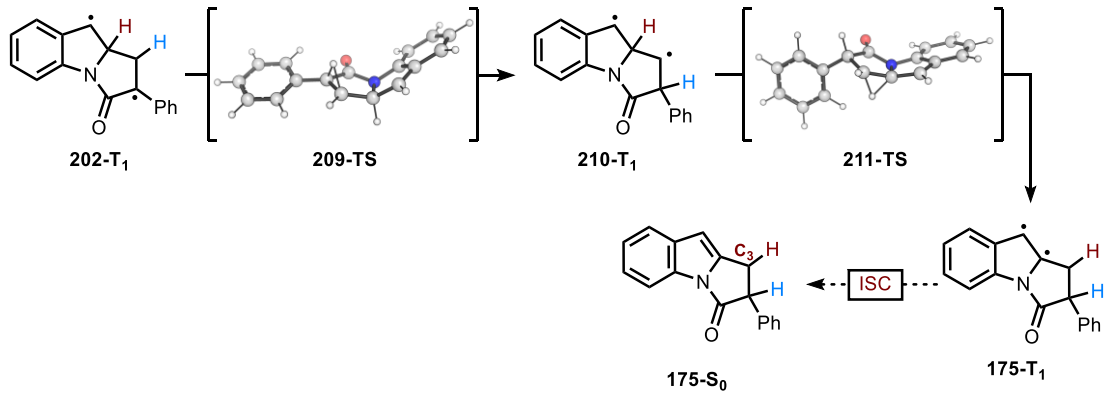



***Figure 23:*** *Proposed alternative mechanism for generating product **175** via a sequence of 1,2-H shifts*

| Entry | $\Delta E_{SPC}$ | $\Delta E$ | $\Delta ZPE$ | $\Delta H_{SPC}$ | $qh.T\Delta S$ | $qh.\Delta G_{SPC}$ |
|---|---|---|---|---|---|---|
| **202-T$_1$** | 0.0 | 0.0 | 0.0 | 0.0 | 0.0 | 0.0 |
| **209-TS** | 49.1 | 49.5 | -3.3 | 45.7 | 0.0 | 45.7 |
| **210-T$_1$** | 17.0 | 16.8 | -0.9 | 16.2 | 0.7 | 15.5 |
| **211-TS** | 64.4 | 64.4 | -3.6 | 60.9 | 0.5 | 60.4 |
| **175-T$_1$** | 21.5 | 21.4 | -0.5 | 21.1 | 0.3 | 20.8 |

***Table 7*****:** *Boltzmann thermochemical parameters in kcal/mol represented relative to **202-S$_0$**, performed at uM06-2x-D3/Def2-QZVPP(SMD=AcOEt)//uM06-2x-D3/6-31++G(d,p)(SMD=AcOEt) level of theory*

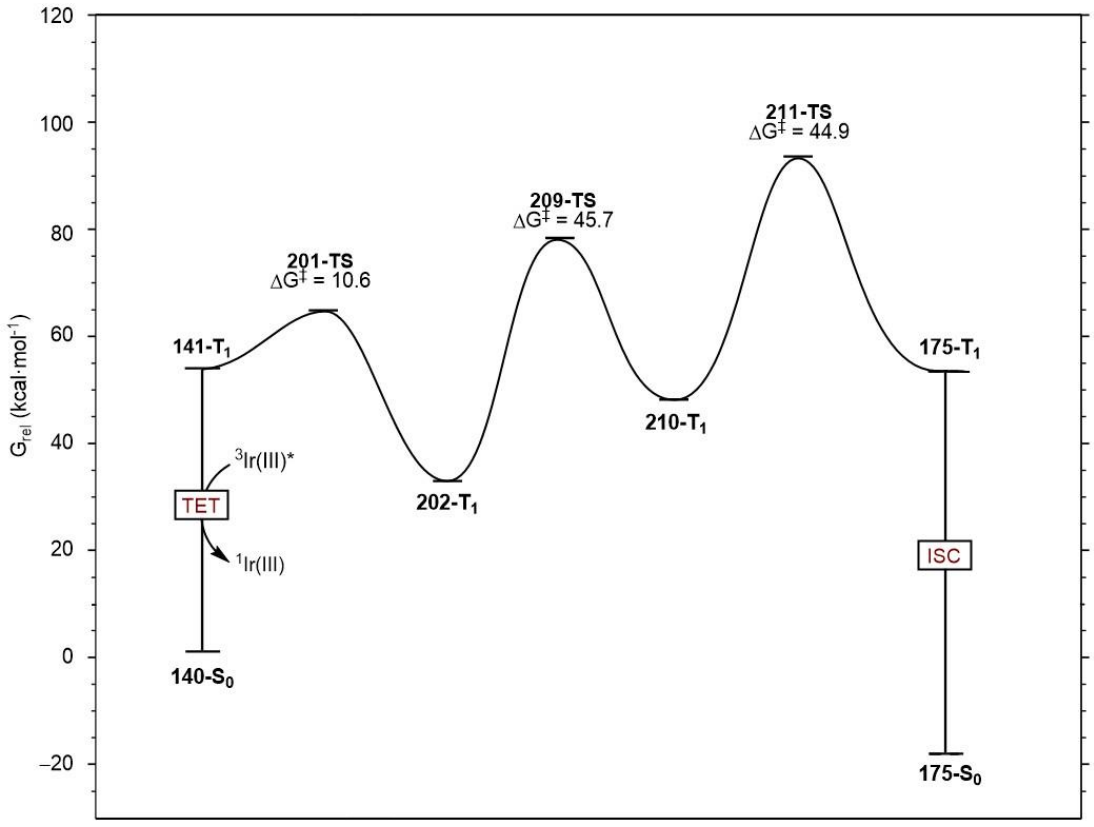
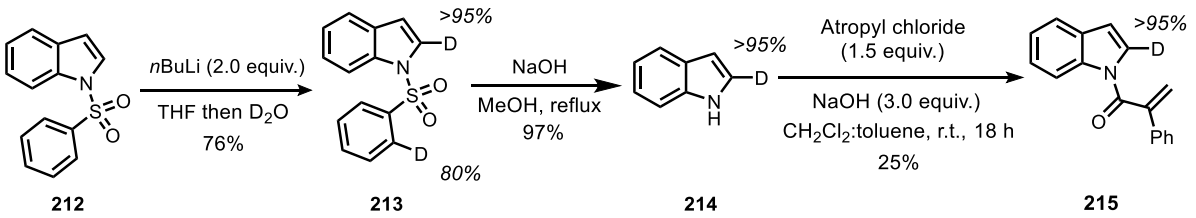



***Figure 24***: *Proposed reaction energy profile based on DFT calculations for alternative 1,2-H shift mechanism in the triplet state*

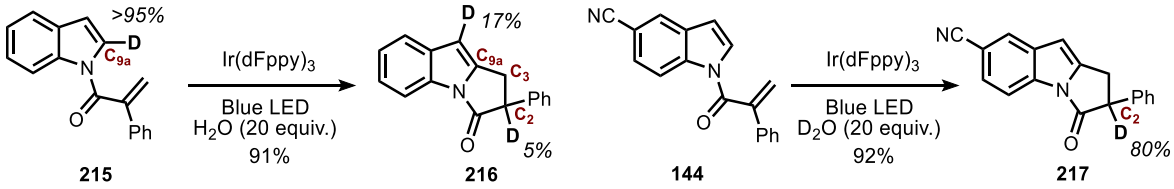
To elucidate the fate of the proton at the C9a position, we proceeded to study this process *via* deuterium labelling experiments. Indole deuterated at the 2-position (**215**), was readily synthesised according to literature procedures (***Scheme 31***) *via* a directed deprotonation-deuteration of *N*-phenylsulfonyl indole **212**, followed by hydrolysis in refluxing methanolic sodium hydroxide.[128] Using the standard phase transfer protocol, deuterated indole was acylated to give the desired product **215** in a modest yield of 25%, but more importantly, with exceptionally high deuterium incorporation.




***Scheme 31*:** Synthesis of deuterated substrate **215**

With the necessary precursor in hand, we proceeded to subject it to the optimized irradiation conditions. By exploiting the water-mediated proton shift pathway, the sodium acetate

additive was removed, and the solvent mixture was saturated with water (***Scheme 32***). Analysis of both the crude reaction mixture and the isolated product revealed a 5% deuterium incorporation at the C2 position of product **216**. Conversely, starting from the non-deuterated precursor **144**, and saturating the system with $D_2O$, an 80% incorporation of deuterium can be observed at the C2 position of product **217**, thus providing evidence for an intermolecular proton transfer process. A subsequent control experiment, where the non-deuterated product **170** was subjected to the same reaction condition, did not lead to any incorporation of deuterium, thus suggesting that the presence of deuterium at the C2 position is not a consequence of post-reaction amide enolization. Additionally, the lack of any deuterium incorporation at the C3 position of the pyrrolo[1,2*a*]indole derivative **216** provides further compelling evidence against a 1,2-H shift mechanism in the triplet state.




***Scheme 32*: *Deuterium labelling experiments***

Intriguingly, analysis of the $^1$H-NMR spectrum of product **214** revealed a loss of signal intensity at the C9 position. This observation suggests the incorporation of 17% deuterium, which was not expected based on our proposed mechanism. We thus hypothesized that a potential 1,2-H shift in the singlet state might be a competitive mechanism.

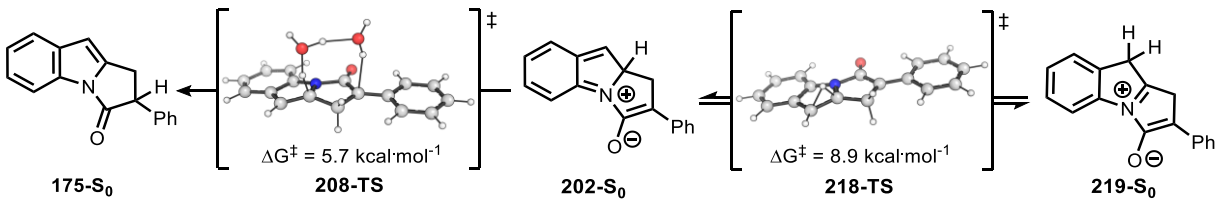



***Figure 25**: Proposed transition states for 1,2-H shift and water catalysed proton shift*

| Entry | $\Delta E_{SPC}$ | $\Delta E$ | $\Delta ZPE$ | $\Delta H_{SPC}$ | $qh.T\Delta S$ | $qh.\Delta G_{SPC}$ |
|---|---|---|---|---|---|---|
| **202-S₀** | 0 | 0 | 0 | 0 | 0 | 0 |
| **218-TS** | 10.9 | 11.7 | -2.1 | 8.5 | -0.3 | 8.9 |
| **219-S₀** | -23.3 | -22.6 | -0.5 | -23.8 | 0.3 | -23.9 |

***Table 8**: Boltzmann thermochemical parameters in kcal/mol represented relative to **202-S₀**, performed at uM06-2x-D3/Def2-QZVPP(SMD=AcOEt)//uM06-2x-D3/6-31++G(d,p)(SMD=AcOEt) level of theory*

Computational investigations revealed the presence of transition state **216-TS**, with a free energy activation barrier of 8.9 kcal·mol$^{-1}$ (***Figure 20***), which is lower than the retrocyclization pathway *via* **205-TS** (9.6 kcal·mol$^{-1}$) but higher than transition sate **208-TS** (5.7 kcal·mol$^{-1}$). Although a $\Delta\Delta G^{\ddagger}$ = 3.2 kcal·mol$^{-1}$ value would make the process highly biased towards transition state **208-TS**, it is to be noted that the water catalyzed process is a trimolecular process and the relative concentration of water needs to be considered, thus making the 1,2-hydrogen shift pathway viable. This opens the possibility that compound **219-S₀** is an actual reaction intermediate, and an alternative proton shift is in operation (***Figure 21***). However, deprotonation of intermediate **219-S₀-D** is expected to lead to at least a 50% incorporation of deuterium at the C9 position, with a potential maximum incorporation of up to ~89% based on a primary kinetic isotope effect of eight. Under the assumption of no solvent cage effects, we can estimate that the 1,2-shift pathway contributes to about 19%-34% of the overall pathways, depending on the value of the kinetic isotope effect. As such, we concluded that the 1,2-shift mechanism is a minor reaction pathway, especially considering that the presence of sodium acetate is expected to further accelerate the rate of the direct deprotonation of **219-S₀-D** under the actual reaction conditions.

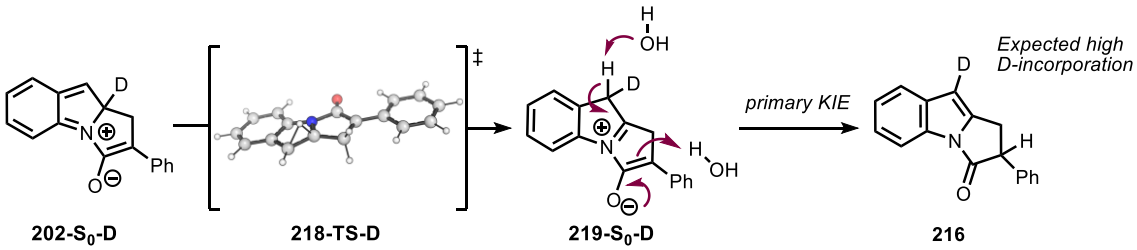



***Figure 26:** Proposed alternative mechanism via intermediate **219***

## 2.3 Mechanistic summary and conclusions

In conclusion, we have developed a novel transformation based on the [2+2] cyclization pathway by preventing the 1,4-diradical recombination. The developed protocol enables us to take readily available feedstock indoles and convert them in two synthetic steps to highly functionalised pyrrolo[1,2a]indoles, an information motif found in natural products. The use of visible light energy transfer catalysis has enabled to develop a highly functional group tolerant transformation and was applied in the synthesis of 23 pyrrolo[1,2a]indoles with isolated yields ranging from 50% to up to 98%. The reaction is scalable with no erosion in isolated yields, making it a useful synthetic tool. We also demonstrated that the reaction conditions are also compatible with other *N*-acryloyl heterocycles such as pyrroles, imidazoles and aza-indoles, which was used to synthesize an additional 5 heterocycles.

Mechanistically, electrochemical measurements excluded a potential photoredox process as the measured oxidation and reduction potentials of the substrates were well outside the redox window of two best performing catalysts $Ir(dFppy)_3$ and $[Ir(dF(CF_3)ppy)_2(dtbbpy)](PF_6)$. Subsequent Stern-Volmer experiments clearly indicated quenching of the $Ir(dFppy)_3$ photocatalyst by the reaction substrate, while comparison of literature triplet energies of catalysts used in the reaction screening revealed a correlation between increased catalyst triplet energy and reaction yield, thus pointing towards an energy transfer mechanism. The triplet energy of the prototypical substrate **139** was determined using DFT at the M06-2X-D3/Def2-QZVPP//M06-2X-D3/6-31++G(d,p) level of theory in conjunction with the SMD solvation model for ethyl acetate. The triplet energy was measured to be 52.2 $kcal \cdot mol^{-1}$, which is lower than that of the best performing catalysts $Ir(dFppy)_3$, thus pointing towards and efficient energy transfer process. Further DFT investigations performed using the M06-2X-D3/Def2-QZVPP//M06-2X-D3/6-31++G(d,p) level of theory in conjunction with the SMD solvation model revealed that the reaction proceeds through zwitterionic intermediate **202**, results which

were further substantiated with the aid of trapping experiments. The computational analysis also revealed that an intramolecular proton shift from zwitterionic intermediate **202** required a high activation energy barrier of 34.9 kcal·mol$^{-1}$. This process can instead be catalysed by sodium acetate with an activation barrier of 3.3 kcal·mol$^{-1}$, thus providing a mechanistic reason for the beneficial role of sodium acetate. This intramolecular proton shift was further emphasised by deuterium labelling experiments.

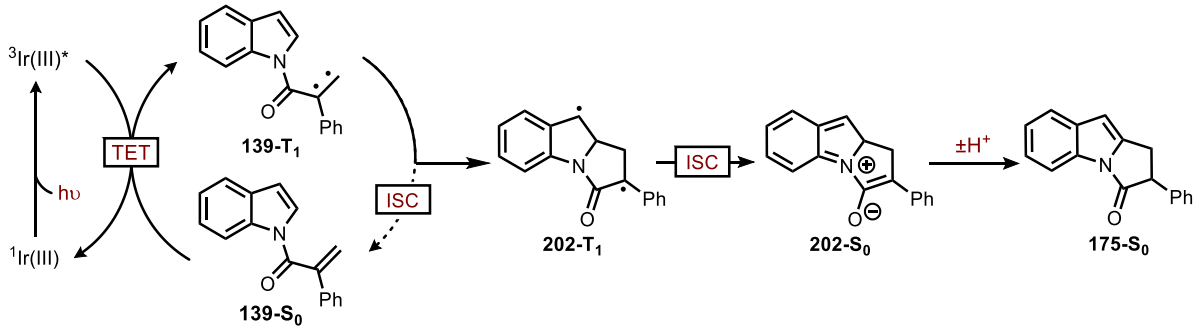
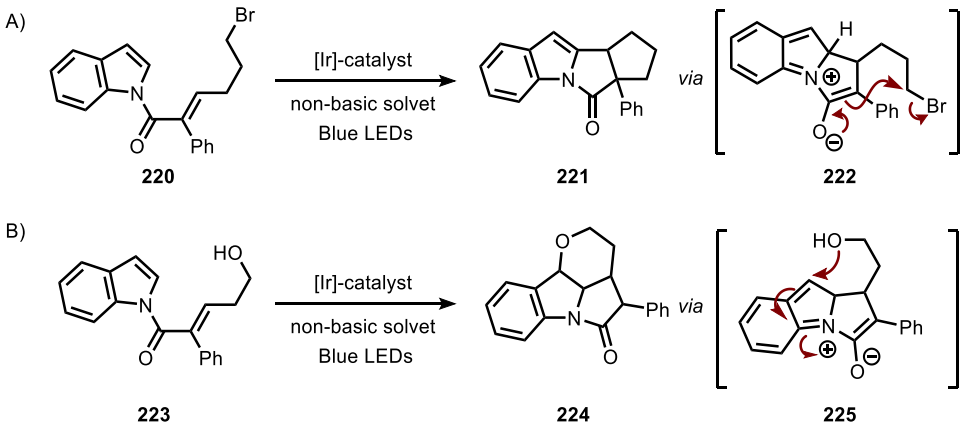



***Figure 27***: *Summary of proposed reaction mechanism*

As such, we have demonstrated the feasibility of interrupted [2+2] processes on nitrogen-based heterocycles. We believe this transformation provides a foundation to explore other interrupted process of nitrogen containing heterocycles, which can expand our understanding or excited state radical reactivity. Based on the mechanistic insights obtained in this reaction, we would like to explore new interrupted [2+2] processes by exploiting other reactivity modes of the newly identified zwitterionic intermediate **202**. One such alternative mode of reactivity would be the trapping of the zwitterionic intermediate by either nucleophiles or electrophiles. Previous trapping experiments of zwitterionic intermediate **202** provide proof of concept for such a transformation, enabling the installation of high chemical complexity in a single step *via* a cascade process. However, our study shows such a process would be inherently challenging due to the low barrier associated with the intermolecular photon shift, which can be catalysed by the solvent. This challenge could be achieved using both intramolecular nucleophiles and electrophiles, as well as reaction conditions that

minimise the 1,3-proton shift, such as using non-basic solvents (e.g. toluene, dichloromethane, etc.) (***Scheme 33***). Two examples of such intramolecular processes are incorporation of alkyl bromides electrophiles (e.g. **220**) or alcohol nucleophiles (e.g. **223**), tethered to the terminal end of the acrylamide moiety which could lead to complex polycyclic derivatives.



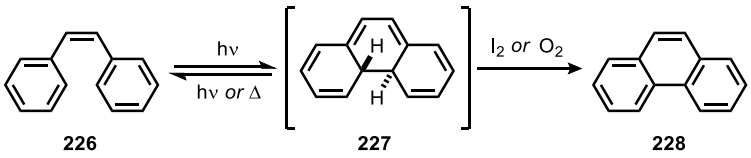

***Scheme 33**: Future directions based on trapping of zwitterionic intermediates*

# Chapter 3: Mechanistic investigations into visible-light-mediated photoeliminative cyclizations of *O*-iodo *N*-2-iodoaryl enaminones

## 3.1 Introduction

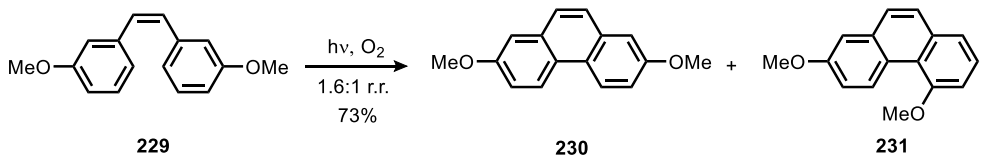
### 3.1.1 Photoeliminative cyclizations

Upon irradiation with UV-light, *cis*-stilbene **226** undergoes 6π electrocyclization to dihydrophenanthrene **227**. The resulting photochemical product is both thermally and photochemically unstable, being prone to reversion to starting material **226**. However, in 1964 Mallory discovered that irreversible oxidation of intermediate **227** to phenanthrene **228** can occur in high yields in the presence of molecular oxygen or iodine (***Scheme 34***).[129] Mechanistic investigations suggest that the reaction is undertaken preferentially in the $S_1$ state.




***Scheme 34**: Photochemical synthesis of phenanthrene from cis-stilbene*

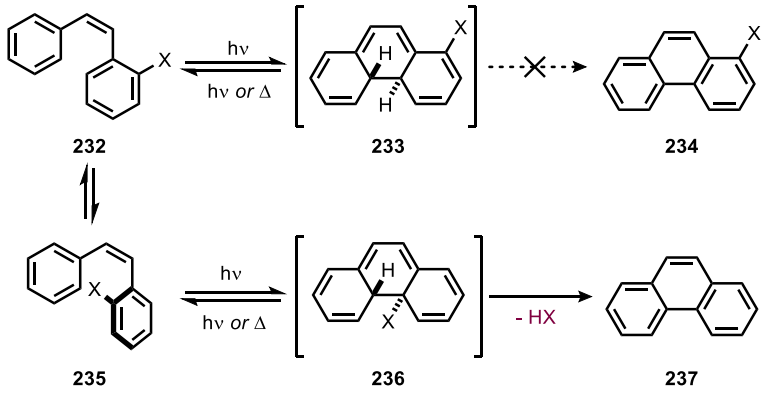
This procedure has found application in the synthesis of polyaromatic hydrocarbons of high structural complexity. Complications arise, however, when the *meta*-positions of one or both of the phenyl rings are differentially substituted; in these cases, mixtures of regioisomers are generally formed, as in the synthesis of **230** and **231** from stilbene **229** (***Scheme 35***).[130]




***Scheme 35**: Generation of a regioisomeric mixture of phenanthrenes form a meta-substituted stilbene*

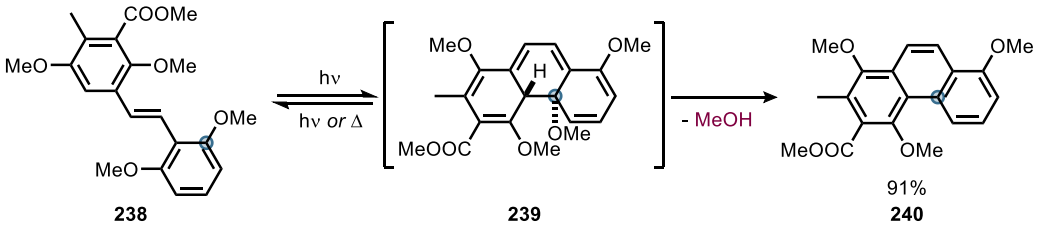
Intriguing behaviour has been observed when substrates bearing an *ortho*-substituent are irradiated in the absence of an external oxidant (***Scheme 36***). Depending on the nature of the *ortho*-substituent 'X', the intermediate **236** resulting from *ipso*-X cyclization can undergo

elimination, resulting in the irreversible formation of phenanthrene **237** in preference to the *ipso*-H cyclization product **234**. In such cases, the *ortho*-substituent acts as both a traceless directing group and an internal oxidant, with regioselectivity arising from the preference of intermediate **233** – formed by *ipso*-H cyclization – to undergo retro-cyclization in the absence of an external oxidant.[131]



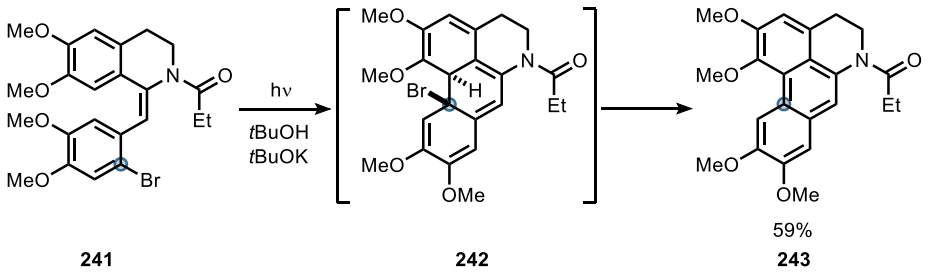

***Scheme 36**: Proposed mechanism of eliminative photocyclization of ortho-substituted stilbenes in the absence of oxidants*

One example is the photocyclization of stilbene-derivative **238**, which upon cyclization and elimination of methanol leads to phenanthrene **240** in 91% yield (***Scheme 37***).[132]




***Scheme 37**: Photoeliminative cyclization of stilbene **238***

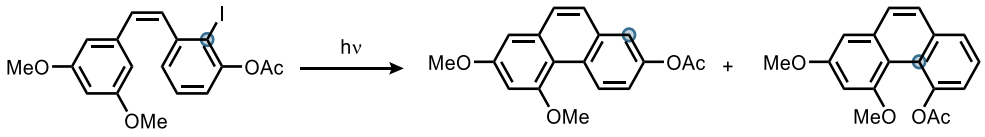
Similarly, *ortho*-bromo substituents can undergo elimination in stilbene photocyclizations (***Scheme 38***). In the presence of base, irradiation of **241** leads to the formation of the polycyclic aromatic compound **243** with elimination of the elements of HBr in 59% yield. The reaction performs best when *t*BuOK is present in the reaction mixture, providing evidence for a bimolecular elimination (E2) mechanism.[133]




241 242 243

***Scheme 38**: Photoeliminative cyclization of ortho-bromo stilbenes.*

When halogens or other photolabile groups are used as *ortho*-substituents, an alternative mechanism involving radical cyclization following homolytic bond cleavage is possible. Such a mechanism is likely operative in the UV-photocyclization of *ortho*-iodo-substituted stilbenes. For example, irradiation of *ortho*-iodo stilbene **244** leads to the formation of a regioisomeric mixture of phenanthrenes **245** and **246**, both of which lack iodo substituents (***Scheme 39***).[134]

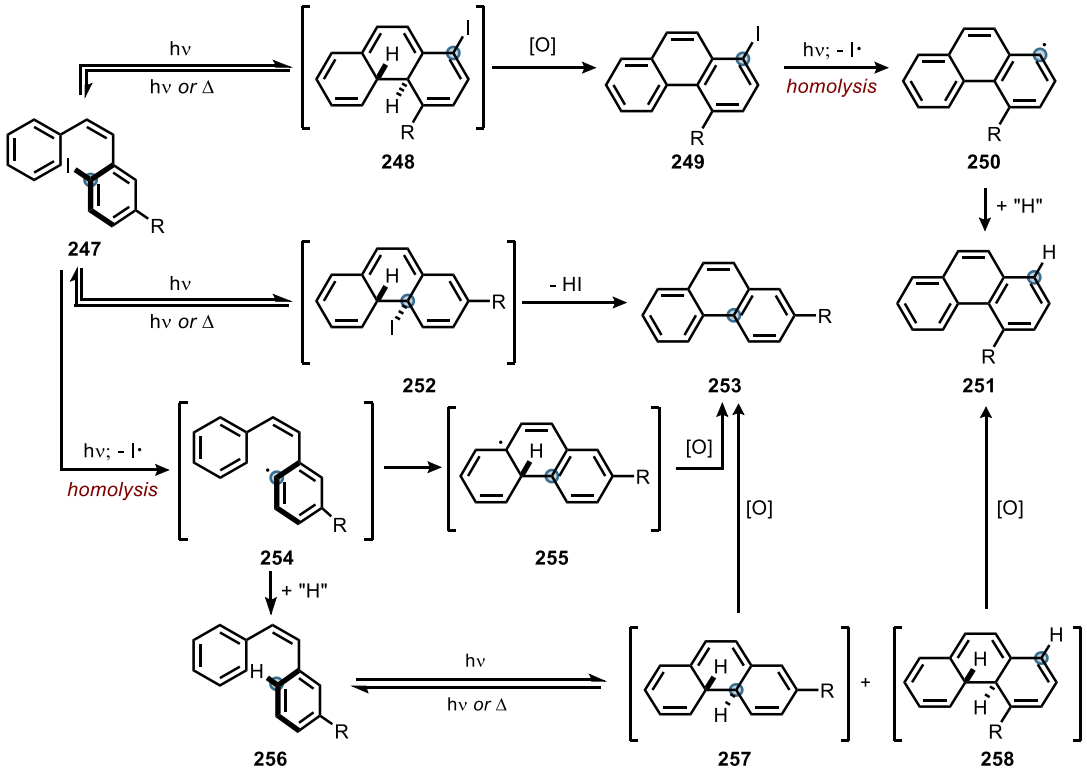



**244** **245** **246**

***Scheme 39**: Photoeliminative cyclization of ortho-iodo stilbenes*

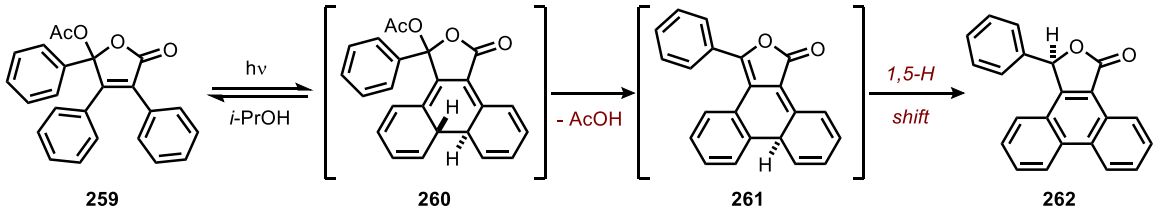
Mechanistically, phenanthrene **251** could be formed *via ipso*-H cyclization of **247** to the dihydrophenanthrene **248** followed by oxidation by trace molecular iodine or other iodine-containing species (***Scheme 40***). The resulting product could then undergo homolysis under the UV-irradiation conditions to form radical **250**, which could then abstract a hydrogen atom from a solvent molecule, leading to the hydrodeiodinated product **251**. Similarly, it could be argued that the iodinated starting material **247** itself undergoes homolysis, leading to radical **254**. Subsequent cyclization and oxidation *via* intermediate **255** would lead to the opposite regioisomer **253**. Another possibility is that the aryl radical **254** abstracts a hydrogen atom from solvent, leading to the hydrodehalogenated stilbene **256**, which then undergoes photocyclization and oxidation by trace iodine-containing species, leading to a mixture of

phenanthrenes **251** and **253**. Since the above pathways lead to the same two products, it is difficult to discern the true reaction mechanism; indeed, all these proposed mechanisms could operate in parallel.



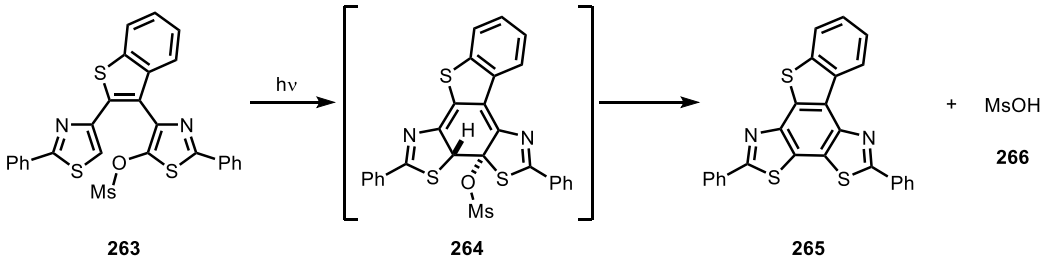

***Scheme 40**: Potential mechanistic pathways for the photochemical cyclization of ortho-iodo stilbenes*

Photoeliminative transformations are not limited to substrates bearing *ortho*-substituents. Stilbene derivative **259**, for instance, undergoes photocyclization with elimination of an *exocyclic* acetoxy substituent. Like the stilbene examples above, irradiation of **259** in isopropanol leads to the formation of a dihydrophenanthrene intermediate (**260**). In this example, however, elimination of the exocyclic acetoxy group leads to the cross-conjugated polyene **261**, which must undergo a subsequent 1,5-H shift to furnish phenanthrene derivative **262**.[135]



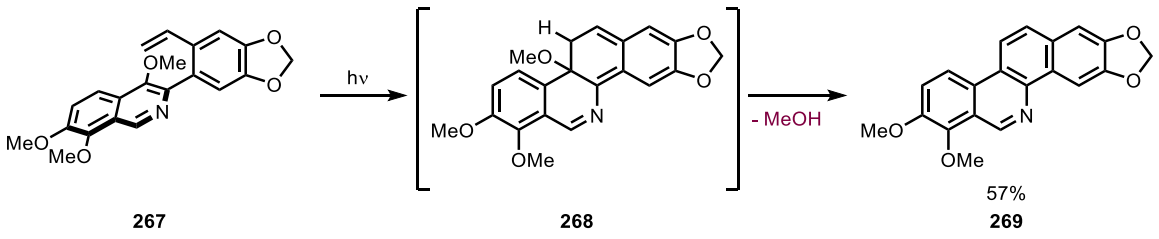

***Scheme 41**: Photoeliminative cyclization of stilbenes with exocyclic substituents*

Photoeliminative cyclizations are also not limited to stilbene-based scaffolds. For instance, the photocyclization of 1,2-disubstituted benzothiophene **263** proceeds with elimination of methanesulfonic acid (**266**). Compounds such as **263** thus have potential applications as photoacids in microlithography and as photoinitiators in polymerization reactions (**Scheme 42**).[136-137]

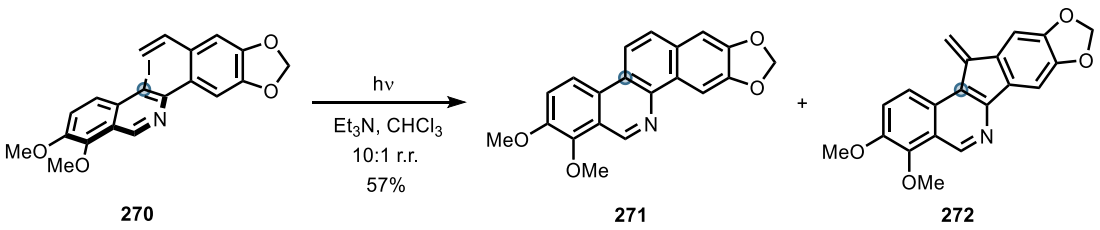



***Scheme 42**: Example of a photoeliminative cyclization in other 6π systems*

Another scaffold that has been shown to undergo photoeliminative cyclization is the 2-aryl-styrene motif. Irradiation of the isoquinoline derivative **267** leads to the formation of natural product norchelerythrine **269** in 57% yield *via* loss of methanol (***Scheme 43***).[138] Similarly, an iodinated analogue **270** leads to the formation of **269** as the major product; however, this was formed alongside regioisomer **271** as a 10:1 mixture in a combined yield of 57% (***Scheme 44***).[139] The formation of exocyclic by-product **271** from iodinated precursor **270**, but not from the methoxy-substituted analogue **267**, suggests that a mechanism involving a homolytically formed aryl radical is operative, though a competing 6π-type photoeliminative pathway cannot be discarded.

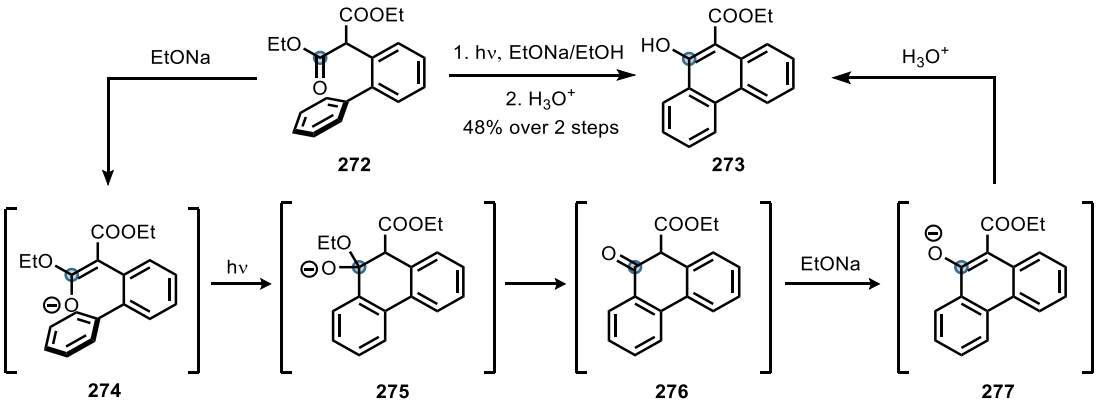



***Scheme 43**: Photoeliminative cyclization of methoxy-substituted 2-aryl-styrene motif*




***Scheme 44**: Photoeliminative cyclization of iodo-substituted 2-aryl-styrene motif*

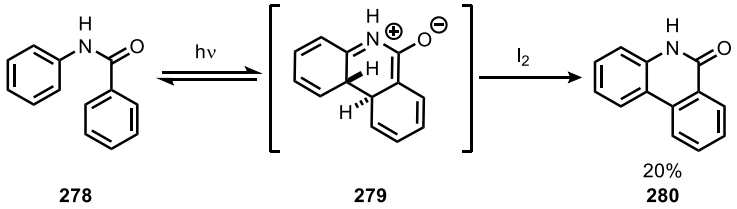
Enols can also participate in electrocyclizations. Like 2-aryl-styrenes, biaryl systems containing an enolizable homo-carbonyl substituent at the *ortho*-position undergo 6π photocyclizations. For example, irradiating malonic acid derivative **272** in presence of sodium ethoxide in ethanol leads to the formation of tetrahedral intermediate **275**, which collapses to β-keto-ester **276**. Subsequent deprotonation and protonation steps generate phenanthrene derivative **273** in 48% yield, in an overall photoeliminative process (***Scheme 45***).[140]



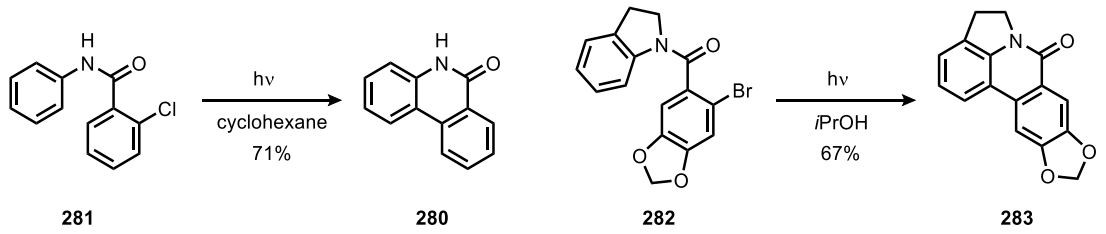

***Scheme 45**: Photoeliminative cyclization of enolates*

*N*-Benzoyl anilines typified by substrate **278** are also capable of 6π electrocyclizations. As in the photocyclization of stilbenes, an external oxidant can be used to drive re-aromatization of the direct photoproduct, leading in the case of **278** to the formation of phenanthridone **280** in a modest 20% yield (***Scheme 46***).[141] Introducing a suitable leaving group at the *ortho*-position of the benzoyl group not only circumvents the need for an external oxidant, but also dictates the regiochemical outcome of the cyclization. Thus, irradiation of 2-chloro-*N*-phenylbenzamide **281** in cyclohexane leads to the isolation of phenanthridone **280** in an improved 71% yield.[142] Replacing the chloro substituent in **281** with iodine is detrimental,

leading to low yields. Under these conditions, homolysis of the highly labile C–I bond competes with the photocyclization, leading to the formation of *N*-benzoyl aniline **278** as the major product *via* hydrogen abstraction from the solvent to the intermediate aryl radical.[141] However, yields can be improved by careful choice of solvent.[143] On the other hand, *ortho*-bromo substrates perform well upon irradiation in alcoholic solvents; substrate **282**, for example, cyclizes regioselectively in 67% yield to form the natural product anhydrolycorine-7-one **283** (***Scheme 47***).[144]

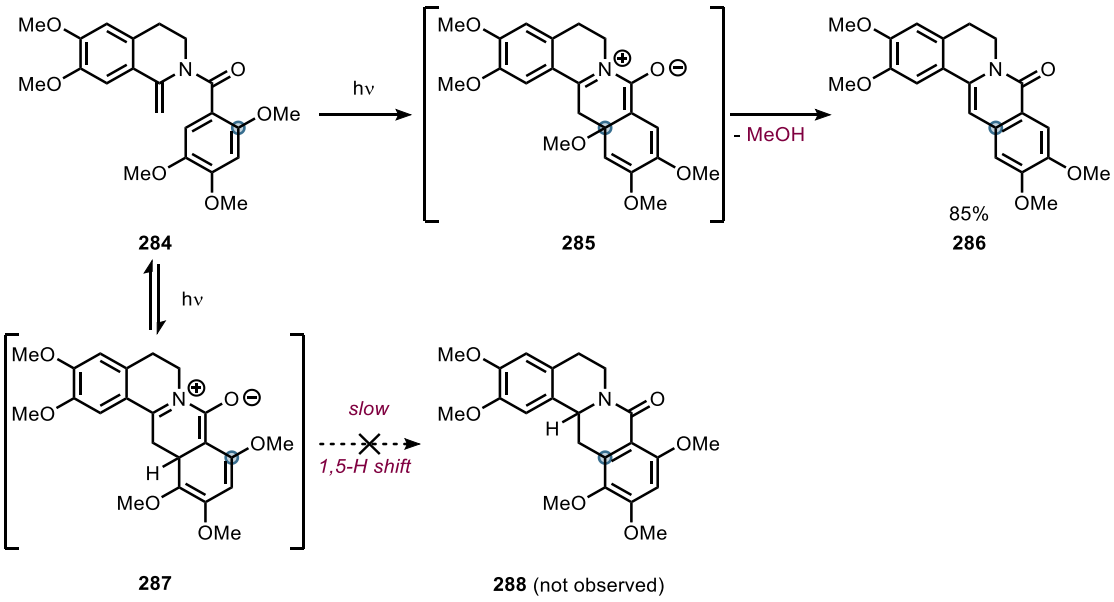



***Scheme 46****: Photochemical synthesis of phenanthridone N-benzoyl aniline*



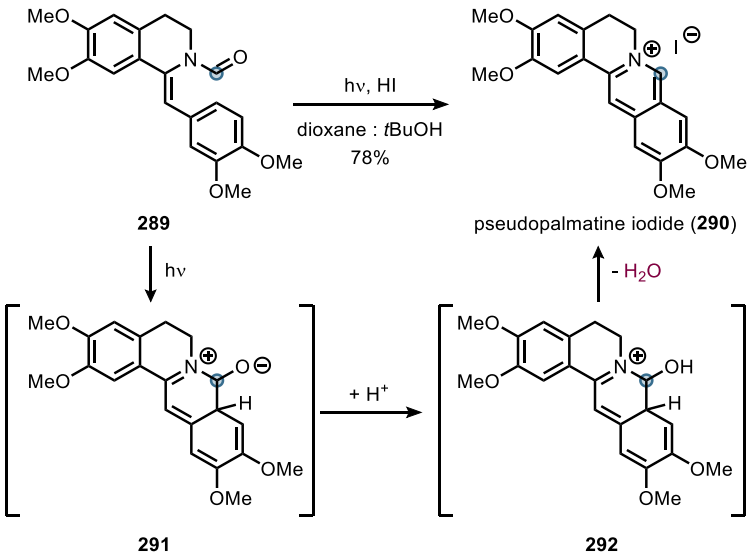

***Scheme 47****: Photochemical syntheses of phenanthridones*

Akin to *N*-benzoyl anilines, *ortho*-substituted *N*-benzoyl enamines can undergo photoeliminative cyclization. Irradiation of *ortho*-methoxy substituted *N*-benzoyl enamine derivative **284** leads to the isolation of tetrahydroisoquinolinone **286** in a very good yield of 85% *via* loss of methanol. Intriguingly, though 1,5-H shifts are known to occur from zwitterionic intermediates resembling **287** in other photocyclizations, the *ipso*-H cyclization product **288** was not observed upon irradiation of **284**. It has been proposed that the 1,5-H shift from the *ipso*-H intermediate **287** to product **288** is slow relative to the retro-cyclization of **287** back the starting material **284**.[145]



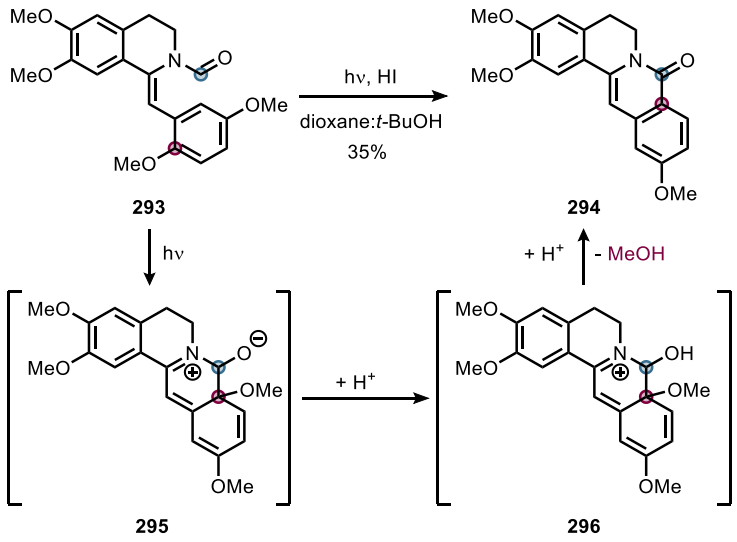

***Scheme 48**: Photoeliminative cyclization of N-benzoyl enaminones*

*N*-Formyl enamides display similar excited state reactivity. Irradiation of *N*-formyl enamides, typified by **289,** in the presence of hydroiodic acid provides access to the berberine and related alkaloid cores in exceptionally high yields. The synthesis of pseudopalmatine iodide **290** from **289**, for example, is believed to proceed *via* cyclization of the arene onto the amide carbon, followed by protonation and acid catalysed elimination of water (***Scheme 49***).[146] Similarly, other amides besides formamides have been shown to be compatible.[147]



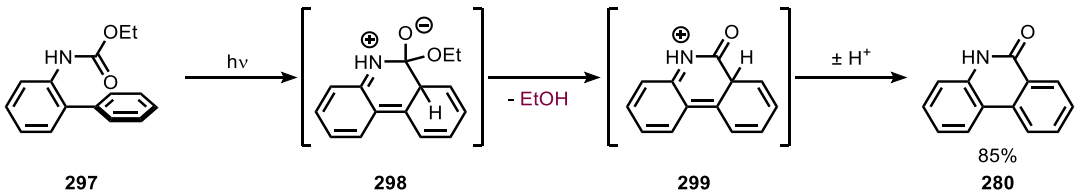

***Scheme 49**: Photoeliminative cyclization of N-formyl enamides*

Interestingly, substrate **293**, bearing an *ortho*-methoxy substituent on the aryl system, cyclizes *via* the vicinally oxygenated intermediate **295**, leading to the isolation of isoquinolinone derivative **294** in 35% yield upon protonation and elimination of methanol (***Scheme 50***).[146]



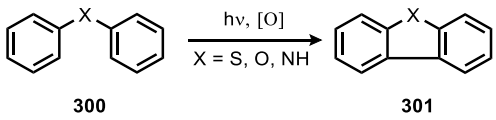

***Scheme 50**: Photoeliminative cyclization of N-formyl enamides*

Similarly, carbamates have been shown to undergo photoeliminative cyclization. Irradiation of *ortho*-carbamate-containing biphenyl **297** led to the isolation of phenanthridone **280** in 85% yield (***Scheme 51***).[148]




***Scheme 51**: Photoeliminative cyclization of ortho-carbamate-containing biaryls*

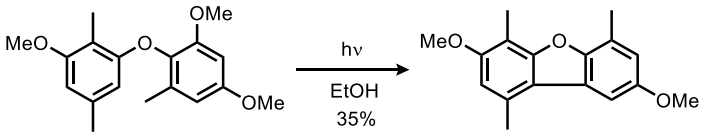
Substrates where one of the π-bonds has been replaced with a heteroatom linker can also undergo 6π photocyclization, leading to the formation of five-membered heterocycles. These reactions proceed smoothly for (thio)ethers and amines when an external oxidant is used (***Scheme 52***). Despite many examples of oxidative photocyclization for both classes of substrate, relatively few examples of photoeliminative cyclizations have been reported for five-membered ring formation compared to six membered ring formation.[149-151]




**300** **301**

***Scheme 51****: Oxidative 6π electrocyclization of heteroatom-bridged biaryls*

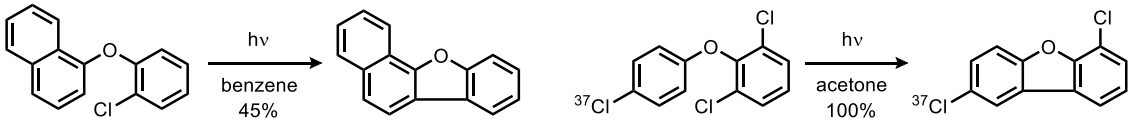
For example, diaryl ethers undergo photocyclization with elimination of methanol when all but one of the *ortho*-positions is blocked – as in **302** – though the yields of the resulting dibenzofurans are generally low (***Scheme 52***).[152]




**302** **303**

***Scheme 52****: Photoeliminative cyclization of ortho-methoxy substituted diaryl ethers*

Examples of successful eliminative photocyclizations of diaryl ethers bearing *ortho*-chloro substituents are known (***Scheme 53***).[153] Mechanistically, however, it is not clear if these reactions proceed *via* a homolytic or photoeliminative pathway (or both). One interesting example occurs upon irradiation of substrate **306**, which bears an isotopically enriched *para*-chloro substituent (***Scheme 53***). Sensitization by acetone leads to quantitative generation of dibenzofuran **307** *via* the $T_1$ state.[154] The high yield of this product, which retains two C–Cl bonds, suggests that the reaction does not proceed via an aryl radical formed by C–Cl homolysis.

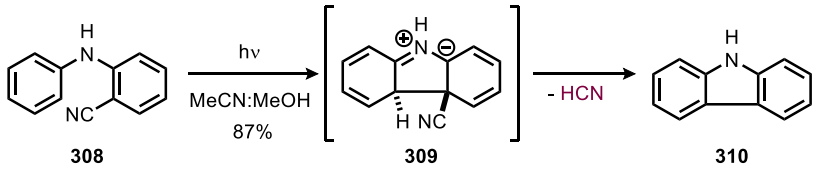



**304** **305** **306** **307**

***Scheme 53****: Cyclization of ortho-chloro substituted biaryl ethers*

Diarylamines bearing *ortho*-chloro substituents lead to the formation of carbazoles in the presence of base; however, these reactions have been proposed to proceed *via* an aryl radical.[155] Intriguingly, irradiation of *ortho*-cyano derivative **308** also leads to the formation

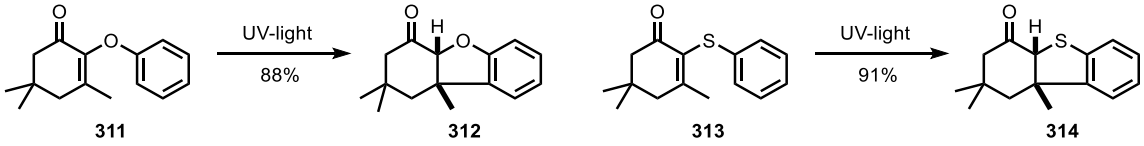
of carbazole **310**, presumably *via* elimination of hydrogen cyanide from intermediate **309** (***Scheme 54***).[156]




***Scheme 54****: Synthesis of carbazoles from ortho-cyano diarylamines*

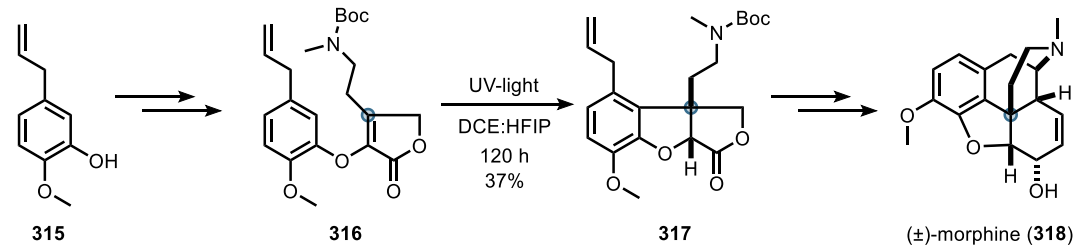
### 3.1.3 Project Aim

Another variation of a heteroatom containing 6π-photocyclization was developed by Schultz and co-workers. Over the course of several papers, the authors reported the UV-light mediated photocyclization of 2-aryloxycyclohexenones **311** and 2-arylthiocyclohexenones **313,** leading to the formation of *cis*-fused dihydrobenzofurans **312** and dihydrobenzothiophenes **314**, respectively (***Scheme 55***).[157-159]



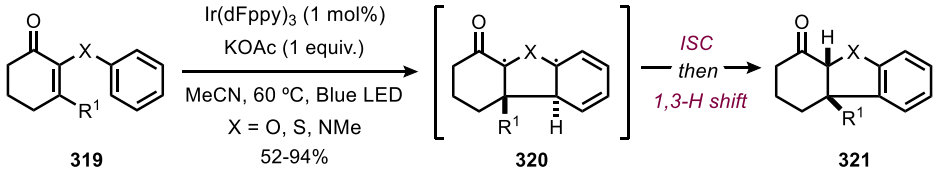

***Scheme 55***: Examples of *6π photocyclizations of 2-aryloxycyclohexenones (left) and 2-arylthiocyclohexenones (right)*

The protocol disclosed by Schultz was later exploited by the Smith group in the total synthesis of (±)-morphine (**318**). Irradiation of **316** with UV-light leads to the formation of the polycyclic lactone **317** in 37% yield, a key synthetic intermediate which was elaborated in a further four steps to the natural product (***Scheme 56***).[160]

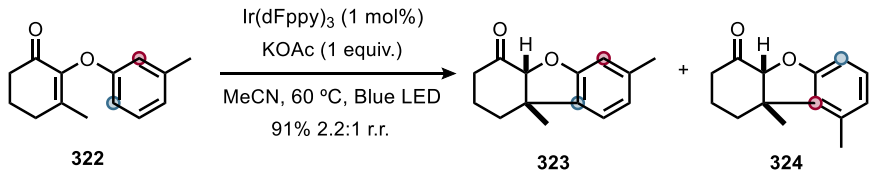



***Scheme 56***: *Total synthesis of (±)-morphine via a 6π photocyclization*

The modest yield of polycyclic lactone **317** prompted the Smith group to develop milder conditions to effect this valuable transformation. To this end, Münster *et al.* discovered that an iridium photocatalyst can be used as a triplet sensitizer in combination with blue light to promote the 6π heterocyclization of substrates such as **319**.[118] The photocatalytic conditions tolerate a wide range of functional groups, enabling the synthesis of diverse C($sp^3$)-rich heterocyclic scaffolds in high yields. Despite these improvements, one major drawback that remained was the poor regioselectivity obtained with respect to the arene cyclization site for this triplet-state reaction (***Scheme 58***).

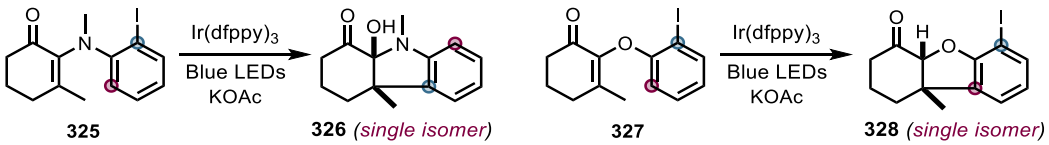



***Scheme 57***: *Visible light mediated 6π photocyclization*




***Scheme 58***: An example of a *6π-photocyclization leading to a mixture of regioisomers*

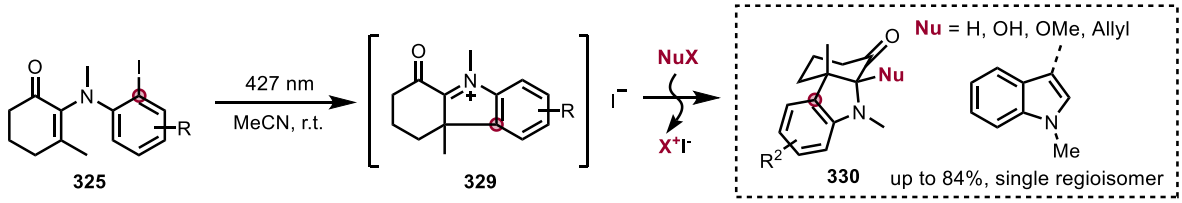
During further investigations of the reaction scope and limitations (***Scheme 59***), 2-((2-iodoaryl)amino)cyclohexenones such as **325** displayed divergent reactivity, leading to the formation of deiodinated hemiaminal **326**. In contrast, 2-iodophenoxy analogue **327** leads to the expected isomerization product **328** upon sensitization.




***Scheme 59***: *Divergent reactivity of 2-substituted enones **325** and **327***

The presence of a hemiaminal group suggested that the reaction could proceed *via* the corresponding iminium ion **329**, that is trapped by water found in the reaction medium. We hypothesized that hemiaminal **326** arose from hydrolysis of the corresponding iminium ion.

This idea was substantiated by the successful formation of iminium trapping products with a wide range of carbon- and heteroatom-centred nucleophiles from the same substrate in the absence of base (***Scheme 60***). Furthermore, it discovered that a triplet sensitizer is not required for this reaction when high-powered 427 nm LEDs are used.




***Scheme 60***: *Synthesis of fully substituted indolines by direct irradiation of **325**; Reaction was developed by Zachariah Lockhart*

Due to the unique mode of reactivity exhibited by these substrates, we decided to investigate the mechanism of this photochemical reaction using computational techniques. We hoped to understand the origin of regioselectivity, with a view to informing the discovery of new photoeliminative cyclizations.

## 3.2 Results and Discussions

### *3.2.1 Geometry Benchmarking*

To our knowledge, no in-depth computational studies have been performed on photoeliminative transformations. As such, a range of different types of functionals were chosen for this investigation: a GGA (B97-D3(BJ)[161]), hybrid-GGA (B3LYP-D3(BJ)[41-44]), hybrid-meta-GGA (M06-2X-D3[35]), as well as range separated functionals (ωB97XD[98], CAM-B3LYP-D3(BJ)[162], LC-ωHPBE[163-166]). Appropriate dispersion corrections were included in all the calculations based of previous benchmarking studies,[36] except for LC-ωHPBE, where dispersion corrections options were not available for the in the default version of Gaussian16.[167] The M06-2X, B3LYP, ωB97XD, CAM-B3LYP were chosen as representative of each family of functionals as they have been previously used in the study of photochemical transformations.[21, 101, 117-118] The B97D-D3(BJ) functionals was chosen as one

of the best performing GGA-type functionals according to previous benchmarking studies,[36] while the LC-ωHPBE was also included as it does not include any Hartree-Fock (HF) exchange at short ranges, contrary to ωB97XD and CAM-B3LYP, which contain 22.2% and 19% HF exchange respectively.[98, 119, 162-166] All calculations included the implicit SMD[80-84] solvation model for acetonitrile. As the C–I bond in the starting material is broken during the reaction, we envisioned that an accurate description of C-I bond lengths is essential, and as such we began our investigation by identifying the best DFT level of theory to accurately describe the geometry of the starting materials. To this extent, an X-ray crystal structure of substrate **331** served as a benchmark against which computed bond lengths and angles were compared using the aforementioned functionals in conjunction with the Def2-TZVP[92-93] basis set. The results were compiled in **Table 9**:

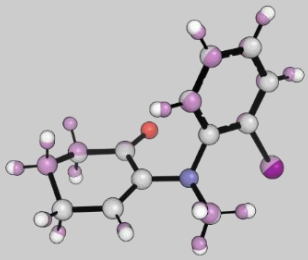
| Functional | $C-I$ | $C=O$ | $C=C$ | $C1-N$ | $C2-N$ | $C3-N$ | Superimposed Structures |
|---|---|---|---|---|---|---|---|
| **M06-2X-D3** | 2.092 (0.3%) | 1.212 (0.7%) | 1.344 (0.2%) | 1.405 (0.7%) | 1.425 (0.1%) | 1.457 (0.7%) |  **331** |
| **B3LYP-D3(BJ)** | 2.113 (0.7%) | 1.219 (0.1%) | 1.350 (0.6%) | 1.404 (0.8%) | 1.424 (0.2%) | 1.459 (0.6%) | |
| **ωB97XD** | 2.094 (0.2%) | 1.213 (0.6%) | 1.344 (0.2%) | 1.404 (0.8%) | 1.424 (0.2%) | 1.454 (1.0%) | |
| **CAM-B3LYP-D3(BJ)** | 2.094 (0.2%) | 1.213 (0.6%) | 1.341 (0.1%) | 1.402 (0.9%) | 1.422 (0.4%) | 1.453 (1.0%) | |
| **LC-ωHPBE** | 2.072 (1.2%) | 1.212 (0.7%) | 1.337 (0.4%) | 1.402 (0.9%) | 1.421 (0.4%) | 1.449 (1.3%) | |
| **B97D-D3(BJ)** | 2.127 (1.4%) | 1.227 (0.6%) | 1.360 (1.3%) | 1.406 (0.6%) | 1.426 (0.1%) | 1.464 (0.3%) | |
| **Experiment** | 2.098(3) | 1.220(4) | 1.342(4) | 1.415(3) | 1.427(3) | 1.468(3) | |

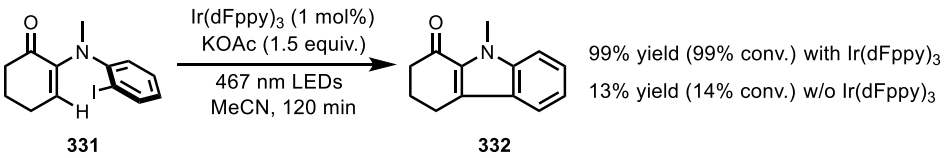
***Table 9**: Relevant bonds lengths obtained experimentally and computationally of **331**, together with superimposed chemical structure (grey – M06-2X-D3; purple – X-ray); variations between experiment and computation are presented in brackets*

Out of the six functionals explored, M06-2X-D3, ωB97XD and CAM-B3LYP-D3(BJ) gave the best description of the key C–I bond (showing <0.3% variation), with variations in the main structural bond lengths (C–C, C–O and C–N) also being minimal (<1.0%), while all other dihedral and bond angles proved to be in excellent agreement with the experimental structure. The next best description of the C–I bond length was provided by B3LYP-D3(BJ), with a variation of 0.7%. Considering that the SMD solvation model (SMD = acetonitrile) employed in the geometry optimizations represents a medium of different polarity to that of the bulk

crystal, and that crystal packing can also affect the geometries observed in X-ray structures, agreement between computed and experimental results is high across all four levels of theory. On the other hand, LC-ωHPBE and B97D-D3(BJ) lead to the largest variations in the description of the C–I bond length (1.2% and 1.4%, respectively), with B97D-D3(BJ) also displaying a significant variation in the enone C=C bond length of 1.3%. To save computational cost, out of the three best performing functionals, M06-2X-D3 was chosen to compute the potential energy surface of the transformation in question, as it has been previously used in the computational study a very similar system lacking the ortho-iodine substituent (**Scheme 57**),[118] thus allowing us to directly compare the two results. Furthermore, the M06-2X functional has been used extensively in the study of triplet state reactivity,[118, 122-126] and it has been shown to accurately describe radicals.[37-38] However, for key selectivity steps that arise thought this study, calculations will be recomputed using the entire ensemble of functionals chosen.

### *3.2.2 Mechanistic investigation*

As this transformation occurs under direct irradiation in the absence of a sensitizer, the reaction could proceed in either $S_1$ or $T_1$ states. Experimental collaborators have shown that the reaction of **331** is substantially accelerated in the presence of $Ir(dFppy)_3$ ($E_T$ = 60.3 kcal·mol$^{-1}$) when a 467 nm LED is used. Although this experiment proves that the reaction can occur efficiently in the $T_1$ state, a competing reaction in the $S_1$ state cannot be excluded. However, the identical product distribution in the presence and absence of a sensitizer, in addition to the efficiency of $S_1$-to-$T_1$ intersystem crossing reported for other cyclohexenones, point towards a transformation on the $T_1$ potential energy surface.




**331** **332**

***Scheme 61***: Rate acceleration in presence of $Ir(dFppy)_3$

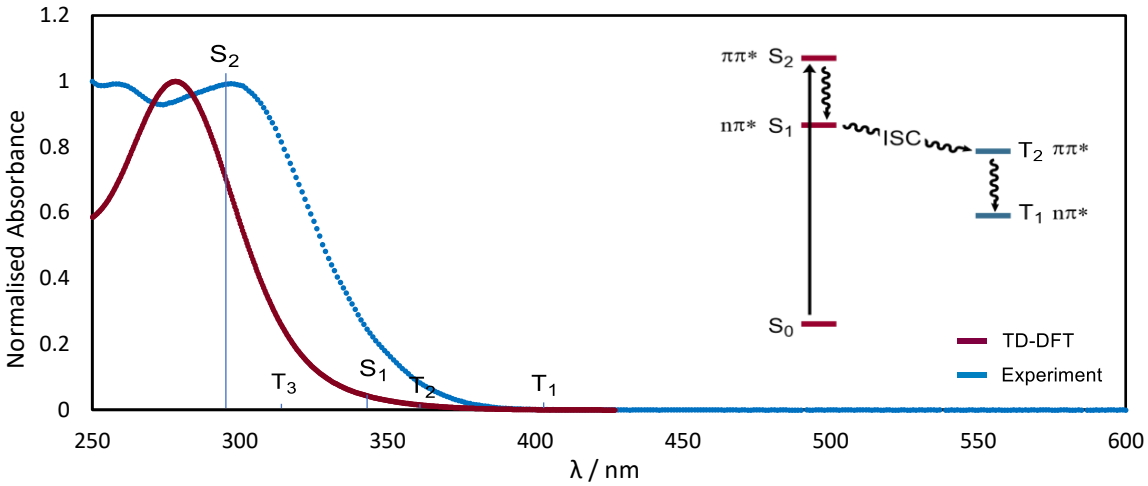



***Figure 28**: Experimental (blue) and TD-DFT (red) UV-Vis absorption spectra of compound **331** computed at the uM06-2X-D3/Def2 TZVP level of theory; Positions of the first two singlet and three triplet bands are indicated by vertical lines; A Jablonski diagram encompassing the proposed mechanistic summary of populating the $T_1$ state of substrate **331** is shown in the top right corner*

An experimental UV-Vis absorption spectrum of compound **331** obtained in acetonitrile (**Figure 28**, *blue outline*) exhibits a broad absorption band ($\lambda_{max}$ = 297 nm) tailing into the visible region and thus overlapping with the emission spectrum of the irradiation source used. To investigate the nature of the absorption, a UV-Vis absorption spectrum of **331** was simulated using DT-DFT at the uM06-2X-D3/Def2-TZVP level of theory with the solvation model for acetonitrile (**Figure 28,** *red outline*). The simulated spectrum was computed for the lowest energy conformer of substrate **331** and displayed an absorption maximum at 280 nm, which is off shifted by 17 nm from the experimentally determined spectrum. Analysis of the TD-DFT computed absorption bands (**Figure 28**) indicated that the absorption maximum at 280 nm corresponds to the $S_2$ state, while the $S_1$ state was found to weakly absorb at 322 nm. Three additional triplet bands were found at 302 nm, 351 nm and 396 nm corresponding to the $T_3$, $T_2$ and $T_1$ states, respectively. Based on these results, it can be assumed that excitation at approximatively 400 nm leads to the preferential population of the $S_2$ state *via* a ππ* transition, followed by rapid thermal relaxation *via* internal conversion to the nπ* $S_1$ state in accordance with Kasha's rule[5-6]. As the $S_1$ state possesses nπ* symmetry, while the $T_1$ and $T_2$ state possess nπ* and ππ* character, respectively, El Sayed's rule suggests that efficient intersystem crossing would take place preferentially between the $S_1$ and $T_2$ state,[168-169] followed by rapid

internal conversion to the $T_1$ state. Overall, these results are consistent with known photophysical behaviour of cyclic enones, and the process is summarised in the Jablonski diagram presented in **Figure 28**.[117, 170]

Having assigned the observed reactivity to the $T_1$ state, the mechanism of the diradical cyclization step immediately following intersystem crossing was investigated. For this investigation, the computational work was performed on substrate **325**, which differs from substate 331 through the presence of an additional methyl group at the 3-position of the eneone. We began by examining a photoeliminative pathway (***Figure 29***), where the triplet diradical **325-T₁** cyclizes onto the *ipso*-I carbon, forming 1,3-diradical intermediate **334-T₁**, from which elimination of an iodine radical then occurs. Similar behaviour has been previously reported in stilbene photocyclizations, albeit these reactions likely occur from an excited singlet state.[129]

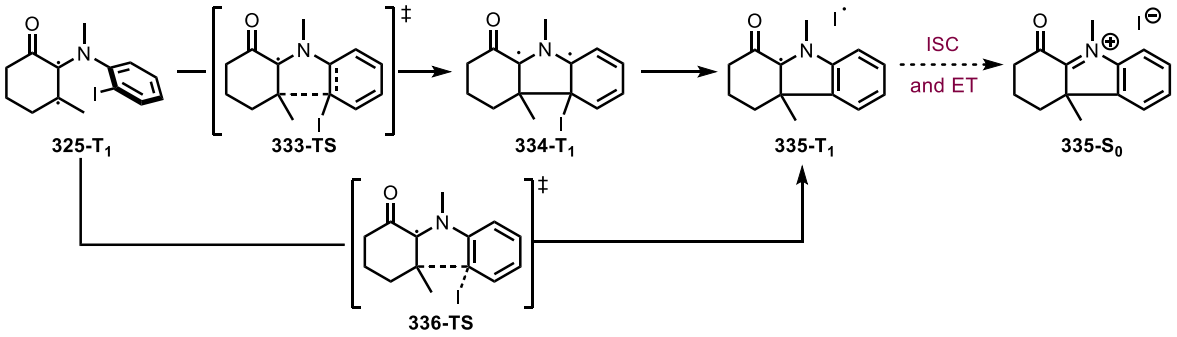



***Figure 29***: *Proposed photoeliminative mechanism of enaminone **331***

| Entry | $\Delta E$ | $\Delta ZPE$ | $\Delta H$ | $T\Delta S$ | $\Delta G$ |
|---|---|---|---|---|---|
| **325-S₀** | -50.7 | 1.2 | -49.7 | -1.4 | -48.3 |
| **325-T₁** | 0.0 | 0.0 | 0.0 | 0.0 | 0.0 |
| **333/336-TS** | 10.9 | -0.4 | 10.0 | -1.6 | 11.6 |
| **335-T₁** | -42.4 | 1.5 | -41.0 | -0.5 | -40.5 |
| **335** (*dissociated*) | -37.1 | 1.5 | -35.9 | 5.3 | -41.2 |
| **335-S₀** | -79.7 | 3.0 | -77.1 | -1.8 | -75.1 |

***Table 10***: *Boltzmann thermochemical parameters for the photoeliminative pathway in kcal·mol$^{-1}$ represented relative to **325-T₁**, performed at uM06-2x-D3/Def2-QZVPP(SMD=MeCN)//uM06-2x-D3/Def2-TZVP(SMD=MeCN) level of theory*

Using uM06-2x-GD3/Def2-QZVPP(SMD=MeCN)//uM06-2x-D3/Def2-TZVP(SMD=MeCN) level of theory, two transition states were found, with a Boltzmann average activation energy barrier of 11.4 kcal·mol$^{-1}$. Natural bond orbital (NBO) analysis of

the transition state connecting intermediates **325-T1** and **334-T1** revealed a Wiberg bond order (WBO) of 0.28 for the forming C–C bond, which is indicative of an early transition state. Intriguingly, the Wiberg bond order of the C–I bond was found to be 0.90, suggesting the partial bond breaking at the transition state. The weakening of the C–I bond is further reflected in the partial radical delocalization on the iodine atom, which displays a natural spin density of 0.13. From a molecular orbital theory perspective, the direct radical aromatic substitution mechanism would require population of the σ* orbital of the C–I bond. Indeed, second order perturbation theory analysis of the Fock matrix in the NBO calculations indicated donation into the C–I σ* bond from adjacent C–C σ and π bonds of the aromatic system worth 14.6 kcal·mol$^{-1}$. This can be also visualised in the SOMO1 and SOMO2 molecular orbitals using a Slater type basis set (STO-3G)[171-172] which indicates partial mixing of the C–I σ* orbital with the p orbital of the aromatic carbon (***Figure 30***). Considering that the transition state is early, these results can be interpreted as a direct radical substitution mechanism on an sp$^2$-hybridised aromatic carbon, rather than a stepwise mechanism involving radical σ-intermediate **334-T1**. On the other hand, the intrinsic reaction coordinates (IRC) of this transition state leads to a chemical structure that could be interpreted as a radical σ-intermediate, with an exceptionally long C–I bond of 2.78131 Å (***Figure 31***). Since subsequent attempts at optimising this structure to a local minimum using small optimization steps ("opt=(maxstep=1)") were unsuccessful, indicating that this intermediate is not stable by DFT, leading instead to the fully dissociated intermediate **335-T1**.

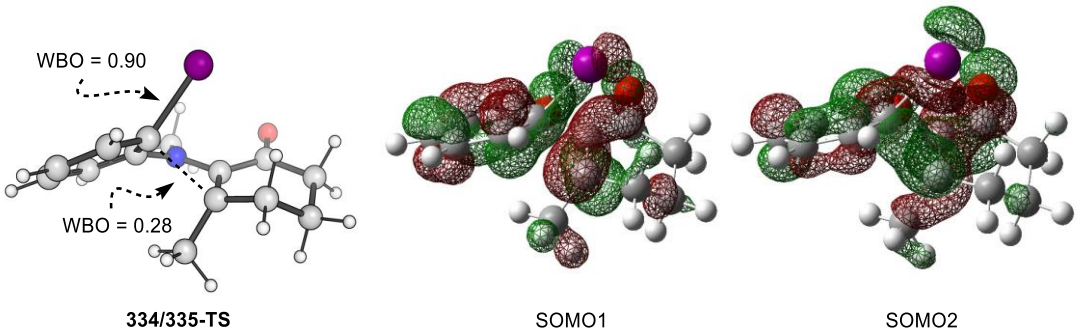



***Figure 30**: DFT optimised structure (left), SOMO1 (middle) and SOMO2 (right) of transition state **333/336-TS***

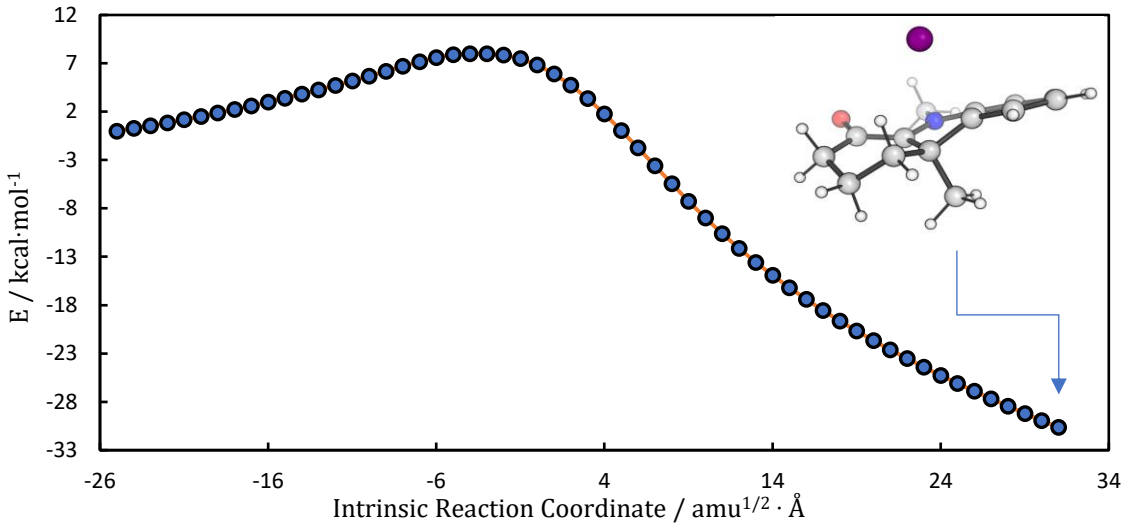



***Figure 31**: IRC plot for transition state **333/336-TS***

Similarities can be drawn between this mechanism and recently identified concerted nucleophilic aromatic substitutions described by Jacobsen.[173] It is unclear at this point if the process can be viewed as truly concerted or borderline-concerted case, involving a hidden σ-intermediate that undergoes barrierless elimination of the iodine radical. A similar radical aromatic substitution mechanism has been recently identified by Glorius and co-workers, where a thiyl radical undergoes direct displacement with a chloro-substituted imidazole.[174] To our knowledge, this latter example of a "concerted radical aromatic substitution" *via* direct displacement that has been previously identified.

The resulting radical pair **335** in the triplet state arising from *ipso*-I cyclization was found to be exceptionally stable relative to the triplet diradical precursor **325-$T_1$,** with a reaction free energy of -40.7 kcal·mol$^{-1}$. The high thermodynamic stability of intermediate **335-$T_1$** means the *ipso*-I cyclization pathway is effectively irreversible. When computed separately, the pair components of **335** were found to be enthalpically less stable than their associated form in the $T_1$ state by 5.1 kcal·mol$^{-1}$. However, when taking in consideration the change in entropy, the separated form of diradical **335** was found to be 0.7 kcal·mol$^{-1}$ more stable with respect to Gibbs free energy at a concentration of 1 mol·L$^{-1}$. Intersystem crossing from $T_1$ to $S_0$ *via* minimum energy crossing point **335-MECP** (***Figure 32***) followed by single-electron transfer

leads to the formation of iminium ion **335-S$_0$**, which is stabilised by an additional 34.7 kcal·mol$^{-1}$. The **335-MECP** was found to be only 0.8 kcal·mol$^{-1}$ higher in energy than its corresponding triplet structure. Coupled with large spin-orbit-coupling constant associated with a radical cantered on the heavy iodine atom, it is expected that the intersystem-crossing $T_1$ to $S_0$ to be very fast.

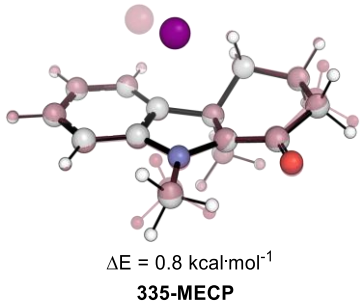



***Figure 32**: Diagram showing structural reorganization between **335-MECP** (gray) overlapped with that of precursor **334-T$_1$** (pink). MECP structure was computed by Dr. Juan Alegre-Requena*

Next, an intramolecular halogen atom transfer ('XAT') pathway was investigated. Recent work from the Leonori group has highlighted that α-amino radicals generated photochemically are capable of abstracting halogen atoms from aryl halides to generate aryl radicals.[175] Based on their observations, it was envisaged that the triplet diradical **325-T$_1$** might also be able to perform a similar process in an intramolecular fashion. This would result in the formation of β-iodo radical **338-T$_1$**, which might be expected to undergo spontaneous elimination, furnishing intermediate **340-T$_1$**. The aryl radical **340-T$_1$** thus formed could then undergo a 5-*endo*-trig cyclization to form radical pair **335-T$_1$**, which, upon intersystem crossing and single-electron transfer, would give the experimentally observed iminium ion **335-S$_0$**.

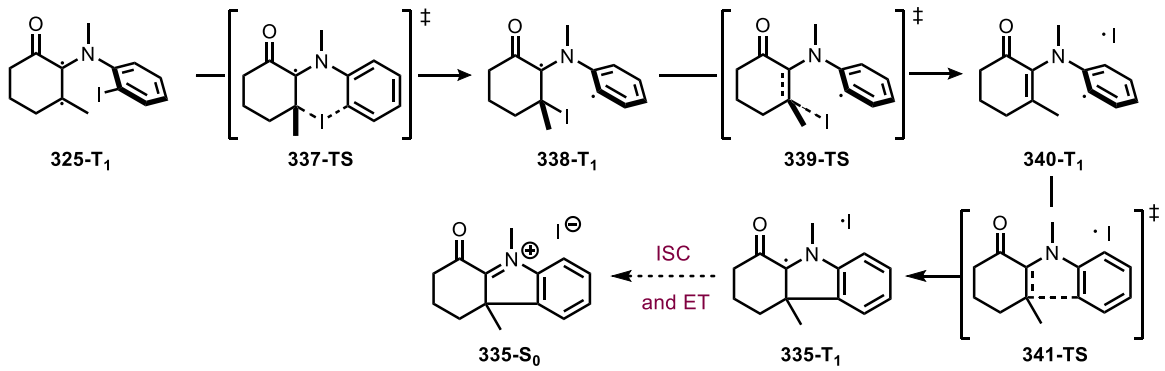



***Figure 33**: Proposed mechanism for an intramolecular halogen atom transfer pathway*

Computational investigations into this proposed pathway indicated two possible transition states **337-TS_a** and **337-TS_b**, differing with respect to the cyclohexyl radical ring conformation (***Figure 34***). Thermochemical analysis of these two structures (***Table 11***) indicates activation energy barriers of 22.8 kcal·mol$^{-1}$ and 24.3 kcal·mol$^{-1}$, respectively. While a barrier of 22.8 kcal·mol$^{-1}$ is surmountable under the reaction conditions, it is more than 10 kcal·mol$^{-1}$ higher than that of the radical aromatic substitution pathway. As such, no further investigations into this mechanism were conducted.

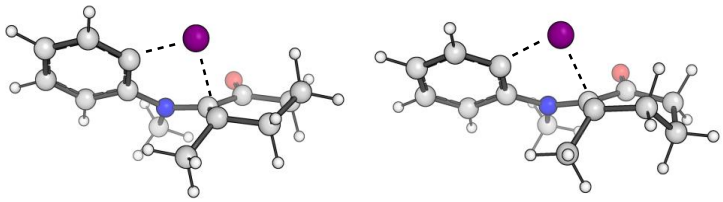



***Figure 34***: *Transition states for intramolecular halogen atom transfer*

| Entry | $\Delta E$ | $\Delta ZPE$ | $\Delta H$ | $T\Delta S$ | $\Delta G$ |
|---|---|---|---|---|---|
| **325-T$_1$[a]** | 0.0 | 0.0 | 0.0 | 0.0 | 0.0 |
| **337-TS_a** | 21.2 | 0.3 | 20.7 | -2.1 | 22.8 |
| **337-TS_b** | 22.5 | 0.5 | 22.2 | -2.2 | 24.3 |

***Table 11***: *Thermochemical parameters for halogen atom transfer in kcal·mol$^{-1}$ represented relative to **325-T$_1$**, performed at uM06-2X-D3/Def2-QZVPP(SMD=MeCN)//uM06-2X-D3/Def2-TZVP(SMD=MeCN) level of theory; [a] thermochemical parameters Boltzmann averaged over two conformers*

Aryl radical **340-T$_1$** (or its equivalent singlet diradical) could be formed *via* homolytic cleavage of the C–I bond (***Figure 35***). Such reactivity is well precedented under UV-irradiation, as bond dissociation enthalpies for aryl iodides have been determined to be around 65 kcal·mol$^{-1}$,[176] which is smaller than the energy provided by UV-photons. Computed C–I bond energies on our system lead to an estimated bond dissociation enthalpy of 59.3 kcal·mol$^{-1}$. As the experimental light source used emits photons with energies up to 71.5 kcal·mol$^{-1}$, the overall energetics transformation is thermodynamically feasible.

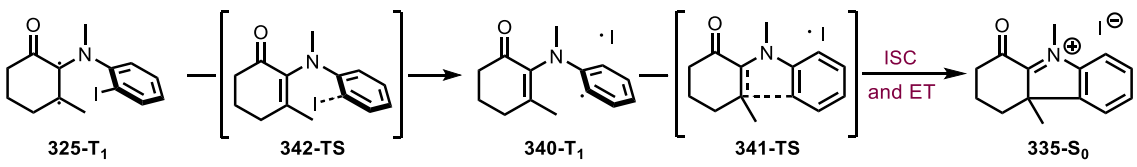



***Figure 35***: *Proposed mechanistic pathway via homolytic cleavage of C–I bond*

To further investigate the possibility of a homolysis mechanism, a radical clock experiment was devised in collaboration with experimentalists. It was envisioned that if radical **340-T$_1$** was formed during the reaction, an intramolecular alkene trap would provide evidence for its presence. To this end, substrate **347** was identified as a promising candidate and studied at the uM06-2x-GD3/Def2QZVPP(SMD=MeCN)//uM06-2x-GD3/Def2TZVP(SMD=MeCN) level of theory (***Figure 36***, ***Scheme 62***). A total of eight transition states were sampled for the 5-*exo*-trig pathway, while four transition states were identified for the 5-*endo*-trig pathway (***Table 12***). These results indicate that under a Curtin-Hammett scenario, a 90:10 ratio between 5-*exo*-trig and 5-*endo*-trig cyclization products would be expected from aryl radical **342**.

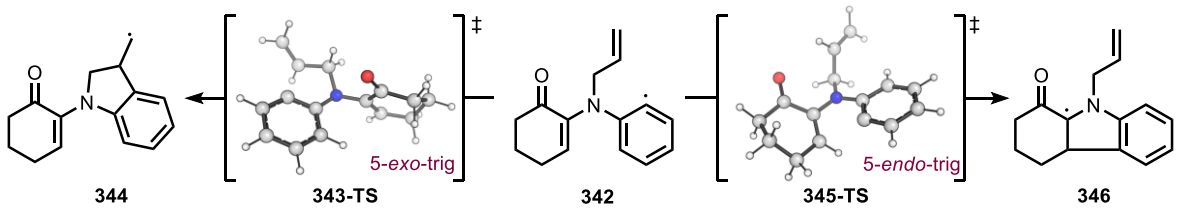
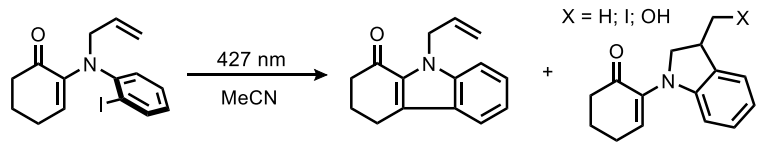



***Figure 36**: Proposed radical trap experiment*

| Entry | $\Delta E$ | $\Delta ZPE$ | $\Delta H$ | $T\Delta S$ | $\Delta G$ |
|---|---|---|---|---|---|
| **346** | -53.2 | 1.7 | -52.0 | -1.0 | -51.0 |
| **345-TS** | 5.7 | -0.7 | 4.6 | -0.6 | 5.2 |
| **342** | 0.0 | 0.0 | 0.0 | 0.0 | 0.0 |
| **343-TS** | 4.5 | -0.9 | 3.2 | -0.7 | 3.9 |
| **344** | -31.0 | -0.3 | -31.5 | -0.3 | -31.2 |

***Table 12**: Boltzmann averaged thermochemical parameters for radical trapping experiment in kcal·mol$^{-1}$ represented relative to **442**, performed at uM06-2x-D3/Def2-QZVPP(SMD=MeCN)//uM06-2x-D3/Def-2TZVP(SMD=MeCN) level of theory*

Substrate **347** was therefore synthesised by experimental collaborators and irradiated with blue light in presence of Ir(dFppy)$_3$. Upon analysis of the crude reaction mixture, indole **348** was identified as the sole reaction product; no 5-*exo*-trig derivatives such as **349** were present (***Scheme 62***). These results provide compelling evidence against the homolysis hypothesis, leaving the radical aromatic substitution pathway as the most promising mechanistic candidate.




| | | | |
|---|---|---|---|
| Predicted Homolysis: | 10 | : | 90 |
| Predicted Photoeliminative: | 100 | : | 0 |
| Experiment: | >95 | : | 5 |

***Scheme 62**: Radical clock experiment used to probe the presence of aryl radicals*

### *3.2.3 Origin of regioselectivity*

Having identified the main mechanistic pathway, two key questions remain, namely: the origin of regioselectivity in the cyclization; and the divergent reactivity of this substrate relative to its *O*-linked analogue **327**. To this end, the *ipso*-H cyclization pathway for substrate **325** was also studied by DFT using the uM06-2X-D3/Def2-QZVPP(SMD=MeCN)//uM06-2X-D3/Def2-TZVP(SMD=MeCN) level of theory (***Figure 37***, ***Table 13***).

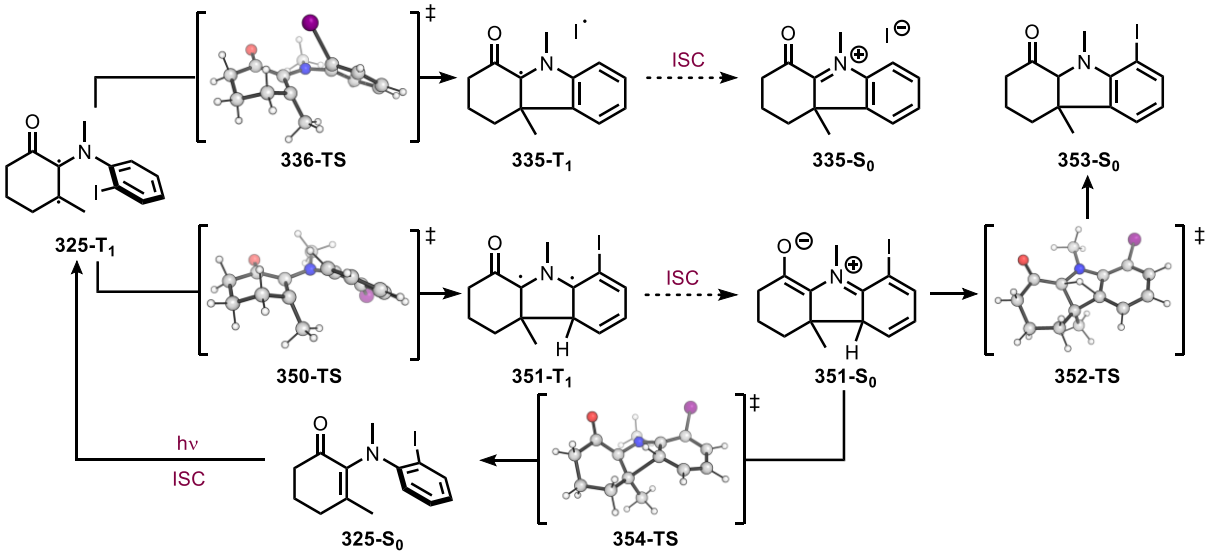



***Figure 37**: Competing mechanistic pathways for the competing ipso-I and ipso-H cyclizations*

| Entry | $\Delta E$ | $\Delta ZPE$ | $\Delta H$ | $T\Delta S$ | $\Delta G$ |
|---|---|---|---|---|---|
| **325-T1** | 0.0 | 0.0 | 0.0 | 0.0 | 0.0 |
| **336-TS** | 10.9 | -0.4 | 9.9 | -1.6 | 11.6 |
| **350-TS** | 11.1 | -0.2 | 10.2 | -1.8 | 12.0 |
| **335-T₁** | -42.4 | 1.5 | -41.1 | -0.5 | -40.7 |
| **351-T₁** | -6.1 | 0.8 | -6.0 | -2.1 | -3.9 |
| **335-S₀** | -79.7 | 2.8 | -77.2 | -2.0 | -75.1 |
| **351-S₀** | -17.2 | 2.0 | -16.1 | -3.1 | -12.9 |
| **352-TS** | 7.0 | -1.1 | 5.0 | -2.9 | 8.0 |
| **354-TS** | 6.5 | 0.1 | 5.8 | -2.8 | 8.7 |
| **353-S₀** | -57.6 | 2.8 | -55.8 | -3.3 | -52.4 |

***Table 13**: Boltzmann averaged thermochemical parameters in kcal·mol$^{-1}$ represented relative to **325-T₁**, performed at uM06-2X-D3/Def2-QZVPP(SMD=MeCN)//uM06-2X-D3/Def2-TZVP(SMD=MeCN) level of theory*

By comparing transition states **336-TS** and **350-TS**, a difference of only -0.4 kcal·mol$^{-1}$ was observed in favour of the *ipso*-I cyclization pathway. Considering the fact that only *ipso*-I products derived from iminium ion **335-S$_0$** have been identified experimentally, this 0.4 kcal·mol$^{-1}$ difference in transition state energy (assuming a Curtin-Hammett scenario) does not adequately account for the observed selectivity. Therefore, DFT errors were considered and benchmarking tests using a wide range of levels of theory in conjunction with the Def2-TZVP basis set and the SMD=MeCN solvation model were used to reoptimize transition states **336-TS** and **350-TS** (***Table 14***).

| Functional | $\Delta\Delta G^{\ddagger}$ / $a.u.$ | $\Delta\Delta G^{\ddagger}$ / $kcal \cdot mol^{-1}$ | C-I / Å | 335-S$_0$ : 353-S$_0$ |
|---|---|---|---|---|
| **uM06-2X-D3** | -0.000701 | -0.5 | 2.174 | 68 : 32 |
| **uωB97XD** | -0.001126 | -0.7 | 2.164 | 77 : 23 |
| **uB3LYP-D3(BJ)** | -0.006162 | -3.9 | 2.229 | >99 : 1 |
| **uLC-ωHPBE** | 0.003758 | 2.4 | 2.119 | 2 : 98 |
| **uB97D-D3(BJ)** | -0.011270 | -7.1 | 2.254 | >99 : 1 |
| **uCAM-B3LYP-D3(BJ)** | -0.000717 | -0.4 | 2.171 | 68:32 |

***Table 14**: Level of theory benchmarking for transition states **336-TS** and **350-TS** using def2-TZVP basis set in conjunction SMD=MeCN solvation model*

Values of $\Delta\Delta G^{\ddagger}$ ranging from -7.1 up to 2.4 kcal·mol$^{-1}$ were obtained from this analysis. While the geometry of transition state **350-TS** does not change significantly with respect to the level of theory, the C–I bond length in transition state **336-TS** displays substantial variation with respect to the level of theory. Plotting the C–I bond lengths vs $\Delta\Delta G^{\ddagger}$ for each level of theory gives a strong correlation (***Figure* 38**), suggesting that the differences in predicted selectivity across the six levels of theory arise from inaccurate modelling of the C–I bond. Comparison of these benchmarking results with those obtained previously by comparison of DFT and X-ray structures (***Table 9***) reveals that functionals that overestimate the C–I bond length (such as uB97D-D3(BJ) and uB3LYP-GD3BJ) predict a lower barrier for the *ipso*-I cyclization pathway. Conversely, the uLC-ωHPBE functional underestimates the C–I bond length while predicting an *ipso*-I cyclization barrier 2.4 kcal·mol$^{-1}$ higher in energy than the corresponding *ipso*-H barrier. Intriguingly, the uM06-2X-D3, uωB97XD and uCAM-B3LYP functionals, which most accurately predict the experimentally determined bond lengths, predict similar

$\Delta\Delta G^{\ddagger}$ values. Based on these observations, it was concluded that these latter three functionals best describe the current system. Furthermore, a $\Delta\Delta G^{\ddagger}$ value of 0.0 kcal·mol$^{-1}$ was also computed using the DLPNO-CCSD(T)/Def2-TZVP(SMD=MeCN)//uM06-2X/Def2-TZVP(SMD=MeCN)[177-180] coupled cluster level of theory was obtained by Dr. Juan Alegre-Requena; this value very similar in energy to that which was obtained using the uM06-2X-D3/Def2-QZVPP(SMD=MeCN)//uM06-2X-D3/Def2-TZVP(SMD=MeCN), suggesting that the latter is an accurate representation for the system of study.

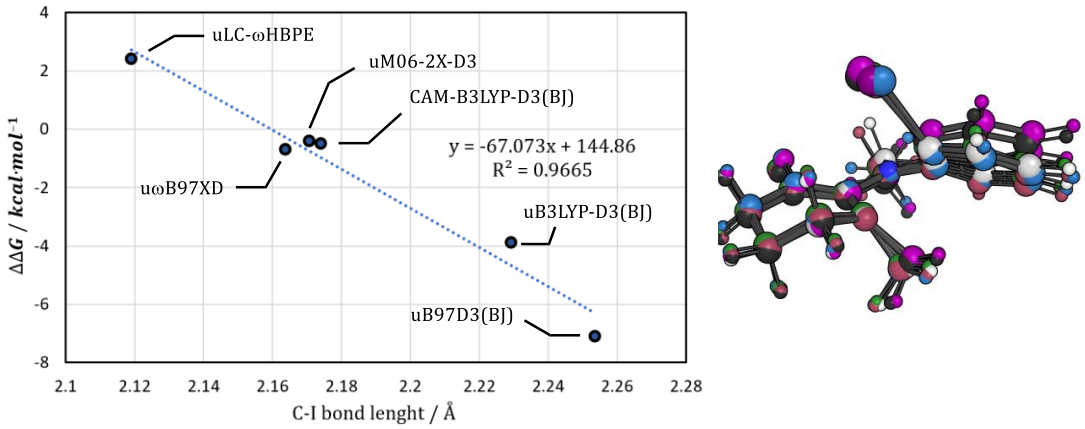



***Figure 38**: Plot of selectivity free energy ΔΔG vs C-I bond length at various levels of theory (left); Optimised transition state **336-TS** at various levels of theory (right).*

As DFT suggested that the small difference in activation energy between the *ipso*-I and *ipso*-H pathways was not due to calculation errors, we turned our attention towards the Curtin-Hammett assumption. Under the prospect that transition states **336-TS** and **350-TS** are not in rapid equilibrium, we question whether pre-excitation dynamics could influence the regiochemical outcome, through preferential population of conformer **325-T1_I**. Thorough analysis of the potential energy surface revealed a viable equilibration mechanism *via* planarization of the C3-centred radical (**355-TS**), with an activation free energy barrier of 7.6 kcal·mol$^{-1}$, which is lower in energy than either the *ipso*-I and *ipso*-H activation energy barriers (***Figure 39***, ***Table 15***). Therefore, we can conclude that conformers **325-T1_I** and **325-T1_H** are indeed in rapid equilibrium, thus validating the Curtin-Hammett scenario.

Alternative interconversion mechanisms *via* rotation about the C–N bonds (transition states **356-TS** and **357-TS**) were found to have prohibitively high activation barriers.

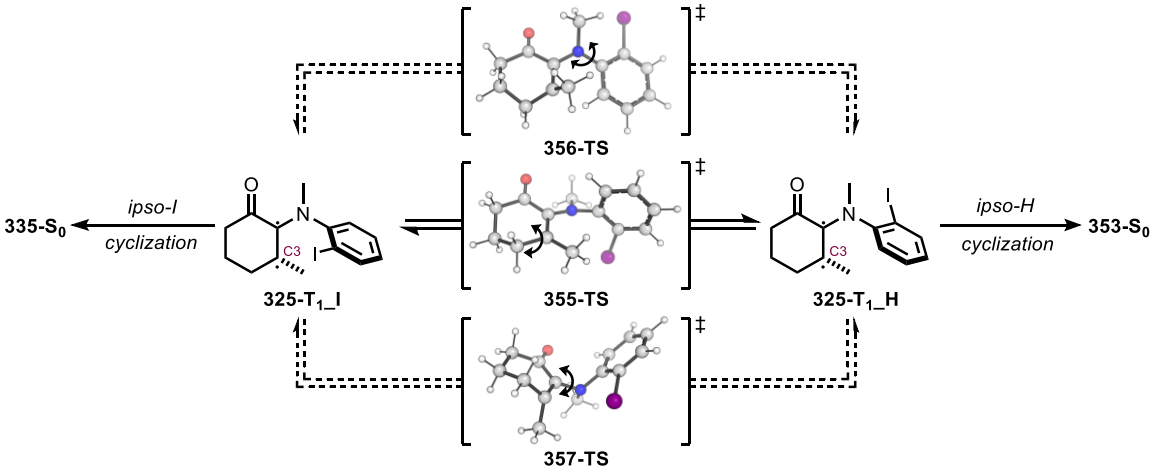



***Figure 39**: Mechanism of interconversion between conformers **325-T1_I** and **334-T1_H***

| Entry | $\Delta E$ | $\Delta ZPE$ | $\Delta H$ | $T\Delta S$ | $\Delta G$ |
|---|---|---|---|---|---|
| **325-T1_I** | 0.0 | 0.0 | 0.0 | 0.0 | 0.0 |
| **355-TS** | 7.0 | -0.2 | 6.3 | -1.4 | 7.6 |
| **356-TS** | 18.4 | -0.8 | 17.1 | -1.2 | 18.3 |
| **357-TS** | 16.2 | -0.1 | 15.5 | -1.2 | 16.7 |
| **325-T1_H** | 0.2 | 0.1 | 0.3 | 0.1 | 0.2 |

***Table 15**: Boltzmann thermochemical parameters for the conformer equilibration pathways in kcal·mol$^{-1}$ represented relative to **325-T1_I**, performed at uM06-2x-GD3/Def2QZVPP(SMD=MeCN)//uM06-2x-GD3/Def2TZVP(SMD=MeCN) level of theory*

The observed regioselectivity could alternatively arise from differences in intersystem crossing behaviour prior to the two cyclization pathways. For instance, if crossing of states occurred along the *ipso*-I reaction coordinate, elimination of the iodine atom could occur from the resulting $S_0$ state, potentially leading to an overall lower "effective" barrier to cyclization. To explore this hypothesis, single point calculations in the $S_0$ state were performed across the IRC of transition state **336-TS** (***Figure 40***). Optimization of points leading up to transition state **336-TS** led to the ground-state starting material **325-S0**. Interestingly, an intersection between the $S_0$ and $T_1$ surfaces was observed at a coordinate following transition state **336-TS** (**Figure 40**), suggesting that the *ipso*-I cyclization and intersystem crossing could occur in concert, effectively circumventing the formation of intermediate **335-T1**. Although this

represents a very fascinating mechanistic detail, the overall reaction outcome is unchanged, as reactivity *via* the *ipso*-I cyclization pathway is irreversible.

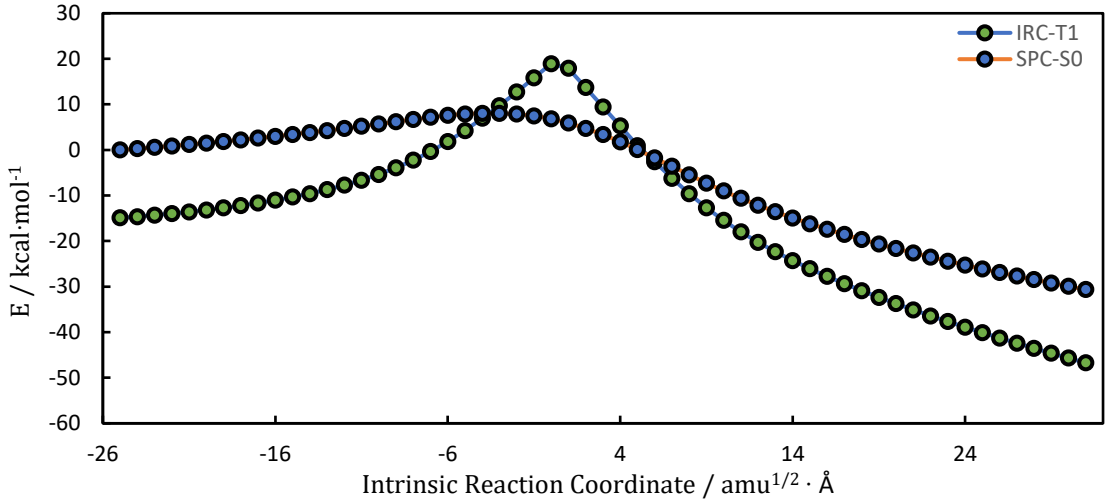
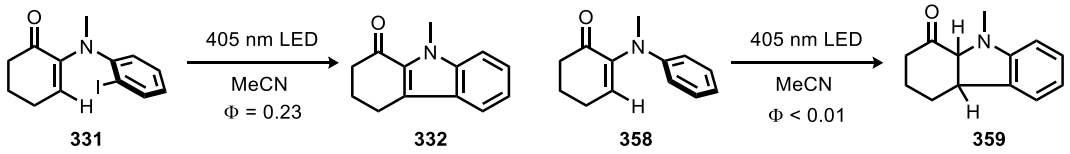



***Figure 40**: IRC plot of transition state **336-TS** and single point calculations in $S_0$*

Another mechanistic possibility that was envisaged is the recycling of molecules following the *ipso*-H cyclization. Upon cyclization *via* transition state **350-TS** and intersystem crossing, the zwitterionic intermediate **351-S$_0$** would be obtained. The resulting intermediate could undergo an intramolecular 1,3-H shift to furnish the classic isomerization product **353-S$_0$**. Alternatively, zwitterion **351-S$_0$** could undergo retro-cyclization *via* fragmentation across the newly formed C–C bond (**354-TS**), which regenerates the starting material. This pathway allows the molecule to re-enter the excited state *via* absorption of a photon, which could lead to slow accumulation of iminium ion **335-S$_0$** over time. However, computational analysis of transition states **352-TS** and **354-TS**, gave a relative free energy of 0.7 kcal·mol$^{-1}$ in favour of the 1,3-H shift pathway, thus pointing away from such a recycling hypothesis.

As DFT had ruled out a recycling mechanism occurring *via* the closed-shell singlet zwitterion **351-S$_0$**, we considered alternative recycling mechanisms in light of quantum yield measurements obtained for substrate **331** and its non-iodinated analogue **358** (***Scheme 63***). While indole **332** was formed in a relatively high quantum yield, Φ, of 0.23 from iodinated substrate **331**, the non-iodinated substrate **358** gave a very small quantum yield, $\Phi < 0.01$. This

difference in quantum yield was not attributed to differences in $S_1$ to $T_1$ intersystem crossing rates for the two substrates, as previous studies on 2-heteroatom substituted cyclohexenones suggest that intersystem crossing is very efficient,[181] in accordance with the El-Sayed rule. As the activation energies for the electrocyclization are small and thermally accessible, we turned our attention to the second intersystem crossing event that might explain the experimentally measured quantum yields.




***Scheme 63**: Quantum yield experiments performed by Zachariah Lockhart*

Minimum energy crossing points computed by Dr. Juan Alegre-Requena revealed a relatively high-energy minimum energy crossing point (**360-MECP)** for the non-iodinated substrate **358**, which is 10.2 kcal·mol$^{-1}$ higher in energy than its $T_1$ precursor **360-$T_1$**. This is in stark contrast to results from the group's previous studies on 2-phenoxycyclohexenones (***Scheme 57***) for which an MECP of approximatively 3 kcal·mol$^{-1}$ was found.[118] The same analysis performed on substrate **331** and the β-methyl derivative **325** revealed very similar results, with $\Delta E_{MECP}$ values of 14.8 and 14.1 kcal·mol$^{-1}$, respectively (***Figure 41***).

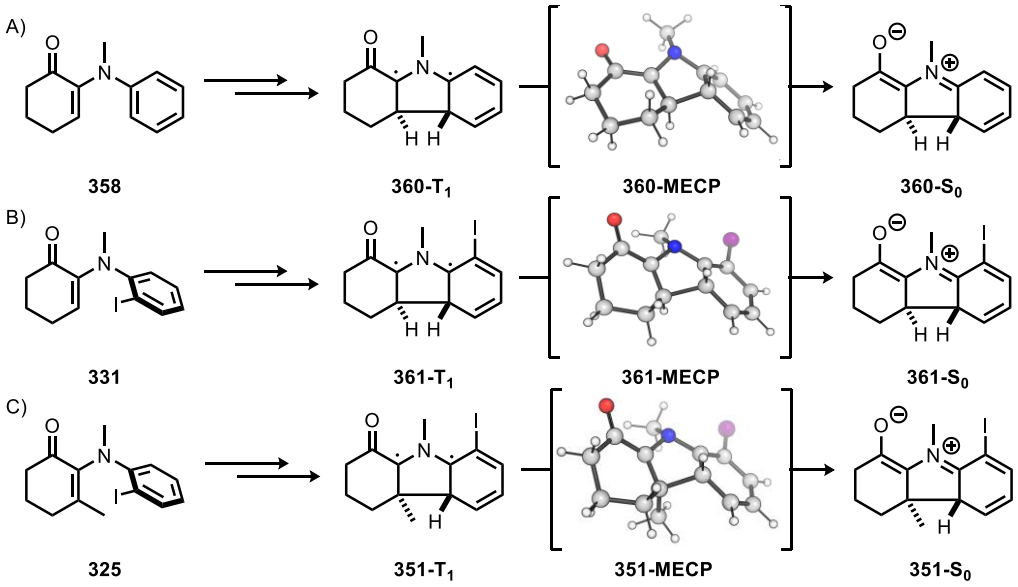



***Figure 41**: Diagram showing the ISC process for substrate **358** (A), **331** (B) and **325** (C) along the ipso-H pathway. MECP structure was computed by Dr. Juan Alegre-Requena*




***Figure 42**: Computed structures of MECPs overlapped with their corresponding $T_1$ precursors. Substantial structural reorganization can be seen in all three examples, emphasizing the high activation barrier required to reach the MECP. the MECP structures computed by Dr. Juan Alegre-Requena*

Taken together with the experimentally measured quantum yields, these results suggest that retro-cyclization in the $T_1$ state could compete with intersystem crossing to $S_0$. In the case of the β-methyl substrate **325**, the ΔE between **351-MECP** and transition state **354-TS** is only 1.8 kcal·mol$^{-1}$. Furthermore, as intersystem crossing operates in accordance with non-adiabatic transition state theory,[182-185] the probability of crossing from the $T_1$ state to $S_0$ is at most 50%. Therefore, it is possible that intersystem crossing from *ipso*-H intermediate **351-S$_0$** is so slow (*i.e.* that the MECP for this step is sufficiently high in energy) that reversion back to the excited-state triplet **325-T$_1$** occurs preferentially (***Figure 43***). In contrast, cyclization *via* transition state **336-T$_1$** is predicted to be irreversible, owing to the high stability of the product **335-T$_1$** and its ease of intersystem crossing (either concerted or stepwise) to the singlet ground state. In combination, these effects might explain the formation of non-iodinated **335-S$_0$** derivatives as the exclusive reaction product from iodinated starting material **325**. Reversibility along the *ipso*-H pathway could also explain the lower quantum yield measured for the non-iodinated analogue **358**. In the absence of an *ipso*-X cyclization pathway, this substrate undergoes less efficient photocyclization, owing to the preference of **361-T$_1$** to undergo

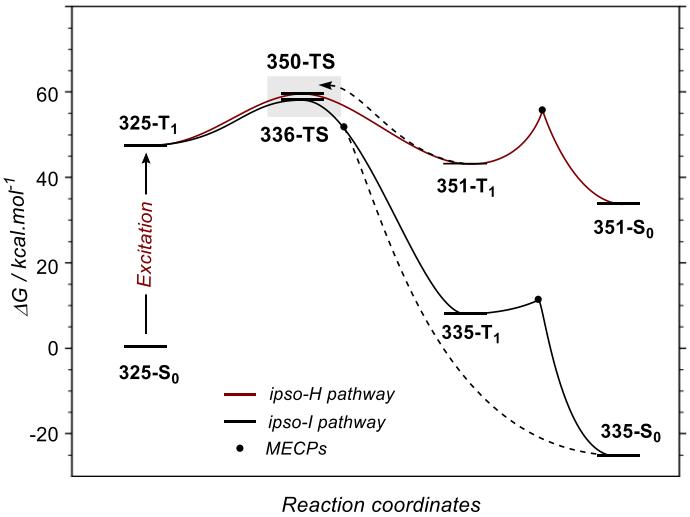



***Figure 43**: Reaction potential energy surface*

cycloreversion following *ipso*-H cyclization. Thus, we propose that it is the slow intersystem crossing that is the regioselectivity determining step of the overall transformation.

### *3.2.4 Comparison to 2-(2-iodophenoxy)-cyclohexenones reactivity*

As previously described, analogue **327** bearing an oxygen linker possesses divergent photochemical behaviour to that of **325**, leading to the formation of iodinated product **328** *via* an *ipso*-H cyclization pathway (***Figure 44***).[118] Although the mechanism of this type of substrate has been studied computationally before, the *ipso*-I pathway has not been previously investigated.

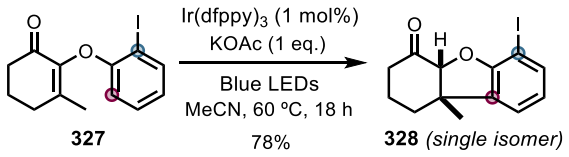



***Figure 44**: Photocyclization of o-iodophenoxy derivative **327***

It was envisaged that by studying the behaviour of this substrate insight into the unique excited state reactivity of its *N*-linked analogue **325** might be gained. As such, the mechanism of this transformation was investigated by DFT using the same level of theory as before (uM06-2x-D3/Def2-QZVPP(SMD=MeCN)//uM06-2x-D3/Def2-TZVP(SMD=MeCN)) (***Figure 45***).

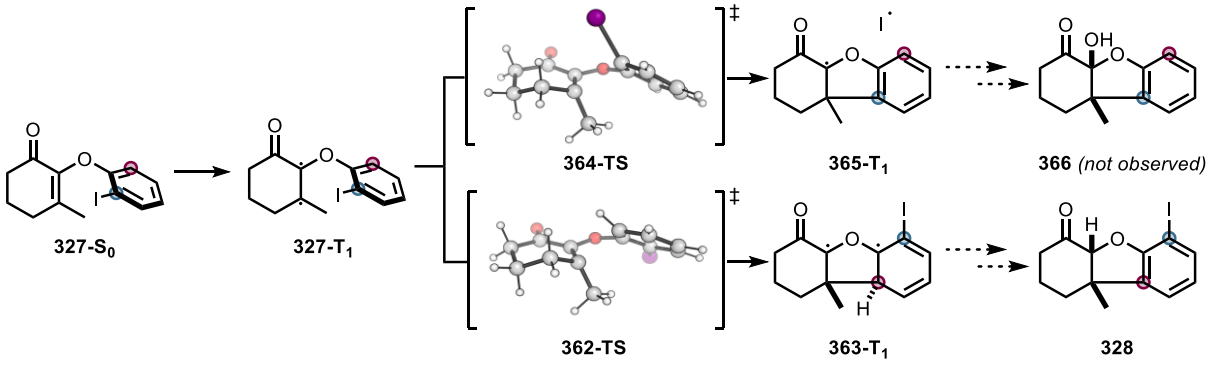



***Figure 45**: Proposed mechanistic pathways for the photocyclization of **327***

| Entry | $\Delta E$ | $\Delta ZPE$ | $\Delta H$ | $T\Delta S$ | $\Delta G$ |
|---|---|---|---|---|---|
| **327-S₀** | -60.4 | 1.4 | -59.1 | -1.0 | -58.1 |
| **327-T₁** | 0.0 | 0.0 | 0.0 | 0.0 | 0.0 |
| **364-TS** | 13.7 | -0.3 | 12.8 | -2.0 | 14.9 |
| **362-TS** | 11.1 | -0.1 | 10.3 | -2.0 | 12.2 |

***Table 16**: Boltzmann thermochemical parameter in kcal·mol$^{-1}$ represented relative to **327-T₁** performed at uM06-2x-D3/Def2-QZVPP(SMD=MeCN)//uM06-2x-D3/Def2-TZVP(SMD=MeCN) level of theory*

Computing the structure of **327** in both $T_1$ and $S_0$ states revealed a triplet state energy of 58.2 kcal·mol$^{-1}$. This is in good agreement with the previous study,[118] and it is within the sensitization capabilities of the photocatalyst used to effect this transformation ($E_T$ = 60.3 kcal·mol$^{-1}$).[115] Once in the triplet state, cyclization *via* the *ipso*-I transition state **364-TS** or either the *ipso*-H transition state **362-TS** is possible, leading to the formation of triplet intermediates **365-$T_1$** or **363-$T_1$** respectively. Although both pathways are thermally accessible, transition state **362-TS** is thermodynamically favoured by 2.7 kcal·mol$^{-1}$. The MECP computed for the resulting $T_1$ intermediate **363-$T_1$** is low in energy ($\Delta E_{MECP}$ = 4.0 kcal·mol$^{-1}$), suggesting a highly efficient intersystem crossing process, which means that the *ipso*-H pathway is likely to be irreversible. Put together, these results are highly consistent with the experimentally observed selectivity. It can therefore be concluded that in the case of the phenol-derived substrate **327**, the selectivity for the *ipso*-H pathway arises from the low energy of transition state **362-TS**. This is in complete contrast to the aniline-derived substrate **325**, where the *ipso*-I selectivity is determined by the competition between the rate of *ipso*-I cyclization *via* transition state **336-TS** and rate of intersystem crossing of triplet *ipso*-H intermediate **351-$T_1$**.

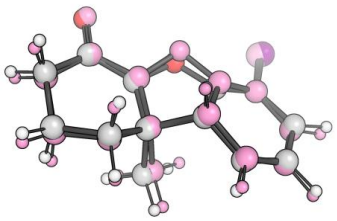



***Figure 46**: Computed structure of **363-MECP** (gray) overlapped with that of precursor **334-$T_1$** (pink). MECP structure was computed by Dr. Juan Alegre-Requena*

As substrates **325** and **327** display orthogonal selectivity in the excited state, it was concluded that a benchmarking test might be able to reinforce the choice of level of theory. We thus compared the relative energies of transition states **362-TS** and **364-TS** against the same ensemble of theory levels used in the selectivity benchmarking of substrate **325** (**Table 14**),

all used in conjunction with the def2-TZVP basis set and SMD=MeCN solvation model. Gratifyingly, the three levels of theory that performed well in the crystal structure benchmarking (uMO6-2X-D3, uωB97XD and uCAM-B3LYP), also predicted the formation of the experimentally observed product **328** from substrate **327**. Similarly, uB3LYP-D3(BJ) and uB97D-D3(BJ), which previously favoured the *ipso*-I transition state while overestimating the C–I bond length observed in the X-ray crystal structure, gave a lower value for the *ipso*-I transition state **364-TS** energy. Therefore, these two levels of theory predict a mixture of products, or preferential formation of **366** in case of the uB97D-D3(BJ) functional, thus contradicting experimental observations. Finally, uLC-ωHPBE, which underestimated the C–I bond length in the previous benchmarking study while predicting a lower-energy *ipso*-H transition state, gave the highest relative free energy of 5.4 kcal·mol$^{-1}$ in favour of the *ipso*-H product **328**. By plotting the relative free energies across the six levels of theory against the C–I bond length in the corresponding *ipso*-I transition state, a similar linear trend was obtained to that of the previous benchmarking analysis of aniline-derived substrate **325** (***Figure 47***). This agreement indicates that the six levels of theory behave similarly across the two systems **325** and **327**. Overall, we can conclude that the chosen level of theory in this study is a good representation for both the aniline **325** and phenol **327**.

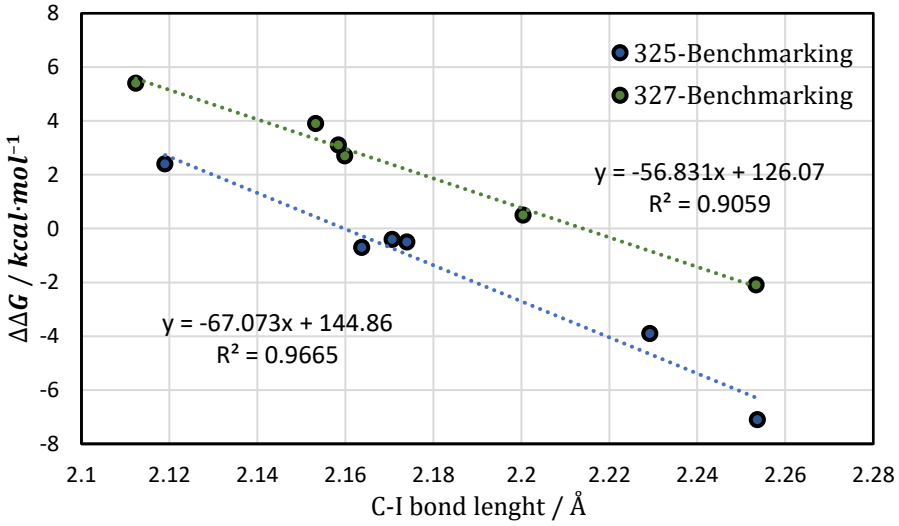


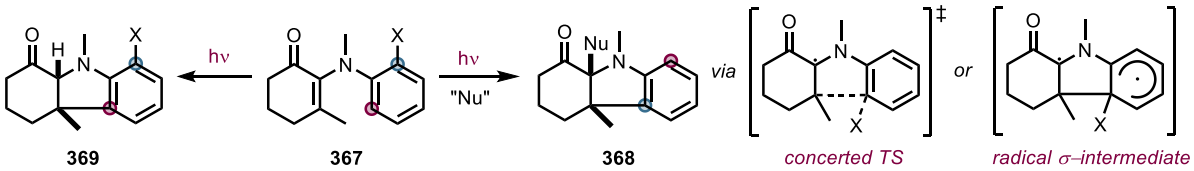

***Figure 47**: Plot of transition state relative energy vs C–I bond length at the photoeliminative transition state for substrates **325** and **327***

| Functional | $\Delta\Delta G$ / $a.u.$ | $\Delta\Delta G$ / $kcal \cdot mol^{-1}$ | C-I / Å | **328** : **366** |
|---|---|---|---|---|
| **uM06-2X-D3** | 0.004253 | 2.7 | 2.160 | 99:1 |
| **uωB97XD** | 0.006263 | 3.9 | 2.153 | >99:1 |
| **uB3LYP-D3(BJ)** | 0.000828 | 0.5 | 2.200 | 71:29 |
| **uLC-ωHPBE** | 0.008734 | 5.4 | 2.112 | >99:1 |
| **uB97D-D3(BJ)** | -0.003389 | -2.1 | 2.253 | 3:97 |
| **uCAM-B3LYP** | 0.005079 | 3.1 | 2.158 | >99:1 |

***Table 17**: Level of theory benchmarking for transition states **362-TS** and **364-TS** using def2-TZVP basis set it conjunction SMD=MeCN solvation model*

### *3.2.5 Influence of ortho-substituents*

Currently, only iodine has been experimentally validated as an effective leaving group for the photoeliminative cyclization of the *ortho*-substituted aniline class of substrate. Due to difficulties involving the synthesis of the necessary precursors, it was decided that a computational screening of *ortho*-substituents would be informative. Using the same computational protocol as before, a range of *ortho*-substituted aniline derivatives were studied, with particular emphasis being placed on the mechanism of photoelimination (***Scheme 64***).




***Scheme 64**: Proposed future investigation into different ortho-substituted derivatives*

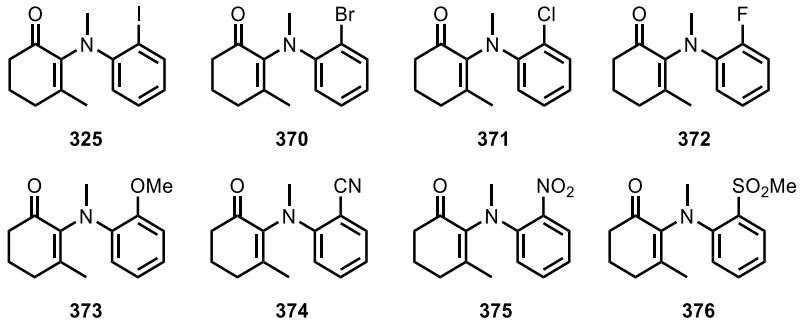



***Figure 48**: Substrates bearing ortho-substituents chosen for investigation*

As iodine proved to be very successful, the rest of the halogens were also investigated (***Figure 48***). Like the iodinated substrate **325**, *ortho*-bromo aniline derivative **370** undergoes competitive cyclization between the *ipso*-H and *ipso*-Br positions; however, the selectivity is slightly biased towards the *ipso*-H transition state **379-TS** ($\Delta\Delta G^{\ddagger}$ = 0.4 kcal·mol$^{-1}$)

(***Figure 49***). Intrinsic reaction coordinate calculations performed on transition state **379-TS**, revealed a potential radical σ-intermediate, although attempts to optimize these structures led to the dissociated diradical **378-T$_1$** (***Figure 50***).

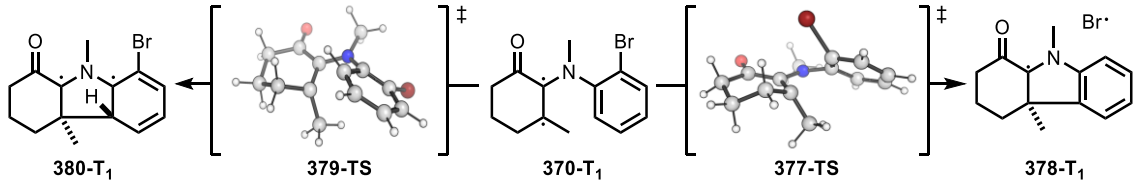



***Figure 49**: Proposed cyclization mechanisms for substrate **370***

| Entry | $\Delta E$ | $\Delta ZPE$ | $\Delta H$ | $T\Delta S$ | $\Delta G$ |
|---|---|---|---|---|---|
| **370-T$_1$** | 0.0 | 0.0 | 0.0 | 0.0 | 0.0 |
| **377-TS** | 11.8 | -0.6 | 10.8 | -1.2 | 11.9 |
| **379-T$_1$** | 10.7 | -0.3 | 9.8 | -1.8 | 11.5 |

***Table 18**: Boltzmann thermochemical parameters for the photocyclization pathways in kcal·mol$^{-1}$ represented relative to **370-T$_1$**, performed at uM06-2x-D3/Def2-QZVPP(SMD=MeCN)//uM06-2x-D3/Def2-TZVP(SMD=MeCN) level of theory*

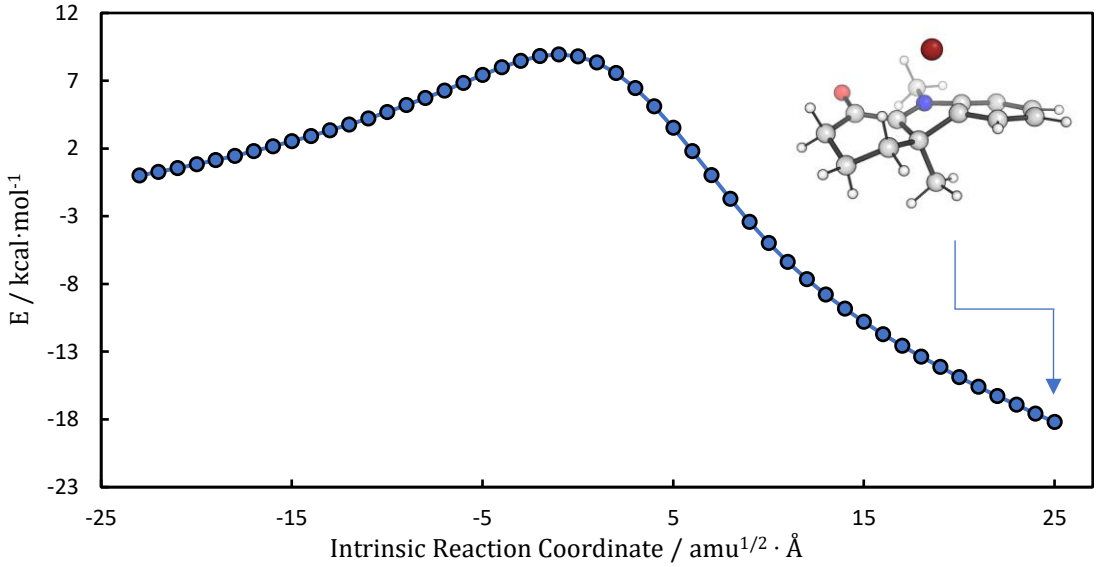



***Figure 50**: IRC plot of transition state **377-TS***

The *ortho*-chloro aniline derivative **371** was also found to possess a low energy photoeliminative cyclization transition state **381-TS** ($\Delta G^{‡}$ = 13.3 kcal·mol$^{-1}$) (***Figure 51***). However, this transition state is substantially higher in energy than the *ipso*-H transition state **383-TS** ($\Delta G^{‡}$ = 11.6 kcal·mol$^{-1}$). Akin to both substrates **325** and **370**, intrinsic reaction coordinate calculations performed on the *ipso*-Cl transition state **381-TS** revealed the presence of a potential σ-intermediate (***Figure 52***). In this case, the structural features of this complex

are much more pronounced (such as the pyramidalization of the carbon bearing the chlorine substituent); however, as in previous cases, it was found to be not stable by DFT.

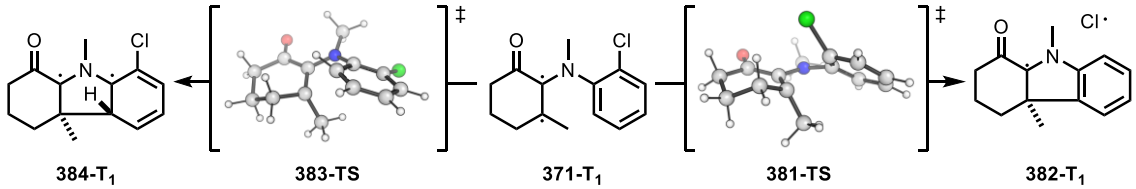



***Figure 51**: Proposed cyclization mechanisms for substrate **371***

| Entry | $\Delta E$ | $\Delta ZPE$ | $\Delta H$ | $T\Delta S$ | $\Delta G$ |
|---|---|---|---|---|---|
| **371-T₁** | 0.0 | 0.0 | 0.0 | 0.0 | 0.0 |
| **381-TS** | 12.5 | -0.4 | 11.5 | -1.8 | 13.3 |
| **383-TS** | 10.6 | -0.3 | 9.8 | -1.8 | 11.6 |

***Table 19**: Boltzmann thermochemical parameters for the photocyclization pathways in kcal·mol$^{-1}$ represented relative to **371-T$_1$**, performed at uM06-2x-D3/Def2-QZVPP(SMD=MeCN)//uM06-2x-D3/Def2-TZVP(SMD=MeCN) level of theory*

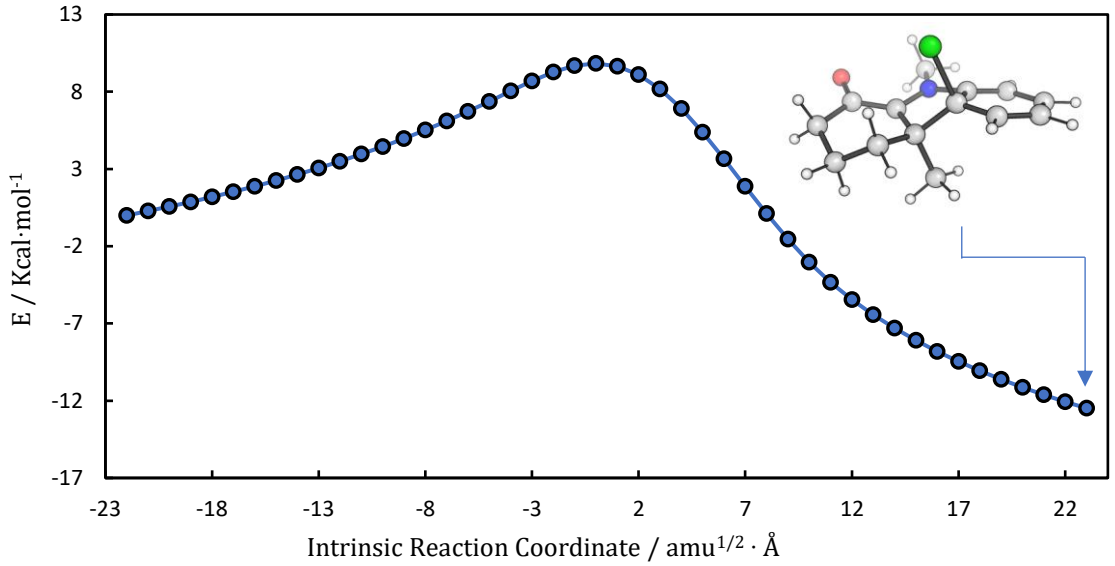



***Figure 52**: IRC plot of transition state **381-TS***

The *ortho*-fluorinated substrate **372** was also investigated (***Figure 53***). Like the brominated and chlorinated analogues **370** and **371**, **372** was also found to undergo preferential *ipso*-H cyclization *via* transition state **385-TS**. Intriguingly, however, the difference in free energy between transition states **385-TS** and **390-TS** was found to be only 1.0 kcal·mol$^{-1}$, which is smaller than the selectivity exhibited by the chlorinated substrate **371** ($\Delta\Delta G^{\ddagger}$=1.7 kcal·mol$^{-1}$). In contrast to the other halogenated substrates, intrinsic reaction coordinate calculations performed on transition state **385-TS** revealed a σ-intermediate **386-T$_1$** that was stable upon

optimization (***Figure 54***). The resulting σ-intermediate **386-T$_1$** is predicted to readily undergo elimination of the fluoride radical, with an activation barrier of 11.8 kcal·mol$^{-1}$. These results suggests that, at least in the case of *ortho*-fluoro substrates, the reaction does indeed proceed *via* a stepwise mechanism involving a radical σ-intermediate.

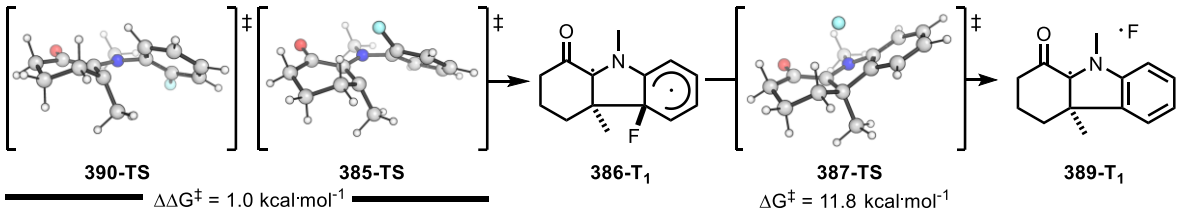



***Figure 53**: Proposed cyclization mechanisms for substrate **372***

| Entry | Δ*E* | Δ*ZPE* | Δ*H* | *T*Δ*S* | Δ*G* |
|---|---|---|---|---|---|
| **372-T$_1$** | 0.0 | 0.0 | 0.0 | 0.0 | 0.0 |
| **385-TS** | 12.2 | -0.5 | 11.1 | -1.6 | 12.7 |
| **390-TS** | 11.0 | -0.4 | 10.1 | -1.6 | 11.7 |
| **386-T$_1$** | -12.1 | 0.6 | -12.0 | -2.0 | -10.0 |
| **387-TS** | 0.6 | 0.0 | 0.2 | -1.5 | 1.8 |

***Table 20**: Boltzmann thermochemical parameters for the photocyclization pathways in kcal·mol$^{-1}$ represented relative to **372-T$_1$**, performed at uM06-2x-D3/Def2-QZVPP(SMD=MeCN)//uM06-2x-D3/Def2-TZVP(SMD=MeCN) level of theory*

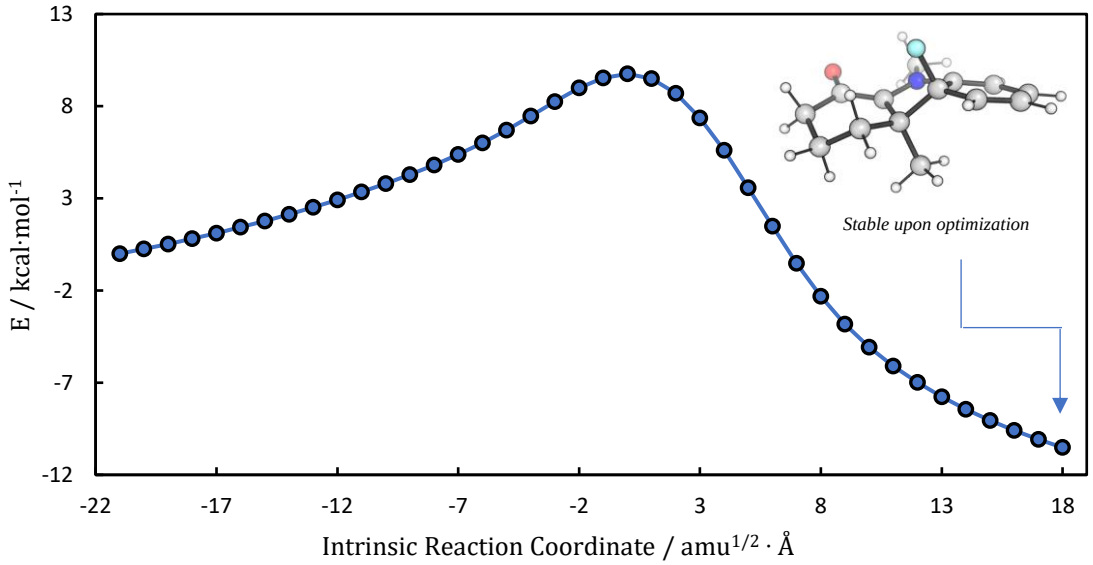



***Figure 54**: IRC plot of transition state **385-TS***

Having investigated the photochemical behaviour of halogens, we then explored groups that have been reported to undergo elimination in other photocyclization systems. The *ortho*-OMe substituted derivative **373** was found to undergo a highly selective *ipso*-H cyclization *via* transition state **395-TS** ($\Delta\Delta G^{\ddagger}$=4.7 kcal·mol$^{-1}$). Intrinsic reaction coordinate calculations

performed on the *ipso*-OMe transition state **391-TS** indicate that the reaction proceeds *via* a σ-intermediate **392-TS** that is stable upon DFT optimization (***Figure 56***), from which elimination of a methoxy radical readily occurs in the triplet state *via* transition state **392-TS** ($\Delta G^{\ddagger}$=10.0 kcal·mol$^{-1}$). As the *ipso*-H transition state **395-TS** is 4.7 kcal·mol$^{-1}$ lower in energy than the *ipso*-OMe transition state **391-TS**, it is expected that substrate **373** will be a poor candidate for a photoeliminative cyclization.

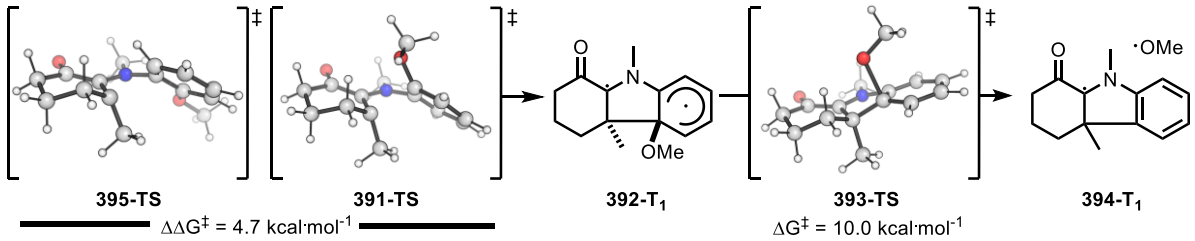



***Figure 55**: Proposed cyclization mechanisms for substrate **373***

| Entry | $\Delta E$ | $\Delta ZPE$ | $\Delta H$ | $T\Delta S$ | $\Delta G$ |
|---|---|---|---|---|---|
| **373-T$_1$** | 0.0 | 0.0 | 0.0 | 0.0 | 0.0 |
| **391-TS** | 16.6 | -0.6 | 15.4 | -1.8 | 17.3 |
| **395-TS** | 11.8 | -0.3 | 10.9 | -1.6 | 12.6 |
| **392-T$_1$** | -2.7 | 0.4 | -2.8 | -2.2 | -0.7 |
| **393TS** | 9.9 | -1.0 | 8.6 | -1.4 | 10.0 |

***Table 21**: Boltzmann thermochemical parameters for the photocyclization pathways in kcal·mol$^{-1}$ represented relative to **373-T$_1$**, performed at uM06-2x-GD3/Def2QZVPP(SMD=MeCN)//uM06-2x-GD3/Def2TZVP(SMD=MeCN) level of theory*

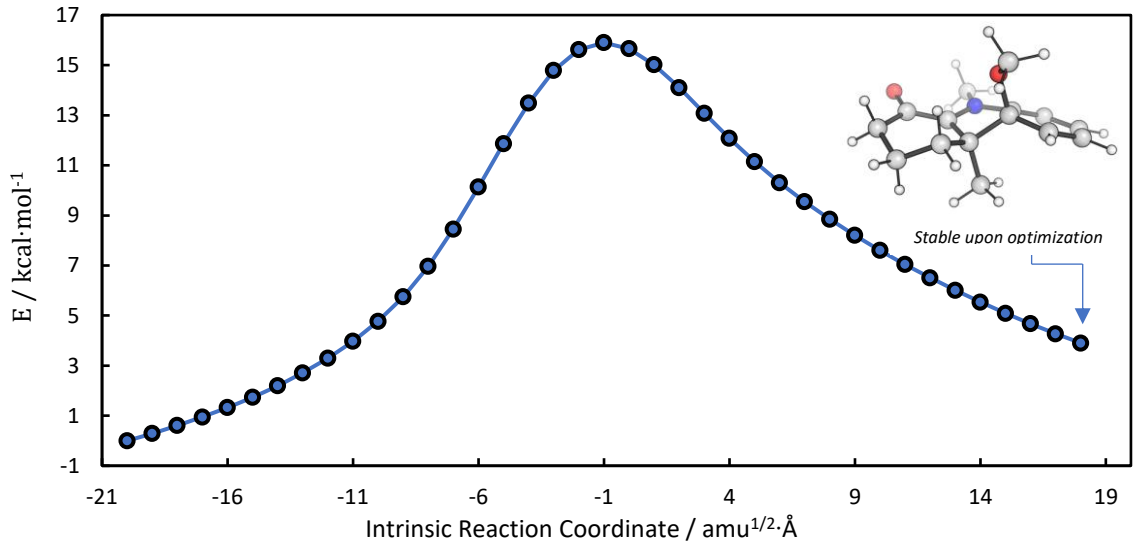



***Figure 56**: IRC plot of transition state **391-TS***

As nitrile groups have been reported to undergo photoeliminative cyclizations (***Figure 57***), substrate **374** was also investigated computationally. Substrate **374** possesses an *ipso*-CN

transition state **396-TS** that is higher in energy than the corresponding *ipso*-H transition state **400-TS** by 1.1 kcal·mol$^{-1}$. Although the difference in energy between the *ipso*-CN and *ipso*-H transition states is small, the intersystem crossing rates could favour the *ipso*-CN pathway overall. Intrinsic reaction coordinate calculations performed on transition state **396-TS** (***Figure 58***)indicate that the reaction proceeds *via* a radical σ-intermediate **397-T$_1$** that requires a high activation energy of 22.1 kcal·mol$^{-1}$. As the barrier to retro-cyclization in the $T_1$ state from radical σ-intermediate **397-T$_1$** *via* transition state **396-TS** requires an activation energy of only 13.6 kcal·mol$^{-1}$, it is expected that elimination of the nitrile radical is unlikely. As such, we expect that the nitrile-derivative **374** is a poor candidate for a photoeliminative cyclization.

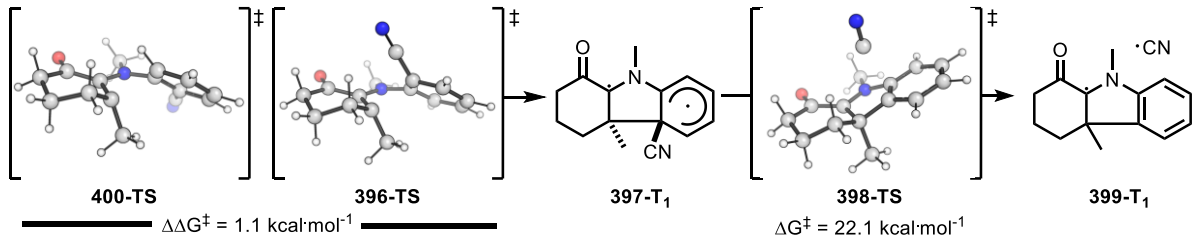



***Figure 57**: Proposed cyclization mechanisms for substrate **374***

| Entry | Δ*E* | Δ*ZPE* | Δ*H* | *T*Δ*S* | Δ*G* |
|---|---|---|---|---|---|
| **374-T$_1$** | 0.0 | 0.0 | 0.0 | 0.0 | 0.0 |
| **396-TS** | 10.8 | -0.6 | 9.7 | -1.4 | 12.1 |
| **400-TS** | 10.9 | -0.6 | 9.9 | -1.2 | 11.0 |
| **397-T$_1$** | -3.3 | 0.2 | -4.0 | -2.5 | -1.4 |
| **398-TS** | 22.4 | -1.1 | 20.4 | -0.2 | 20.6 |

***Table 22**: Boltzmann thermochemical parameters for the photocyclization pathways in kcal·mol$^{-1}$ represented relative to **374-T$_1$**, performed at uM06-2x-D3/Def2-QZVPP(SMD=MeCN)//uM06-2x-D3/Def2-TZVP(SMD=MeCN) level of theory*

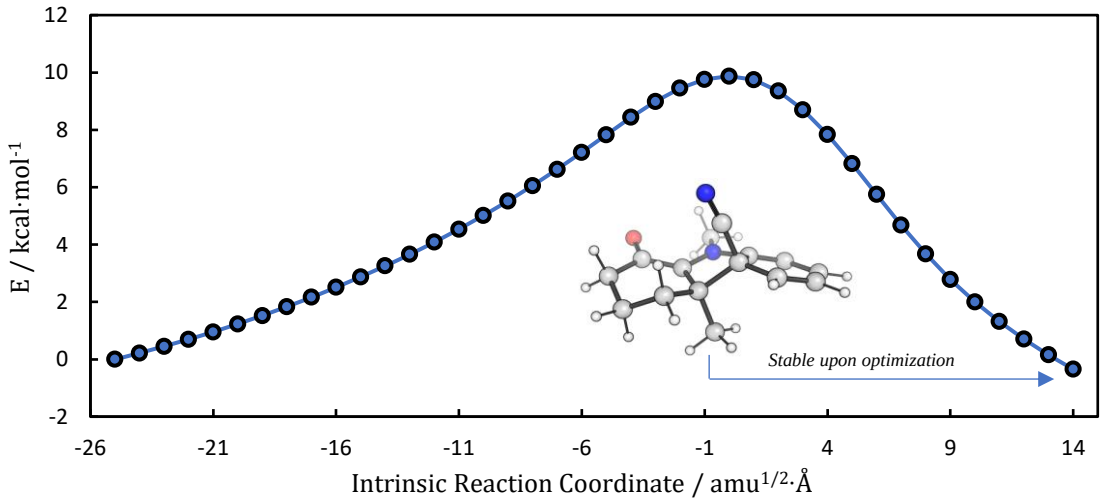



***Figure 58**: IRC plot of transition state **396-TS***

The *ortho*-$NO_2$ substituted derivative **375** was found to undergo highly selective *ipso*-$NO_2$ cyclization *via* transition state **401**-TS, which is lower in energy than the *ipso*-H transition state **405-TS** by 4.9 kcal·mol$^{-1}$. Analysis of the two transition states structures revealed deconjugation of the nitro group in the *ipso*-H transition state **405-TS**, presumably arising from allylic strain interactions between the $NO_2$ group and the methyl substituent of the aniline nitrogen. Like the fluorinated derivative **372**, intrinsic reaction coordinate calculations performed on transition state **401-TS** also indicate that this transformation proceeds *via* a radical σ-intermediate **402-T$_1$**, which readily undergoes elimination of the nitrite radical *via* transition state **403-TS** ($\Delta G^{\ddagger}$=0.9 kcal·mol$^{-1}$). As such, it is expected that substrate **375** is a good candidate for photoeliminative cyclization. However, side reactivity involving the nitro group cannot be excluded as nitroaromatic compounds are known to be photo-reactive.[186]

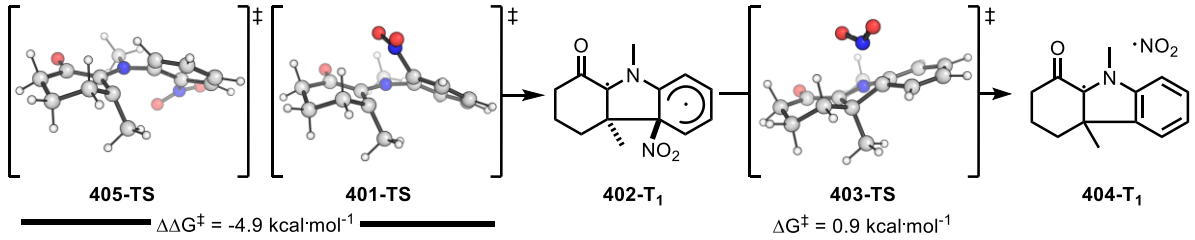



***Figure 59**: Proposed cyclization mechanisms for substrate **375***

| Entry | $\Delta E$ | $\Delta ZPE$ | $\Delta H$ | $T\Delta S$ | $\Delta G$ |
|---|---|---|---|---|---|
| **XX-T1** | 0.0 | 0.0 | 0.0 | 0.0 | 0.0 |
| **401-TS** | 10.6 | 0.1 | 10.1 | -0.8 | 10.9 |
| **405-TS** | 15.7 | 0.1 | 15.4 | -0.4 | 15.8 |
| **402-T1** | -7.6 | 0.7 | -7.0 | -0.5 | -6.6 |
| **402-TS** | -5.8 | -0.1 | -6.1 | -0.5 | -5.6 |

***Table 23**: Boltzmann thermochemical parameters for the photocyclization pathways in kcal·mol$^{-1}$ represented relative to **375-T$_1$**, performed at uM06-2x-D3/Def2-QZVPP(SMD=MeCN)//uM06-2x-D3/Def2-TZVP(SMD=MeCN) level of theory*

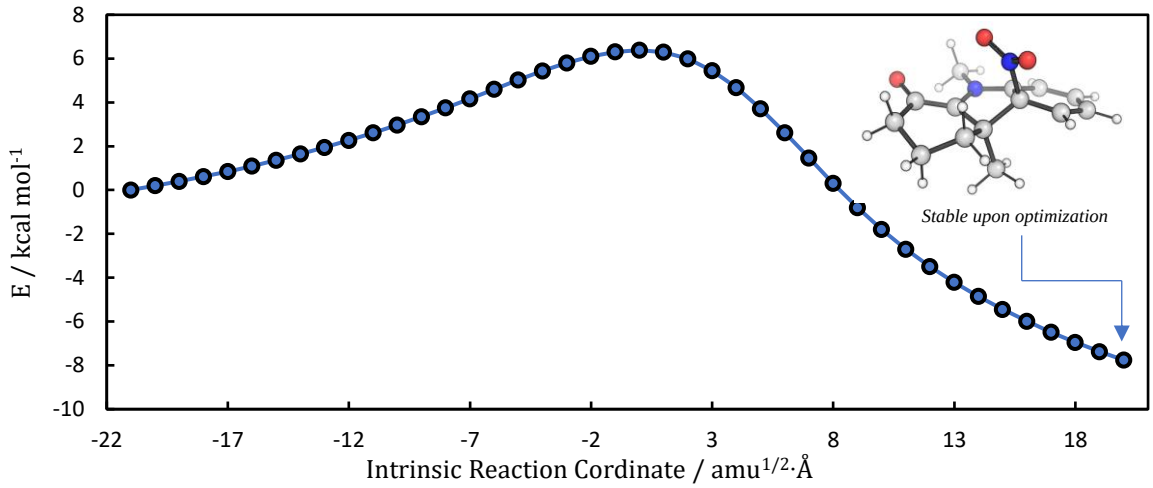



***Figure 60**: IRC plot of transition state **401-TS***

Like the *ortho*-$NO_2$ derivatives **375**, the derivative **376** bearing an *ortho*-$SO_2Me$ substituent is also expected to undergo cyclization at carbon bearing the non-hydrogen substituent. DFT calculations suggests that the *ipso*-$SO_2Me$ transition state **406-TS** requires an activation energy of only 8.0 kcal·mol$^{-1}$, while the *ipso*-H transition state **410-TS** requires an activation energy of 11.4 kcal·mol$^{-1}$. Akin to both *ortho*-$NO_2$ and *ortho*-F derivative **372** and **374**, the *ipso*-$SO_2Me$ pathway proceeds through a radical σ-intermediate **407-T$_1$**, which readily undergoes elimination of the sulfinic radical *via* transition state **408-TS** ($\Delta G^{\ddagger}$=0.9 kcal·mol$^{-1}$), thus making the process overall irreversible. As such, due to the high selectivity towards the *ipso*-$SO_2Me$ pathway and the ease of sulfinic radical elimination from the resulting σ-intermediate **407-T$_1$**, substrate **376** represents a very good candidate to study experimentally.

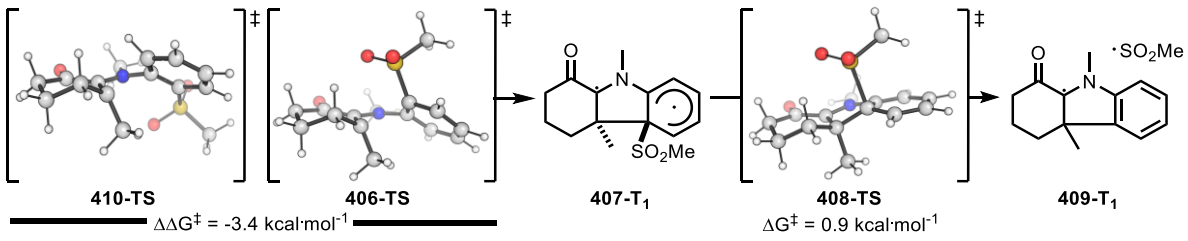



***Figure 61**: Proposed cyclization mechanisms for substrate **376***

| Entry | $\Delta E$ | $\Delta ZPE$ | $\Delta H$ | $T\Delta S$ | $\Delta G$ |
|---|---|---|---|---|---|
| **376-T$_1$** | 0.0 | 0.0 | 0.0 | 0.0 | 0.0 |
| **406-TS** | 6.9 | -0.3 | 6.0 | -2.1 | 8.0 |
| **410-TS** | 10.1 | 0.0 | 9.4 | -2.1 | 11.4 |
| **407-T$_1$** | -15.5 | 0.5 | -15.5 | -2.1 | -13.4 |
| **408-TS** | -13.7 | -0.3 | -14.5 | -2.0 | -12.5 |

***Table 24**: Boltzmann thermochemical parameters for the photocyclization pathways in kcal·mol$^{-1}$ represented relative to **376-T$_1$**, performed at uM06-2x-D3/Def2-QZVPP(SMD=MeCN)//uM06-2x-D3/Def2-TZVP(SMD=MeCN) level of theory*

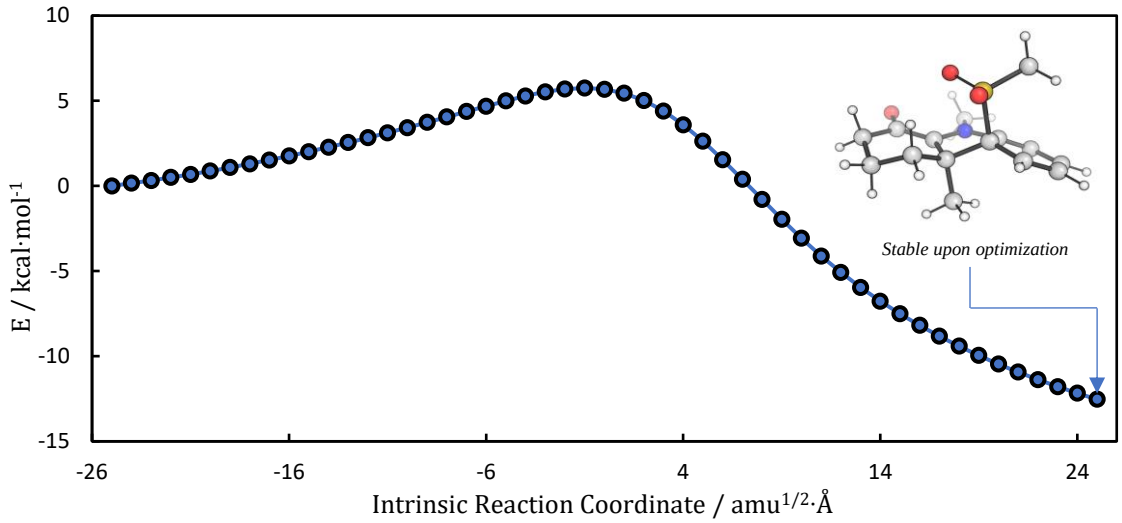



***Figure 66**: IRC plot of transition state **406-TS***

## 3.3 Mechanistic summary and conclusions

In conclusion, we have investigated the mechanism of a novel photoeliminative transformation using a combination of computational and experimental techniques. The reaction likely proceeds in the triplet state, where a range of mechanistic pathways are available. Homolysis of the C–I bond, as well as intramolecular halogen atom transfer were disproven by a computationally designed radical trapping experiment. The remaining mechanistic pathway involves a concerted radical aromatic substitution reaction occurring *via* cyclization onto the carbon bearing the iodine substituent. This is the most energetically favourable pathway that explains the experimentally observed product; however, the *ipso*-I and *ipso*-H cyclization transition states were similar in energy. As the *ipso*-I product forms exclusively in this reaction, DFT errors were considered. Benchmarking studies against crystallographic data suggest the uM06-2X-D3/Def2-QZVPP(SMD=MeCN)//uM06-2X-D3/Def2-

TZVP(SMD=MeCN) level of theory is the most appropriate across the chosen ensemble. Further benchmarking on a phenol-derived substrate reinforced our choice of level of theory, as it accurately predicted the experimentally observed *ipso*-H selectivity for this substrate. Investigations of intersystem crossing rates of this transformation indicated surprisingly high minimum energy crossing points, suggesting slow rates of intersystem crossing to the $S_0$ state from the triplet intermediate formed immediately following the *ipso*-H cyclization. This proposal is consistent with the lower reaction quantum yields measured experimentally for a non-iodinated analogue. As such, molecules cyclizing by the *ipso*-H pathway fragment back to the triplet starting material, irreversibly transformed to the observed product *via* the *ipso*-I pathway. Thus, it was concluded that the observed experimental selectivity arises from the irreversibility of the ipso-I cyclization pathway coupled with the slow rate of intersystem crossing from **351-T$_1$** to **351-S$_0$**.

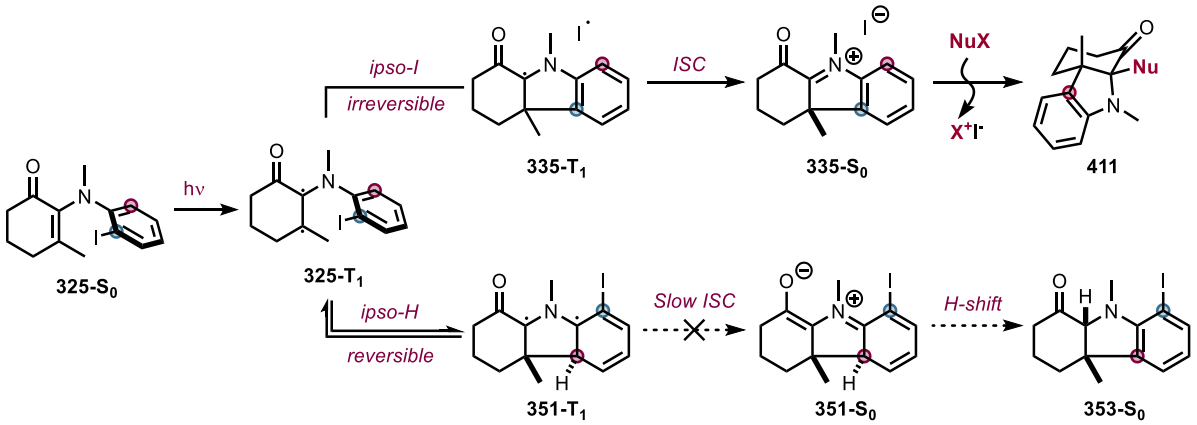



***Figure 67**: Summary of the proposed mechanism*

The mechanistic insight obtained from this transformation will enable us to design and explain new photoeliminative transformations. Preliminary computational investigations into other *ortho*-substituted derivatives suggested that the other halogens could undergo photoeliminative cyclization, although less selectively. Intriguingly, nitro and sulfonate groups are expected to undergo highly selective cyclizations in favour of the photoeliminative products. As such, we would like to investigate the fluorine, chlorine, bromine, nitro and sulfonate substrate experimentally and study their cyclization selectivity.

As the current synthetic protocol has been developed by trapping iminium ion **335** with nucleophiles, radical methods should also be explored through the reduction of iminium ion **335** to its corresponding radical **413** (**Figure 48**). A very compelling strategy for reducing iminium ion **335** would be through the use of photoredox-catalysis. Not only has the photo-reduction of iminium ions by photochemical methods been well established,[187] but we have also demonstrated that the reaction is compatible to iridium based photocatalysts commonly used in these transformations.

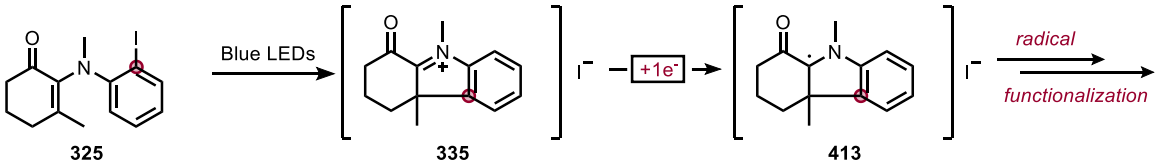
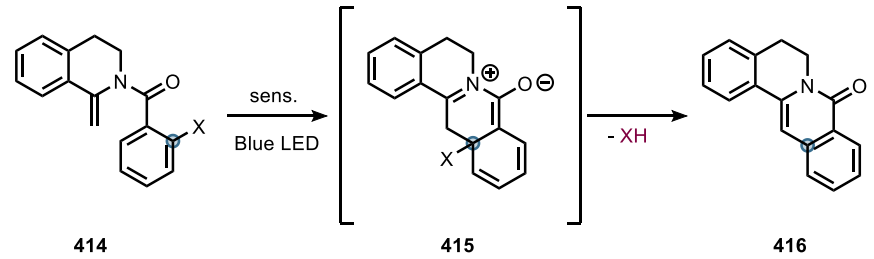
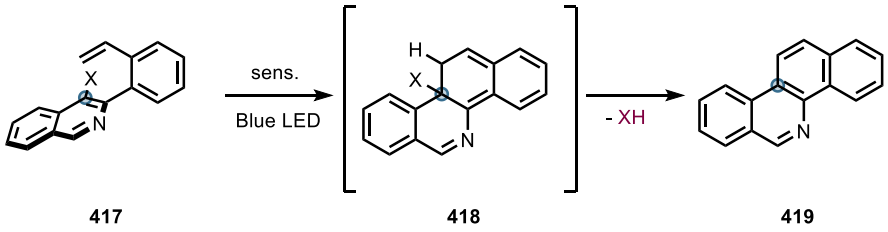



***Figure 68**: Proposed further functionalization of substrate via reduction of iminium ion **335***

Although numerous photoeliminative cyclization have been identified, very little mechanistic detail regarding these transformations is known. As our mechanistic investigation indicated that the photocyclization of 2-((2-iodoaryl)amino)cyclohexenones proceeds in the triplet state, it opens the possibility that other previously reported photoeliminative transformations could occur in the triplet state. As most photoeliminative transformations have been performed under direct UV-irradiation in the absence of a sensitizer, it is hard to assess based on current experimental evidence if they proceed *via* an excited state singlet or triplet pathway (or both). This opens numerous avenues of research by studying these transformations using both experimental and computational methods. We have identified two interesting transformations (***Scheme 69** and **Scheme 70***) that are expected to possess low triplet energies, due to the presence of styrene chromophores, and thus may be amenable to visible light sensitization. By restudying these transformations using both visible light sensitization and UV-light direct irradiation, coupled with computational studies using DFT, we can attempt to elucidate their mechanisms.




***Scheme 65**: Proposed transformation that could be investigated by visible light energy transfer catalysis*




***Scheme 66**: Proposed transformation that could be investigated by visible light energy transfer catalysis*

# Supplementary Information

## 1. Instrumentation, methods and materials

All reagents and solvents were used as supplied commercially without further purification. Dry dichloromethane, tetrahydrofuran and diethyl ether were purified through activated alumina columns. Water was purified using an Elix® UV-10 system. HPLC grade solvents for photochemical reactions were degassed by sparging the solvent with argon or nitrogen gas for at least 30 minutes. The solvents used in the photochemical reactions were used as received, without additional drying. Petrol ether (PE) 40–60 refers to the fraction of petroleum ether which boils in the range 40–60 ºC. Photochemical reactions were performed using a Kessil PR440 blue LED lamp. Optimization reactions were performed in sealed microwave vials, whilst larger scale reactions were performed in sealed Schlenk tubes. In both cases the LED lamp was placed approximately 1 cm away from the edge of the reaction vessel. Cooling was provided by a stream of nitrogen, which kept the reaction at approximatively 25 ºC.

Thin Layer Chromatography was performed using pre-coated aluminium-backed Merck TLC Silica Gel 60 F254 plates and visualised using 254 nm light or by staining with a $KMnO_4$ solution. Flash column chromatography was performed with Merck Geduran® Si 60 Silicagel (40–63 μm particle size) or with Sigma-Aldrich Silica gel (technical grade, pore size 60 Å, 40–63 μm particle size). All solvents used for chromatographic purification were HPLC grade or equivalent and supplied by Sigma-Aldrich.

All Nuclear Magnetic Resonance spectra were recorded on Bruker AVIIIHD 400 nanobay spectrometers at room temperature in solutions of $CDCl_3$ and the deuterated solvent acted as the deuterium lock. $^{1}$H-NMR spectra were recorded at 400 MHz, $^{13}$C NMR spectra at 101 MHz with broadband proton decoupling and $^{19}$F NMR spectra at 377 MHz. Residual protic solvent signal acted as an internal reference for $^{1}$H-NMR and the deuterated solvent carbon

signal acted as an internal reference for $^{13}C$ NMR ($CDCl_3$: $^{1}H$ NMR = 7.26 ppm, $^{13}C$ NMR = 77.16 ppm). $^{19}F$ NMR spectra were referenced externally to $CFCl_3$. Chemical shifts, δ, are given in parts per million (ppm) to the nearest 0.01 ppm for $^{1}H$ and $^{19}F$ and 0.1 ppm for $^{13}C$ NMR. The multiplicity of a signal is reported as such: s–singlet, d–doublet, t–triplet, q–quartet, quint–quintet, m–multiplet, or combinations thereof. Coupling constants, *J*, are reported as observed in Hz. Additional 2D-NMR experiments (COSY, HSQC, HMBC and NOESY) were used to assist in structural assignment in conjunction with the carbon shift predicting algorithm CASCADE.[188]

Fourier-transform infrared (FT-IR) spectra were recorded from evaporated films on a Bruker Tensor 27 spectrometer equipped with a Pike Miracle Attenuated Total Reflectance (ATR) sampling accessory. Absorption maxima are quoted in wavenumbers, $\nu_{max}$ /$cm^{-1}$, for the range 3500–600 $cm^{-1}$.

High resolution mass spectrometry (HRMS) using electrospray ionization (ESI) was carried out on a Thermo Exactive orbitrap spectrometer equipped with a Waters Equity LC system. HRMS using chemical ionization (CI) or electron ionization (EI) was carried out on a Waters GCT system equipped with a Time of Flight (TOF) spectrometer. Low resolution mass spectrometry was carried out using ESI and was performed on a Micromass LCT Premier Spectrometer. In both cases the mass reported is that containing the most abundant isotopes.

Melting points were determined using a Reichert melting point apparatus or a Leica VMTG heated-stage microscope equipped with a Testo 720 thermometer and are reported uncorrected. All compounds were crystallised from chloroform ($CHCl_3$) unless stated otherwise. Systematic names were generated using ChemDraw 16.0 in accordance with the guidelines specified by the International Union of Pure and Applied Chemistry (IUPAC). Compounds labelled with the prefix “AM” have been synthesised by Dr. Aroonroj Makareeya.

*2. General synthetic procedures*

**Phase-transfer method [A]**

To a solution of carboxylic acid (1.0 equiv.) and oxalyl chloride (1.2 equiv.) in anhydrous $CH_2Cl_2$ (2 mL), was added one drop of anhydrous DMF. The reaction mixture was stirred at room temperature for 3 h, when anhydrous toluene (4 mL), tetrabutylammonium bromide (0.34 equiv.), freshly ground KOH (2.4 equiv.) and indole or *N*-heterocycle (1.0 equiv.) were added to the reaction mixture. The resulting suspension was stirred vigorously at room temperature until completion (as indicated by TLC). Water (15 mL) was then added to the reaction mixture and the aqueous layer was extracted with EtOAc (3 × 10 mL). The combined organic layer was washed with brine (5 mL), dried over $MgSO_4$, and concentrated in vacuo.

**Amidation *via* $NEt_3$/DMAP/oxalyl chloride [B]**

To a solution of carboxylic acid (1.0 equiv.) and oxalyl chloride (1.2 equiv.) in anhydrous $CH_2Cl_2$ (2.4 mL), was added one drop of anhydrous DMF. The reaction mixture was stirred at room temperature for 3 h, when anhydrous triethylamine (1.67 equiv.) was added dropwise *via* syringe under a strong flow of $N_2$ (in some cases, an ice bath was required to prevent a thermal runaway), followed by an addition of DMAP (0.17 equiv.). After approximatively 1 min, indole or *N*-heterocycle (0.83 equiv.) was added, and the reaction mixture was then stirred overnight. After completion (as indicated by TLC), water (20 mL) was added, and the aqueous layer was extracted with EtOAc (3 × 15 mL). The combined organic layer was washed with brine (10 mL), dried over $MgSO_4$, and concentrated in vacuo.

**Amidation *via* DCC coupling [C]**

Carboxylic acid (1.2 equiv.), indole (1.0 equiv.), DMAP (0.12 equiv.) and DCC (1.2 equiv.) were dissolved in anhydrous $CH_2Cl_2$ (11.3 mL). The reaction was stirred at room temperature overnight until completion (as indicated by TLC). The reaction mixture was then passed

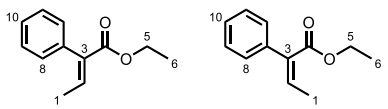
through a plug of silica, and filtrate was concentrated in vacuo. The crude residue was then purified by flash column chromatography.

**Photocyclisation *via* triplet energy transfer [D]**

Amide substrate (1.0 equiv.), $Ir(dFppy)_3$ (0.01 equiv.) and NaOAc (0.1 equiv.) were transferred to glass vial. The vial was sealed and flushed with argon for 5 min. The vial was then charged with degassed EtOAc (10 mL/mmol amide). The reaction mixture was then irradiated with blue light and stirred under a stream of $N_2$. Once the reaction was completed, the excess solvent was evaporated and the residue was purified by flash column chromatography.

***3. Characterization of compounds***

*(E*/*Z*)-2-phenylbut-2-enoic acid (**136**)

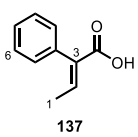


**136**

To a suspension of ethyltriphenylphosphonium bromide (1.78 g, 10 mmol, 1 equiv.) in anhydrous THF (20 mL) cooled to –78 ºC, KHMDS (10 mL, 1M in THF, 10 mmol, 1 equiv.) was added dropwise and the resulting mixture was stirred at –78 ºC for 15 minutes. The reaction was then allowed to worm to room temperature and stirred for an additional 1 h when it was cooled back to –78 ºC. A solution of **135** (3.71 g, 10 mmol, 1 equiv.) in anhydrous THF (5 mL) was added dropwise and the reaction was further stirred for 1 h at –78 ºC, when the reaction was allowed to warm to room temperature over 16 h. The reaction was then quenched with 1M HCl, extracted with $CH_2Cl_2$, dried of $MgSO_4$ and evaporated. The resulting crude oil was purified by column chromatography (5% $Et_2O$/pentane) to give **136** compound as a clear liquid (1.05 g, 5.5 mmol, 55%); $\boldsymbol{\delta_H}$ (400 MHz, $CDCl_3$): 7.41– 7.14 (6.1H, m, $H2^E$, Ph*H*), 6.27 (0.1H, q, *J* = 7.2 Hz, $H2^z$), 4.31 (0.2H, q, *J* = 7.1 Hz, $H5^Z$), 4.21 (2H, q, *J* = 7.1 Hz, $H5^E$), 2.05 (0.3H, d, *J* = 7.2 Hz, $H1^Z$), 1.75 (3H, d, *J* = 7.2 Hz, $H1^E$), 1.33 (0.3H, t, *J* = 7.1 Hz, $H6^Z$), 1.26

(3H, t, $J$ = 7.1 Hz, H6$^{E}$); **δC** (100 MHz, $CDCl_3$): 167.28, 139.75, 135.28, 135.12, 134.46, 129.92, 128.36, 128.05, 127.54, 127.43, 127.22, 60.84, 16.07, 15.57, 14.40, 14.36. Data is in accordance with literature values.[189]

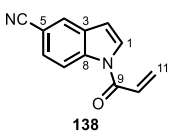
(*E*/*Z*)-2-phenylbut-2-enoic acid (**137**)



**137**

A solution of **137** (920 mg, 4.84 mmol, 1 equiv.), $LiOH{\cdot}H_2O$ (1.02 g, 24.2 mmol, 5 equiv.) in mixture of THF (9.7 mL) and $H_2O$ (9.7 mL) was heated to 80 ºC for 24 h. The reaction was quenched with 1M HCl, extracted with $Et_2O$, dried of $MgSO_4$ and evaporated. The resulting oil was triturated with pentane to give an off-white solid of the compound **137** (697 mg, 4.21 mmol, 89%); **δH** (400 MHz, $CDCl_3$): 7.42 – 7.28 (4H, m, H2, Ph*H*), 7.22 – 7.16 (2H, m, Ph*H*), 1.78 (3H, d, $J$ = 7.2 Hz, H1). **δC** (100 MHz, $CDCl_3$): 172.54, 142.93, 134.55, 134.29, 129.99, 129.95, 128.29, 128.21, 128.08, 127.77, 15.92. Data is in accordance with literature values.[190]

1-acryloyl-1H-indole-5-carbonitrile (**138**)

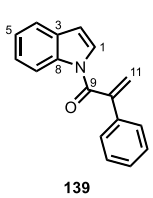


**138**

To a suspension of 1H-indole-5-carbonitrile (142.2 mg, 1.0 mmol, 1.0 equiv.), tetrabutylammonium bromide (161.2 mg, 0.5 mmol, 0.5 equiv.) and NaOH (60 mg, 1.5 mmol, 1.5 equiv.) in $CH_2Cl_2$, was added acryloyl chloride (0.12 mL, 1.5 mmol, 1.5 equiv.). The reaction was stirred at room temperature for 16 h, concentrated. The resulting residue was purified by column chromatography (7% acetone/pentane) to give compound **138** as an off-white solid (80 mg, 0.41 mmol, 41%); **m.p.** >300 ºC (decomposition); **δH** (400 MHz, $CDCl_3$): 8.61 (1H, dt, $J$ = 8.7, 0.8 Hz, H7), 7.92 (1H, dd, $J$ = 1.7, 0.7 Hz, H4), 7.72 – 7.60 (2H, m, H1, H6), 6.96 (1H, dd, $J$ = 16.8, 10.4 Hz, H10), 6.78 – 6.69 (2H, m, H2, H11, H2), 6.13 (1H, dd, $J$ = 10.4, 1.3 Hz, H11); **δC** (100 MHz, $CDCl_3$): 163.99, 137.77, 133.75, 130.71, 128.41, 127.36, 126.83, 125.83, 119.64, 117.76, 108.98, 107.55; **IR** (thin film) $\nu_{max}/cm^{-1}$:

2224, 1691, 1610, 1404, 1202; **HRMS** *m/z* ($ESI^+$) found $[M+H]^+$ 197.0712; $C_{12}H_9N_2O^+$ requires 197.0709.

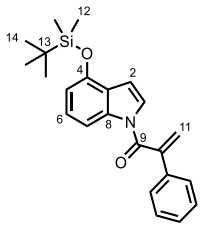
1-(1H-indol-1-yl)-2-phenylprop-2-en-1-one (**139**)



139

Synthesised from atropic acid (0.5 g, 3.375 mmol) and indole (264 mg, 2.25 mmol) using **General Procedure [A]**. The resulting crude material was purified by column chromatography (2.5% $Et_2O$/pentane) to give compound **139** as a colourless oil (239 mg, 0.97 mmol, 43%); $\delta_H$ (400 MHz, $CDCl_3$): 8.57 (1H, dq, *J* = 8.2, 0.9 Hz, H7), 7.57 (1H, dt, *J* = 7.6, 1.1 Hz, H4), 7.54 – 7.45 (2H, m, H5, H6), 7.45 – 7.28 (6H, m, H1, Ph*H*), 6.55 (1H, dd, *J* = 3.8, 0.8 Hz, H2), 6.08 (1H, s, H11), 5.70 (1H, s, H11); $\delta_C$ (100 MHz, $CDCl_3$): 168.66, 144.52, 135.67, 135.46, 131.05, 129.20, 129.16, 127.07, 126.23, 125.27, 124.32, 121.02, 118.60, 116.84, 109.26.; **IR** (thin film) $\nu_{max}/cm^{-1}$: 1689, 1536, 1471, 1379; **HRMS** *m/z* ($ESI^+$) found $[M+H]^+$ 248.1071; $C_{17}H_{14}NO^+$ requires 248.1070.

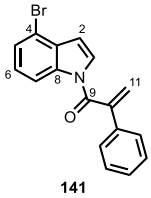
1-(4-((*tert*-butyldimethylsilyl)oxy)-1H-indol-1-yl)-2-phenylprop-2-en-1-one (**140**)



140

Synthesised from atropic acid (0.5 g, 3.375 mmol) and 4-((*tert*-butyldimethylsilyl)oxy)-1H-indole (556 mg, 2.25 mmol) using **General Procedure [A]**. The resulting crude material was purified by column chromatography (3% $Et_2O$/pentane) to give compound **140** as a colourless oil (249 mg, 0.65 mmol, 29%); $\delta_H$ (400 MHz, $CDCl_3$): 8.17 (1H, dt, *J* = 8.3, 0.8 Hz, H7), 7.51 – 7.45 (2H, m, Ph*H*), 7.41 – 7.33 (3H, m, Ph*H*), 7.25 (1H, t, *J* = 8.3 Hz, H6), 7.20 (1H, d, *J* = 3.8 Hz, H1), 6.74 (1H, dd, *J* = 7.9, 0.8 Hz, H5), 6.60 (1H, dd, *J* = 3.8, 0.8 Hz, H2), 6.07 (1H, s, H11), 5.69 (1H, s, H11), 1.04 (9H, s, H14), 0.24 (6H, s, H12); $\delta_C$ (100 MHz, $CDCl_3$): 168.71, 148.79, 144.62, 137.28, 135.51, 129.17, 129.14, 126.26, 126.12, 125.61, 124.10, 118.55, 113.86, 110.41, 106.67, 25.86, 18.42, -4.17; **IR** (thin film) $\nu_{max}/cm^{-1}$: 1695, 1481, 1419, 1344, 1246; **HRMS** *m/z* ($ESI^+$) found $[M+H]^+$ 378.1884; $C_{23}H_{28}NO_2Si^+$ requires 378.1884.

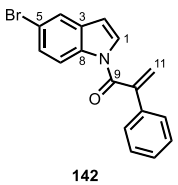
1-(4-bromo-1H-indol-1-yl)-2-phenylprop-2-en-1-one (**141**)



141

Synthesised from atropic acid (0.5 g, 3.375 mmol) and 4-bromoindole (442 mg, 2.25 mmol) using **General Procedure [A]**. The resulting crude material was purified by column chromatography (3% $Et_2O$/pentane) to give compound **141** as a white solid (535 mg, 1.64 mmol, 73%); **m.p.** 33-34 °C; **$\delta_H$** (400 MHz, $CDCl_3$): 8.51 (1H, dd, *J* = 8.4, 1.1 Hz, H7), 7.51 – 7.42 (3H, m, H5, Ph*H*), 7.42 – 7.33 (4H, m, H1, Ph*H*), 7.26 (1H, t, *J* = 8.0 Hz, H6), 6.62 (1H, dd, *J* = 3.8, 0.7 Hz, H2), 6.10 (1H, s, H11), 5.72 (1H, s, H11); **$\delta_C$** (100 MHz, $CDCl_3$): 168.70, 144.26, 136.04, 135.27, 131.68, 129.36, 129.25, 127.62, 127.22, 126.32, 126.22, 119.24, 115.84, 114.76, 108.97; **IR** (thin film) $\nu_{max}/cm^{-1}$: 1682, 1532, 1419, 1345, 1174; **HRMS** *m/z* ($ESI^+$) found $[M+H]^+$ 326.0175; $C_{17}H_{13}NBrO^+$ requires 326.0175.

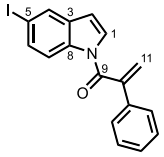
1-(5-bromo-1H-indol-1-yl)-2-phenylprop-2-en-1-one (**142**)



142

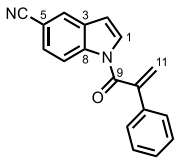
Synthesised from atropic acid (4.0 g, 27.0 mmol) and 5-bromoindole (3.38 g, 18.0 mmol) using **General Procedure [A]**. The resulting crude material was purified by column chromatography (4% $Et_2O$/pentane) to give compound **142** as an off-white solid (3.46 g, 10.62 mmol, 59%); **m.p.** 75-76 °C; **$\delta_H$** (400 MHz, $CDCl_3$): 8.43 (1H, d, *J* = 8.8 Hz, H7), 7.70 (1H, d, *J* = 2.0 Hz, H4), 7.55 – 7.41 (3H, m, H6, Ph*H*), 7.42 – 7.33 (3H, m, Ph*H*), 7.30 (1H, d, *J* = 3.8 Hz, H1), 6.47 (1H, dd, *J* = 3.8, 0.8 Hz, H2), 6.09 (1H, s, H11), 5.71 (1H, s, H11); **$\delta_C$** (100 MHz, $CDCl_3$): 168.49, 144.23, 135.30, 134.38, 132.76, 129.33, 129.23, 128.17, 128.11, 126.21, 123.74, 119.11, 118.17, 117.61, 108.37. **IR** (thin film) $\nu_{max}/cm^{-1}$: 1693, 1407, 1331; **HRMS** *m/z* ($ESI^+$) found $[M+H]^+$ 326.0176; $C_{17}H_{13}NBrO^+$ requires 326.0175.

1-(5-iodo-1H-indol-1-yl)-2-phenylprop-2-en-1-one (**143**)


143

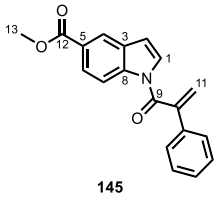
Synthesised from atropic acid (1.0 g, 6.75 mmol) and 5-iodoindole (1.09 g, 4.5 mmol) using **General Procedure [A]** where toluene was replaced by $CH_2Cl_2$. The resulting crude material was purified by column chromatography (2% $Et_2O$/pentane) to give compound **143** as a white solid (494 mg, 1.31 mmol, 29%); **m.p.** 63 ºC; **$\delta_H$** (400 MHz, $CDCl_3$): 8.31 (1H, dt, *J* = 8.7, 0.7 Hz, H7), 7.91 (1H, dd, *J* = 1.7, 0.5 Hz, H4), 7.67 (1H, dd, *J* = 8.7, 1.7 Hz, H6), 7.48 – 7.41 (2H, m, Ph*H*), 7.41 – 7.34 (3H, m, Ph*H*), 7.26 (1H, d, *J* = 3.8 Hz, H1), 6.46 (1H, dd, *J* = 3.8, 0.8 Hz, H2), 6.09 (1H, s, H11), 5.71 (1H, s, H11); **$\delta_C$** (100 MHz, $CDCl_3$): 168.54, 144.25, 135.29, 134.94, 133.79, 133.28, 129.92, 129.33, 129.23, 127.82, 126.20, 119.12, 118.56, 108.14, 88.47; **IR** (thin film) $\nu_{max}/cm^{-1}$: 1691, 1537, 1442, 1366; **HRMS** *m/z* ($ESI^+$) found $[M+H]^+$ 374.0037; $C_{17}H_{13}NIO^+$ requires 374.0036.

1-(2-phenylacryloyl)-1H-indole-5-carbonitrile (**144**)


144

Synthesised from atropic acid (222 mg, 1.5 mmol) and indole (142 mg, 1.0 mmol) using a modified **General Procedure [A]** where toluene was replaced by $CH_2Cl_2$. The resulting crude material was purified by column chromatography (10% AcOEt/pentane) to give compound **144** as a white solid (155 mg, 0.57 mmol, 57%); **m.p.** 144 °C; **$\delta_H$** (400 MHz, $CDCl_3$): 8.64 (1H, dt, *J* = 8.6, 0.8 Hz, H7), 7.90 (1H, dd, *J* = 1.6, 0.7 Hz, H4), 7.65 (1H, dd, *J* = 8.6, 1.6 Hz, H6), 7.49 – 7.35 (6H, m, H1, Ph*H*), 6.59 (1H, dd, *J* = 3.8, 0.8 Hz, H2), 6.13 (1H, s, H11), 5.76 (1H, s, H11); **$\delta_C$** (100 MHz, $CDCl_3$): 168.62, 143.99, 137.51, 135.04, 131.03, 129.51, 129.33, 129.30, 129.14, 128.45, 126.21, 125.77, 119.88, 119.60, 117.57, 108.62, 107.73; **IR** (thin film) $\nu_{max}/cm^{-1}$: 2227, 1684, 1540; **HRMS** *m/z* ($ESI^+$) found $[M+H]^+$ 273.1024; $C_{18}H_{13}N_2O^+$ requires 273.1028.

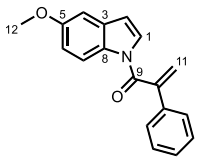
methyl 1-(2-phenylacryloyl)-1H-indole-5-carboxylate (**145**)



**145**

Synthesised from atropic acid (0.5 g, 3.375 mmol) and methyl 1H-indole-5-carboxylate (394 mg, 2.25 mmol) using **General Procedure [A]**. The resulting crude material was purified by column chromatography (7.5% AcOEt/pentane) to give compound **145** as a white solid (162 mg, 0.54 mmol, 24%); **m.p.** 171-173 °C; **$\delta_H$** (400 MHz, $CDCl_3$): 8.58 (1H, dt, *J* = 8.8, 0.7 Hz, H7), 8.29 (1H, dd, *J* = 1.8, 0.7 Hz, H4), 8.09 (1H, dd, *J* = 8.7, 1.7 Hz, H6), 7.51 – 7.43 (2H, m, Ph*H*), 7.43 – 7.32 (4H, m, H1, Ph*H*), 6.60 (1H, dd, *J* = 3.8, 0.7 Hz, H2), 6.10 (1H, s, H11), 5.74 (1H, s, H11), 3.95 (3H, s, H13); **$\delta_C$** (100 MHz, $CDCl_3$): 168.64, 167.41, 144.31, 138.32, 135.27, 130.87, 129.37, 129.25, 129.23, 128.25, 126.60, 126.25, 123.23, 119.28, 116.45, 109.48, 52.25; **IR** (thin film) $\nu_{max}/cm^{-1}$: 1708, 1695, 1493, 1209; **HRMS** *m/z* ($ESI^+$) found $[M+H]^+$ 306.1126; $C_{19}H_{16}NO_3^+$ requires 306.1125.

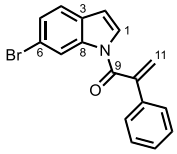
1-(5-methoxy-1H-indol-1-yl)-2-phenylprop-2-en-1-one (**146**)



**146**

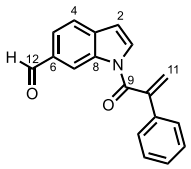
Synthesised from atropic acid (0.5 g, 3.375 mmol) and indole (331 mg, 2.25 mmol) using **General Procedure [A]**. The resulting crude material was purified by column chromatography (7% $Et_2O$/pentane) to give t compound **146** as a colourless oil (253 mg, 0.90 mmol, 40%); **$\delta_H$** (400 MHz, $CDCl_3$): 8.45 (1H, dt, *J* = 8.9, 0.8 Hz, H7), 7.50 – 7.45 (2H, m, Ph*H*), 7.40 – 7.33 (3H, m, Ph*H*), 7.28 (1H, d, *J* = 3.8 Hz, H1), 7.05 – 6.98 (2H, m, H4, H6), 6.47 (1H, dd, *J* = 3.8, 0.8 Hz, H2), 6.06 (1H, s, H11), 5.68 (1H, s, H11), 3.87 (3H, s, H12); **$\delta_C$** (100 MHz, $CDCl_3$): 168.32, 157.04, 144.44, 135.56, 132.11, 130.35, 129.18, 129.14, 127.76, 126.23, 118.51, 117.61, 113.54, 109.21, 103.95, 55.85; **IR** (thin film) $\nu_{max}/cm^{-1}$: 1684, 1470, 1244; **HRMS** *m/z* ($ESI^+$) found $[M+H]^+$ 278.1178; $C_{18}H_{16}NO_2^+$ requires 287.1176.

1-(6-bromo-1H-indol-1-yl)-2-phenylprop-2-en-1-one (**147**)


147

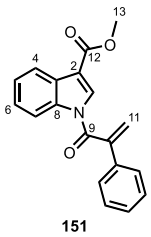
Synthesised from atropic acid (0.5 g, 3.375 mmol) and 6-bromoindole (422 mg, 2.25 mmol) using **General Procedure [A]**. The resulting crude material was purified by column chromatography (3% $Et_2O$/pentane) to give compound **147** as a white solid (350 mg, 1.08 mmol, 48%); **m.p.** 75-76 ºC; **$\delta_H$** (400 MHz, $CDCl_3$): 8.78 (1H, dt, *J* = 1.6, 0.7 Hz, H7), 7.56 – 7.29 (7H, m, H4, H5, Ph*H*), 7.26 (1H, d, *J* = 3.8 Hz, H1), 6.49 (1H, dd, *J* = 3.8, 0.8 Hz, H2), 6.09 (1H, s, H11), 5.71 (1H, s, H11); **$\delta_C$** (100 MHz, $CDCl_3$): 168.52, 144.21, 136.30, 135.27, 129.81, 129.34, 129.27, 129.23, 127.58, 127.51, 126.20, 122.04, 119.96, 119.09, 118.98, 108.92; **IR** (thin film) $\nu_{max}/cm^{-1}$: 1692, 1496, 1317, 1347, 1200; **HRMS** *m/z* ($ESI^+$) found $[M+H]^+$ 326.0177; $C_{17}H_{13}NBrO^+$ requires 326.0175.

1-(2-phenylacryloyl)-1H-indole-6-carbaldehyde (**148**)


148

Synthesised from atropic acid (0.5 g, 3.375 mmol) and 1H-indole-6-carbaldehyde (327 mg, 2.25 mmol) using **General Procedure [A]**. The resulting crude material was purified by column chromatography (15% AcOEt/pentane) to give compound **148** as an off-white solid (405 mg, 1.46 mmol, 65%); **m.p**: 103-105 ºC; **$\delta_H$** (400 MHz, $CDCl_3$): 10.12 (1H, s, H12), 9.04 (1H, dt, *J* = 1.5, 0.7 Hz, H7), 7.89 (1H, dd, *J* = 8.1, 1.4 Hz, H4), 7.67 (1H, d, *J* = 8.1 Hz, H4), 7.53 – 7.44 (3H, m, Ph*H*), 7.44 – 7.34 (3H, m, H1, Ph*H*), 6.61 (1H, dd, *J* = 3.7, 0.8 Hz, H2), 6.13 (1H, s, H11), 5.76 (1H, s, H11); **$\delta_C$** (100 MHz, $CDCl_3$): 192.31, 168.53, 144.07, 135.94, 135.38, 135.19, 133.95, 130.65, 129.44, 129.34, 129.29, 126.22, 124.11, 121.58, 120.61, 119.58, 109.16. **IR** (thin film) $\nu_{max}/cm^{-1}$: 1732, 1674, 1453, 1365, 1327; **HRMS** *m/z* ($ESI^+$) found $[M+H]^+$ 276.1020; $C_{18}H_{14}NO_2^+$ requires 276.1019.

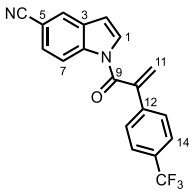
methyl 1-(2-phenylacryloyl)-1H-indole-3-carboxylate (**151**)



**151**

Synthesised from atropic acid (0.5 g, 3.375 mmol) and methyl 1H-indole-3-carboxylate (394 mg, 2.25 mmol) using **General Procedure [A]**. The resulting crude material was purified by column chromatography (7.5% AcOEt/pentane) to give compound **151** as a white solid (449 mg, 1.46 mmol, 65%); **m.p.** 85-86 ºC; **$\delta_H$** (400 MHz, $CDCl_3$): 8.59 – 8.52 (1H, m, H7), 8.20 – 8.13 (1H, m, H4), 8.02 (1H, s, H1), 7.53 – 7.33 (7H, m, H5, H6, Ph*H*), 6.16 (1H, s, H11), 5.73 (1H, s, H11), 3.89 (3H, s, H13); **$\delta_C$** (100 MHz, $CDCl_3$): 168.77, 164.41, 143.63, 136.09, 134.92, 132.93, 129.52, 129.29, 127.98, 126.25, 126.14, 125.39, 121.86, 119.69, 116.70, 114.04, 51.70; **IR** (thin film) $\nu_{max}/cm^{-1}$: 1682, 1717, 1701, 1622, 1192; **HRMS** *m/z* ($ESI^+$) found $[M+H]^+$ 306.1126; $C_{19}H_{16}NO_3^+$ requires 306.1125.

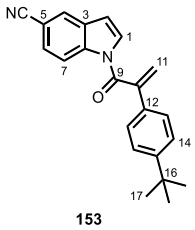
1-(2-(4-(trifluoromethyl)phenyl)acryloyl)-1H-indole-5-carbonitrile (**152**)



**152**

Synthesised from 2-(4-(trifluoromethyl)phenyl)acrylic acid[6] (324.3 mg, 1.50 mmol) and 1H-indole-5-carbonitrile (142 mg, 1.0 mmol) using **General Procedure [B]**. The resulting crude material was purified by column chromatography (20% AcOEt/pentane) to give compound **152** as a yellow oil (60.4 mg, 0.18 mmol, 18%); **$\delta_H$** (400 MHz, $CDCl_3$): 8.63 (1H, dt, *J* = 8.6, 0.8 Hz, H7), 7.91 (1H, dd, *J* = 1.6, 0.7 Hz, H4), 7.70 – 7.55 (5H, m, H6, H13, H14), 7.40 (1H, d, *J* = 3.8 Hz, H1), 6.64 (1H, dd, *J* = 3.8, 0.8 Hz, H2), 6.24 (1H, s, H11), 5.88 (1H, s, H11); **$\delta_C$** (100 MHz, $CDCl_3$): 167.75, 142.82, 138.46, 137.54, 131.11, 128.77, 128.66, 126.73, 126.33 (q, *J* = 3.8 Hz), 125.89, 122.16, 119.46, 117.61, 109.10, 108.08; **$\delta_F$** (376 MHz, $CDCl_3$): -62.87; **IR** (thin film) $\nu_{max}/cm^{-1}$: 2227, 1699, 1461, 1325; **HRMS** *m/z* ($ESI^+$) found $[M-H]^-$ 339.0750; $C_{19}H_{10}N_2OF_3^-$ requires 339.0751.

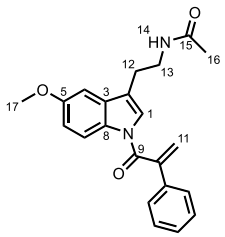
1-(2-(4-(*tert*-butyl)phenyl)acryloyl)-1H-indole-5-carbonitrile (**153**)



**153**

Synthesised from 2-(4-(*tert*-butyl)phenyl)acrylic acid (306.4 mg, 1.5 mmol) and 1H-indole-5-carbonitrile (142 mg, 1.0 mmol) using **General Procedure [B]**. The resulting crude material was purified by column chromatography (15% $Et_2O$/pentane) to give compound **153** as a white solid (240.3 mg, 0.73 mmol, 73%); **m.p.** 103-104 ºC; $\delta_H$ (400 MHz, $CDCl_3$): 8.64 (1H, dt, *J* = 8.6, 0.8 Hz, H7), 7.90 (1H, dd, *J* = 1.7, 0.7 Hz, H4), 7.65 (1H, dd, *J* = 8.5, 1.7 Hz, H6), 7.44 (1H, d, *J* = 3.8 Hz, H1), 7.43 – 7.35 (4H, m, H13, H14), 6.59 (1H, dd, *J* = 3.8, 0.8 Hz, H2), 6.09 (1H, s, H11), 5.68 (1H, s, H11), 1.31 (9H, s, H17); $\delta_C$ (100 MHz, $CDCl_3$): 168.84, 152.87, 143.80, 137.53, 132.13, 131.09, 129.29, 128.40, 126.26, 125.94, 125.74, 119.62, 118.75, 117.59, 108.52, 107.71, 34.88, 31.31; **IR** (thin film) $\nu_{max}/cm^{-1}$: 2227, 1702, 1460, 1365, 1337; **HRMS** *m/z* ($ESI^+$) found $[M+H]^+$ 329.1649; $C_{22}H_{21}N_2O^+$ requires 329.1648.

*N*-(2-(5-methoxy-1-(2-phenylacryloyl)-1H-indol-3-yl)ethyl)acetamide (**154**)

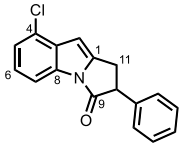


**154**

To a solution of atropic acid (0.5 g, 3.37 mmol, 1.5 equiv.) and oxalyl chloride (0.35 mL, 2.7 mmol, 1.2 equiv.) in anhydrous $CH_2Cl_2$ (6.8 mL), was added one drop of anhydrous DMF. The reaction mixture was stirred at room temperature for 3 h. Once the reaction completed, anhydrous toluene (14.5 mL), tetrabutylammonium bromide (363 mg, 1.13 mmol, 0.5 equiv.), freshly ground KOH (455 mg, 8.11 mmol, 3.6 equiv.) and melatonin (523 mg, 2.25 mmol, 1 equiv.) were added to the reaction mixture. The reaction was heated to 40 ºC and further stirred for 16 h. The resulting mixture was then cooled to room temperature, concentrated and purified by column chromatography (25% MeCN/pentane) to give compound **154** as a viscous oil (178 mg, 0.50 mmol, 22%); $\delta_H$ (400 MHz, $CDCl_3$): 8.47 – 8.40 (1H, m, H7), 7.49 – 7.45 (2H, m, Ph*H*), 7.41 – 7.31 (3H, m, Ph*H*), 7.08 (1H, d, *J* = 1.1 Hz, H4), 7.06 – 6.97 (2H, m, H4, H6), 6.05 (1H, s, H11), 5.66 (1H, s, H11), 5.40 (1H, s, H14), 3.88 (3H, s, H17), 3.49 (2H, q, *J* = 6.6

Hz, H13), 2.80 (2H, td, *J* = 6.9, 1.1 Hz, H12), 1.85 (3H, s, H16); **δC** (100 MHz, $CDCl_3$): 170.14, 167.88, 157.15, 144.46, 135.54, 132.08, 130.68, 129.19, 129.15, 126.18, 124.81, 119.60, 118.29, 117.88, 113.68, 102.18, 55.94, 38.90, 25.25, 23.40; **IR** (thin film) $\nu_{max}/cm^{-1}$: 3290, 1679, 1551, 1475, 1384, 1204; **HRMS** *m/z* ($ESI^+$) found $[M+H]^+$ 363.1704; $C_{22}H_{23}N_2O_3^+$ requires 363.1703.

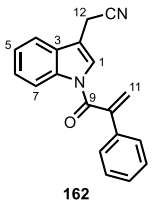
8-chloro-2-phenyl-1,2-dihydro-3H-pyrrolo[1,2-a]indol-3-one (**155**)



**155**

Synthesised from compound **S3** (84.5 mg, 0.3 mmol) using **General Procedure [D]**. The resulting crude material was purified by column chromatography (5% AcOEt/pentane) to give compound **155** as a white solid (66.8 mg, 0.24 mmol, 79%); **m.p.** 85-86 ºC; **δH** (400 MHz, $CDCl_3$): 7.99 (1H, dt, *J* = 7.9, 0.9 Hz, H7), 7.43 – 7.18 (7H, m, H5, H6, Ph*H*), 6.51 (1H, q, *J* = 1.5 Hz, H2), 4.40 (1H, dd, *J* = 9.2, 4.7 Hz, H10), 3.73 (1H, ddd, *J* = 17.6, 9.2, 1.5 Hz, H11), 3.30 (1H, ddd, *J* = 17.6, 4.8, 1.6 Hz, H11); **δC** (100 MHz, $CDCl_3$): 172.01, 142.54, 138.14, 134.10, 131.44, 129.33, 128.06, 127.80, 125.65, 124.42, 124.25, 112.42, 99.14, 52.82, 29.73; **IR** (thin film) $\nu_{max}/cm^{-1}$: 1718, 1608, 1585 1424, 1136; **HRMS** *m/z* ($ESI^+$) found $[M+H]^+$ 282.0680; $C_{17}H_{13}ClNO_2^+$ requires 282.0681.

2-(1-(2-phenylacryloyl)-1H-indol-3-yl)acetonitrile (**162**)

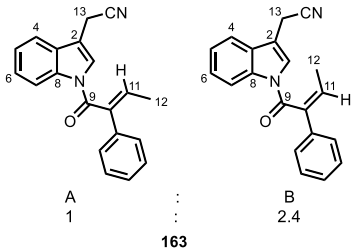


**162**

Synthesised from atropic acid (367 mg, 2.48 mmol) and 2-(1H-indol-3-yl)acetonitrile (352 mg, 2.25 mmol) using **General Procedure [C]**. The resulting crude material was purified by column chromatography (10% AcOEt/pentane) to give compound **162** as a white solid (351 mg, 1.23 mmol, 54%); **m.p.** 94 ºC; **δH** (400 MHz, $CDCl_3$): 8.57 (1H, dt, *J* = 8.2, 0.9 Hz, H7), 7.54 (1H, ddd, *J* = 7.8, 1.3, 0.8 Hz, H4), 7.51 – 7.44 (3H, m, H5, H6, Ph*H*), 7.43 – 7.32 (5H, m, H1, Ph*H*), 6.11 (1H, s, H11), 5.70 (1H, s, H11), 3.71 (2H, d, *J* = 1.3 Hz, H12); **δC** (100 MHz, $CDCl_3$): 168.32, 144.10,

136.07, 135.12, 129.42, 129.27, 129.11, 126.34, 126.21, 125.23, 124.68, 118.96, 118.40, 117.24, 116.79, 111.63, 14.52; **IR** (thin film) $\nu_{max}/cm^{-1}$: 1678, 1372, 1224; **HRMS** *m/z* ($ESI^+$) found $[M+H]^+$ 287.1180; $C_{19}H_{15}N_2O^+$ requires 287.1179.

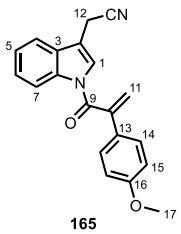
(*E*/*Z*)-2-(1-(2-phenylbut-2-enoyl)-1H-indol-3-yl)acetonitrile (**163**)



**163**

Synthesised from (*E*)-2-phenylbut-2-enoic acid (401 mg, 2.47 mmol) and 2-(1H-indol-3-yl)acetonitrile (352 mg, 2.25 mmol) using **General Procedure [C]**. The resulting crude material was purified by column chromatography (10% AcOEt/pentane) to give compound **163** as a yellow oil (252 mg, 0.83 mmol, 37%); **$\delta_H$** (400 MHz, $CDCl_3$): 8.48 (1H, dt, *J* = 8.3, 0.9 Hz, $H7^B$), 7.58 – 7.28 (11.7H m, $H4^A$, $H5^A$, $H6^A$, $H7^A$, Ph$H^A$, $H4^B$, $H5^B$, $H6^B$, Ph$H^B$), 6.48 (1.3H, m, $H1^A$, $H1^B$), 3.71 (0.7H, d, *J* = 1.3 Hz, $H12^A$), 3.70 (2H, d, *J* = 1.3 Hz, $H13^B$), 2.00 (3H, d, *J* = 7.2 Hz, $H12^B$), 1.88 (1.2H, d, *J* = 7.2 Hz, $H12^A$); **$\delta_C$** (100 MHz, $CDCl_3$): 168.82, 137.68, 136.34, 135.74, 135.30, 134.55, 129.20, 129.15, 129.04, 128.97, 128.94, 128.81, 128.47, 128.43, 128.39, 126.32, 126.00, 125.55, 125.36, 124.71, 124.64, 124.27, 118.36, 118.19, 117.06, 116.94, 116.84, 112.01, 110.79, 15.86, 15.30, 14.53, 14.50; **IR** (thin film) $\nu_{max}/cm^{-1}$: 1678, 1372, 1224; **HRMS** *m/z* ($ESI^+$) found $[M+H]^+$ 301.1336; $C_{20}H_{17}N_2O^+$ requires 301.1335.

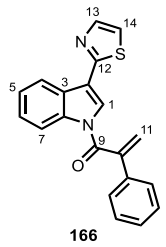
2-(1-(2-(4-methoxyphenyl)acryloyl)-1H-indol-3-yl)acetonitrile (**165**)


**165**

Synthesised from 2-(4-methoxyphenyl)acrylic acid (441 mg, 2.48 mmol) and 2-(1H-indol-3-yl)acetonitrile (352 mg, 2.25 mmol) using **General Procedure [C]**. The resulting crude material was purified by column chromatography (20% AcOEt/pentane) followed by recrystallization from minimum amount of hot isopropanol to give compound **165** as a white solid (327 mg, 1.04 mmol, 46%); **m.p.** 124 °C; **$\delta_H$** (400 MHz, $CDCl_3$): 8.56 (1H, dt, *J* = 8.3, 0.9 Hz, H7), 7.54 (1H, ddd, *J* = 7.8, 1.3,

0.7 Hz, H4), 7.47 (1H, ddd, *J* = 8.4, 7.2, 1.3 Hz, H6), 7.43 – 7.35 (4H, m, H5, H1, H14), 6.99 – 6.84 (2H, m, H15), 5.99 (1H, s, H11), 5.57 (1H, s, H11), 3.81 (3H, s, H17), 3.71 (2H, d, *J* = 1.3 Hz, H12); **δC** (100 MHz, $CDCl_3$): 168.64, 160.52, 143.46, 136.03, 129.10, 127.59, 127.53, 126.27, 125.33, 124.61, 118.38, 117.21, 116.84, 116.73, 114.63, 111.47, 55.49, 14.51; **IR** (thin film) $\nu_{max}/cm^{-1}$: 1683, 1606, 1514, 1500, 1372; **HRMS** *m/z* ($ESI^+$) found $[M+H]^+$ 317.1285; $C_{20}H_{17}N_2O_2^+$ requires 317.1285.

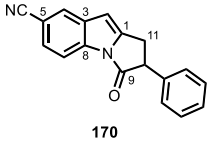
2-phenyl-1-(3-(thiazol-2-yl)-1H-indol-1-yl)prop-2-en-1-one (**166**)



166

Synthesised from atropic acid (183.4 mg, 1.24 mmol) and camalexin (225 mg, 1.12 mmol) using **General Procedure [C]**. The resulting crude material was purified by column chromatography (10% AcOEt/pentane) to give compound **166** as a white solid (276.5 mg, 0.83 mmol, 74%); **m.p.** 139-140 ºC; **δH** (400 MHz, $CDCl_3$): 8.67 – 8.57 (1H, m, H7), 8.33 – 8.24 (1H, m, H4), 7.95 (1H, s, H1), 7.88 (1H, d, *J* = 3.3 Hz, H13), 7.54 – 7.44 (4H, m, H5, H6, Ph*H*) 7.42 – 7.31 (4H, m, H14, Ph*H*), 6.16 (1H, s, H11), 5.75 (1H, s, H11); **δC** (100 MHz, $CDCl_3$): $^{13}C$ NMR (101 MHz, $CDCl_3$) δ 168.61, 160.79, 143.90, 143.37, 136.30, 135.08, 129.42, 129.25, 127.90, 126.30, 126.28, 125.94, 125.19, 121.16, 119.23, 117.90, 117.52, 116.99; **IR** (thin film) $\nu_{max}/cm^{-1}$: 1686, 1616, 1472, 1374, 1194; **HRMS** *m/z* ($ESI^+$) found $[M+H]^+$ 331.0899; $C_{20}H_{15}N_2SO^+$ requires 331.0900.

3-oxo-2-phenyl-2,3-dihydro-1H-pyrrolo[1,2-a]indole-7-carbonitrile (**170**)

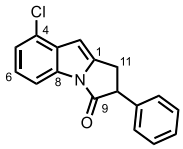


170

Synthesised from compound **145** (81.7 mg, 0.3 mmol) using **General Procedure [D]**. The resulting crude material was purified by column chromatography (15% AcOEt/pentane) to give compound **170** as a white solid (76.0 mg, 0.28 mmol, 93%); **m.p.** 163 ºC; **δH** (400 MHz, $CDCl_3$): 8.09 (1H, dt, *J* = 8.4, 0.8 Hz, H7), 7.81 (1H, dd, *J* = 1.6, 0.7 Hz, H4), 7.48 (1H, dd, *J* = 8.3, 1.5 Hz, H6), 7.37 – 7.12 (5H, m, Ph*H*), 6.36 (1H, td, *J* = 1.6, 0.8 Hz, H2), 4.36 (1H, dd, *J* = 9.3, 4.9 Hz, H10), 3.69 (1H, ddd, *J* = 17.8, 9.2,

1.5 Hz, H11), 3.26 (1H, ddd, *J* = 17.7, 4.9, 1.6 Hz, H11). **δC** (100 MHz, $CDCl_3$): 171.94, 144.08, 137.66, 135.47, 132.49, 129.40, 128.22, 127.78, 126.98, 125.57, 119.72, 114.63, 107.83, 100.52, 52.69, 29.69; **IR** (thin film) $\nu_{max}/cm^{-1}$: 2220, 1733, 1585, 1462, 1383, 1350; **HRMS** *m/z* ($ESI^+$) found $[M+H]^+$ 273.1024; $C_{18}H_{13}N_2O^+$ requires 273.1022.

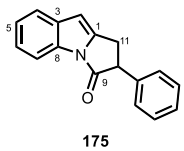
8-chloro-2-phenyl-1,2-dihydro-3H-pyrrolo[1,2-a]indol-3-one (**171**)



171

Synthesised from compound **156** (84.5 mg, 0.3 mmol) using **General Procedure [D]**. The resulting crude material was purified by column chromatography (5% AcOEt/pentane) to give compound **171** as a white solid (66.8 mg, 0.24 mmol, 79%); **m.p.** 85-86 ºC; **δH** (400 MHz, $CDCl_3$): 7.99 (1H, dt, *J* = 7.9, 0.9 Hz, H7), 7.43 – 7.18 (7H, m, H5, H6, Ph*H*), 6.51 (1H, q, *J* = 1.5 Hz, H2), 4.40 (1H, dd, *J* = 9.2, 4.7 Hz, H10), 3.73 (1H, ddd, *J* = 17.6, 9.2, 1.5 Hz, H11), 3.30 (1H, ddd, *J* = 17.6, 4.8, 1.6 Hz, H11); **δC** (100 MHz, $CDCl_3$): 172.01, 142.54, 138.14, 134.10, 131.44, 129.33, 128.06, 127.80, 125.65, 124.42, 124.25, 112.42, 99.14, 52.82, 29.73; **IR** (thin film) $\nu_{max}/cm^{-1}$: 1718, 1608, 1585 1424, 1136; **HRMS** *m/z* ($ESI^+$) found $[M+H]^+$ 282.0680; $C_{17}H_{13}ClNO_2^+$ requires 282.0681.

2-phenyl-1,2-dihydro-3H-pyrrolo[1,2-a]indol-3-one (**175**)

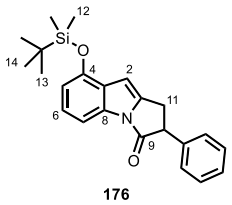


175

Synthesised from compound **140** (74.2 mg, 0.30 mmol) using **General Procedure [D]**. The resulting crude material was purified by flash column chromatography (2.5→5% $Et_2O$/petroleum ether) to yield compound **175** as an off-white solid (72.6 mg, 0.29 mmol, 98%); **m.p.** 160-162 ºC; **δH** (400 MHz, $CDCl_3$) 8.07 (1H, m, H7), 7.51 (1H, m, H4), 7.39-7.18 (7H, m, Ph*H*, H5, H6), 6.31 (1H, s, H2), 4.31 (1H, dd, *J* = 9.5, 5.0 Hz, H10), 3.63 (1H, dd, *J* = 17.4, 5.0 Hz, H11), 3.21 (1H, dd, *J* = 17.4, 9.5 Hz, H11); **δC** (100 MHz, $CDCl_3$) 29.63, 52.81, 100.71, 113.90, 120.74, 123.52, 124.36, 127.78,

127.82, 129.18, 130.75, 135.52, 138.50, 141.83, 171.89; **IR** (thin film) $\nu_{max}/cm^{-1}$ 1729, 1365; **HRMS** *m/z* ($ESI^+$) found $[M+H]^+$ 248.1071; $C_{17}H_{14}NO^+$ requires 248.1075.

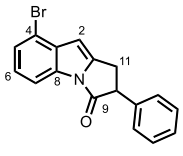
8-((*tert*-butyldimethylsilyl)oxy)-2-phenyl-1,2-dihydro-3H-pyrrolo[1,2-a]indol-3-oneone (**176**)



176

Synthesised from compound **141** (113.3 mg, 0.3 mmol) using **General Procedure [D]**. The resulting crude material was purified by column chromatography (2.5% $Et_2O$/pentane) to give compound **176** as a white solid (96.2 mg, 0.26 mmol, 85%); **m.p.** 117-120 ºC; $\delta_H$ (400 MHz, $CDCl_3$): 7.72 (1H, dt, *J* = 8.0, 0.8 Hz, H7), 7.40 – 7.25 (5H, m, Ph*H*), 7.15 (1H, t, *J* = 8.0 Hz, H6), 6.74 (1H, dd, *J* = 7.9, 0.8 Hz, H5), 6.41 (1H, td, *J* = 1.6, 0.7 Hz, H2), 4.38 (1H, dd, *J* = 9.2, 4.8 Hz, H10), 3.69 (1H, ddd, *J* = 17.4, 9.2, 1.5 Hz, H11), 3.25 (1H, ddd, *J* = 17.4, 4.8, 1.6 Hz, H11), 1.07 (9H, s, H14), 0.26 (6H, d, *J* = 1.5 Hz, H12); $\delta_C$ (100 MHz, $CDCl_3$): 172.03, 148.41, 140.27, 138.61, 132.35, 129.23, 128.36, 127.87, 124.48, 114.16, 107.69, 98.26, 53.01, 29.68, 25.90, 18.45, -4.13; **IR** (thin film) $\nu_{max}/cm^{-1}$: 1742, 1691, 1591, 1480, 1142; **HRMS** *m/z* ($ESI^+$) found $[M+H]^+$ 378.1885; $C_{23}H_{28}NO_2Si^+$ requires 378.1884.

8-bromo-2-phenyl-1,2-dihydro-3H-pyrrolo[1,2-a]indol-3-one (**177**)

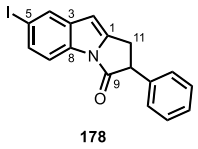


177

Synthesised from compound **142** (97.9 mg, 0.3 mmol) using **General Procedure [D]**. The resulting crude material was purified by column chromatography (5% AcOEt/pentane) to give compound **177** as a white solid (92.2 mg, 0.28 mmol, 94%); **m.p.** 101-102 ºC; $\delta_H$ (400 MHz, $CDCl_3$): 7.96 (1H, dt, *J* = 8.0, 0.9 Hz, H7), 7.38 (1H, dd, *J* = 7.9, 0.8 Hz, H5), 7.34 – 7.17 (5H, m, Ph*H*), 7.08 (1H, t, *J* = 7.9 Hz, H6), 6.39 (1H, td, *J* = 1.6, 0.7 Hz, H2), 4.32 (1H, dd, *J* = 9.2, 4.7 Hz, H10), 3.65 (1H, ddd, *J* = 17.6, 9.2, 1.5 Hz, H11), 3.22 (1H, ddd, *J* = 17.6, 4.7, 1.6 Hz, H11); $\delta_C$ (100 MHz, $CDCl_3$): 171.74, 142.27, 137.81, 135.72, 130.80, 129.02, 127.75, 127.48, 127.00, 124.37, 113.77,

112.61, 100.52, 52.46, 29.43; **IR** (thin film) $\nu_{max}/cm^{-1}$: 1724, 1421, 1156; **HRMS** *m/z* ($ESI^+$) found $[M+H]^+$ 326.0176; $C_{17}H_{13}BrNO_2^+$ requires 326.0175.

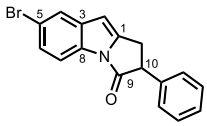
7-iodo-2-phenyl-1,2-dihydro-3H-pyrrolo[1,2-a]indol-3-one (**178**)



**178**

Synthesised from compound **144** (112.0 mg, 0.3 mmol) using **General Procedure [D]**. The resulting crude material was purified by column chromatography (5% AcOEt/pentane) to give compound **178** as a white solid (93.3 mg, 0.25 mmol, 83%); **m.p.** 141-145 ºC; **$\delta_H$** (400 MHz, $CDCl_3$): 7.82 (1H, d, *J* = 1.6 Hz, H4), 7.77 (1H, dd, *J* = 8.5, 0.7 Hz, H7), 7.50 (1H, dd, *J* = 8.5, 1.6 Hz, H6), 7.34 – 7.17 (5H, m, Ph*H*), 6.22 (1H, q, *J* = 1.1 Hz, H2), 4.30 (1H, dd, *J* = 9.2, 4.8 Hz, H10), 3.63 (1H, ddd, *J* = 17.6, 9.2, 1.5 Hz, H11), 3.20 (1H, ddd, *J* = 17.6, 4.8, 1.6 Hz, H11); **$\delta_C$** (100 MHz, $CDCl_3$): 71.85, 142.79, 138.16, 137.69, 132.17, 129.94, 129.73, 129.32, 128.04, 127.85, 127.81, 115.58, 99.85, 88.65, 52.76, 29.65; **IR** (thin film) $\nu_{max}/cm^{-1}$: 1722, 1587, 1443, 1391, 1351; **HRMS** *m/z* ($ESI^+$) found $[M+H]^+$ 374.0038; $C_{17}H_{13}INO^+$ requires 374.0036.

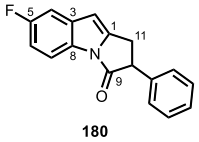
7-bromo-2-phenyl-1,2-dihydro-3H-pyrrolo[1,2-a]indol-3-one (**179**)



**179**

Synthesised from compound **143** (97.9 mg, 0.3 mmol) using **General Procedure [D]**. The resulting crude material was purified by column chromatography (5% AcOEt/pentane) to give compound **179** as a white solid (92.0 mg, 0.28 mmol, 94%); **m.p.** 112 ºC; **$\delta_H$** (400 MHz, $CDCl_3$): 7.87 (1H, dt, *J* = 8.5, 0.7 Hz, H7), 7.61 (1H, d, *J* = 1.8 Hz, H4), 7.35 – 7.16 (6H, m, Ph*H*, H6), 6.26 – 6.20 (1H, m, H2), 4.30 (1H, dd, *J* = 9.2, 4.8 Hz, H10), 3.63 (1H, ddd, *J* = 17.6, 9.2, 1.5 Hz, H11), 3.20 (1H, ddd, *J* = 17.6, 4.8, 1.6 Hz, H11); **$\delta_C$** (100 MHz, $CDCl_3$): 172.10, 143.49, 138.48, 137.51, 129.76, 129.63, 128.35, 128.12, 126.82, 123.89, 118.06, 115.47, 100.45, 53.03, 30.01; **IR** (thin film) $\nu_{max}/cm^{-1}$: 1731, 1584, 1449, 1384, 1349; **HRMS** *m/z* ($ESI^+$) found $[M+H]^+$ 326.0175; $C_{17}H_{13}BrNO_2^+$ requires 326.0175.

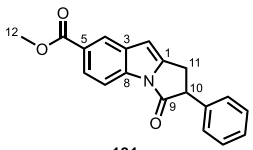
7-floro-2-phenyl-1,2-dihydro-3H-pyrrolo[1,2-a]indol-3-one (**180**)



**180**

Synthesised from compound **AM-157** (79.6 mg, 0.3 mmol) using **General Procedure [D]**. The resulting crude material was purified by column chromatography (5% AcOEt/pentane) to give compound **180** as a white solid (75.9 mg, 0.25 mmol, 83%); **m.p.** 148 ºC; **$\delta_H$** (400 MHz, $CDCl_3$): 8.02 (1H, dd, *J* = 8.8, 4.7 Hz, H7), 7.41 – 7.27 (5H, m, Ph*H*), 7.20 (1H, dd, *J* = 9.2, 2.5 Hz, H4), 7.02 (1H, td, *J* = 9.0, 2.5 Hz, H6), 6.33 (1H, q, *J* = 1.3 Hz, H2), 4.38 (1H, dd, *J* = 9.1, 4.7 Hz, H10), 3.71 (1H, ddd, *J* = 17.6, 9.2, 1.5 Hz, H11), 3.27 (1H, ddd, *J* = 17.6, 4.7, 1.6 Hz, H11); **$\delta_C$** (100 MHz, $CDCl_3$): 171.62, 160.30 (d, *J* = 240.4 Hz), 143.67, 138.30, 136.63 (d, *J* = 10.1 Hz), 129.29, 127.99, 127.81, 127.24, 114.71 (d, *J* = 9.8 Hz), 111.36 (d, *J* = 25.5 Hz), 106.65 (d, *J* = 24.2 Hz), 100.74 (d, *J* = 3.8 Hz), 52.64, 29.74; **$\delta_F$** (376 MHz, $CDCl_3$): -117.86 (td, *J* = 9.4, 4.8 Hz); **IR** (thin film) $\nu_{max}/cm^{-1}$: 1726, 1497, 1165; **HRMS** *m/z* ($ESI^+$) found $[M+H]^+$ 266.0975; $C_{17}H_{13}FNO_2^+$ requires 266.0976.

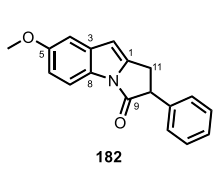
methyl 3-oxo-2-phenyl-2,3-dihydro-1H-pyrrolo[1,2-a]indole-7-carboxylate (**181**)



**181**

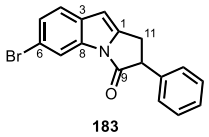
Synthesised from compound **146** (91.6 mg, 0.3 mmol) using **General Procedure [D]**. The resulting crude material was purified by column chromatography (10% AcOEt/pentane) to give compound **181** as a white solid (56.5 mg, 0.19 mmol, 62%); **m.p.** 171-173 ºC; **$\delta_H$** (400 MHz, $CDCl_3$): 8.27 (1H, dd, *J* = 1.6, 0.7 Hz, H4), 8.09 (1H dt, *J* = 8.6, 0.7 Hz, H7), 7.99 (1H, dd, *J* = 8.5, 1.6 Hz, H6), 7.40 – 7.24 (5H, m, Ph*H*), 6.42 (1H, td, *J* = 1.6, 0.7 Hz, H2), 4.39 (1H, dd, *J* = 9.2, 4.9 Hz, H10), 3.93 (3H, s, H12), 3.71 (1H, ddd, *J* = 17.6, 9.3, 1.5 Hz, H11), 3.29 (1H, ddd, *J* = 17.6, 4.9, 1.7 Hz, H11); **$\delta_C$** (100 MHz, $CDCl_3$): 171.99, 167.52, 142.99, 138.08, 135.32, 133.30, 129.32, 128.05, 127.82, 126.29, 125.08, 123.05, 113.55, 101.20, 52.78, 52.28, 29.71; **IR** (thin film) $\nu_{max}/cm^{-1}$: 1739, 1709, 1381, 1295; **HRMS** *m/z* ($ESI^+$) found $[M+H]^+$ 306.1125; $C_{19}H_{16}NO_3^+$ requires 306.1125.

7-methoxy-2-phenyl-1,2-dihydro-3H-pyrrolo[1,2-a]indol-3-one (**182**)


182

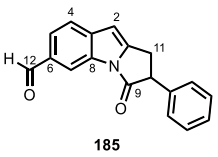
Synthesised from compound **147** (83.2 mg, 0.30 mmol) using **General Procedure [D]**. The crude material was purified by flash column chromatography (5% $Et_2O$/petroleum ether) to obtain compound **182** as a white solid (58.1 mg, 0.21 mmol, 70%); **m.p.** 165-166 ºC; **$\delta_H$** (400 MHz, $CDCl_3$): 7.96 (1H, d, *J* = 8.7 Hz, H7), 7.39-7.32 (2H, m, *o*-Ph*H*), 7.32-7.24 (3H, m, *p*-Ph*H*, *m*-Ph*H*), 7.01 (1H, d, *J* = 2.5 Hz, H4), 6.89 (1H, dd, *J* = 8.7, 2.5 Hz, H6), 6.28 (1H, s, H2), 4.33 (1H, dd, *J* = 9.1, 4.7 Hz, H10), 3.85 (3H, s, C*H*$_3$), 3.65 (1H, ddd, *J* = 17.5, 9.1, 1.5 Hz, H11), 3.21 (1H, ddd, *J* = 17.5, 4.7, 1.5 Hz, H11); **$\delta_C$** (100 MHz, $CDCl_3$): 29.72, 52.69, 55.81, 100.74, 103.94, 111.81, 114.49, 125.48, 127.80, 129.18, 136.66, 138.61, 142.80, 157.18, 171.48; **IR** (thin film) $\nu_{max}/cm^{-1}$: 1723, 1445; **HRMS** *m/z* ($ESI^+$) found $[M+H]^+$ 278.1185; $C_{18}H_{16}NO_2^+$ requires 278.1181.

6-bromo-2-phenyl-1,2-dihydro-3H-pyrrolo[1,2-a]indol-3-one (**183**)


183

Synthesised from compound **148** (97.9 mg, 0.3 mmol) using **General Procedure [D]**. The resulting crude material was purified by column chromatography (5% $Et_2O$/pentane) to give compound **183** as a white solid (92.9 mg, 0.28 mmol, 94%); **m.p.** 135-137 ºC; **$\delta_H$** (400 MHz, $CDCl_3$): 8.18 (1H, dt, *J* = 1.6, 0.9 Hz, H7), 7.37 – 7.16 (7H, m, Ph*H*, H4, H5), 6.25 (1H, td, *J* = 1.6, 0.7 Hz, 1H, H2), 4.30 (dd, *J* = 9.2, 4.8 Hz, H10), 3.61 (1H, ddd, *J* = 17.5, 9.2, 1.5 Hz, H11), 3.17 (1H, ddd, *J* = 17.6, 4.8, 1.6 Hz, H11). **$\delta_C$** (100 MHz, $CDCl_3$): 171.77, 142.30, 138.20, 134.32, 131.32, 129.30, 128.02, 127.83, 127.80, 127.78, 127.62, 121.91, 117.08, 116.98, 100.58, 52.73, 29.75; **IR** (thin film) $\nu_{max}/cm^{-1}$: 1732, 1602, 1441; **HRMS** *m/z* ($ESI^+$) found $[M+H]^+$ 326.0177; $C_{17}H_{13}BrNO_2^+$ requires 326.0175.

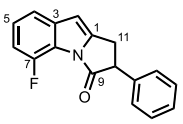
3-oxo-2-phenyl-2,3-dihydro-1H-pyrrolo[1,2-a]indole-6-carbaldehyde (**185**)



**185**

Synthesised from compound **149** (82.6 mg, 0.3 mmol) using **General Procedure B2**. The resulting crude material was purified by column chromatography (15% AcOEt/pentane) to give compound **185** as a white solid (26.8 mg, 0.1 mmol, 32%); **m.p.** 179 ºC; **$\delta_H$** (400 MHz, $CDCl_3$): 9.98 (1H, s, H12), 8.48 (1H, dt, *J* = 1.6, 0.8 Hz, H7), 7.79 (1H, dd, *J* = 8.2, 1.5 Hz, H5), 7.58 (1H, d, *J* = 8.2 Hz, H4), 7.35 – 7.18 (5H, m, Ph*H*), 6.38 (1H, q, *J* = 1.3 Hz, H2), 4.37 (1H, dd, *J* = 9.2, 4.7 Hz, H10), 3.70 (1H, ddd, *J* = 17.9, 9.2, 1.5 Hz, H11), 3.26 (1H, ddd, *J* = 17.8, 4.8, 1.6 Hz, H11); **$\delta_C$** (100 MHz, $CDCl_3$): 191.89, 171.81, 146.36, 140.60, 137.86, 132.47, 130.42, 129.37, 128.14, 127.79, 124.70, 121.24, 116.87, 101.18, 52.62, 30.05; **IR** (thin film) $\nu_{max}/cm^{-1}$: 1732, 1674, 1452, 1364, 1327; **HRMS** *m/z* ($ESI^+$) found $[M+H]^+$ 276.1019; $C_{18}H_{14}NO_2^+$ requires 256.1019.

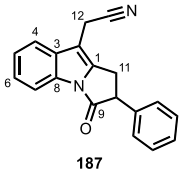
5-fluoro-2-phenyl-1,2-dihydro-3H-pyrrolo[1,2-a]indol-3-one (**186**)



**186**

Synthesised from compound **AM-162** (79.6 mg, 0.3 mmol) using **General Procedure [D]**. The resulting crude material was purified by column chromatography (5% AcOEt/pentane) to give compound **186** as a white solid (65.6 mg, 0.25 mmol, 82%); **m.p.** 125 ºC; **$\delta_H$** (400 MHz, $CDCl_3$): 7.42 – 7.27 (6H, m, H4, Ph*H*), 7.22 (1H, td, *J* = 7.9, 4.3 Hz, H6), 7.01 (1H, ddd, *J* = 10.9, 8.0, 1.0 Hz, H5), 6.41 (1H, q, *J* = 1.7 Hz, H2), 4.40 (1H, dd, *J* = 9.3, 4.9 Hz, H10), 3.72 (1H, ddd, *J* = 17.4, 9.3, 1.5 Hz, H11), 3.31 (1H, ddd, *J* = 17.5, 4.9, 1.6 Hz, H11); **$\delta_C$** (100 MHz, $CDCl_3$):170.19, 150.80 (d, *J* = 253.4 Hz), 143.39, 138.99 (d, *J* = 4.8 Hz), 138.31, 129.23, 127.96, 127.83, 125.27 (d, *J* = 6.4 Hz), 118.36 (d, *J* = 13.7 Hz), 116.42 (d, *J* = 3.7 Hz), 110.51 (d, *J* = 18.7 Hz), 101.13 (d, *J* = 1.9 Hz), 52.42, 29.39; **$\delta_F$** (376 MHz, $CDCl_3$): -117.64 (ddd, *J* = 10.8, 4.5, 2.1 Hz); **IR** (thin film) $\nu_{max}/cm^{-1}$: 1747, 1642, 1432, 1274; **HRMS** *m/z* ($ESI^+$) found $[M+H]^+$ 266.0976; $C_{17}H_{13}FNO_2^+$ requires 266.0976.

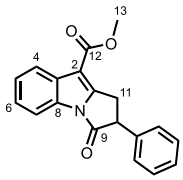
2-(3-oxo-2-phenyl-2,3-dihydro-1H-pyrrolo[1,2-a]indol-9-yl)acetonitrile (**187**)



**187**

Synthesised from compound **163** (85.9 mg, 0.3 mmol) using **General Procedure [D]**. The resulting crude material was purified by column chromatography (20% AcOEt/pentane) to give compound **187** as a yellow solid (79.4 mg, 0.83 mmol, 92%); **m.p.** 106 ºC; **$\delta_H$** (400 MHz, $CDCl_3$): 8.20 – 8.06 (1H, m, H7), 7.55 – 7.46 (1H, m, H4), 7.44 – 7.22 (7H, m, Ph*H*, H5, H6), 4.43 (1H, dd, *J* = 9.1, 4.8 Hz, H10), 3.90 – 3.73 (3H, m, H11, H12), 3.37 (ddt, *J* = 17.4, 4.6, 1.2 Hz, H11); **$\delta_C$** (100 MHz, $CDCl_3$): 171.54, 139.55, 137.95, 133.57, 130.52, 129.34, 128.10, 127.81, 124.78, 124.63, 118.19, 116.84, 114.31, 102.07, 52.54, 28.81, 13.48; **IR** (thin film) $\nu_{max}/cm^{-1}$: 1735, 1629, 1456, 1359; **HRMS** *m/z* ($ESI^+$) found $[M+H]^+$ 287.1180; $C_{19}H_{15}N_2O^+$ requires 287.1179.

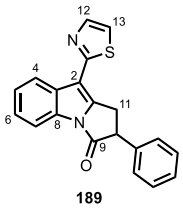
methyl 3-oxo-2-phenyl-2,3-dihydro-1H-pyrrolo[1,2-a]indole-9-carboxylate (**188**)



**188**

Synthesised from compound **152** (91.6 mg, 0.3 mmol) using **General Procedure [D]**. The resulting crude material was purified by column chromatography (10% AcOEt/pentane) to give compound **188** as a pale orange solid (77.1 mg, 0.25 mmol, 84%); **m.p.** 135-137 ºC; **$\delta_H$** (400 MHz, $CDCl_3$): 8.13 (1H, ddd, *J* = 7.7, 1.4, 0.7 Hz, H7), 8.11 – 8.06 (1H, ddd, *J* = 7.8, 1.4, 0.7 Hz, H4), 7.45 – 7.27 (7H, m, Ph*H*, H5, H6), 4.42 (1H, dd, *J* = 9.0, 4.4 Hz, H10), 4.03 – 3.92 (4H, m, H11, H13), 3.55 (1H, dd, *J* = 19.2, 4.4 Hz, H11); **$\delta_C$** (100 MHz, $CDCl_3$): 172.39, 164.76, 150.55, 137.51, 132.16, 130.66, 129.37, 128.16, 127.78, 125.57, 124.68, 121.79, 113.87, 106.30, 51.93, 51.56, 31.17; **IR** (thin film) $\nu_{max}/cm^{-1}$: 1742, 1716, 1591, 1457, 1158; **HRMS** *m/z* ($ESI^+$) found $[M+H]^+$ 306.1126; $C_{19}H_{16}NO_3^+$ requires 306.1125.

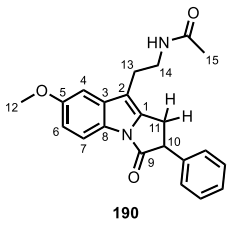
2-phenyl-9-(thiazol-2-yl)-1,2-dihydro-3H-pyrrolo[1,2-a]indol-3-one (**189**)



**189**

Synthesised from compound **167** (99.1 mg, 0.3 mmol) using **General Procedure [D]**. The resulting crude material was purified by column chromatography (10% AcOEt/pentane) to give the compound **189** as an off-white solid (49.5 mg, 0.15 mmol, 50%); **m.p.** 157-160 ºC; **$\delta_H$** (400 MHz, $CDCl_3$): 8.39 – 8.32 (1H, m, H4), 8.19 – 8.12 (1H, m, H7), 7.93 (1H, d, *J* = 3.3 Hz, H12), 7.51 – 7.29 (8H, m, Ph*H*, H5, H6, H13), 4.50 (1H, dd, *J* = 9.1, 4.5 Hz, H10), 3.99 (1H, dd, *J* = 18.5, 9.1 Hz, H11), 3.55 (1H, dd, *J* = 18.5, 4.5 Hz, H11); **$\delta_C$** (100 MHz, $CDCl_3$): 171.99, 161.14, 143.23, 142.22, 137.91, 132.08, 130.87, 129.36, 128.11, 127.87, 125.39, 124.74, 121.49, 117.22, 114.06, 109.89, 52.55, 31.10; **IR** (thin film) $\nu_{max}/cm^{-1}$: 1728, 1597, 1492, 1350; **HRMS** *m/z* ($ESI^+$) found $[M+H]^+$ 331.0900; $C_{20}H_{15}N_2OS^+$ requires 331.0900.

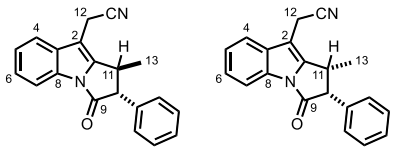
*N*-(2-(7-methoxy-3-oxo-2-phenyl-2,3-dihydro-1H-pyrrolo[1,2-a]indol-9-yl)ethyl)acetamide (**190**)



**190**

Synthesised from compound **155** (108.7 mg, 0.3 mmol) using **General Procedure [D]**. The resulting crude material was purified by column chromatography (50% MeCN/toluene) to give compound **190** as a yellow solid (54.7 mg, 0.15 mmol, 50%); **m.p.** 151-154 ºC; **$\delta_H$** (400 MHz, $CDCl_3$): 7.88 (1H, dd, *J* = 8.7, 0.5 Hz, H7), 7.34 – 7.14 (5H, m, *Ph*H), 6.92 (1H, d, *J* = 2.3 Hz, H4), 6.83 (1H, dd, *J* = 8.8, 2.4 Hz, H6), 5.60 (1H, s, N*H*), 4.23 (1H, dd, *J* = 9.2, 4.6 Hz, H10), 3.81 (3H, s, H12), 3.59 – 3.40 (3H, m, H11, H14), 3.08 (1H, dd, *J* = 17.3, 4.6 Hz, H11), 2.81 (2H, td, *J* = 6.9, 1.8 Hz, H13), 1.85 (3H, s, H15); **$\delta_C$** (100 MHz, $CDCl_3$): 171.13, 170.24, 157.35, 139.42, 138.66, 136.69, 129.25, 127.89, 127.71, 125.46, 114.77, 111.91, 110.63, 102.33, 55.96, 52.64, 39.17, 29.03, 24.48, 23.48.; **IR** (thin film) $\nu_{max}/cm^{-1}$: 3271, 1728, 1634, 1473, 1232; **HRMS** *m/z* ($ESI^+$) found $[M+H]^+$ 363.1704; $C_{22}H_{23}N_2O_3^+$ requires 363.1703.

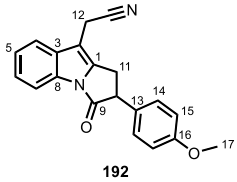
2-(1-methyl-3-oxo-2-phenyl-2,3-dihydro-1H-pyrrolo[1,2-a]indol-9-yl)acetonitrile (**191**)




**191**

Synthesised from compound **164** (90.1 mg, 0.3 mmol) using **General Procedure [D]**. The resulting crude material was purified by column chromatography (2.5% $Et_2O$/pentane) to give compound **191** as a pale yellow solid (78.9 mg, 0.26 mmol, 88%); **m.p.** 112-114 ºC; **$\delta_H$** (400 MHz, $CDCl_3$, mixture of isomers): 8.21 – 8.11 (0.9H, m, $H7^B$), 8.15 – 8.07 (1H, m, $H7^A$), 7.61 – 7.51 (1.9H, m, $H4^A$, $H4^B$), 7.44 – 7.33 (10H, m, Ph$H^A$, $H5^A$, $H6^A$, Ph$H^B$, $H5^B$, $H6^B$), 7.29 – 7.22 (2H, m, Ph$H^A$, Ph$H^B$), 7.22 – 7.15 (2H, m, Ph$H^A$, Ph$H^B$), 4.64 (0.9H, d, *J* = 8.6 Hz, $H10^B$), 4.05 – 3.93 (0.9H, m, $H11^B$), 3.91 (1H, d, *J* = 4.7 Hz, $H10^A$), 3.88 – 3.71 (4H, m, $H12^A$, $H12^B$), 3.72 – 3.60 (1H, m, $H11^A$), 1.65 (3H, d, *J* = 7.0 Hz, $H13^A$), 1.04 (2.7H, d, *J* = 7.4 Hz, $H13^B$); **$\delta_C$** (100 MHz, $CDCl_3$): 171.46, 171.07, 144.88, 144.06, 137.24, 134.48, 133.66, 133.51, 130.24, 130.20, 129.84, 129.35, 128.92, 128.16, 128.06, 127.99, 124.81, 124.80, 124.76, 124.74, 118.37, 118.30, 116.91, 114.44, 114.38, 102.09, 101.93, 62.09, 57.45, 37.62, 32.47, 19.38, 17.39, 13.17, 13.10; **IR** (thin film) $\nu_{max}/cm^{-1}$: 1724, 1457, 1395; **HRMS** *m/z* ($ESI^+$) found $[M+H]^+$ 301.1336; $C_{20}H_{17}N_2O^+$ requires 301.1335.

2-(2-(4-methoxyphenyl)-3-oxo-2,3-dihydro-1H-pyrrolo[1,2-a]indol-9-yl)acetonitrile (**192**)

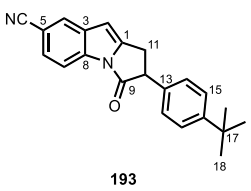


**192**

Synthesised from compound **166** (94.9 mg, 0.3 mmol) using **General Procedure [D]**. The resulting crude material was purified by column chromatography (30% AcOEt/pentane) to give compound **192** as a yellow solid (84.1 mg, 0.28 mmol, 92%); **m.p.** 127 ºC; **$\delta_H$** (400 MHz, $CDCl_3$): 8.15 – 8.03 (1H, m, H7), 7.55 – 7.45 (1H, m, H4), 7.43 – 7.32 (2H, m, H5, H6), 7.25 – 7.16 (2H, m, H14), 6.97 – 6.82 (2H, m, H15), 4.36 (1H, dd, *J* = 9.3, 4.9 Hz, H10), 3.84 – 3.74 (6H, m, H11, H12, H17), 3.31 (1H, ddt, *J* = 17.8, 5.3, 1.3 Hz, H11); **$\delta_C$** (100 MHz, $CDCl_3$): 171.86, 159.39, 139.60, 133.53, 130.51, 129.92, 128.89, 124.71, 124.56, 118.15, 116.86, 114.71, 114.27, 101.98,

55.47, 51.80, 28.84, 13.44; **IR** (thin film) $\nu_{max}/cm^{-1}$: 1724, 1516, 1455; **HRMS** *m/z* ($ESI^+$) found $[M+H]^+$ 317.1285; $C_{20}H_{17}N_2O_2^+$ requires 317.1285.

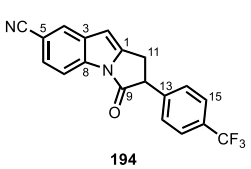
2-(4-(*tert*-butyl)phenyl)-3-oxo-2,3-dihydro-1H-pyrrolo[1,2-a]indole-7-carbonitrile (**193**)



**193**

Synthesised from compound **154** (98.0 mg, 0.3 mmol) using **General Procedure [D]**. The resulting crude material was purified by column chromatography (10% AcOEt/pentane) to give compound **193** as an off-white solid (89.0 mg, 0.27 mmol, 91%); **m.p.** 149 ºC; $\delta_H$ (400 MHz, $CDCl_3$): 8.15 (1H, dt, *J* = 8.3, 0.8 Hz, H7), 7.87 (1H, dd, *J* = 1.6, 0.7 Hz, H4), 7.54 (1H, dd, *J* = 8.3, 1.5 Hz, H6), 7.46 – 7.34 (2H, m, H15), 7.26 – 7.18 (2H, m, H14), 6.43 (1H, td, *J* = 1.5, 0.7 Hz, H2), 4.41 (1H, dd, *J* = 9.2, 4.9 Hz, H10), 3.74 (1H, ddd, *J* = 17.7, 9.2, 1.5 Hz, H11), 3.34 (1H, ddd, *J* = 17.7, 4.9, 1.6 Hz, H11), 1.31 (9H, s, H18); $\delta_C$ (100 MHz, $CDCl_3$): 172.19, 151.21, 144.24, 135.46, 134.52, 132.49, 127.41, 126.91, 126.32, 125.52, 119.74, 114.60, 107.75, 100.42, 52.27, 34.70, 31.40, 29.60; **IR** (thin film) $\nu_{max}/cm^{-1}$: 2221, 1737, 1438, 1384, 1348; **HRMS** *m/z* ($ESI^+$) found $[M+H]^+$ 329.1649; $C_{22}H_{21}N_2O^+$ requires 329.1648.

3-oxo-2-(4-(trifluoromethyl)phenyl)-2,3-dihydro-1H-pyrrolo[1,2-a]indole-7-carbonitrile (**194**)

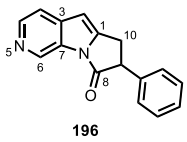


**194**

Synthesised from compound **153** (34.0 mg, 0.1 mmol) using **General Procedure [D]**. The resulting crude material was purified by column chromatography (20% AcOEt/pentane) to give compound **194** as an off white (23.2 mg, 0.07 mmol, 68%); **m.p.** 160 ºC; $\delta_H$ (400 MHz, $CDCl_3$): 8.15 (1H, dd, *J* = 8.4, 0.8 Hz, H7), 7.92 – 7.84 (1H, m, H4), 7.65 (2H, d, *J* = 8.1 Hz, H15), 7.56 (1H, dd, *J* = 8.4, 1.5 Hz, H6), 7.44 (2H, d, *J* = 8.1 Hz, H14), 6.46 (1H, q, *J* = 1.3 Hz, H12), 4.51 (1H, dd, *J* = 9.3, 5.1 Hz, H12), 3.80 (1H, ddd, *J* = 17.7, 9.3, 1.5 Hz, H11), 3.34 (1H, ddd, *J* = 17.7, 5.1, 1.7 Hz, H11); $\delta_C$ (100 MHz, $CDCl_3$): 170.99, 143.41, 141.43, 135.47, 132.47, 130.76, 130.44, 128.31,

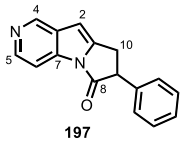
127.17, 126.36 (q, *J* = 3.8 Hz), 125.66, 119.57, 114.66, 108.09, 100.93, 52.35, 29.37; **$\delta_F$** (376 MHz, $CDCl_3$): -62.73; **IR** (thin film) $\nu_{max}/cm^{-1}$: 2225, 1744, 1463, 1325; **HRMS** *m/z* ($ESI^+$) found $[M+H]^+$ 341.0896; $C_{19}H_{12}N_2OF_3^-$ requires 341.0896.

7-phenyl-6,7-dihydro-8H-pyrido[4,3-b]pyrrolizin-8-one (**196**)


196

Synthesised from compound **AM-160** (74.5 mg, 0.3 mmol) using **General Procedure [D]**. The resulting crude material was purified by column chromatography (100% AcOEt) to give compound **196** as a white solid (57.6 mg, 0.23 mmol, 77%); **m.p.** 141-144 ºC; **$\delta_H$** (400 MHz, $CDCl_3$): 9.35 (1H, d, *J* = 1.0 Hz, H6), 8.47 (1H, d, *J* = 5.4 Hz, H5), 7.48 (1H, dd, *J* = 5.4, 1.1 Hz, H4), 7.43 – 7.27 (5H, m, Ph*H*), 6.39 (1H, q, *J* = 1.3 Hz, H2), 4.44 (1H, dd, *J* = 9.1, 4.7 Hz, H9), 3.78 (1H, ddd, *J* = 17.8, 9.2, 1.4 Hz, H10), 3.35 (1H, ddd, *J* = 17.8, 4.8, 1.6 Hz, H10); **$\delta_C$** (100 MHz, $CDCl_3$): 171.41, 145.75, 143.93, 141.09, 137.69, 136.01, 129.37, 128.17, 127.98, 127.76, 115.66, 99.91, 52.47, 30.01; **IR** (thin film) $\nu_{max}/cm^{-1}$: 1725, 1599, 1452; **HRMS** *m/z* ($ESI^+$) found $[M+H]^+$ 249.1024; $C_{16}H_{13}N_2O^+$ requires 249.1022;

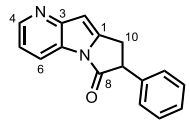
7-phenyl-7,8-dihydro-6H-pyrido[3,4-b]pyrrolizin-6-one (**197**)


197

Synthesised from compound **AM-159** (74.5 mg, 0.3 mmol) using **General Procedure [D]**. The resulting crude material was purified by column chromatography (70% AcOEt/$CH_2Cl_2$) to give compound **197** as a white solid (97.2 mg, 0.27 mmol, 90%); **m.p.** 170 ºC; **$\delta_H$** (400 MHz, $CDCl_3$): 8.90 (1H, d, *J* = 1.1 Hz, H4), 8.50 (1H, d, *J* = 5.5 Hz, H5), 7.94 (1H, dt, *J* = 5.5, 1.0 Hz, H6), 7.43 – 7.25 (5H, m, Ph*H*), 6.43 (1H, q, *J* = 1.2 Hz, H2), 4.43 (1H, dd, *J* = 9.3, 4.9 Hz, H9), 3.75 (1H, ddd, *J* = 17.7, 9.3, 1.5 Hz, H10), 3.33 (1H, ddd, *J* = 17.7, 5.0, 1.7 Hz, H10); **$\delta_C$** (100 MHz, $CDCl_3$): 172.45, 144.03, 143.84, 142.83, 138.03, 135.17, 131.85, 129.68, 128.49, 128.10, 109.07, 99.22, 53.19, 30.02; **IR** (thin

film) $\nu_{max}/cm^{-1}$: 1734, 1583, 1384; **HRMS** *m/z* ($ESI^+$) found $[M+H]^+$ 249.1024; $C_{16}H_{13}N_2O^+$ requires 249.1022.

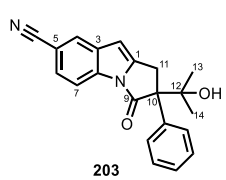
7-phenyl-7,8-dihydro-6H-pyrido[2,3-b]pyrrolizin-6-one (**198**)



198

Synthesised from compound **AM-161** (74.5 mg, 0.3 mmol) using **General Procedure [D]**. The resulting crude material was purified by column chromatography (100% AcOEt) to give compound **198** as a white solid (65.4 mg, 0.26 mmol, 88%); **m.p.** 135-136 ºC; **$\delta_H$** (400 MHz, $CDCl_3$): 8.56 (1H, dd, *J* = 4.9, 1.5 Hz, H4), 8.29 (1H, dt, *J* = 8.1, 1.0 Hz, H6), 7.43 – 7.25 (5H, m, Ph*H*), 7.20 (1H, dd, *J* = 8.1, 4.9 Hz, H5), 6.59 (1H, q, *J* = 1.3 Hz, H2), 4.37 (1H, dd, *J* = 9.2, 4.7 Hz, H9), 3.80 (1H, ddd, *J* = 17.8, 9.2, 1.5 Hz, H10), 3.38 (1H, ddd, *J* = 17.8, 4.7, 1.6 Hz, H10); **$\delta_C$** (100 MHz, $CDCl_3$): 172.38, 153.55, 146.83, 145.15, 137.87, 129.35, 128.12, 127.79, 124.57, 120.71, 118.23, 102.07, 51.83, 30.28; **IR** (thin film) $\nu_{max}/cm^{-1}$: 1737, 1607, 1407; **HRMS** *m/z* ($ESI^+$) found $[M+H]^+$ 249.1024; $C_{16}H_{13}N_2O^+$ requires 249.1022.

2-(2-hydroxypropan-2-yl)-3-oxo-2-phenyl-2,3-dihydro-1H-pyrrolo[1,2-a]indole-7-carbonitrile (**203**)

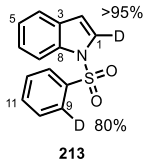


203

Synthesised from compound **145** (27.2 mg, 0.10 mmol) and degassed anhydrous acetone (2.5 mL) was used as solvent using **General Procedure [A]**. The resulting crude material was purified by column chromatography (5% $Et_2O$/petroleum ether) to give the compound **203** as a minor product in the form of a colourless oil (3.63 mg, 0.011 mmol, 11%); **$\delta_H$** (400 MHz, $CDCl_3$) 8.20 (1H, d , *J* = 8.3 Hz, H7), 7.82 (1H, d, *J* = 1.5 Hz, H4), 7.76 (2H, m, 2 × *m*-Ph*H*), 7.55 (1H, dd, *J* =8.3 and 1.5 Hz, H6), 7.39 (2H, m, 2 × *o*-Ph*H*), 7.33 (1H, m, *p*-Ph*H*), 6.32 (1H, t, *J* = 1.5 Hz, H2), 3.98 (1H, dd, *J* =17.8 and 1.5 Hz, H11'), 3.69 (1H, dd, *J* = 17.8 and 1.5 Hz, H11"), 1.43 (1H, s, O*H)*, 1.30 (3H, s, H14), 1.26 (3H, s, H13); **$\delta_C$** (100 MHz, $CDCl_3$) 173.12, 143.33, 138.12,

135.48, 132.47, 128.50, 128.25, 127.95, 126.83, 125.41, 119.75, 114.62 107.83, 99.63, 75.12, 66.06, 32.48, 27.07, 25.45; **IR** (thin film) $\nu_{max}/cm^{-1}$ 3426, 1725, 1372, 1091; **HRMS** *m/z* ($ESI^+$) found $[M+H]^+$ 331.3948; $C_{21}H_{19}N_2O_2^+$ requires 331.3950.

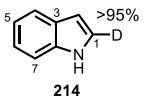
1-((phenyl-2-d)sulfonyl)-1H-indole-2-d (**213**)



**213**

To a solution of **212** (2.0 g, 7.77 mmol, 1 equiv.) in anhydrous THF (90 mL) at -78 ºC, *n*BuLi (9.72 mL, 1.6 M, 15.55 mmol, 2 equiv.) was added dropwise and the resulting mixture was stirred for 3 h at -78 ºC. The reaction was then quenched with $D_2O$ (2 mL, 101 mmol, 13 equiv.) and was allowed to slowly warm up to room temperature over the course of 1 h. The reaction was then extracted with $CH_2Cl_2$, dried and evaporated. The resulting solid was purified by recrystallization from hot hexane to give compound **213** as a white solid (1.52 g, 5.91 mmol, 76%); $\delta_H$ (400 MHz, $CDCl_3$): 8.00 – 7.93 (1H, m), 7.86 – 7.81 (1H, m), 7.52 – 7.43 (2H, m), 7.42 – 7.34 (2H, m), 7.27 (1H, ddd, *J* = 8.4, 7.2, 1.3 Hz), 7.23 – 7.15 (0.2H, m), 6.62 (1H, d, *J* = 0.8 Hz); $\delta_C$ (100 MHz, $CDCl_3$): 138.39, 138.31, 134.94, 133.93, 130.87, 129.37, 129.26, 126.86, 126.84, 126.60, 126.51, 126.35, 126.21, 125.92, 124.76, 123.50, 121.54, 113.64, 109.19. Data are consistent with literature values.[128]

1H-indole-2-d (**214**)

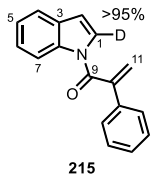


**214**

To a solution of **213** (1.3 g, 5.0 mmol, 1 equiv.) in methanol (14.3 mL) was added an aqueous solution of sodium hydroxide (18.2 mL, 2M, 36.4 mmol, 7.28 equiv.). The mixture was refluxed for 16 h, when it was allowed to cool to room temperature and extracted with AcOEt. The organic layer was separated, dried, and evaporated. The resulting residue was dissolved in $CHCl_3$, filtered and evaporated to give compound **214** as an off-white solid (576 mg, 4.88 mmol, 97%); $\delta_H$ (400 MHz, $CDCl_3$): 8.09 (1H, s, N*H*), 7.69 (1H, dq, *J* = 7.8, 1.0 Hz, H4), 7.41 (1H, dq, *J* = 8.1, 1.0 Hz, H7), 7.23 (1H, ddd, *J* = 8.2, 7.0, 1.2

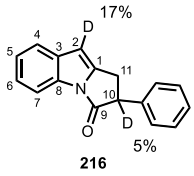
Hz, H6), 7.15 (1H, ddd, *J* = 8.0, 7.0, 1.1 Hz, H5), 6.58 (1H, dd, *J* = 2.1, 0.9 Hz, H2); **δC** (100 MHz, $CDCl_3$): 135.87, 127.98, 124.32, 124.04, 123.82, 122.10, 120.86, 119.97, 119.95, 111.15, 102.58. Data are consistent with literature values.[128]

1-(1H-indol-1-yl-2-d)-2-phenylprop-2-en-1-one (**215**)




Synthesised from atropic acid (0.5 g, 3.375 mmol) and **214** (331 mg, 2.25 mmol) using **General Procedure [A]**. The reaction mixture was then concentrated and purified by FCC (2.5% $Et_2O$/pentane) to give compound **215** as a clear oil (141 mg, 0.56 mmol, 25%); **m.p.** 148 °C; **δH** (400 MHz, $CDCl_3$): 8.57 (1H, dd, *J* = 8.2, 1.0 Hz, H7), 7.57 (1H, dt, *J* = 7.8, 1.0 Hz, H4), 7.52 – 7.46 (2H, m, H5, H6), 7.44 – 7.30 (5H, m, Ph*H*), 6.54 (1H, d, *J* = 0.8 Hz, H2), 6.08 (1H, s, H11), 5.70 (1H, s, H11); **δC** (100 MHz, $CDCl_3$): 168.63, 144.52, 135.65, 135.47, 131.05, 129.20, 129.16, 126.23, 125.26, 124.31, 121.02, 118.61, 116.84, 109.08; **IR** (thin film) $\nu_{max}/cm^{-1}$: 1735, 1584, 1383, 1347; **HRMS** *m/z* ($ESI^+$) found $[M+H]^+$ 249.1133; $C_{17}H_{13}{}^2HNO^+$ requires 249.1133.

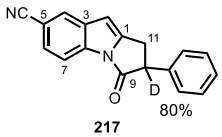
2-phenyl-1,2-dihydro-3H-pyrrolo[1,2-a]indol-3-one-2,9-$d_2$ (**216**)




Compound **215** (74.5 mg, 0.3 mmol, 1 equiv.) and $Ir(dFppy)_3$ (2.3 mg, 0.003 mmol, 0.01 equiv.) were added to a dry microwave vial. The container was sealed, evacuated, and backfilled with argon three times. Ethyl acetate (5 mL) and $H_2O$ (2 mL) were placed in a vial. The container was sealed and vigorously shaken. The layers were allowed to separate, and the organic phase was transferred to a dry container and sparged with argon for 30 minutes. The deoxygenated solution (3 mL) was then transferred to the microwave vial and the suspension was stirred until homogeneous. The container was irradiated with blue LED light for 16 h, when the reaction was concentrated and purified by column chromatography (10% $Et_2O$/pentane) to give compound **216** as a white solid (68 mg, 0.27 mmol, 91%); **m.p.** 68 ºC; **δH** (400 MHz, $CDCl_3$): 8.11 – 7.96 (1H, m, H7), 7.53 – 7.46

(1H, m, H4), 7.34 – 7.21 (7H, m, Ph*H*, H5, H6), 6.30 (0.83H, d, *J* = 1.8 Hz, H2), 4.32 (0.95H, dd, *J* = 9.2, 4.8 Hz, H10), 3.64 (1H, ddd, *J* = 17.5, 9.2, 1.5 Hz, H11), 3.21 (1H, ddd, J = 17.4, 4.8, 1.6 Hz, H11); **δC** (100 MHz, $CDCl_3$): 171.90, 141.84, 138.54, 135.55, 130.81, 129.23, 127.87, 127.82, 124.40, 123.57, 120.77, 113.96, 100.76, 52.87, 29.69; **IR** (thin film) $\nu_{max}/cm^{-1}$: 1688, 1517, 1344; **HRMS** *m/z* ($ESI^+$) found $[M+H]^+$ 249.1126; $C_{17}H_{13}{}^2HNO^+$ requires 249.1133.

7-isocyano-2-phenyl-1,2-dihydro-3H-pyrrolo[1,2-a]indol-3-one-2-d (**217**)



80%

**217**

Compound **144** (74.5 mg, 0.3 mmol, 1 equiv.) and $Ir(dFppy)_3$ (2.3 mg, 0.003 mmol, 0.01 equiv.) were added to a dry microwave vial. The container was sealed, evacuated, and backfilled with argon three times. Ethyl acetate (5 mL) and $D_2O$ (2 mL) were placed in a dry vial. The container was sealed and vigorously shaken. The layers were allowed to separate, and the organic phase was transferred to a dry container and sparged with argon for 30 minutes. The deoxygenated solution (3 mL) was then transferred to the microwave vial and the suspension was stirred until homogeneous. The container was irradiated with blue LED light for 16 h, when the reaction was concentrated and purified by column chromatography (15% AcOEt/pentane) to give compound **217** as a white solid (75.4 mg, 0.27 mmol, 92%); **m.p.** 163 ºC; **δH** (400 MHz, $CDCl_3$): 8.16 (1H, dt, *J* = 8.3, 0.8 Hz, H7), 7.88 (1H, dd, *J* = 1.6, 0.7 Hz, H4), 7.55 (1H, dd, *J* = 8.3, 1.5 Hz, H6), 7.42 – 7.26 (5H, m, Ph*H*), 6.44 (1H, td, *J* = 1.6, 0.7 Hz, H2), 4.43 (0.2H, dd, *J* = 9.2, 4.9 Hz, H10), 3.81-3.72 (1H, m, H11), 3.37-3.30 (1H, m, H11); **δC** (100 MHz, $CDCl_3$): 171.96, 144.11, 144.08, 137.65, 137.63, 135.46, 132.47, 129.39, 128.21, 127.77, 127.75, 126.96, 125.55, 119.73, 114.62, 107.79, 100.51, 52.68, 52.54, 52.33, 52.13, 29.68, 29.58; **IR** (thin film) $\nu_{max}/cm^{-1}$: 2220, 1735, 1584, 1383, 1347; **HRMS** *m/z* ($ESI^+$) found $[M+H]^+$ 274.1088; $C_{18}H_{12}{}^2HN_2O^+$ requires 249.1085.

### *4. Large Scale Synthesis of compound 179*

Amide substrate **142** (1.5 g, 4.6 mmol, 1 equiv.), $Ir(dFppy)_3$ (35 mg, 0.046 mmol, 0.01 equiv.) and NaOAc (38 mg, 0.46 mmol, 0.1 equiv.) were transferred to an appropriately sized Schlenk tube. The Schlenk tube was evacuated and backfilled with Ar three times. The reaction vessel was then charged with EtOAc (46 mL) that was previously sparged with Ar for 15 min. The reaction mixture was then irradiated with blue light and stirred while maintaining at room temperature by a stream of $N_2$. Once the reaction was completed, the excess solvent was evaporated and the resulting solid was purified by column chromatography (5% AcOEt/pentane) to give compound **179** as a white solid (1.39 g, 4.28 mmol, 93%). Characterization data are consistent with small scale reaction.

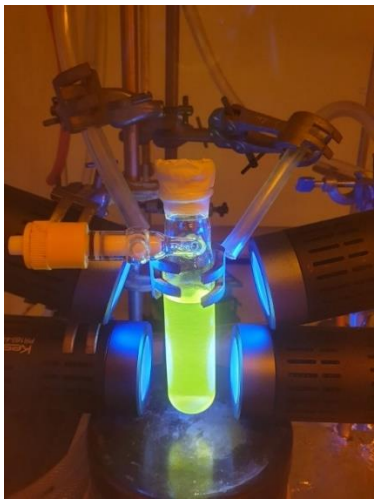


***Figure 68**: Experimental setup for large scale synthesis*

### *5. Stern-Volmer Quenching*

A stock solution of $Ir(dFppy)_3$ (2.0 mg) in EtOAc (10.0 mL; 0.26 mM) was prepared by adding argon sparged EtOAc to a volumetric flask under argon containing the photocatalyst. A stock solution of substrate **144** (10.9 mg) in EtOAc (2.0 mL; 20 mM) was prepared in a similar manner by adding argon sparged EtOAc to a vial containing substrate **144** sealed with a septum under an atmosphere of argon.

Samples were prepared in 4.0 mL quartz cuvettes equipped with a septum under an argon atmosphere by adding 2.0 mL of the photocatalyst stock solution which was diluted with a further 1.0 mL of argon sparged EtOAc (final concentration of photocatalyst = 0.175 mM). The resulting solution was excited at 400 nm and three emission spectra recorded from 430 to 700 nm. To this solution was then added 50 µL of substrate **144** stock solution under argon,

and three emission spectra recorded as before. This process was then repeated five further times.

### *6. Square wave voltammetry*

Voltammetry measurements were made using an Autolab PGSTAT 12 with a 3 mm glassy carbon working electrode, platinum wire counter electrode and $Ag/AgNO_3$ (0.01 M in acetonitrile) reference electrode. Voltammograms were referenced to the $Fc/Fc^+$ couple (0.40 V vs SCE) as an internal reference. Square wave voltammograms were acquired with a 5 mV step potential, 50 mV modulation amplitude and 2 Hz frequency. The supporting electrolyte, (tetra-*n*-butylammonium hexafluorophosphate) was prepared as a 0.1 M solution in dry MeCN. A stock solution of **144** (2.7 mg) in dry MeCN (1.0 mL; 10 mM) was prepared and then further diluted with the electrolyte solution to a concentration of 1 mM.

### *7. General Computational Methods*

Gaussian 16[167] was employed for all density functional theory (DFT) calculations, using an "ultrafine" pruned grid for numerical integration of the exchange-correlation functional and its derivatives.

For structures reported in **Chapter 2**, the range-separated dispersion-corrected M06-2X[35] density functional and the 6-31++G(d,p)[76-79] basis set were used with Grimme's D3[39] correction using the original D3 damping function to optimize the geometries of all stationary points. To these optimized structures, single-point energy corrections (M06-2X-D3/Def2-QZVPP) [35, 39, 92-93] were applied. All the calculations included the solvation model based on density (SMD)[80-84] to account for solvent effects (solvent=ethylethanoate). The solvent model was chosen as it has been developed by parametrization using the Minnesota family of functionals (M05-2X[99]).

For structures reported in **Chapter 3**, the range-separated dispersion-corrected M06-2X[35] density functional in conjunction with the def2-TZVP[92-93] basis set and D3[39] corrections were used for optimization. Single point corrections were performed at the M06-2X-D3/Def2-QZVPP[35, 39, 92-93] level of theory. All the calculations (both optimization and single point corrections) included the SMD[80-84] solvation model (solvent = acetonitrile) to account for solvent effects.

We performed vibrational frequency calculations to verify that stationary points were either minima or first-order saddle points on the potential energy surface, and to calculate thermal corrections to Gibbs free energies. Moreover, intrinsic reaction coordinate (IRC) calculations were performed to ensure that the transition structures connected to their corresponding starting and final geometries.[191] Where IRC calculations failed for transition states possessing small negative vibrations, structures were reoptimized to local minima *via* manual displacement along the negative vibration vector to confirm the identity of the intermediated connected by the saddle point.

Low lying normal vibrational modes are not well described by the rigid-rotor-harmonic-oscillator, leading to inaccuracies in thermochemical calculations. Once solution to improve accuracy is to employ Grimme's quasi-harmonic model for entropy.[192] Under Grimme's approach, vibrational modes below a certain frequency are recomputed instead using the free rotor approximation [**EQ7**]:

$$S_R = R\left[\frac{1}{2} + ln\left\{\left(\frac{8\pi\mu' kT}{h^2}\right)^{\frac{1}{2}}\right\}\right] \qquad [\boldsymbol{EQ7}]$$

where $S_R$ is the recomputed entropy for a given vibration mode, $\mu'$ is the effective moment of inertia, $k$ is the Boltzmann constant and $h$ is Plank's constant. Using this equation, a cut-off was chosen for 100 $cm^{-1}$ and was applied automatically using the Goodvibes program at

298.15 K.[193] The software also automatically applies a 1 M standard concentration corrections to all individual calculations to account for reactions in solution (*i.e.* change in standard concentration from 1 atm to 1 M, which accounts for an additional increase in entropy of 1.89 kcal·mol$^{-1}$ due to changes in translational entropy).

Multi-conformational corrections were added to all final Boltzmann weighted free energy to include the entropic stabilization created by multiple accessible low-lying conformers.[194] The resulting conformationally stabilised entropies were calculated using equation [**EQ8**]

$$S_{conf} = \sum_i S_i \cdot p_i - R \sum_i p_i \cdot ln(p_i) \qquad [\boldsymbol{EQ8}]$$

$$p_i = \frac{e^{\frac{-(G_i - G_1)}{RT}}}{\sum_i \left( e^{\frac{-(G_i - G_1)}{RT}} \right)} \qquad [\boldsymbol{EQ9}]$$

where $S_{conf}$ is the conformationally corrected entropy, $S_i$ is the computed enthalpy and entropy for conformer *i*, $p_i$ is the probably of the molecules existing as conformer *i*, and $G_1$ is the Gibbs free energy of the lowest energy conformer. Throughout this Thesis, thermochemical parameters correspond Boltzmann averaged values unless otherwise stated.

Reaction intermediates on the ground state singlet surface discussed in **Chapters 2** and **3** can be expressed as either open shell singlet-biradicals or closed shell zwitterions. All calculation were performed under the unrestricted formalism. The wavefunction stability of intermediates were carried out with the *stable* keyword in two different ways: (i) "*stable"* and (ii) "*guess=mix stable=opt"*. Both methods led to the same result, with $\langle \hat{S}^2 \rangle = 0$ as the most stable value and as such all intermediates in the singlet state are best described as closed shell zwitterions. The same protocol was applied for open shell triplet, with $\langle \hat{S}^2 \rangle = 2$ as the most stable value. No spin contamination issues were thus encountered. To account for potential open-shell biradical forms of closed shell zwitterionic intermediates, additional calculations

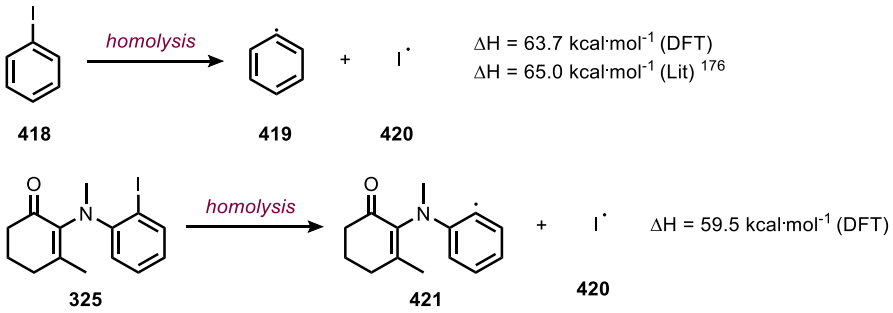
were performed using "*guess=mix stable=opt"* at various distorted geometries followed by a linked optimization calculation. In all cases, no open-shell singlet biradicals were found.

Minimum energy crossing points of the intersystem crossings (ISC) were calculated with MECPro, interfaced to Gaussian 16. All calculation were performed by Dr. Juan Alegre-Requena.[195] As MECPs are neither minima or saddle points, energy E was used for analysis. Natural bonding orbital calculations were performed using NBO version 6.0 interfaced with Gaussian 16.[196] Graphical structures of computed structures were generated using PyMol.[197]

Nomenclature of computed structures is based on the numerical order in which they were reported. Transition state structures are labelled with the suffix "TS". Stationary points may contain a suffix denoting the multiplicity of the system (*i.e.* $S_0$ *or* $T_1$). For structures that display multiple conformers, the corresponding structures are labelled with an alphabetical suffix (*e.g.* 100_a, 100_b, *etc.*). Structures computed in benchmarking studies are labelled with the appropriate functional as a suffix (e.g. 100_m062x-gd3). Minimum energy structures used in the calculation of activation energies barrier for the base catalysed proton shift pathways in **Chapter 2** are labelled with the suffix "precursor" added to the name of the transition state they connect to (e.g. 208-TS-precursor_a). Minimum energy crossing points are labelled with the suffix "MECP".

Reported triplet energies refer to adiabatic triplet energies, which are calculated as the difference in energy between the optimised triplet state structure and the optimised singlet ground state structure.

Bond dissociation enthalpies and free energies were calculated at the M06-2X-D3[35, 39] level of theory in conjunction with the Def2-TZVP[92-93] basis set and the SMD[80-84] solvation model for acetonitrile (***Scheme 67***).




***Scheme 67:*** *Homolysis of iodobenzene* ***418*** *and enaminone* ***325***

### *9. Thermochemical Data*

Compiled thermochemical data are presented in the tables below, where $E_{SPC}$ and $E$ are the computed energies with and without single point energy corrections, $ZPE$ is the computed zero point energy, $H_{SPC}$ is the enthalpy including single point energy corrections, $T$ is temperature, $S$ is the entropy, $qh.T{\cdot}S$ is the product between temperature and entropy including quasi-harmonic corrections, $G_{SPC}$ is the Gibbs free energy with single point energy corrections and $qh.G_{SPC}$ is the Gibbs free energy with single point energy corrections and quasi-harmonic corrections.

| Entry | $E_{SPC}$ | $E$ | $ZPE$ | $H_{SPC}$ | $T \cdot S$ | $qh.T \cdot S$ | $G_{SPC}$ | $qh.G_{SPC}$ | Imag. $\upsilon$ / $cm^{-1}$ |
|---|---|---|---|---|---|---|---|---|---|
| **149-S0_a** | -785.657367 | -785.340763 | 0.255966 | -785.385759 | 0.059058 | 0.056496 | -785.444817 | -785.442256 | |
| **149-S0_b** | -785.655075 | -785.338516 | 0.25574 | -785.383663 | 0.059114 | 0.056559 | -785.442777 | -785.440222 | |
| **149-S0_c** | -785.658035 | -785.341753 | 0.255683 | -785.386614 | 0.059441 | 0.056669 | -785.446055 | -785.443283 | |
| **149-S0_d** | -785.656144 | -785.339833 | 0.255418 | -785.384956 | 0.059566 | 0.056705 | -785.444522 | -785.441661 | |
| **149-T1_a** | -785.538178 | -785.221744 | 0.250453 | -785.271205 | 0.061723 | 0.059064 | -785.332928 | -785.330269 | |
| **149-T1_b** | -785.536071 | -785.219599 | 0.250307 | -785.269175 | 0.061946 | 0.059209 | -785.331121 | -785.328384 | |
| **149-T1_c** | -785.540331 | -785.224665 | 0.250147 | -785.273754 | 0.061368 | 0.058717 | -785.335122 | -785.332471 | |
| **149-T1_d** | -785.542845 | -785.227663 | 0.251385 | -785.275364 | 0.060215 | 0.057888 | -785.335579 | -785.333253 | |
| **175-S0** | -785.691161 | -785.376348 | 0.258127 | -785.418135 | 0.057849 | 0.055259 | -785.475984 | -785.473393 | |
| **175-T1** | -785.571238 | -785.257080 | 0.253819 | -785.302109 | 0.058972 | 0.056714 | -785.361080 | -785.358823 | |
| **201-TS** | -785.552605 | -785.23761 | 0.251563 | -785.285837 | 0.058275 | 0.056373 | -785.344113 | -785.342211 | -597.85 |
| **202-S0** | -785.608288 | -785.29338 | 0.256369 | -785.336952 | 0.056549 | 0.054907 | -785.3935 | -785.391858 | |
| **202_MECP** | -785.600503 | N/A | N/A | N/A | N/A | N/A | N/A | N/A | |
| **202-T1** | -785.605542 | -785.291217 | 0.254653 | -785.335765 | 0.058013 | 0.056229 | -785.393778 | -785.391993 | |
| **204-TS** | -785.552798 | -785.237092 | 0.251072 | -785.287016 | 0.055862 | 0.054296 | -785.342878 | -785.341312 | -1367.99 |
| **205-TS** | -785.591516 | -785.276857 | 0.254709 | -785.32212 | 0.055928 | 0.054296 | -785.378047 | -785.376416 | -592.98 |
| **206-TS-precursor_a** | -1176.492999 | -1176.055065 | 0.308717 | -1176.161874 | 0.074146 | 0.070399 | -1176.23602 | -1176.232273 | |
| **206-TS-precursor_b** | -1176.500522 | -1176.062659 | 0.308934 | -1176.169115 | 0.07554 | 0.070733 | -1176.244655 | -1176.239848 | |
| **206-TS-precursor_c** | -1176.49815 | -1176.05899 | 0.30878 | -1176.16662 | 0.07722 | 0.071808 | -1176.24384 | -1176.238428 | |
| **206-TS_a** | -1176.478237 | -1176.039875 | 0.304847 | -1176.151389 | 0.075617 | 0.070496 | -1176.227007 | -1176.221885 | -228.2 |
| **206-TS_b** | -1176.492223 | -1176.054789 | 0.305054 | -1176.165407 | 0.07359 | 0.069316 | -1176.238997 | -1176.234723 | -524.06 |
| **207-TS-precursor_a** | -1054.033088 | -1053.59821 | 0.348559 | -1053.662073 | 0.07409 | 0.070238 | -1053.736163 | -1053.732312 | |

| | | | | | | | | | |
|---|---|---|---|---|---|---|---|---|---|
| **207-TS-precursor_b** | -1054.032815 | -1053.597819 | 0.348693 | -1053.661799 | 0.073595 | 0.06991 | -1053.735395 | -1053.731709 | |
| **207-TS-precursor_b** | -1054.029319 | -1053.593877 | 0.348223 | -1053.658437 | 0.07591 | 0.071088 | -1053.734347 | -1053.729524 | |
| **207-TS-precursor_d** | -1054.030393 | -1053.595654 | 0.348508 | -1053.659356 | 0.074479 | 0.070436 | -1053.733835 | -1053.729793 | |
| **207-TS_a** | -1054.015938 | -1053.580378 | 0.343014 | -1053.650824 | 0.074076 | 0.069886 | -1053.724899 | -1053.720709 | -748.2 |
| **207-TS_b** | -1054.012094 | -1053.576223 | 0.343006 | -1053.646854 | 0.074702 | 0.070293 | -1053.721557 | -1053.717147 | -817.66 |
| **208-TS-precursor** | -938.510784 | -938.119291 | 0.304962 | -938.184118 | 0.073459 | 0.068923 | -938.257578 | -938.253041 | |
| **208-TS** | -938.500242 | -938.109479 | 0.301009 | -938.179182 | 0.068155 | 0.064832 | -938.247337 | -938.244014 | -589.15 |
| **209-TS_a** | -785.527565 | -785.212560 | 0.249386 | -785.263111 | 0.057909 | 0.056027 | -785.321021 | -785.319138 | |
| **209-TS_b** | -785.525095 | -785.209868 | 0.249240 | -785.260769 | 0.057990 | 0.056075 | -785.318759 | -785.316845 | |
| **210-T1_a** | -785.578595 | -785.264591 | 0.253150 | -785.310145 | 0.059453 | 0.056829 | -785.369598 | -785.366974 | |
| **210-T1-b** | -785.577676 | -785.263712 | 0.253184 | -785.309156 | 0.059008 | 0.056652 | -785.368165 | -785.365809 | |
| **211-TS_a** | -785.503071 | -785.188759 | 0.248920 | -785.238970 | 0.058748 | 0.056428 | -785.297718 | -785.295398 | |
| **211-TS_b** | -785.502575 | -785.188112 | 0.248951 | -785.238440 | 0.058512 | 0.056331 | -785.296952 | -785.294771 | |
| **218-TS** | -785.591047 | -785.274677 | 0.252960 | -785.323398 | 0.055647 | 0.054303 | -785.379045 | -785.377701 | -959.77 |
| **219-S0** | -785.645487 | -785.329415 | 0.255524 | -785.374778 | 0.056968 | 0.055296 | -785.431746 | -785.430074 | |

***Table 25:*** *Thermochemical data for structures reported in* ***Chapter 2***

| **Entry** | $E_{SPC}$ | $E$ | $ZPE$ | $H_{SPC}$ | $T \cdot S$ | $qh.T \cdot S$ | $G_{SPC}$ | $qh.G_{SPC}$ | **Imag. ʋ / cm$^{-1}$** |
|---|---|---|---|---|---|---|---|---|---|
| **325-S0_a** | -970.759029 | -970.698800 | 0.263967 | -970.477449 | 0.063056 | 0.060788 | -970.540506 | -970.538238 | |
| **325-S0_b** | -970.760038 | -970.699822 | 0.263939 | -970.478554 | 0.062768 | 0.060571 | -970.541322 | -970.539125 | |
| **325-S0_c** | -970.755617 | -970.695518 | 0.263495 | -970.474235 | 0.064324 | 0.061784 | -970.538559 | -970.536019 | |
| **325-S0_d** | -970.756378 | -970.696304 | 0.263696 | -970.474916 | 0.063869 | 0.061457 | -970.538784 | -970.536373 | |
| **325-T1_a** | -970.679345 | -970.618956 | 0.262124 | -970.399321 | 0.064702 | 0.062345 | -970.464023 | -970.461666 | |
| **325-T1_b** | -970.677491 | -970.617092 | 0.261563 | -970.397816 | 0.065273 | 0.062832 | -970.463090 | -970.460648 | |
| **325-T1_c** | -970.678955 | -970.618560 | 0.262260 | -970.398866 | 0.064772 | 0.062436 | -970.463638 | -970.461302 | |
| **325-T1_d** | -970.677277 | -970.616886 | 0.261711 | -970.397539 | 0.065425 | 0.062873 | -970.462964 | -970.460412 | |
| **327-S0_a** | -951.327905 | -951.271388 | 0.224188 | -951.087572 | 0.061399 | 0.058675 | -951.148972 | -951.146247 | |
| **327-S0_b** | -951.327529 | -951.271030 | 0.224208 | -951.087161 | 0.061491 | 0.058728 | -951.148653 | -951.145890 | |
| **327-S0_c** | -951.320219 | -951.263551 | 0.224125 | -951.079970 | 0.060575 | 0.058162 | -951.140545 | -951.138132 | |
| **327-S0_d** | -951.321221 | -951.264577 | 0.224156 | -951.081020 | 0.060291 | 0.057941 | -951.141311 | -951.138961 | |
| **327-T1_a** | -951.232018 | -951.175002 | 0.222077 | -950.993582 | 0.062295 | 0.059876 | -951.055878 | -951.053458 | |
| **327-T1_b** | -951.229847 | -951.172810 | 0.221538 | -950.991759 | 0.062997 | 0.060315 | -951.054757 | -951.052074 | |
| **327-T1_c** | -951.231656 | -951.174614 | 0.222142 | -950.993149 | 0.062186 | 0.059699 | -951.055334 | -951.052847 | |
| **327-T1_d** | -951.230082 | -951.173019 | 0.221683 | -950.991904 | 0.062381 | 0.059972 | -951.054285 | -951.051875 | |
| **335-S0_a** | -970.805708 | -970.746585 | 0.266739 | -970.521676 | 0.063126 | 0.060510 | -970.584801 | -970.582186 | |
| **335-S0_b** | -970.799347 | -970.740229 | 0.266210 | -970.515541 | 0.064353 | 0.061269 | -970.579894 | -970.576810 | |
| **335_a_MECP** | -970.667122 | N/A | N/A | N/A | N/A | N/A | N/A | N/A | |
| **335_b_MECP** | -970.669720 | N/A | N/A | N/A | N/A | N/A | N/A | N/A | |

| | | | | | | | | | |
|---|---|---|---|---|---|---|---|---|---|
| **335-T1_a** | -970.746360 | -970.686322 | 0.264424 | -970.464203 | 0.066215 | 0.062673 | -970.530418 | -970.526876 | |
| **335-T1_b** | -970.744814 | -970.684790 | 0.264617 | -970.462583 | 0.065152 | 0.062167 | -970.527735 | -970.524749 | |
| **336-TS_a** | -970.661666 | -970.601287 | 0.261443 | -970.383086 | 0.061961 | 0.060615 | -970.445047 | -970.443701 | -361.07 |
| **336-TS_b** | -970.660471 | -970.600125 | 0.261302 | -970.382031 | 0.061868 | 0.060600 | -970.443900 | -970.442632 | -384.27 |
| **337-TS_a** | -970.645051 | -970.584188 | 0.262413 | -970.365915 | 0.060985 | 0.059632 | -970.426900 | -970.425547 | -398.39 |
| **337-TS_b** | -970.643011 | -970.582017 | 0.262737 | -970.363599 | 0.061029 | 0.059555 | -970.424628 | -970.423155 | -323.88 |
| **342_a** | -711.122916 | -711.060922 | 0.267107 | -710.839184 | 0.060945 | 0.058572 | -710.900129 | -710.897756 | |
| **342_b** | -711.123794 | -711.061805 | 0.267221 | -710.839996 | 0.060679 | 0.058447 | -710.900675 | -710.898443 | |
| **343-TS_a** | -711.116624 | -711.054585 | 0.265838 | -710.834897 | 0.059014 | 0.057000 | -710.893911 | -710.891897 | -385.44 |
| **343-TS_b** | -711.116351 | -711.054307 | 0.265708 | -710.834697 | 0.059343 | 0.057152 | -710.894040 | -710.891849 | -385.37 |
| **343-TS_c** | -711.113676 | -711.051696 | 0.265685 | -710.832009 | 0.059428 | 0.057258 | -710.891437 | -710.889267 | -409.74 |
| **343-TS_d** | -711.113914 | -711.051938 | 0.265659 | -710.832261 | 0.059464 | 0.057270 | -710.891725 | -710.889531 | -411.17 |
| **344_a** | -711.172204 | -711.110317 | 0.267070 | -710.888958 | 0.059508 | 0.057515 | -710.948465 | -710.946473 | |
| **344_b** | -711.172024 | -711.110131 | 0.266986 | -710.888836 | 0.059605 | 0.057580 | -710.948441 | -710.946417 | |
| **344_c** | -711.173157 | -711.111219 | 0.266713 | -710.890075 | 0.060330 | 0.057882 | -710.950405 | -710.947957 | |
| **345-TS_a** | -711.111772 | -711.049801 | 0.266194 | -710.829699 | 0.058678 | 0.056939 | -710.888377 | -710.886638 | -453.29 |
| **345-TS_b** | -711.115194 | -711.053235 | 0.266165 | -710.833184 | 0.058536 | 0.056880 | -710.891721 | -710.890065 | -434.82 |
| **345-TS_c** | -711.113669 | -711.051532 | 0.266138 | -710.831533 | 0.059647 | 0.057355 | -710.891179 | -710.888888 | -449.34 |
| **345-TS_d** | -711.112891 | -711.050854 | 0.265870 | -710.830981 | 0.059420 | 0.057357 | -710.890401 | -710.888338 | -440.30 |
| **345-TS_f** | -711.112591 | -711.050565 | 0.265977 | -710.830662 | 0.059189 | 0.057152 | -710.889851 | -710.887814 | -427.01 |
| **345-TS_g** | -711.110321 | -711.048166 | 0.266167 | -710.828176 | 0.059480 | 0.057277 | -710.887655 | -710.885453 | -462.53 |
| **345-TS_h** | -711.109582 | -711.047527 | 0.265824 | -710.827684 | 0.059549 | 0.057417 | -710.887233 | -710.885101 | -455.33 |
| **345-TS_i** | -711.108797 | -711.046744 | 0.266085 | -710.826753 | 0.059070 | 0.057116 | -710.885823 | -710.883869 | -433.27 |
| **346_a** | -711.208688 | -711.146789 | 0.269962 | -710.923145 | 0.058511 | 0.056470 | -710.981655 | -710.979615 | |
| **346_b** | -711.206475 | -711.144656 | 0.270063 | -710.920805 | 0.058271 | 0.056452 | -710.979076 | -710.977257 | |
| **346_c** | -711.204418 | -711.142591 | 0.269988 | -710.918557 | 0.059395 | 0.057166 | -710.977952 | -710.975723 | |
| **346_d** | -711.205546 | -711.143736 | 0.269917 | -710.919752 | 0.059425 | 0.057182 | -710.979177 | -710.976934 | |
| **346_e** | -711.208104 | -711.146312 | 0.269980 | -710.922492 | 0.058423 | 0.056497 | -710.980916 | -710.978990 | |
| **350-TS_a** | -970.661427 | -970.600953 | 0.261764 | -970.382745 | 0.061858 | 0.060355 | -970.444602 | -970.443100 | -418.86 |
| **350-TS_b** | -970.659505 | -970.599020 | 0.261266 | -970.381199 | 0.062259 | 0.060628 | -970.443457 | -970.441827 | -449.88 |
| **351-S0_a** | -970.706181 | -970.645933 | 0.265159 | -970.424413 | 0.059983 | 0.058619 | -970.484396 | -970.483032 | |
| **351-S0_b** | -970.701913 | -970.641767 | 0.264850 | -970.420322 | 0.060782 | 0.059019 | -970.481103 | -970.479341 | |
| **351-T1_a** | -970.688644 | -970.628114 | 0.263343 | -970.408381 | 0.061605 | 0.060205 | -970.469986 | -970.468586 | |
| **351-T1_b** | -970.685452 | -970.624946 | 0.263050 | -970.405414 | 0.062018 | 0.060344 | -970.467432 | -970.465759 | |
| **352-TS_a** | -970.667611 | -970.607637 | 0.260353 | -970.390596 | 0.060856 | 0.059041 | -970.451452 | -970.449638 | -1483.71 |
| **352-TS_b** | -970.663313 | -970.603373 | 0.260194 | -970.386391 | 0.061251 | 0.059140 | -970.447642 | -970.445530 | -1478.09 |
| **353-S0_a** | -970.770564 | -970.710373 | 0.266583 | -970.487544 | 0.059473 | 0.058339 | -970.547017 | -970.545883 | |
| **353-S0_b** | -970.766783 | -970.706607 | 0.266247 | -970.484023 | 0.059619 | 0.058466 | -970.543642 | -970.542489 | |
| **354-TS_a** | -970.666317 | -970.605605 | 0.262305 | -970.387266 | 0.060526 | 0.058985 | -970.447792 | -970.446252 | -825.53 |
| **354-TS_b** | -970.668517 | -970.607866 | 0.262234 | -970.389586 | 0.060301 | 0.058869 | -970.449887 | -970.448455 | -805.52 |

| | | | | | | | | | |
|---|---|---|---|---|---|---|---|---|---|
| **355-TS** | -970.667656 | -970.607127 | 0.261609 | -970.388964 | 0.062898 | 0.060825 | -970.451862 | -970.449789 | -66.42 |
| **356-TS_a** | -970.653500 | -970.592887 | 0.262048 | -970.374638 | 0.061835 | 0.060278 | -970.436473 | -970.434916 | -37.49 |
| **356-TS_b** | -970.651926 | -970.591268 | 0.261507 | -970.373361 | 0.062730 | 0.060844 | -970.436091 | -970.434205 | -38.49 |
| **357-TS** | -970.649594 | -970.589316 | 0.260645 | -970.371691 | 0.062945 | 0.061120 | -970.434635 | -970.432810 | -43.37 |
| **360-S0_a** | -634.365491 | -634.309702 | 0.247822 | -634.103732 | 0.053700 | 0.052355 | -634.157432 | -634.156087 | |
| **360-S0_b** | -634.371242 | -634.315411 | 0.248203 | -634.109402 | 0.052034 | 0.051432 | -634.161436 | -634.160834 | |
| **360_a_MECP** | -634.330613 | N/A | N/A | N/A | N/A | N/A | N/A | N/A | |
| **360_b_MECP** | -634.332919 | N/A | N/A | N/A | N/A | N/A | N/A | N/A | |
| **360-T1_a** | -634.344604 | -634.288451 | 0.246049 | -634.084488 | 0.054664 | 0.053380 | -634.139152 | -634.137867 | |
| **360-T1_b** | -634.349108 | -634.292915 | 0.246212 | -634.088963 | 0.053915 | 0.053035 | -634.142878 | -634.141998 | |
| **361-S0_a** | -931.388812 | -931.332879 | 0.237743 | -931.135631 | 0.058768 | 0.056857 | -931.194399 | -931.192488 | |
| **361-S0_b** | -931.394339 | -931.338343 | 0.237897 | -931.141216 | 0.057490 | 0.056202 | -931.198706 | -931.197418 | |
| **361_a_MECP** | -931.361617 | N/A | N/A | N/A | N/A | N/A | N/A | N/A | |
| **361_b_MECP** | -931.351125 | N/A | N/A | N/A | N/A | N/A | N/A | N/A | |
| **361-T1_a** | -931.370643 | -931.314336 | 0.236120 | -931.118937 | 0.059571 | 0.057896 | -931.178508 | -931.176833 | |
| **361-T1_b** | -931.374779 | -931.318474 | 0.236156 | -931.123098 | 0.059140 | 0.057762 | -931.182238 | -931.180860 | |
| **362-TS_a** | -951.214112 | -951.156988 | 0.221814 | -950.976980 | 0.058861 | 0.057422 | -951.035841 | -951.034402 | -430.19 |
| **362-TS_b** | -951.211941 | -951.154832 | 0.221442 | -950.975094 | 0.059144 | 0.057616 | -951.034238 | -951.032710 | -461.74 |
| **363-S0_a** | -951.243852 | -951.186656 | 0.224513 | -951.004278 | 0.056867 | 0.055695 | -951.061146 | -951.059973 | |
| **363-S0_b** | -951.238741 | -951.181591 | 0.224133 | -950.999403 | 0.057950 | 0.056186 | -951.057352 | -951.055589 | |
| **363_a_MECP** | -951.236481 | N/A | N/A | N/A | N/A | N/A | N/A | N/A | |
| **363_b_MECP** | -951.234617 | N/A | N/A | N/A | N/A | N/A | N/A | N/A | |
| **363-T1_a** | -951.242803 | -951.185694 | 0.223358 | -951.004124 | 0.058623 | 0.057265 | -951.062747 | -951.061388 | |
| **363-T1_b** | -951.239652 | -951.182578 | 0.223225 | -951.001098 | 0.058792 | 0.057265 | -951.059889 | -951.058363 | |
| **364-TS_a** | -951.209866 | -951.152782 | 0.221645 | -950.972847 | 0.058490 | 0.057263 | -951.031336 | -951.030110 | -406.44 |
| **364-TS_b** | -951.208442 | -951.151383 | 0.221435 | -950.971628 | 0.058260 | 0.057215 | -951.029888 | -951.028843 | -436.77 |
| **370_T1_a** | -3247.304255 | -3247.185076 | 0.262669 | -3247.023914 | 0.063866 | 0.061616 | -3247.087780 | -3247.085530 | |
| **370_T1_b** | -3247.302513 | -3247.183340 | 0.262019 | -3247.022565 | 0.064794 | 0.062227 | -3247.087359 | -3247.084792 | |
| **370_T1_c** | -3247.304272 | -3247.185149 | 0.262721 | -3247.023858 | 0.063663 | 0.061467 | -3247.087521 | -3247.085324 | |
| **370_T1_d** | -3247.302356 | -3247.183237 | 0.261995 | -3247.022408 | 0.064477 | 0.062068 | -3247.086885 | -3247.084475 | |
| **371-T1_a** | -1133.265637 | -1133.191353 | 0.263248 | -1132.984951 | 0.062791 | 0.060608 | -1133.047742 | -1133.045560 | |
| **371-T1_b** | -1133.263795 | -1133.189515 | 0.262532 | -1132.983541 | 0.063822 | 0.061303 | -1133.047363 | -1133.044844 | |
| **371-T1_c** | -1133.265600 | -1133.191383 | 0.263350 | -1132.984853 | 0.062355 | 0.060342 | -1133.047208 | -1133.045195 | |
| **371-T1_d** | -1133.263644 | -1133.189456 | 0.262507 | -1132.983388 | 0.063456 | 0.061174 | -1133.046844 | -1133.044562 | |
| **372-T1_a** | -772.905986 | -772.839776 | 0.264556 | -772.624328 | 0.061659 | 0.059651 | -772.685987 | -772.683979 | |
| **372-T1_b** | -772.904022 | -772.837793 | 0.264071 | -772.622665 | 0.062221 | 0.060055 | -772.684886 | -772.682720 | |
| **372-T1_c** | -772.905941 | -772.839716 | 0.264686 | -772.624207 | 0.061172 | 0.059417 | -772.685379 | -772.683624 | |
| **372-T1_d** | -772.903931 | -772.837740 | 0.264168 | -772.622503 | 0.061964 | 0.059898 | -772.684467 | -772.682401 | |
| **373-T1_a** | -788.185596 | -788.116024 | 0.304550 | -787.862223 | 0.065546 | 0.063092 | -787.927769 | -787.925315 | |
| **373-T1_b** | -788.183534 | -788.113951 | 0.304027 | -787.860487 | 0.066233 | 0.063533 | -787.926720 | -787.924020 | |

| | | | | | | | | | |
|---|---|---|---|---|---|---|---|---|---|
| **373-T1_c** | -788.184707 | -788.115126 | 0.304688 | -787.861261 | 0.065117 | 0.062806 | -787.926378 | -787.924067 | |
| **373-T1_d** | -788.183020 | -788.113453 | 0.304007 | -787.859990 | 0.065791 | 0.063395 | -787.925781 | -787.923384 | |
| **374-T1_a** | -765.906708 | -765.840599 | 0.271408 | -765.617298 | 0.063683 | 0.061561 | -765.680981 | -765.678859 | |
| **374-T1_b** | -765.904962 | -765.838848 | 0.270843 | -765.615918 | 0.064298 | 0.061995 | -765.680216 | -765.677913 | |
| **374-T1_c** | -765.908830 | -765.842730 | 0.271559 | -765.619348 | 0.062986 | 0.061202 | -765.682334 | -765.680550 | |
| **374-T1_d** | -765.907062 | -765.840973 | 0.271119 | -765.617852 | 0.063470 | 0.061585 | -765.681321 | -765.679437 | |
| **375-T1_a** | -878.174199 | -878.100471 | 0.275621 | -877.879966 | 0.065187 | 0.062882 | -877.945153 | -877.942848 | |
| **375-T1_b** | -878.172434 | -878.098723 | 0.274776 | -877.878764 | 0.066124 | 0.063526 | -877.944888 | -877.942290 | |
| **375-T1_c** | -878.178369 | -878.104750 | 0.275125 | -877.884658 | 0.064824 | 0.062639 | -877.949482 | -877.947296 | |
| **375-T1_d** | -878.183007 | -878.109296 | 0.274538 | -877.889978 | 0.064544 | 0.062205 | -877.954522 | -877.952183 | |
| **376-T1_a** | -1261.618593 | -1261.527810 | 0.310073 | -1261.287550 | 0.070576 | 0.067534 | -1261.358126 | -1261.355084 | |
| **376-T1_b** | -1261.616701 | -1261.525913 | 0.309498 | -1261.285984 | 0.071550 | 0.068154 | -1261.357534 | -1261.354139 | |
| **376-T1_c** | -1261.618603 | -1261.527945 | 0.310015 | -1261.287571 | 0.070046 | 0.067368 | -1261.357617 | -1261.354939 | |
| **376-T1_d** | -1261.616632 | -1261.526054 | 0.309583 | -1261.285911 | 0.070382 | 0.067636 | -1261.356293 | -1261.353547 | |
| **377-TS_a** | -3247.284478 | -3247.165420 | 0.261393 | -3247.005927 | 0.063304 | 0.060968 | -3247.069231 | -3247.066896 | -400.40 |
| **377-TS_b** | -3247.285591 | -3247.166494 | 0.261770 | -3247.006845 | 0.061171 | 0.059842 | -3247.068015 | -3247.066687 | -380.04 |
| **379-TS_a** | -3247.287147 | -3247.167908 | 0.262146 | -3247.008229 | 0.060945 | 0.059573 | -3247.069174 | -3247.067802 | -414.22 |
| **379-TS_b** | -3247.285223 | -3247.165973 | 0.261593 | -3247.006712 | 0.061436 | 0.059907 | -3247.068148 | -3247.066619 | -447.19 |
| **381-TS_a** | -1133.244325 | -1133.170108 | 0.262202 | -1132.965440 | 0.059683 | 0.058679 | -1133.025122 | -1133.024118 | -429.60 |
| **381-TS_b** | -1133.245469 | -1133.171186 | 0.262507 | -1132.966364 | 0.059449 | 0.058461 | -1133.025813 | -1133.024825 | -405.10 |
| **383-TS_a** | -1133.248384 | -1133.174014 | 0.262658 | -1132.969173 | 0.059806 | 0.058588 | -1133.028979 | -1133.027761 | -417.17 |
| **383-TS_b** | -1133.246488 | -1133.172108 | 0.262306 | -1132.967545 | 0.060075 | 0.058775 | -1133.027619 | -1133.026320 | -445.04 |
| **385-TS_a** | -772.885108 | -772.818975 | 0.263439 | -772.605332 | 0.058673 | 0.057749 | -772.664005 | -772.663081 | -479.52 |
| **385-TS_b** | -772.886507 | -772.820328 | 0.263772 | -772.606450 | 0.058647 | 0.057655 | -772.665096 | -772.664104 | -457.06 |
| **386-T1** | -772.924825 | -772.858626 | 0.265493 | -772.643004 | 0.058641 | 0.057557 | -772.701645 | -772.700561 | |
| **387-TS** | -772.904549 | -772.837326 | 0.264477 | -772.623526 | 0.059454 | 0.058333 | -772.682979 | -772.681859 | -131.71 |
| **390-TS_a** | -772.888425 | -772.822113 | 0.264055 | -772.608166 | 0.058649 | 0.057625 | -772.666815 | -772.665791 | -413.97 |
| **390-TS_b** | -772.886493 | -772.820180 | 0.263510 | -772.606594 | 0.059518 | 0.058121 | -772.666113 | -772.664715 | -440.29 |
| **391-TS_a** | -788.156393 | -788.086831 | 0.302833 | -787.835357 | 0.063042 | 0.061466 | -787.898399 | -787.896823 | -499.59 |
| **391-TS_b** | -788.159067 | -788.089416 | 0.303759 | -787.837471 | 0.061589 | 0.060581 | -787.899060 | -787.898052 | -484.80 |
| **392-T1** | -788.189226 | -788.119604 | 0.305140 | -787.866117 | 0.061917 | 0.060718 | -787.928035 | -787.926835 | |
| **393-TS** | -788.169132 | -788.099687 | 0.302892 | -787.847845 | 0.063880 | 0.061964 | -787.911725 | -787.909809 | -447.26 |
| **395-T1_a** | -788.166574 | -788.096880 | 0.304158 | -787.844522 | 0.062408 | 0.060979 | -787.906930 | -787.905501 | -426.43 |
| **395-T1_b** | -788.164621 | -788.094921 | 0.303639 | -787.842942 | 0.062935 | 0.061324 | -787.905876 | -787.904265 | -456.79 |
| **396-TS_a** | -765.888340 | -765.822219 | 0.270204 | -765.600875 | 0.060986 | 0.059692 | -765.661861 | -765.660568 | -384.97 |
| **396-TS_b** | -765.889764 | -765.823574 | 0.270693 | -765.601985 | 0.060309 | 0.059249 | -765.662294 | -765.661234 | -354.55 |
| **397-T1** | -765.914290 | -765.848079 | 0.271831 | -765.625126 | 0.059227 | 0.059665 | -765.686146 | -765.684791 | |
| **398-TS** | -765.874008 | -765.807858 | 0.269662 | -765.586184 | 0.061020 | 0.061944 | -765.650574 | -765.648128 | -123.00 |
| **400-TS_a** | -765.891025 | -765.824813 | 0.270512 | -765.603253 | 0.061420 | 0.059898 | -765.664674 | -765.663151 | -408.52 |
| **400-TS_b** | -765.889185 | -765.822976 | 0.270142 | -765.601682 | 0.061827 | 0.060130 | -765.663508 | -765.661811 | -438.79 |

| | | | | | | | | | |
|---|---|---|---|---|---|---|---|---|---|
| **401-TS_a** | -878.165988 | -878.092492 | 0.274633 | -877.873821 | 0.061043 | 0.060091 | -877.934864 | -877.933912 | -438.79 |
| **401-TS_b** | -878.166232 | -878.092579 | 0.274762 | -877.873825 | 0.061696 | 0.060465 | -877.935521 | -877.934290 | -326.44 |
| **402-T1** | -878.195056 | -878.121415 | 0.275735 | -877.901134 | 0.063355 | 0.061507 | -877.964489 | -877.962641 | -307.23 |
| **403-TS** | -878.192146 | -878.118467 | 0.274339 | -877.899702 | 0.063358 | 0.061481 | -877.963060 | -877.961183 | |
| **405-TS_a** | -878.158471 | -878.084701 | 0.274854 | -877.865844 | 0.062486 | 0.060928 | -877.928330 | -877.926772 | -316.48 |
| **405-TS_b** | -878.156495 | -878.082719 | 0.274231 | -877.864282 | 0.063365 | 0.061438 | -877.927647 | -877.925720 | -410.10 |
| **406-TS_a** | -1261.605279 | -1261.514710 | 0.309231 | -1261.275960 | 0.067145 | 0.065258 | -1261.343104 | -1261.341218 | -443.08 |
| **406-TS_b** | -1261.607484 | -1261.516813 | 0.309482 | -1261.277965 | 0.066578 | 0.065046 | -1261.344543 | -1261.343011 | -294.43 |
| **407-T1** | -1261.642852 | -1261.552158 | 0.310706 | -1261.311863 | 0.066981 | 0.065366 | -1261.378844 | -1261.377230 | -287.54 |
| **408-TS** | -1261.640007 | -1261.549390 | 0.309501 | -1261.310271 | 0.067544 | 0.065548 | -1261.377815 | -1261.375819 | |
| **410-TS_a** | -1261.602489 | -1261.511640 | 0.309999 | -1261.272647 | 0.066703 | 0.064784 | -1261.339350 | -1261.337431 | -287.72 |
| **410-TS_b** | -1261.600535 | -1261.509678 | 0.309409 | -1261.271085 | 0.067321 | 0.065262 | -1261.338406 | -1261.336347 | -407.21 |
| **410-TS_b** | -970.759029 | -970.698800 | 0.263967 | -970.477449 | 0.063056 | 0.060788 | -970.540506 | -970.538238 | -438.74 |
| **418** | -529.286133 | -529.265052 | 0.088063 | -529.191184 | 0.038634 | 0.038626 | -529.229818 | -529.229810 | |
| **419** | -231.567937 | -231.547533 | 0.085480 | -231.477070 | 0.033452 | 0.033452 | -231.510519 | -231.510522 | |
| **420** | -297.615013 | -297.614276 | 0.000000 | -297.612652 | 0.019863 | 0.019863 | -297.632515 | -297.632515 | |
| **421_a** | -673.047849 | -672.988431 | 0.261377 | -672.770300 | 0.059676 | 0.057512 | -672.829976 | -672.827812 | |
| **421_b** | -673.048655 | -672.989248 | 0.261590 | -672.771026 | 0.059037 | 0.059037 | -672.830064 | -672.828112 | |

***Table 26:*** *Thermochemical data for structures reported in* ***Chapter 3***

| Entry | $E$ | $ZPE$ | $H_{SPC}$ | $T \cdot S$ | $qh.T \cdot S$ | $G$ | $qh.G$ | Imag. $\upsilon$ / $cm^{-1}$ |
|---|---|---|---|---|---|---|---|---|
| **311_b3lyp-gd3bj** | -931.892534 | 0.241979 | -931.634877 | 0.059374 | 0.057222 | -931.694251 | -931.692099 | |
| **311_cam-b3lyp-gd3bj** | -931.425079 | 0.24491 | -931.164691 | 0.058913 | 0.056838 | -931.223605 | -931.22153 | |
| **311_lc-whpbe** | -931.315013 | 0.24649 | -931.05304 | 0.058947 | 0.056866 | -931.111987 | -931.109906 | |
| **311_m062x-D3** | -931.387201 | 0.244398 | -931.127313 | 0.058806 | 0.056811 | -931.186118 | -931.184124 | |
| **311_wb97xd** | -931.596922 | 0.244558 | -931.336891 | 0.058881 | 0.056812 | -931.395772 | -931.393703 | |
| **336-TS_a_B3LYP-gd3bj** | -970.640558 | 0.269786 | -970.354057 | 0.061167 | 0.059874 | -970.415223 | -970.413931 | -204.84 |
| **336-TS_a_B97D-gd3bj** | -971.076237 | 0.260593 | -970.798091 | 0.063505 | 0.061655 | -970.861596 | -970.859746 | -127.69 |
| **336-TS_a_CAM-B3LYP** | -970.5966 | 0.269542 | -970.310301 | 0.06131 | 0.059977 | -970.371611 | -970.370278 | -364.61 |
| **336-TS_a_LC-wHPBE-gd3bj** | -970.524472 | 0.271308 | -970.23634 | 0.061771 | 0.06014 | -970.298111 | -970.296481 | -460.69 |
| **336-TS_a_m062x-gd3** | -970.601287 | 0.269252 | -970.315292 | 0.06118 | 0.059884 | -970.376472 | -970.375176 | -361.07 |
| **336-TS_a_wb97xd** | -970.821916 | 0.269419 | -970.535761 | 0.061247 | 0.059902 | -970.597008 | -970.595664 | -390.57 |
| **336-TS_b_B3LYP-gd3bj** | -971.14584 | 0.266554 | -970.862234 | 0.062148 | 0.060616 | -970.924382 | -970.92285 | -204.83 |
| **336-TS_b_B97D-gd3bj** | -971.07693 | 0.260916 | -970.798579 | 0.063187 | 0.061402 | -970.861766 | -970.859981 | -116.59 |
| **336-TS_b_CAM-B3LYP-gd3bj** | -970.641905 | 0.269997 | -970.355248 | 0.061075 | 0.059765 | -970.416323 | -970.415013 | -340.35 |
| **336-TS_b_LC-wHPBE-gd3bj** | -970.525831 | 0.271589 | -970.237521 | 0.061334 | 0.059944 | -970.298855 | -970.297464 | -433.75 |
| **336-TS_b_m062x-gd3** | -970.600125 | 0.269106 | -970.314276 | 0.061086 | 0.059865 | -970.375362 | -970.374141 | -384.27 |
| **336-TS_b_wb97xd** | -970.823312 | 0.269695 | -970.536966 | 0.060969 | 0.05969 | -970.597935 | -970.596656 | -367.63 |
| **350-TS_a_B3LYP-gd3bj** | -971.141142 | 0.267041 | -970.857388 | 0.061579 | 0.060041 | -970.918967 | -970.917429 | -417.24 |
| **350-TS_a_B97D-gd3bj** | -971.066256 | 0.261224 | -970.787929 | 0.062482 | 0.060782 | -970.850411 | -970.848711 | -435.80 |

| | | | | | | | | |
|---|---|---|---|---|---|---|---|---|
| **350-TS_a_CAM-B3LYP-gd3bj** | -970.641376 | 0.270202 | -970.354672 | 0.061069 | 0.059623 | -970.415741 | -970.414295 | -469.21 |
| **350-TS_a_LC-wHPBE-gd3bj** | -970.529912 | 0.271868 | -970.241507 | 0.061191 | 0.059716 | -970.302698 | -970.301222 | -501.91 |
| **350-TS_a_m062x-gd3** | -970.600953 | 0.269582 | -970.314847 | 0.061083 | 0.059628 | -970.37593 | -970.374475 | -418.86 |
| **350-TS_a_wb97xd** | -970.824577 | 0.269898 | -970.538182 | 0.061082 | 0.0596 | -970.599265 | -970.597782 | -465.47 |
| **350-TS_b_B3LYP-gd3bj** | -971.139362 | 0.266621 | -970.855928 | 0.061997 | 0.060267 | -970.917925 | -970.916195 | -443.58 |
| **350-TS_b_B97D-gd3bj** | -971.064749 | 0.261116 | -970.786584 | 0.062302 | 0.060581 | -970.848886 | -970.847165 | -461.70 |
| **350-TS_b_CAM-B3LYP-gd3bj** | -970.639436 | 0.269745 | -970.35308 | 0.061505 | 0.059869 | -970.414585 | -970.412948 | -506.20 |
| **350-TS_b_LC-wHPBE-gd3bj** | -970.528016 | 0.271476 | -970.239899 | 0.061575 | 0.05994 | -970.301474 | -970.299839 | -546.58 |
| **350-TS_b_m062x-gd3** | -970.59902 | 0.269069 | -970.313304 | 0.061481 | 0.059901 | -970.374785 | -970.373206 | -449.88 |
| **350-TS_b_wb97xd** | -970.822756 | 0.269742 | -970.536526 | 0.061116 | 0.059538 | -970.597643 | -970.596064 | -499.43 |
| **362-TS_a_b3lyp-gd3bj** | -951.673014 | 0.226194 | -951.431771 | 0.058292 | 0.056901 | -951.490063 | -951.488672 | -382.75 |
| **362-TS_a_b97D-gd3bj** | -951.622325 | 0.221278 | -951.385714 | 0.058827 | 0.057361 | -951.444541 | -951.443075 | -390.35 |
| **362-TS_a_cam-b3lyp-gd3bj** | -951.206497 | 0.228875 | -950.962694 | 0.058099 | 0.056722 | -951.020792 | -951.019416 | -469.96 |
| **362-TS_a_lc-whpbe** | -951.089618 | 0.230293 | -950.844326 | 0.058337 | 0.05691 | -950.902663 | -950.901236 | -516.17 |
| **362-TS_a_m062x-gd3** | -951.156988 | 0.228439 | -950.913584 | 0.058174 | 0.056782 | -950.971758 | -950.970366 | -430.19 |
| **362-TS_a_wb97xd** | -951.371123 | 0.228589 | -951.127576 | 0.058183 | 0.056775 | -951.18576 | -951.184352 | -479.26 |
| **362-TS_b_b3lyp** | -951.671092 | 0.225954 | -951.430055 | 0.058402 | 0.056957 | -951.488457 | -951.487011 | -394.32 |
| **362-TS_b_b97D-gd3bj** | -951.620717 | 0.221019 | -951.384343 | 0.058854 | 0.057384 | -951.443197 | -951.441727 | -402.74 |
| **362-TS_b_cam-b3lyp-gd3bj** | -951.204346 | 0.22863 | -950.960751 | 0.058231 | 0.056787 | -951.018981 | -951.017538 | -497.96 |
| **362-TS_b_lc-whpbe** | -951.087456 | 0.230104 | -950.842332 | 0.058418 | 0.056936 | -950.90075 | -950.899268 | -554.99 |
| **362-TS_b_m062x-gd3** | -951.154832 | 0.228055 | -950.911723 | 0.058456 | 0.056976 | -950.970179 | -950.968699 | -461.74 |
| **362-TS_b_wb97xd** | -951.369015 | 0.228288 | -951.125699 | 0.058411 | 0.056923 | -951.184109 | -951.182621 | -509.64 |
| **364-TS_a_b3lyp-gd3bj** | -951.672172 | 0.226081 | -951.430913 | 0.058151 | 0.056929 | -951.489064 | -951.487842 | -273.16 |
| **364-TS_a_b97D-gd3bj** | -951.625288 | 0.221017 | -951.388661 | 0.059241 | 0.057802 | -951.447903 | -951.446464 | -176.29 |
| **364-TS_a_cam-b3lyp-gd3bj** | -951.201566 | 0.228793 | -950.957808 | 0.057707 | 0.05653 | -951.015515 | -951.014337 | -384.43 |
| **364-TS_a_lc-whpbe** | -951.081174 | 0.23024 | -950.835972 | 0.057674 | 0.056529 | -950.893647 | -950.892502 | -449.51 |
| **364-TS_a_m062x-gd3** | -951.152782 | 0.228265 | -950.909498 | 0.057799 | 0.056614 | -950.967297 | -950.966112 | -406.44 |
| **364-TS_a_wb97xd** | -951.364945 | 0.228434 | -951.121521 | 0.057744 | 0.056567 | -951.179265 | -951.178088 | -407.57 |
| **364-TS_b_b3lyp-gd3bj** | -951.670594 | 0.225889 | -951.429504 | 0.058043 | 0.056951 | -951.487548 | -951.486455 | -290.71 |
| **364-TS_b_b97D-gd3bj** | -951.62372 | 0.220733 | -951.38731 | 0.059299 | 0.057919 | -951.446609 | -951.445229 | -179.57 |
| **364-TS_b_cam-b3lyp-gd3bj** | -951.199887 | 0.228621 | -950.956283 | 0.057529 | 0.056518 | -951.013812 | -951.012801 | -409.66 |
| **364-TS_b_lc-whpbe** | -951.079564 | 0.230067 | -950.834532 | 0.057462 | 0.056478 | -950.891994 | -950.891009 | -479.43 |
| **364-TS_b_m062x-gd3** | -951.151383 | 0.228048 | -950.908311 | 0.057568 | 0.056561 | -950.965879 | -950.964872 | -436.77 |
| **364-TS_b_wb97xd** | -951.363255 | 0.228366 | -951.119926 | 0.05741 | 0.05645 | -951.177336 | -951.176376 | -433.08 |

***Table 27:*** *Thermochemical data for structures reported in* ***Chapter 3*** *used in benchmarking studies*

### *10. TD-DFT results*

Absorption spectra of compounds **331** and **358** were determined using TD-DFT at the M06-2X-D3[35, 39] level of theory in conjunction with the def2-TZVP[92-93] basis set and the SMD[80-84] solvation model (solvent = acetonitrile). The first ten excited singlet states and excited triplet states were computed.

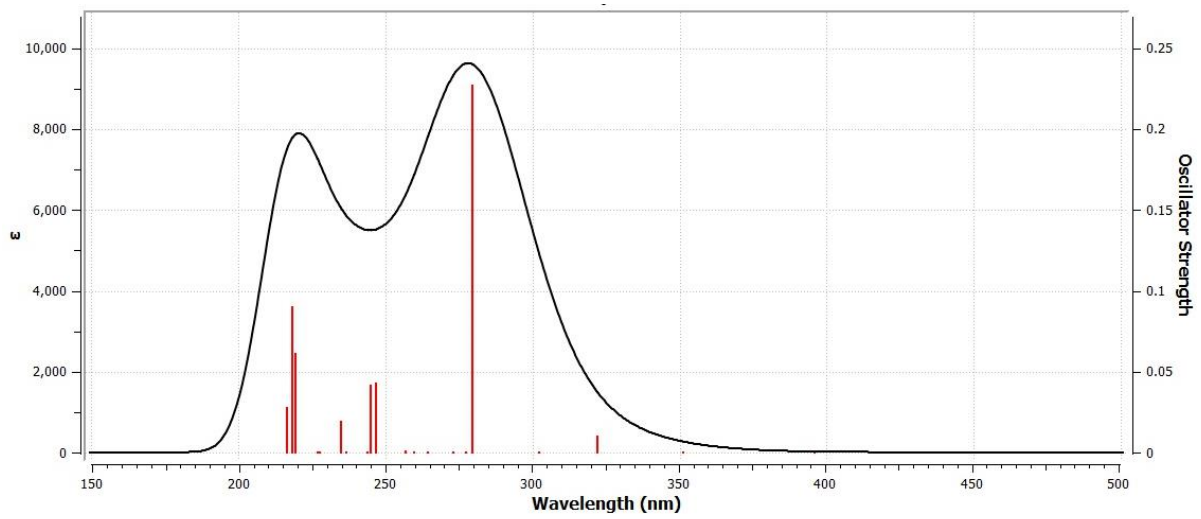



***Figure 62:*** *Computed absorption spectrum of* ***331***

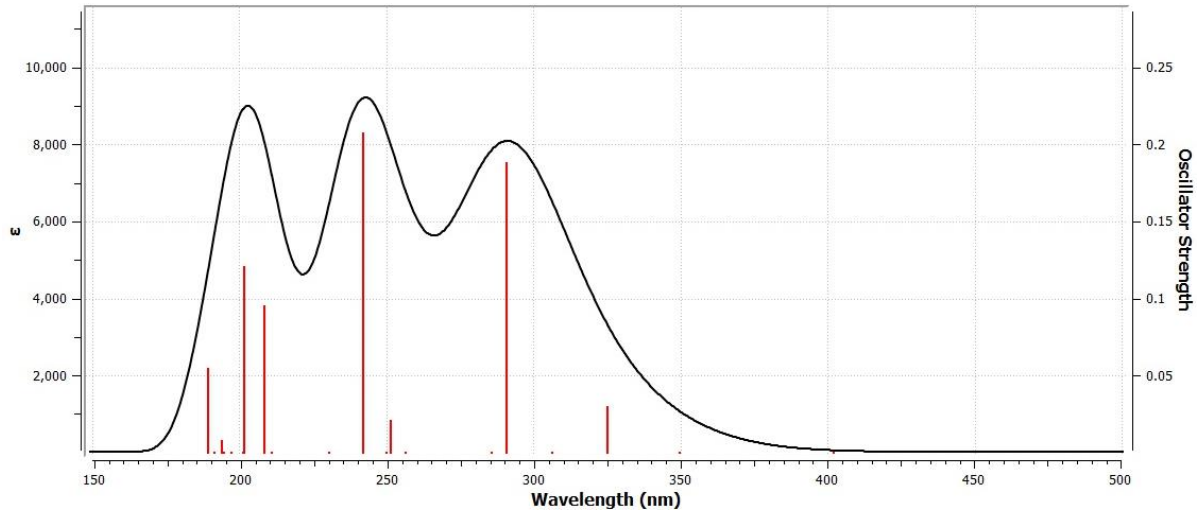



***Figure 63:*** *Computed absorption spectrum of* ***358***

Excitation energies and oscillator strengths for compound **331** are presented below:

Excited State 1: 3.000-A 3.1308 eV 396.01 nm f=0.0000 <S**2>=2.000
60A -> 67A -0.10021
62A -> 67A 0.19266
65A -> 67A -0.11711
66A -> 67A 0.62623
60B -> 67B 0.10021
62B -> 67B -0.19266
65B -> 67B 0.11711
66B -> 67B -0.62623

This state for optimization and/or second-order correction.
Total Energy, E(TD-HF/TD-DFT) = -931.272143977
Copying the excited state density for this state as the 1-particle RhoCI density.

Excited State 2: 3.000-A 3.5308 eV 351.15 nm f=0.0000 <S**2>=2.000
62A -> 67A 0.37796
62A -> 70A 0.10448
63A -> 67A -0.25141
64A -> 67A 0.41371
64A -> 70A 0.10009
65A -> 67A 0.14224
62B -> 67B -0.37796
62B -> 70B -0.10448
63B -> 67B 0.25141
64B -> 67B -0.41371
64B -> 70B -0.10009
65B -> 67B -0.14224

Excited State 3: 1.000-A 3.8496 eV 322.07 nm f=0.0096 <S**2>=0.000
62A -> 67A 0.40681
62A -> 70A 0.10934
63A -> 67A -0.20661
64A -> 67A 0.36650
66A -> 67A 0.26687
62B -> 67B 0.40681
62B -> 70B 0.10934
63B -> 67B -0.20661
64B -> 67B 0.36650
66B -> 67B 0.26687

Excited State 4: 3.000-A 4.1014 eV 302.30 nm f=0.0000 <S**2>=2.000
61A -> 68A -0.12281
61A -> 70A 0.10706
62A -> 69A -0.17307
64A -> 69A 0.23482
65A -> 67A 0.15794
65A -> 68A 0.31513
65A -> 70A -0.14485
66A -> 68A 0.22194
66A -> 69A 0.31175
66A -> 70A -0.23540
61B -> 68B 0.12281
61B -> 70B -0.10706
62B -> 69B 0.17307
64B -> 69B -0.23482
65B -> 67B -0.15794
65B -> 68B -0.31513
65B -> 70B 0.14485
66B -> 68B -0.22194
66B -> 69B -0.31175
66B -> 70B 0.23540

Excited State 5: 1.000-A 4.4327 eV 279.71 nm f=0.2266 <S**2>=0.000
62A -> 67A -0.12407
63A -> 67A 0.12468
64A -> 67A -0.16389
65A -> 67A -0.12459
66A -> 67A 0.63825
62B -> 67B -0.12407
63B -> 67B 0.12468
64B -> 67B -0.16389
65B -> 67B -0.12459
66B -> 67B 0.63825

Excited State 6: 3.000-A 4.4673 eV 277.54 nm f=0.0000 <S**2>=2.000
64A -> 69A -0.16265
65A -> 68A 0.37128
65A -> 69A 0.14357

65A -> 70A 0.30724
66A -> 68A 0.31942
66A -> 69A -0.13827
66A -> 70A 0.21841
64B -> 69B 0.16265
65B -> 68B -0.37128
65B -> 69B -0.14357
65B -> 70B -0.30724
66B -> 68B -0.31942
66B -> 69B 0.13827
66B -> 70B -0.21841

Excited State 7: 3.000-A 4.5423 eV 272.95 nm f=0.0000 <S**2>=2.000
61A -> 68A 0.12677
62A -> 69A -0.12699
64A -> 68A -0.14950
64A -> 69A 0.14370
65A -> 67A -0.14354
65A -> 69A 0.17525
65A -> 70A 0.27724
66A -> 67A -0.11135
66A -> 68A -0.23550
66A -> 69A 0.40920
66A -> 70A 0.18698
61B -> 68B -0.12677
62B -> 69B 0.12699
64B -> 68B 0.14950
64B -> 69B -0.14370
65B -> 67B 0.14354
65B -> 69B -0.17525
65B -> 70B -0.27724
66B -> 67B 0.11135
66B -> 68B 0.23550
66B -> 69B -0.40920
66B -> 70B -0.18698

Excited State 8: 3.000-A 4.6869 eV 264.53 nm f=0.0000 <S**2>=2.000
61A -> 69A 0.12656
62A -> 68A 0.16908
63A -> 68A 0.13520
63A -> 70A 0.11063
64A -> 67A -0.13538
64A -> 68A -0.18407
64A -> 69A 0.11213
64A -> 70A 0.15853
65A -> 68A 0.32393
65A -> 69A -0.22729
66A -> 68A -0.25860
66A -> 69A -0.19606
66A -> 70A 0.14442
61B -> 69B -0.12656
62B -> 68B -0.16908
63B -> 68B -0.13520
63B -> 70B -0.11063
64B -> 67B 0.13538
64B -> 68B 0.18407
64B -> 69B -0.11213
64B -> 70B -0.15853
65B -> 68B -0.32393
65B -> 69B 0.22729
66B -> 68B 0.25860
66B -> 69B 0.19606
66B -> 70B -0.14442

Excited State 9: 3.000-A 4.7706 eV 259.89 nm f=0.0000 <S**2>=2.000
63A -> 68A 0.33919
63A -> 69A 0.18545
63A -> 70A 0.35111

64A -> 68A 0.20914
65A -> 69A 0.18495
65A -> 70A 0.17727
66A -> 70A -0.23597
63B -> 68B -0.33919
63B -> 69B -0.18545
63B -> 70B -0.35111
64B -> 68B -0.20914
65B -> 69B -0.18495
65B -> 70B -0.17727
66B -> 70B 0.23597

Excited State 10: 1.000-A 4.8282 eV 256.79 nm f=0.0007 <S**2>=0.000
65A -> 68A 0.34200
65A -> 69A 0.12442
65A -> 70A 0.32526
66A -> 68A 0.41297
66A -> 69A 0.16129
66A -> 70A 0.17648
65B -> 68B 0.34200
65B -> 69B 0.12442
65B -> 70B 0.32526
66B -> 68B 0.41297
66B -> 69B 0.16129
66B -> 70B 0.17648

Excited State 11: 1.000-A 5.0245 eV 246.76 nm f=0.0426 <S**2>=0.000
64A -> 68A -0.13390
65A -> 69A 0.23426
66A -> 68A -0.35386
66A -> 69A 0.49118
64B -> 68B -0.13390
65B -> 69B 0.23426
66B -> 68B -0.35386
66B -> 69B 0.49118

Excited State 12: 1.000-A 5.0601 eV 245.02 nm f=0.0417 <S**2>=0.000
65A -> 68A -0.13915
65A -> 69A -0.20199
65A -> 70A -0.14051
66A -> 68A 0.29883
66A -> 69A 0.38626
66A -> 70A -0.37454
65B -> 68B -0.13915
65B -> 69B -0.20199
65B -> 70B -0.14051
66B -> 68B 0.29883
66B -> 69B 0.38626
66B -> 70B -0.37454

Excited State 13: 3.000-A 5.0819 eV 243.97 nm f=0.0000 <S**2>=2.000
61A -> 69A -0.17560
62A -> 69A 0.12020
64A -> 69A -0.18847
64A -> 70A 0.10036
65A -> 67A 0.15892
65A -> 69A 0.46235
65A -> 70A -0.30753
66A -> 68A -0.13205
61B -> 69B 0.17560
62B -> 69B -0.12020
64B -> 69B 0.18847
64B -> 70B -0.10036
65B -> 67B -0.15892
65B -> 69B -0.46235
65B -> 70B 0.30753
66B -> 68B 0.13205

Excited State 14: 3.000-A 5.2378 eV 236.71 nm f=0.0000 <S**2>=2.000
48A -> 67A -0.10065
53A -> 67A -0.13628
57A -> 67A -0.19898
60A -> 67A 0.35198
61A -> 67A -0.14520
62A -> 67A -0.26732
64A -> 67A 0.15773
65A -> 67A 0.13374
66A -> 67A 0.19709
66A -> 68A -0.15296
48B -> 67B 0.10065
53B -> 67B 0.13628
57B -> 67B 0.19898
60B -> 67B -0.35198
61B -> 67B 0.14520
62B -> 67B 0.26732
64B -> 67B -0.15773
65B -> 67B -0.13374
66B -> 67B -0.19709
66B -> 68B 0.15296

Excited State 15: 1.000-A 5.2751 eV 235.04 nm f=0.0193 <S**2>=0.000
63A -> 68A -0.29070
63A -> 69A -0.15757
63A -> 70A -0.28490
64A -> 68A -0.11944
65A -> 68A -0.21015
65A -> 70A -0.22952
66A -> 70A 0.38810
63B -> 68B -0.29070
63B -> 69B -0.15757
63B -> 70B -0.28490
64B -> 68B -0.11944
65B -> 68B -0.21015
65B -> 70B -0.22952
66B -> 70B 0.38810

Excited State 16: 3.000-A 5.4461 eV 227.66 nm f=0.0000 <S**2>=2.000
61A -> 68A -0.10331
61A -> 70A -0.11359
63A -> 68A 0.17223
63A -> 70A 0.17318
64A -> 68A 0.11499
64A -> 69A 0.18287
64A -> 70A 0.10910
65A -> 68A -0.14332
65A -> 70A -0.14867
66A -> 68A 0.26547
66A -> 70A 0.44816
61B -> 68B 0.10331
61B -> 70B 0.11359
63B -> 68B -0.17223
63B -> 70B -0.17318
64B -> 68B -0.11499
64B -> 69B -0.18287
64B -> 70B -0.10910
65B -> 68B 0.14332
65B -> 70B 0.14867
66B -> 68B -0.26547
66B -> 70B -0.44816

Excited State 17: 3.000-A 5.4646 eV 226.89 nm f=0.0000 <S**2>=2.000
60A -> 69A 0.12198
62A -> 69A 0.17384
62A -> 70A -0.12893
64A -> 67A -0.10778
64A -> 68A -0.11157

64A -> 69A -0.30552
64A -> 70A 0.28993
65A -> 69A -0.19679
66A -> 68A 0.15043
66A -> 69A 0.31254
60B -> 69B -0.12198
62B -> 69B -0.17384
62B -> 70B 0.12893
64B -> 67B 0.10778
64B -> 68B 0.11157
64B -> 69B 0.30552
64B -> 70B -0.28993
65B -> 69B 0.19679
66B -> 68B -0.15043
66B -> 69B -0.31254

Excited State 18: 1.000-A 5.6487 eV 219.49 nm f=0.0613 <S**2>=0.000
63A -> 68A 0.21087
63A -> 70A 0.19510
64A -> 67A -0.10115
64A -> 69A 0.11527
64A -> 70A 0.18439
65A -> 67A 0.39782
65A -> 69A 0.17930
65A -> 70A -0.24505
66A -> 68A 0.21075
66A -> 70A 0.17123
63B -> 68B 0.21087
63B -> 70B 0.19510
64B -> 67B -0.10115
64B -> 69B 0.11527
64B -> 70B 0.18439
65B -> 67B 0.39782
65B -> 69B 0.17930
65B -> 70B -0.24505
66B -> 68B 0.21075
66B -> 70B 0.17123

Excited State 19: 1.000-A 5.6757 eV 218.45 nm f=0.0900 <S**2>=0.000
62A -> 67A -0.11052
63A -> 68A -0.17339
63A -> 70A -0.15781
64A -> 68A -0.13271
64A -> 70A -0.15789
65A -> 67A 0.45874
65A -> 68A 0.29268
66A -> 68A -0.15617
66A -> 70A -0.14837
62B -> 67B -0.11052
63B -> 68B -0.17339
63B -> 70B -0.15781
64B -> 68B -0.13271
64B -> 70B -0.15789
65B -> 67B 0.45874
65B -> 68B 0.29268
66B -> 68B -0.15617
66B -> 70B -0.14837

Excited State 20: 1.000-A 5.7263 eV 216.52 nm f=0.0275 <S**2>=0.000
62A -> 67A 0.10466
63A -> 68A -0.10605
64A -> 67A -0.11084
64A -> 68A -0.29408
65A -> 69A 0.40546
66A -> 68A 0.14398
66A -> 69A -0.20053
66A -> 70A -0.30099
62B -> 67B 0.10466

63B -> 68B -0.10605
64B -> 67B -0.11084
64B -> 68B -0.29408
65B -> 69B 0.40546
66B -> 68B 0.14398
66B -> 69B -0.20053
66B -> 70B -0.30099
SavETr: write IOETrn= 770 NScale= 10 NData= 16 NLR=1 NState= 20 LETran= 370.

Excitation energies and oscillator strengths for compound **258** are presented below:

Excited State 1: 3.000-A 3.0833 eV 402.11 nm f=0.0000 <S**2>=2.000
51A -> 55A -0.24662
52A -> 55A 0.11903
54A -> 55A 0.62205
51B -> 55B 0.24662
52B -> 55B -0.11903
54B -> 55B -0.62205
This state for optimization and/or second-order correction.
Total Energy, E(TD-HF/TD-DFT) = -634.242588363
Copying the excited state density for this state as the 1-particle RhoCI density.

Excited State 2: 3.000-A 3.5469 eV 349.55 nm f=0.0000 <S**2>=2.000
51A -> 55A 0.42414
52A -> 55A 0.39699
53A -> 55A 0.26559
51B -> 55B -0.42414
52B -> 55B -0.39699
53B -> 55B -0.26559

Excited State 3: 1.000-A 3.8118 eV 325.26 nm f=0.0292 <S**2>=0.000
51A -> 55A 0.43597
51A -> 57A -0.10012
52A -> 55A 0.26379
53A -> 55A 0.18776
54A -> 55A -0.38489
51B -> 55B 0.43597
51B -> 57B -0.10012
52B -> 55B 0.26379
53B -> 55B 0.18776
54B -> 55B -0.38489

Excited State 4: 3.000-A 4.0449 eV 306.52 nm f=0.0000 <S**2>=2.000
51A -> 57A 0.14214
52A -> 55A -0.13400
52A -> 56A 0.15758
52A -> 57A -0.13547
53A -> 56A -0.16478
53A -> 57A -0.12880
54A -> 56A -0.17390
54A -> 57A 0.55728
51B -> 57B -0.14214
52B -> 55B 0.13400
52B -> 56B -0.15758
52B -> 57B 0.13547
53B -> 56B 0.16478
53B -> 57B 0.12880
54B -> 56B 0.17390
54B -> 57B -0.55728

Excited State 5: 1.000-A 4.2649 eV 290.71 nm f=0.1878 <S**2>=0.000
51A -> 55A 0.24224
52A -> 55A 0.24277
53A -> 55A 0.13223
54A -> 55A 0.58034
51B -> 55B 0.24224
52B -> 55B 0.24277
53B -> 55B 0.13223

54B -> 55B 0.58034

Excited State 6: 3.000-A 4.3400 eV 285.68 nm f=0.0000 <S**2>=2.000
51A -> 56A 0.14581
52A -> 56A -0.15437
53A -> 56A -0.12922
54A -> 56A 0.61292
54A -> 57A 0.19483
51B -> 56B -0.14581
52B -> 56B 0.15437
53B -> 56B 0.12922
54B -> 56B -0.61292
54B -> 57B -0.19483

Excited State 7: 3.000-A 4.8313 eV 256.63 nm f=0.0000 <S**2>=2.000
52A -> 56A -0.32578
53A -> 55A -0.16353
53A -> 56A 0.53610
54A -> 57A 0.20652
52B -> 56B 0.32578
53B -> 55B 0.16353
53B -> 56B -0.53610
54B -> 57B -0.20652

Excited State 8: 1.000-A 4.9284 eV 251.57 nm f=0.0203 <S**2>=0.000
52A -> 57A -0.12389
53A -> 57A 0.16541
54A -> 56A 0.64668
52B -> 57B -0.12389
53B -> 57B 0.16541
54B -> 56B 0.64668

Excited State 9: 3.000-A 4.9570 eV 250.12 nm f=0.0000 <S**2>=2.000
48A -> 55A -0.14204
50A -> 55A 0.31604
51A -> 55A 0.32113
52A -> 55A -0.17728
53A -> 55A -0.22659
53A -> 56A -0.14687
54A -> 55A 0.24790
54A -> 56A 0.10722
54A -> 57A -0.16736
48B -> 55B 0.14204
50B -> 55B -0.31604
51B -> 55B -0.32113
52B -> 55B 0.17728
53B -> 55B 0.22659
53B -> 56B 0.14687
54B -> 55B -0.24790
54B -> 56B -0.10722
54B -> 57B 0.16736

Excited State 10: 1.000-A 5.1219 eV 242.07 nm f=0.2074 <S**2>=0.000
54A -> 57A 0.68019
54B -> 57B 0.68019

Excited State 11: 3.000-A 5.3744 eV 230.69 nm f=0.0000 <S**2>=2.000
52A -> 55A -0.15946
52A -> 57A -0.30247
53A -> 55A 0.20346
53A -> 57A 0.56283
52B -> 55B 0.15946
52B -> 57B 0.30247
53B -> 55B -0.20346
53B -> 57B -0.56283

Excited State 12: 3.000-A 5.8732 eV 211.10 nm f=0.0000 <S**2>=2.000
42A -> 55A -0.12535

48A -> 55A -0.15606
50A -> 55A 0.10499
50A -> 57A 0.12515
51A -> 55A -0.11063
51A -> 57A -0.19281
52A -> 55A 0.16316
52A -> 57A 0.35018
53A -> 57A 0.20425
54A -> 57A 0.22288
54A -> 58A -0.12309
54A -> 59A 0.11756
42B -> 55B 0.12535
48B -> 55B 0.15606
50B -> 55B -0.10499
50B -> 57B -0.12515
51B -> 55B 0.11063
51B -> 57B 0.19281
52B -> 55B -0.16316
52B -> 57B -0.35018
53B -> 57B -0.20425
54B -> 57B -0.22288
54B -> 58B 0.12309
54B -> 59B -0.11756

Excited State 13: 1.000-A 5.9486 eV 208.43 nm f=0.0947 <S**2>=0.000
50A -> 55A -0.14546
51A -> 55A -0.37950
52A -> 55A 0.23849
53A -> 55A 0.47444
54A -> 56A -0.11144
50B -> 55B -0.14546
51B -> 55B -0.37950
52B -> 55B 0.23849
53B -> 55B 0.47444
54B -> 56B -0.11144

Excited State 14: 1.000-A 6.1489 eV 201.64 nm f=0.1205 <S**2>=0.000
50A -> 55A -0.10559
51A -> 55A -0.18837
51A -> 56A -0.10130
52A -> 55A 0.40483
52A -> 56A 0.11263
52A -> 57A 0.19211
53A -> 55A -0.22751
53A -> 56A 0.25247
53A -> 57A -0.23298
54A -> 56A 0.18740
50B -> 55B -0.10559
51B -> 55B -0.18837
51B -> 56B -0.10130
52B -> 55B 0.40483
52B -> 56B 0.11263
52B -> 57B 0.19211
53B -> 55B -0.22751
53B -> 56B 0.25247
53B -> 57B -0.23298
54B -> 56B 0.18740

Excited State 15: 3.000-A 6.1563 eV 201.39 nm f=0.0000 <S**2>=2.000
42A -> 55A -0.14826
43A -> 55A 0.10619
48A -> 55A -0.19204
50A -> 55A -0.19047
50A -> 56A 0.10101
50A -> 57A -0.13700
51A -> 56A -0.12933
52A -> 55A 0.15647
52A -> 56A 0.25485

52A -> 57A -0.22637
53A -> 55A -0.20617
53A -> 56A 0.12186
54A -> 55A -0.11155
54A -> 56A 0.10563
54A -> 59A 0.10904
42B -> 55B 0.14826
43B -> 55B -0.10619
48B -> 55B 0.19204
50B -> 55B 0.19047
50B -> 56B -0.10101
50B -> 57B 0.13700
51B -> 56B 0.12933
52B -> 55B -0.15647
52B -> 56B -0.25485
52B -> 57B 0.22637
53B -> 55B 0.20617
53B -> 56B -0.12186
54B -> 55B 0.11155
54B -> 56B -0.10563
54B -> 59B -0.10904

Excited State 16: 3.000-A 6.2850 eV 197.27 nm f=0.0000 <S**2>=2.000
48A -> 55A 0.13432
50A -> 56A 0.18361
51A -> 55A 0.10084
51A -> 56A -0.18679
52A -> 55A -0.19624
52A -> 56A 0.35959
52A -> 57A 0.21839
53A -> 56A 0.23976
54A -> 56A 0.20872
54A -> 59A 0.11016
48B -> 55B -0.13432
50B -> 56B -0.18361
51B -> 55B -0.10084
51B -> 56B 0.18679
52B -> 55B 0.19624
52B -> 56B -0.35959
52B -> 57B -0.21839
53B -> 56B -0.23976
54B -> 56B -0.20872
54B -> 59B -0.11016

Excited State 17: 3.000-A 6.3585 eV 194.99 nm f=0.0000 <S**2>=2.000
49A -> 55A 0.13373
50A -> 55A 0.14336
50A -> 57A -0.14054
52A -> 55A -0.22639
52A -> 57A -0.10016
53A -> 55A 0.34280
53A -> 57A -0.23377
54A -> 58A -0.24773
54A -> 59A 0.17728
54A -> 61A -0.12122
54A -> 63A 0.13076
49B -> 55B -0.13373
50B -> 55B -0.14336
50B -> 57B 0.14054
52B -> 55B 0.22639
52B -> 57B 0.10016
53B -> 55B -0.34280
53B -> 57B 0.23377
54B -> 58B 0.24773
54B -> 59B -0.17728
54B -> 61B 0.12122
54B -> 63B -0.13076

Excited State 18: 1.000-A 6.3833 eV 194.23 nm f=0.0074 <S**2>=0.000
51A -> 56A -0.11132
52A -> 55A -0.31125
52A -> 56A 0.24647
52A -> 57A 0.16470
53A -> 55A 0.35922
53A -> 56A 0.11160
53A -> 57A -0.35004
54A -> 56A 0.12230
51B -> 56B -0.11132
52B -> 55B -0.31125
52B -> 56B 0.24647
52B -> 57B 0.16470
53B -> 55B 0.35922
53B -> 56B 0.11160
53B -> 57B -0.35004
54B -> 56B 0.12230

Excited State 19: 3.000-A 6.4652 eV 191.77 nm f=0.0000 <S**2>=2.000
48A -> 55A -0.15565
49A -> 55A 0.12987
52A -> 57A 0.11385
53A -> 55A 0.30305
54A -> 58A 0.45825
54A -> 61A 0.13955
54A -> 63A -0.11371
48B -> 55B 0.15565
49B -> 55B -0.12987
52B -> 57B -0.11385
53B -> 55B -0.30305
54B -> 58B -0.45825
54B -> 61B -0.13955
54B -> 63B 0.11371

Excited State 20: 1.000-A 6.5400 eV 189.58 nm f=0.0543 <S**2>=0.000
50A -> 55A -0.14366
52A -> 56A 0.24133
52A -> 57A -0.16306
53A -> 55A -0.10278
53A -> 56A -0.35034
53A -> 57A -0.14184
54A -> 58A 0.43414
50B -> 55B -0.14366
52B -> 56B 0.24133
52B -> 57B -0.16306
53B -> 55B -0.10278
53B -> 56B -0.35034
53B -> 57B -0.14184
54B -> 58B 0.43414
SavETr: write IOETrn= 770 NScale= 10 NData= 16 NLR=1 NState= 20 LETran= 370.

## *11. X-Ray Crystallography*

Experimental measurement of crystallographic parameters of compound **331** were measured by Owen Smith.

| | | |
|---|---|---|
| **Identification code** | 7065 | |
| **Empirical formula** | $C_{13}H_{14}INO$ | |
| **Formula weight** | 327.16 | |
| **Temperature** | 150 K | |
| **Wavelength** | 1.54184 Å | |
| **Crystal system** | Monoclinic | |
| **Space group** | P 21/c | |
| **Unit cell dimensions:** | a = 7.8494(2) Å<br>b = 24.2754(5) Å<br>c = 6.71270(10) Å | α= 90°.<br>β= 106.052(2)°.<br>γ = 90°. |
| **Volume 1229.22(5)** | $Å^3$ | |
| Z | **4** | |
| **Density (calculated)** | 1.768 $Mg/m^3$ | |
| **Absorption coefficient** | 20.291 $mm^{-1}$ | |
| **F(000)** | 640 | |
| **Crystal size** | 0.17 x 0.10 x 0.05 $mm^3$ | |
| **Theta range for data collection** | 3.642 to 76.217°. | |
| **Index ranges** - | 9<=h<=9, -30<=k<=29, -7<=l<=8 | |
| **Reflections collected** | 7616 | |
| **Independent reflections** | 2540 [R(int) = 0.035] | |
| **Completeness to theta = 73.930°** | 99.7 % | |
| **Absorption correction** | Semi-empirical from equivalents | |
| **Max. and min. transmission** | 0.35 and 0.08 | |
| **Refinement method** | Full-matrix least-squares on F2 | |
| **Data / restraints / parameters** | 2540 / 0 / 145 | |
| **Goodness-of-fit on $F^2$** | 1.0000 | |
| **Final R indices [I>2sigma(I)]** | R1 = 0.0228, wR2 = 0.0534 | |
| **R indices (all data)** | R1 = 0.0269, wR2 = 0.0559 | |
| **Largest diff. peak and hole** | 0.94 and -0.51 $e.Å^{-3}$ | |

***Table 26:*** *Crystallographic parameters for compound* ***331***

| Atom | X | Y | Z | U(eq) |
|---|---|---|---|---|
| **I(1)** | 5592(1) | 3115(1) | 2090(1) | 27 |
| **C(2)** | 2872(4) | 3189(1) | 610(4) | 22 |
| **C(3)** | 1689(4) | 2849(1) | 1247(5) | 28 |
| **C(4)** | -108(4) | 2892(1) | 283(6) | 34 |
| **C(5)** | -731(4) | 3267(1) | -1289(6) | 32 |
| **C(6)** | 458(4) | 3603(1) | -1926(5) | 27 |
| **C(7)** | 2280(4) | 3575(1) | -969(4) | 21 |
| **N(8)** | 3487(3) | 3917(1) | -1653(4) | 21 |
| **C(9)** | 3000(3) | 4477(1) | -1991(4) | 19 |
| **C(10)** | 3054(4) | 4767(1) | -3676(4) | 23 |
| **C(11)** | 2624(4) | 5371(1) | -3943(5) | 28 |
| **C(12)** | 1377(4) | 5544(1) | -2682(5) | 28 |
| **C(13)** | 2163(4) | 5369(1) | -435(5) | 25 |
| **C(14)** | 2626(3) | 4766(1) | -189(4) | 21 |
| **O(15)** | 2766(3) | 4527(1) | 1448(3) | 30 |
| **C(16)** | 4102(4) | 3654(1) | -3297(5) | 27 |

***Table 27:*** *Crystallographic coordinates for compound* ***331***

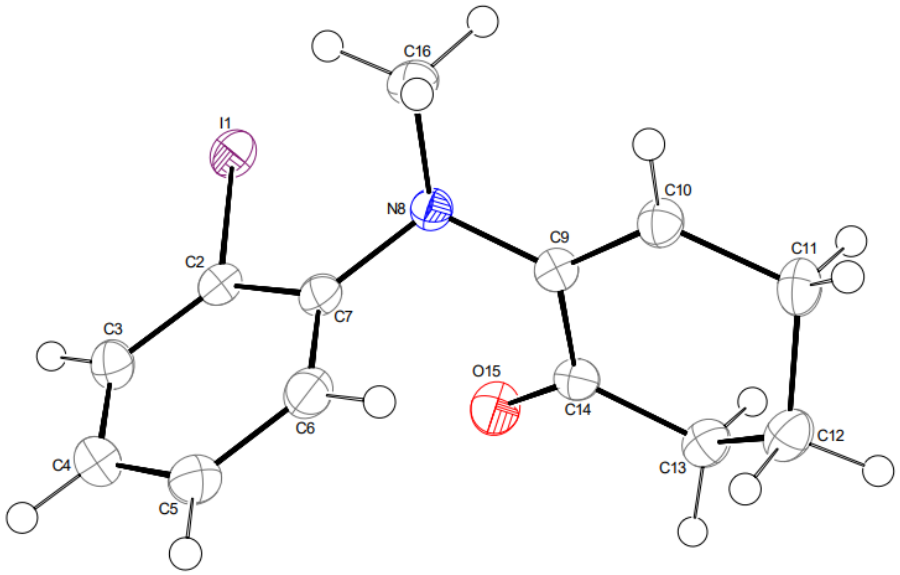



***Figure 64:*** *X-Ray structure of compound* ***331***

# References


1. J.D.Coyle, *Introduction to organic photochemistry*. John Wiley & Sons: Chichester, 1986.

2. V.Balzani; P.Ceroni; A.Juris, *Photochemistry and Photophysics*. Wiley-VCH: Weinheim, 2014.

3. R.S.H.Liu; G.S.Hammond, *J. Am. Chem. Soc.* **1964,** *86*, 1892-1893.

4. J.M.Luis; D.M.Bishop; B.Kirtman, *J. Chem. Phys.* **2004,** *120*, 813-822.

5. M.Kasha, *Discuss. Faraday Soc.* **1950,** *9*, 14-19.

6. M.Bixon; J.Jortner, *J. Chem. Phys. Soc.* **1968,** *48*, 715-726.

7. G.Baryshnikov; B.Minaev; H.Agren, *Chem. Rev.* **2017,** *117*, 6500-6537.

8. G-S.Kim; T.L.Nguyen; A.M.Mebel; S.H.Lin; M.T.Nguyen, *J. Phys. Chem. A.* **2003,** *107*, 1788-1796.

9. E.Condon, *Phys. Rev.* **1928,** *32*, 858-872.

10. E.Condon, *Phys. Rev.* **1926,** *28*, 1182-1201.

11. J.Franck, *Trans. Faraday Soc.* **1925,** *21*, 536-542.

12. J.Saltiel; S.Ganapathy; C.Werking, *J. Phys. Chem.* **1986,** *91*, 2788-2758.

13. K.Singh; S.J.Staig; J.D.Weaver, *J. Am. Chem. Soc.* **2014,** *136*, 5275-5278.

14. C.Garcia-Iriepa; M.Marazzi; L.M.Frutos; D.Sampedro, *RSC adv.* **2012,** *3*, 6241-6266.

15. R.A.Caldwell; C.V.Cao, *J. Am. Chem. Soc.* **1982,** *104*, 6174-6180.

16. R.A.Caldwell; L.D.Jacobs; T.R.Furlani; E.A.Nalley; J.Laboy, *J. Am. Chem. Soc.* **1992,** *114*, 1623–1625.

17. T.Kumagai; K.Shimizu; Y.Kawamura; T.Mukai, *Tetrahedron* **1981,** *37*, 3365-3376.

18. L.Salem; C.Rowland, *Angew. Chem. Int. Ed.* **1972,** *11*, 92-111.

19. M.R.Becker; E.R.Wearing; C.S.Schindler, *Nat. Chem.* **2020,** *12*, 898–905.

20. R.A.Caldwell; M.Singh, *J. Am. Chem. Soc.* **1983,** *105*, 5139–5140.

21. F.Strieth-Kalthoff; M.J.James; M.Teders; L.Pitzer; F.Glorius, *Chem. Soc. Rev.* **2018,** *47*, 7190-7202.

22. T.Forster, *Ann. Phys.* **1948,** *437*, 55-75.

23. D.L.Dexter, *J. Chem. Phys. Soc.* **1953,** *21*, 599-610.

24. H.E.Zimmerman; R.J.Boettcher; N.E.Buehler; G.E.Keck; M.G.Steinmetz, *J. Am. Chem. Soc.* **1975,** *98*, 7680-7698.

25. C.K.Prier; D.A.Rankic; D.W.C.MacMillan, *Chem. Rev.* **2013,** *113*, 5322-5363.

26. F.Strieth-Kalthoff; F.Glorius, *Chem* **2020,** *6*, 1888-1903.

27. K.Teegardin; J.Day; J.Chan; J.Weaver, *Org. Process Res. Dev.* **2016,** *20*, 1156-1163.

28. H.Yersin, *Highly Efficient OLEDs with Phosphorescent Materials*. Wiley-VCH: Darmstadt, 2008.

29. S.DiLuzio; V.Mdluli; T.U.Connell; J.Lewis; V.VanBenschoten; S.Bernhard, *J. Am. Chem. Soc.* **2021,** *143*, 1179-1194.

30. J.E.Baldwin, *J. Chem. Soc., Chem. Commun.* **1976**, 734-736.

31. K.Gilmore; I.V.Alabugin, *Chem. Rev.* **2011,** *111*, 6513-6556.

32. P.Hohenberg; W.Kohn, *Phys. Rev.* **1964,** *136*, B864-B871.

33. W.Kohn; L.J.Sham, *Phys. Rev.* **1965,** *140*, A1133-A1138.

34. C.J.Cramer, *Essentials of Computational Chemistry, Theories and Models*. 2nd ed.; John Wiley & Sons: Chichester, 2004.

35. Y.Zhao; D.G.Truhlar, *Theor. Chem. Acc.* **2008,** *120*, 215-241.

36. L.Goerigk; A.Hansen; C.Bauer; S.Ehrlich; A.Najibi; S.Grimme, *Phys. Chem. Chem. Phys.* **2017,** *19*, 32184-32215.

37. P.C.St.John; Y.Guan; Y.Kim; S.Kim; R.S.Paton, *Nat. Commun.* **2020,** *11*.

38. Y.Zhao; D.G.Truhlar, *J. Phys. Chem. A* **2008,** *112*, 1095-1099.

39. S.Grimme; J.Anthony; S.Ehrlich; H.Krieg, *J. Chem. Phys.* **2010,** *132*, 154104-154119.

40. S.Grimme, *Wiley Interdiscip. Rev. Comput. Mol. Sci.* **2011,** *1*, 211-228.

41. P.J.Stephens; F.J.Devlin; C.F.Chabalowski; M.J.Frisch, *J. Phys. Chem.* **1994,** *98*, 11623-11627.

42. S.H.Vosko; L.Wilk; M.Nusair, *Can. J. Phys.* **1980,** *58*, 1200-1211.

43. C.Lee; W.Yang; R.G.Parr, *Phys. Rev. B* **1988,** *37*, 785-789.

44. A.D.Becke, *J. Chem. Phys.* **1993,** *98*, 5648-5652.

45. M.Zhu; C.Zheng; X.Zhang; S.-L.You, *J. Am. Chem. Soc.* **2019,** *141*, 2636–2644.

46. N.Ferre; N.Guihery; Malriu, J.-P., *Phys. Chem. Chem. Phys.* **2015,** *17*, 14375-14382.

47. B.O.Roos; P.R.Taylor; P.E.M.Sigbahn, *Chem. Phys.* **1980,** *48*, 157-173.

48. K.Andersson; P.A.Malmqvist; B.O.Roos; A.J.Sadlej; K.Wolinski, *J. Chem. Phys.* **1990,** *94*, 5483-5488.

49. K.Andersson; P.A.Malmqvist; B.O.Roos, *J. Chem. Phys.* **1992,** *96*, 1218-1226.

50. G.Yang; K.Sivalingam; E.F.Valeen; F.Neese, *J. Chem. Phys.* **2016,** *144*.

51. P.G.Szalay, *Chem. Rev.* **2012,** *112*, 108-181.

52. R.R.Valiev; V.N.Cherepanov; G.V.Baryshnikov; D.Sundholm, *Phys. Chem. Chem. Phys.* **2018,** *20*, 6121-6133.

53. D.A.Fedorov; S.R.Pruitt; K.Keipert; M.S.Gordon; S.A.Varganov, *J. Phys. Chem.* **2016,** *120*, 2911-2919.

54. D.A.Fedorov; A.O.Lykhin; S.A.Varganov, *J. Phys. Chem.* **2018,** *122*, 3480-3488.

55. M.Richter; P.Marquetand; J.Gonzalez-Vazquez; I.Sola; L.Gonzalez, *J. Chem. Theory Comput.* **2011,** *7*, 1253-1258.

56. T.P.Yoon; M.A.Ischay; J.Du, *Nat. Chem.* **2010,** *2*, 527-532.

57. F.Bohlmann; R.K.Gupta; J.Jakupovic, *Phytochemistry* **1981,** *20*, 831-832.

58. C.M.Hasan; T.M.Healey; P.G.Waterman; C.H.Schwalbe, *J. Chem. Soc., Perkin Trans. 1* **1982**, 2807-2812.

59. J.-F.Liu; Z.-Y.Jiang; R.-R.Wang; Y.-T.Zeng; J.-J.Chen; X.-M.Zhang; Y.-B.Ma, *Org. Lett.* **2007,** *9*, 4127-4129.

60. L.S.Fernandez; M.L.Sykesa; K.T.Andrews; V.M.Avery, *Int. J. Antimicrob. Agents* **2010,** *36*, 275-279.

61. A.M.Balde; L.A.Pieters; A.Gergely; V.Wray; M.Claeys; A.J.Vlietinck, *Phytochemistry* **1991,** *30*, 997-1000.

62. A.Thakur; A.Singh; N.Kaur; R.Ojha; K.Nepali, *Bioorg. Chem.* **2020,** *94*.

63. M.D.Karkas; J.A.Porco Jr.; C.R.J.Stephenson, *Chem. Rev.* **2016,** *116*, 9683−9747.

64. H.Nagaoka; M.Shimano; Y.Yamada, *Tet. Lett.* **1989**, 971-974.

65. S.Poplata; A.Tröster; Y.-Q.Zou; T.Bach, *Chem. Rev.* **2016,** *116*, 9748−9815.

66. M.A.Ischay; M.E.Anzovino; J.Du; T.P.Yoon, *J. Am. Chem. Soc.* **2008,** *130*, 12886–12887.

67. M.A.Ischay; Z.Lu; T.P.Yoon, *J. Am. Chem. Soc.* **2010,** *132*, 8572–8574.

68. J.Du; T.P.Yoon, *J. Am. Chem. Soc.* **2009,** *41*, 14604-14605.

69. J.Du; K.L.Skubi; D.M.Schultz; T.P.Yoon, *Science* **2014,** *344*, 392-396.

70. Z.Lu; T.P.Yoon, *Angew. Chem. Int. Ed.* **2012,** *51*, 10329-10332.

71. J.Zhao; J.L.Brosmer; Q.Tang; Z.Zang; K.N.Houk; P.L.Diaconescu; O.Kwon, *J. Am. Chem. Soc.* **2017,** *139*.

72. X.Li; J.Großkopf; C.Jandl; T.Bach, *Angew. Chem. Int. Ed.* **2020,** *60*, 2684-2688.

73. K.A.Rykaczewski; C.S.Schindler, *Org. Lett.* **2020,** *22*, 6516-6519.

74. J.Zheng; X.Dong; T.P.Yoon, *Org. Lett.* **2020,** *22*, 6520-6525.

75. P.-S.Song; W.E.Kurtin, *J. Am. Chem. Soc.* **1969,** *91*, 4892-4906.

76. M.M.Francl; W.J.Pietro; W.J.Hehre; J.S.Binkley; M.S.Gordon; D.J.DeFrees; J.A.Pople, *J. Chem. Phys.* **1982,** *77*, 3654-3665.

77. R.Krishnan; J.S.Binkley; R.Seeger; J.A.Pople, *J. Chem. Phys.* **1980,** *72*, 650-654.

78. P.C.Hariharan; J.A.Pople, *Theor. Chim. Acta* **1973,** *28*, 213-222.

79. W.J.Hehre; R.Ditchfield; J.A.Pople, *J. Chem. Phys.* **1972,** *56*, 2257-2261.

80. A.V.Marenich; C.J.Cramer; D.G.Truhlar, *J. Phys. Chem. B* **2009,** *113*, 6378-6396.

81. J.Tomasi; B.Mennucci; E.Cances, *J. Molec. Struct. THEOCHEM* **1999,** *132*, 114110-114115.

82. B.Mennucci; J.Tomasi, *J. Chem. Phys.* **1997,** *106*, 5151-5158.

83. B.Mennucci; E.Cances; J.Tomasi, *J. Phys. Chem. B* **1997,** *101*, 10506-10517.

84. E.Cances; B.Mennucci; J.Tomasi, *J. Chem. Phys.* **1997,** *107*, 3032-3041.

85. A.B.Rolka; B.Koening, *Org. Lett.* **2020,** *22*, 5035-5040.

86. N.Arai; T.Ohkuma, *Org. Lett.* **2019,** *21*, 1506-1510.

87. M.Zhu; X.-L.Huang; H.Xu; X.Zhang; C.Zheng; S.-L.You, *CCS Chem.* **2020,** *2*, 652-664.

88. M.Zhu; X.Zhang; C.Zheng; S.-L.You, *ACS Catal.* **2020,** *21*, 12618-12626.

89. Y.-Z.Cheng; X.-L.Huang; W.-H.Zhuang; Q.-R.Zhao; X.Zhang; T.-S.Mei; S.-L.You, *Angew. Chem. Int. Ed.* **2020,** *59*, 18062-18067.

90. M.J.James; J.L.Schwarz; F.Strieth-Kalthoff; B.Wibbeling; F.Glorius, *J. Am. Chem. Soc.* **2018,** *140*, 8624-8628.

91. Z.Zhang; D.Yi; M.Zhang; J.Wei; J.Lu; L.Yang; J.Wang; N.Hao; X.Pan; S.Zhang; S.Wei; Q.Fu, *ACS Catal.* **2020,** *10*, 10149–10156.

92. F.Weigend, *Phys. Chem. Chem. Phys.* **2006,** *8*, 1057-1065.

93. F.Weigend; R.Ahlrichs, *Phys. Chem. Chem. Phys.* **2005,** *7*, 3297-3305.

94. M.S.Oderinde; E.Mao; A.Ramirez; J.Pawluczyk; C.Jorge; L.A.M.Cornelius; J.Kempson; M.Vetrichelvan; M.Pitchai; A.Gupta; A.K.Gupta; N.A.Meanwell; A.Mathur; T.G.M.Dhar, *J. Am. Chem. Soc.* **2020,** *142*, 3094-3103.

95. M.S.Oderinde; A.Ramirez; T.G.M.Dhar; L.A.M.Cornelius; C.Jorge; D.Aulakh; B.Sandhu; J.Pawluczyk; A.A.Sarjeant; N.A.Meanwell; A.Mathur; J.Kempson, *J. Org. Chem.* **2021,** *86*, 1730-1747.

96. J.Ma; F.Schafers; C.Daniliuc; K.Bergander; C.A.Strassert; F.Glorius, *Angew. Chem. Int. Ed.* **2020,** *132*, 9726-9732.

97. J.Mateos; A.Vega-Penaloza; P.Franceschi; F.Rigodanza; P.Andreetta; X.Companyo; G.Pelosi; M.Bonchio; D.Dell'Amico, *Chem. Sci.* **2020,** *11*, 6532-6538.

98. J.-D.Chai; M.Head-Gordon, *Phys. Chem. Chem. Phys.* **2008,** *10*, 6615-6620.

99. Y.Zhao; N.Schultz; D.G.Truhlar, *J. Chem. Theory Comput.* **2006,** *2*, 364-382.

100. C.Adamo, *J. Chem. Phys.* **1999,** *110*.

101. X.-P.Mu; Y.-H.Li; N.Zheng; J.-Y.Long; S.-J.Chen; B.-Y.Liu; C.-B.Zhao; Z.Yang, *Angew. Chem. Int. Ed.* **2021,** *60*, 11211-11216.

102. D.Becker; N.Morlender; N.Haddad, *Tet. Lett.* **1995,** *36*, 1921-1924.

103. D.Becker; N.Haddad; Y.Sahali, *Tet. Lett.* **1989,** *30* (2661-2664).

104. N.Haddad; N.Galili, *Tet. Lett.* **1997,** *38*, 6083-6086.

105. A.R.Matlin; C.F.George; S.Wolff; W.C.Agosta, *J. Am. Chem. Soc.* **1986,** *108*, 3385-3394.

106. S.Wolff; W.C.Agosta, *J. Am. Chem. Soc.* **1983,** *105*, 1292-1299.

107. F.Strieth-Kalthoff; C.Henkel; M.Teders; A.Kahnt; W.Knolle; A.Gómez-Suárez; K.Dirian; W.Alex; K.Bergander; C.G.Daniliuc; B.Abel; D.M.Guldi; F.Glorius, *Chem* **2019,** *5*, 2183-2194.

108. N.Chadha; O.Silakari, *Eur. J. Med. Chem.* **2019,** *134*, 159-184.

109. T.Saget; B.Konig, *Chem. Eur. J.* **2020,** *26*, 7004-7007.

110. H.Huang; M.Yu; X.Su; P.Guo; J.Zhao; J.Zhou; Y.Li, *J. Org. Chem.* **2018,** *83*, 2425-2437.

111. J.W.Tucker; J.M.R.Narayanam; S.W.Krabbe; C.R.J.Stephenson, *Org. Lett.* **2010,** *12*, 368-371.

112. Y.Yang; X.-H.Duan; J.-Y.Deng; B.Jin; H.-M.Jia; B.-L.Liu, *Bioorg. Med. Chem. Lett.* **2011,** *21*, 5594-5597.

113. M.J.Eichberg; R.L.Dorta; K.Lamottke; K.P.C.Vollhardt, *Org. Lett.* **2000,** *2*, 2497-2481.

114. Y.Takahashi; H.Ikeda; Y.Kanase; K.Makino; H.Tabata; T.Oshitari; S.Inagaki; Y.Otani; H.Natsugari; H.Takahashi; T.Ohwada, *J. Org. Chem.* **2017,** *82*, 11370–11382.

115. A.Singh; K.Teegardin; M.Kelly; K.S.Prasad; S.Krishnan; J.D.Weaver, *J. Organomet. Chem.* **2014,** *776*, 51-59.

116. K.K.-W.Lo; J.S.-W.Chan; L.-H.Lui; C.-K.Chung, *Organomet.* **2004,** *23*, 3108-3116.

117. S.G.Modha; A.Pothig; A.Dreuw; T.Bach, *J. Org. Chem.* **2019,** *84*, 1139-1153.

118. N.Munster; N.A.Parker; L. van Dijk; R.S.Paton; M.D.Smith, *Angew. Chem. Int. Ed.* **2017,** *56*, 9468-9472.

119. J.Ma; S.Chen; P.Bellotti; R.Guo; F.Schafer; A.A.Heusler; X.Zhang; C.Daniliuc; M.K.Brown; K.N.Houk; F.Glorius, *Science* **2021,** *371*, 1338-1345.

120. S.Grimme; S.Ehrlich; L.Goerigk, *J. Comp. Chem.* **2011,** *32*, 1456-1465.

121. A.D.McLean; G.S.Chandler, *J. Chem. Phys.* **1980,** *72*, 5639-6548.

122. E.Gorobets; N.E.Wong; R.S.Paton; D.J.Derksen, *Org. Lett.* **2017,** *19*, 484-487.

123. R.K.Mohamed; S.Mondal; K.Jorner; T.F.Delgado; V.V.Lobodin; H.Ottosson; I.V.Alabugin, *J. Am. Chem. Soc.* **2015,** *137*, 15441-15450.

124. G.Jimenez-Oses; P.Liu; R.A.Matute; K.N.Houk, *Angew. Chem.* **2014,** *53*.

125. R.A.Matute; M.A.Garcia-Garibay; K.N.Houk, *Org. Lett.* **2014,** *16*.

126. R.A.Matute; K.N.Houk, *Angew. Chem.* **2012,** *51*, 13097-13100.

127. E.M.Greer; K.Kwon; A.Greer; C.Doubleday, *Tetrahedron* **2016,** *72*, 7357-7373.

128. J.J.Maresh; L.-A.Giddings; A.Friedrich; E.A.Loris; S.Panjikar; B.L.Trout; J.Stockigt; B.Peters; S.E.O'Connor, *J. Am. Chem. Soc.* **2008,** *130*, 710-723.

129. F.B.Mallory; C.S.Wood; J.T.Gordon, *J. Am. Chem. Soc.* **1964,** *86*, 3094-3102.

130. P.Hugelschofer; J.Kalvoda; K.Schaffner, *Helv. Chim. Acta* **1960,** *43*, 1322-1332.

131. K.B.Jorgensen, *Molecules* **2010,** *15*, 4334-4358.

132. R.G.F.Giles; P.R.K.Mitchell; M.V.Sargent, *J. Chem. Soc., Perkin Trans. 1* **1983**, 2147-2152.

133. M.P.Cava; P.Stern; K.Wakisaka, *Tet. Lett.* **1973,** *29*, 2245-2249.

134. R.M.Letcher; Wong, K.-M., *J. Chem. Soc., Perkin Trans. 1* **1977**, 178-180.

135. G.Rio; J.-C.Hardy, *Bull. Soc. Chim. Fr.* **1970,** *3578-3584*.

136. R.Li; T.Nakashima; O.Galangau; T.Kawai, *Chem. Eur. J.* **2016,** *22*, 16250-16257.

137. T.Nakashima; K.Tsuchie; R.Kanazawa; R.Li; S.Iijima; O.Galangau; H.Nakagawa; K.Mutoh; Y.Kobayashi; J.Abe; T.Kawai, *J. Am. Chem. Soc.* **2015,** *137*, 7023-7026.

138. V.Smula; R.H.F.Manske; R.Rodrigo, *Can. J. Chem.* **1972,** *50*, 1544-1547.

139. D.Fischer; H.Tomeba; N.K.Pahadi; N.T.Patil; Z.Huo; Y.Yamamoto, *J. Am. Chem. Soc.* **2008,** *130*, 15720–15725.

140. Y.N.Chu; L.C.Lin; A.Shani; S.S.Yang, *J. Org. Chem.* **1969,** *34*, 1845-1848.

141. B.S.Thyagarajan; N.Kharasch; H.B.Lewis; W.Wolf, *Chem. Commun.* **1967**, 614-615.

142. J.Grimshaw; A.Prasanna de Silva, *J. Chem. Soc., Chem. Commun.* **1980**, 302-303.

143. S.Lalitha; S.Rajeswari; R.B.Pai; H.Suguna, *Indian J. Chem. Sect. B* **1977,** *15*, 180-182.

144. H.Hara; O.Hoshino; B.Umezawa, *Tet. Lett.* **1977,** *49*, 5031-5034.

145. G.R.Lenz, *Tet. Lett.* **1673,** *14*, 1963-1966.

146. G.R.Lenz, *J. Org. Chem.* **1977,** *42* (1117-1122).

147. G.R.Lenz; N.C.Yang, *Chem. Commun.* **1967**, 1136b-1137.

148. N.C.Yang; A.Shani; G.R.Lenz, *J. Am. Chem. Soc.* **1966,** *88*, 5369.

149. K.-P.Zeller; S.Berger, *J. Chem. Soc., Perkin Trans. 2* **1977**, 54-58.

150. K.-P.Zeller; H.Petersen, *Synthesis* **1975,** *8*, 532-533.

151. V.M.Clark; A.Cox; E.J.Herbert, *J. Chem. Soc. C* **1968**, 831-833.

152. J.A.Ejlx; D.P.H.Murphy; M.V.Sargent, *Synth. Commun.* **1972,** *2*, 427-430.

153. W.A.Henderson Jr.; Zweig, A., *Tet. Lett.* **1969,** *10*, 625-626.

154. Y.-S.Chang; M.L.Deinzer, *J. Label. Compd. Radiopharm* **1991,** *29*, 43-62.

155. M.E.Buden; V.A.Vaillard; S.E.Martin; R.A.Rossi, *J. Org. Chem.* **2009,** *74*, 4490-4498.

156. J.P.Ferris; F.R.Antonucci, *J. Am. Chem. Soc.* **1974,** *96*, 2010-2014.

157. A.G.Schultz; R.D.Lucci; W.Y.Fu; M.H.Berger; J.Erhardt; W.K.Hagmann, *J. Am. Chem. Soc.* **1978,** *100*, 2150-2162.

158. A.G.Schultz; W.Y.Fu; R.D.Lucci; B.G.Kurr; K.M.Lo; M.Boxer, *J. Am. Chem. Soc.* **1978,** *100*, 2140-2149.

159. A.G.Schultz, *J. Org. Chem.* **1974,** *39*, 3185-3186.

160. S.Chu; N.Munster; T.Balan; M.D.Smith, *Angew. Chem. Int. Ed.* **2016,** *55*, 14306-14309.

161. S.Grimme, *J. Comp. Chem.* **2006,** *27*, 1787-1799.

162. T.Yanai; D.Tew; N.Handy, *Chem. Phys. Lett.* **2004,** *393*, 51-57.

163. O.A.Vydrov; G.E.Scuseria; J.P.Perdew, *J. Chem. Phys.* **2007,** *126*, 154109.

164. O.A.Vydrov; J.Heyd; A.Krukau; G.E.Scuseria, *J. Chem. Phys.* **2006,** *125*, 074106.

165. O.A.Vydrov; G.E.Scuseria, *J. Chem. Phys.* **2006,** *125*, 234109.

166. T.M.Henderson; A.F.Izmaylov; G.Scalmani; G.E.Scuseria, *J. Chem. Phys.* **2009,** *131*, 044108.

167. M.J.Frisch; G.W.Trucks; H.B.Schlegel; G.E.Scuseria; M.A.Robb; J.R.Cheeseman; G.Scalmani; V.Barone; G.A.Petersson; H.Nakatsuji; X.Li; M.Caricato; V.Marenich, A.; J.Bloino; B.G.Janesko; R.Gomperts; B.Mennucci; H.P.Hratchian; J.V.Ortiz; A.F.Izmaylov; J.L.Sonnenberg; D.Williams-Young; F.Ding; F.Lipparini; F.Egidi; J.Goings; B.Peng; A.Petrone; T.Henderson; D.Ranasinghe; V.G.Zakrzewski; J.Gao; N.Rega; G.Zheng; W.Liang; M.Hada; M.Ehara; K.Toyota; R.Fukuda; J.Hasegawa; M.Ishida; T.Nakajima; Y.Honda; O.Kitao; H.Nakai; T.Vreven; K.Throssell; J.A.Montgomery Jr; J.E.Peralta; F.Ogliaro; M.J.Bearpark; J.J.Heyd; E.N.Brothers; K.N.Kudin; V.N.Staroverov; T.A.Keith; R.Kobayashi; J.Normand; K.Raghavachari; A.P.Rendell; J.C.Burant; S.S.Iyengar; J.Tomasi; M.Cossi; J.M.Millam; M.Klene; C.Adamo; R.Cammi; J.W.Ochterski; R.L.Martin; K.Morokuma; O.Farkas; J.B.Foresman; D.J.Fox *Gaussian 16*, Revision C.01; Gaussian Inc.: Wallingford CT, 2016.

168. M.Baba, *J. Phys. Chem. A* **2011,** *115*, 9514-9519.

169. M.A.El-Sayed, *J. Phys. Chem.* **1963,** *38*, 2834-2838.

170. M.T.Peschel; P.Kabacinski; D.P.Schwinger; E.Thyrhaug; G.Cerullo; T.Bach; J.Hauer; R.de Vivie-Riedle, *Angew. Chem. Int. Ed.* **2021,** *60*, 10155-10163.

171. W.J.Hehre; R.F.Stewart; J.A.Pople, *J. Chem. Phys.* **1969,** *51*, 2657-2664.

172. J.B.Collins; P.v.R.Schleyer; J.S.Binkley; J.A.Pople, *J. Chem. Phys.* **1974,** *64*, 5142-5151.

173. E.W.Kwan; Y.Zheng; H.A.Besser; E.N.Jacobsen, *Nat. Chem.* **2018,** *10*, 917-923.

174. F.Sandfort; T.Knecht; T.Pinkert; C.G.Daniliuc; F.Glorius, *J. Am. Chem. Soc.* **2020,** *142*, 6913-6919.

175. T.Constantin; M.Zanini; A.Regni; N.S.Shikh; F.Julia; D.Leonori, *Science* **2020,** *367*, 1021-1026.

176. Y.-R.Luo, *Handbook of bond dissociation energiesin organic compounds*. CRC Press, London, 2003.

177. Y.Guo; C.Riplinger; U.Becker; D.G.Liakos; Y.Minenkov; L.Cavallo; F.Neese, *J. Chem. Phys.* **2018,** *148*, 011101.

178. C.Riplinger; P.Pinski; U.Becker; E.F.Valeen; F.Neese, *J. Chem. Phys.* **2016,** *144*, 024109.

179. M.Saitow; U.Becker; C.Riplinger; E.F.Valeen; F.Neese, *J. Chem. Phys.* **2017,** *146*, 164105.

180. C.Riplinger; F.Neese, *J. Chem. Phys.* **2013,** *138*, 034106.

181. T.Wolff, *J. Org. Chem.* **1981,** *46*, 978-983.

182. C.M.Marian, *Annu. Rev. Phys. Chem.* **2021,** *72*, 617-640.

183. T.J.Penfold; E.Gindensperger; C.Daniel; C.M.Marian, *Chem. Rev.* **2018,** *118*, 6975-7025.

184. J.C.Lorquet; B.Leyh-Nihant, *J. Phys. Chem.* **1988,** *92*, 4778-4783.

185. J.Suchan; J.Janoš; P.Slavíček, *J. Chem. Theory Comput.* **2020,** *16*, 5809-5820.

186. T.Schmierer; S.Laimbruber; K.Haiser; K.Keiwisch; J.Neugebauer; P.Glich, *Phys. Chem. Chem. Phys.* **2010,** *12* (15653-15664).

187. J.A.Leitch; T.Rossolini; R.Rogova; J.A.P.Maitland; D.J.Dixon, *ACS Catal.* **2020,** *10*, 2009-2025.

188. Y.Guan; S.V.S.Sowndarya; L.C.Gallegos; P.C.St.John; R.S.Paton, *Chem. Sci.* **2021**, doi.org/10.1039/D1SC03343C.

189. F.N.Palmer; F.Lach; C.Poriel; A.G.Pepper; M.C.Bagley; A.M.Z.Slawin; C.J.Moody, *Org. Biomol. Chem.* **2005,** *3*, 3805-3811.

190. T.Fujihara; T.Xu; K.Semba; J.Terao; Y.Tsuji, *Angew. Chem. Int. Ed.* **2011,** *50*, 523-527.

191. K.Fukui, *Acc. Chem. Res.* **1981,** *14*, 363-368.

192. S.Grimme, *Chem. Eur. J.* **2012,** *18*, 9955-9964.

193. G.Luchini; J.V.Alegre-Requena; Y.Guan; I.Funes-Ardoiz; R.S.Paton *GoodVibes 3.0.1*, 2019.

194. R.E.Plata; D.A.Singleton, **2015,** *137*, 3811-3826.

195. J.D.Snyder; L.-A.Hamill; K.E.Faleumu; D.H.Ess *MECPro Version 1.0.5: Minimum Energy Crossing Program*, Brigham Young University: 2019.

196. E.D.Glendening; J.K.Badenhoop; A.E.Reed; J.E.Carpenter; J.A.Bohmann; C.M.Morales; C.R.Landis; F.Weinhold *NBO*, Version 6.0; Theoretical Chemistry Institute, University of Wisconsin, Madison WI: 2013.

197. *The PyMOL Molecular Graphics System, version 2.0.7*, Schrödinger, LLC.